CHALMERS
UNIVERSITY OF TECHNOLOGY

Design with Regard to Collision Impact
Comparison between 2DOF and FE Analysis for Collision Impact on Concrete Slabs

Master's Thesis in the Master's Programme Structural Engineering and Building Technology

JONATAN ANDERSSON
JOHAN ANTONSSON

Design with Regard to Collision Impact

Comparison between 2DOF and FE Analysis for Collision Impact on Concrete Slabs

Master's Thesis in the Master's Programme Structural Engineering and Building Technology

JONATAN ANDERSSON

JOHAN ANTONSSON

Design with Regard to Collision Impact
Comparison between 2DOF and FE Analysis for Collision Impact on Concrete Slabs

Master's Thesis in the Master's Programme Structural Engineering and Building Technology
JONATAN ANDERSSON
JOHAN ANTONSSON

Department of Civil and Environmental Engineering
Division of Structural Engineering
Concrete Structures
Chalmers University of Technology
SE-412 96 Göteborg
Sweden
Telephone: + 46 (0)31-772 1000

Cover:
Illustration of a how a vehicle impact on a simply supported slab can be simplified in FEM and to a 2DOF system. Comparison of response in displacement u_2 and velocity v_2 over time between FEM and 2DOF, with a $\kappa_{mF} = 0.1$.

Design with Regard to Collision Impact

Comparison between 2DOF and FE Analysis for Collision Impact on Concrete Slabs

Master's Thesis in the Master's Programme Structural Engineering and Building Technology

JONATAN ANDERSSON

JOHAN ANTONSSON

Department of Civil and Environmental Engineering

Division of Structural Engineering

Concrete Structures

Chalmers University of Technology

ABSTRACT

During collisions between a moving object and a resisting structure, an impact load is obtained which can act very different from a static load. Examples of such collisions are when a structure is exposed to a vehicle crash, or if a strong wind throws an object at it. These scenarios will create a dynamic response which can be of great importance for the behaviour of the structure. The methods that regard collision impact in Eurocode are very simplified and further studies of the subject are needed. Therefore, the purpose of this master's thesis is to evaluate how the design with regard to collision impact between an incoming object and a reinforced concrete member, can be carried out using both advanced and simplified methods. This thesis compares impact loaded finite element (FE) models, with two degree of freedom (2DOF) mass-spring systems. The resisting structure and the incoming object are simplified to have either an elastic behaviour, or an elastic and plastic (elasto-plastic) bilinear behaviour. The structures studied are mainly simply supported quadratic slabs.

Basic theory of dynamics and collision impact is described and a parametric study of collisions using 2DOF is performed for the understanding of basic principles of collision impact. It is described how beams and slabs can be transformed into a mass and a spring, so it can be used in the 2DOF, in addition it is also described how the used FE models are built.

When modelling a slab with FE software in this thesis, the target was first to use a grid of beams (beam grillage), which in turn are made of 3D beam elements. However, it appears that the beam grillage has the wrong behaviour when acting plastically compared to both theory and alternative FE models made of shell elements. So for slabs with elasto-plastic behaviour, shell elements are used instead. It is shown that the 2DOF and FE models correspond well for beams, particularly when the collision impact is in the centre of the beam and especially for elastic beams. For elastic slabs, 2DOF and FE models correspond quite well but less so when the impact is far from the centre. For elasto-plastic slabs however, the correspondence is not so good, but a corresponding maximum displacement can be found between the 2DOF and FE. It is believed that the 2DOF model can be improved in several ways, which are discussed, to be able to fully describe the elasto-plastic behaviour of a simply supported reinforced concrete slab.

Key words: Collision impact, impulse load, 2DOF, FEM, dynamic response, transformation factor, beam grillage, elasto-plastic

Dimensionering med hänsyn till kollisionsstöt
Jämförelse mellan 2DOF och FE-analys för kollisionsstöt på betongplattor
Examensarbete inom mastersprogrammet Structural Engineering and Building Technology
JONATAN ANDERSSON
JOHAN ANTONSSON
Institutionen för bygg- och miljöteknik
Avdelningen för konstruktionsteknik
Betongbyggnad
Chalmers tekniska högskola

SAMMANFATTNING

Vid kollisioner mellan en kropp i rörelse och en mothållande konstruktion så kommer en stötlast att skapas som kan agera mycket olikt en statisk last. Exempel på sådana kollisioner är när en konstruktion blir påkört av ett fordon, eller om en stark vind får ett objekt att flyga in i den från sidan. Dessa scenarier kommer att skapa en dynamisk respons som kan spela en stor roll i beteendet av konstruktionen. Eurocode behandlar kollisionsstötar med mycket förenklade metoder och mer fördjupade studier av ämnet behövs. Därför är syftet med detta examensarbete att undersöka hur dimensionering med hänsyn till kollisionsstöt, mellan ett inkommande objekt och en armerad betongstruktur, kan utföras med både avancerade och förenklade beräkningsmetoder. Denna rapport jämför stötbelastade finita element- (FE) modeller, med två frihetsgraders (2DOF) massa-fjäder-system. Den mothållande konstruktionens och det inkommande objektet är förenklat till att ha antingen ett elastiskt beteende, eller ett elastiskt och plastiskt (elastoplastiskt) bilinjärt beteende. Det som studeras främst i den här rapporten är kollisionsstöt på fritt upplagda kvadratiska betongplattor.

Grundläggande teori om dynamik och kollisionsstötar beskrivs och en parameter-studie av kollisioner med hjälp av 2DOF genomförs för att skapa en grundläggande förståelse av kollisionsstöt. Det är också beskrivit hur balkar och plattor kan bli transformerade till en massa och en fjäder för användning i 2DOF, och hur de använda FE-modellerna är uppbyggda.

Det var meningen att FE-modellerna av plattor, skulle byggas upp med ett rutnät av balkar (balkrost), utgjorda av tredimensionella balkelement. Det visar sig dock att denna balkrost har fel beteende när plattan plasticerar jämfört med både teori och alternativa FE-modeller utgjorda av skalelement. Därför används skalelement för plattor med elastoplastiskt beteende. För balkar så stämmer 2DOF och FE-modellerna väl överens med varandra, särskilt för elastiska balkar utsatta för stöt i mittpunkten. För elastiska plattor, så har 2DOF och FE-modellerna ganska likt beteende, men också för dessa så skiljer modellerna sig mer från varandra ju längre stöten sker från mitten av plattan. För elastoplastiska plattor är dock korrespondensen inte så bra, men en motsvarande maximal nedböjning kan hittas mellan 2DOF och FE. 2DOF-modellen kan förbättras på flera sätt, vilka diskuteras, för att mer fullständigt kunna beskriva det elastoplastiska beteendet av en fritt upplagd armerad betongplatta.

Nyckelord: Kollisionsstöt, impulslast, 2DOF, FEM, dynamisk respons, transformationsfaktor, balkrost, elasto-plastisk

Contents

Preface

In this master's thesis, the response of a simply supported concrete structure subjected to an impact load is evaluated, and how this can be used in design with regard to collision impact. A comparison between a simplified method, consisting of a 2DOF mass-spring system, and FE models is carried out.

The work has been carried out at the office of Reinertsen Sverige AB in Gothenburg during the period of January to June 2015. This master's thesis is a collaboration between Reinertsen Sverige AB and the Department of Civil and Environmental Engineering, Division of Structural Engineering, Concrete Structures research group at Chalmers University of Technology.

We would like to thank our supervisor and examiner Adjunct Professor Morgan Johansson for his guidance and his helpful feedback throughout the project. We would also like to thank Reinertsen Sverige AB for the time at their office. Finally we would like to thank our fellow thesis worker colleagues who have been our closest company during this study.

Gothenburg, June 2015

Jonatan Andersson and Johan Antonsson

Abbreviations

2DOF	Two Degrees of Freedom
CDM	Central Difference Method
FE	Finite Element
FEM	Finite Element Method
SDOF	Single Degree of Freedom

Notations

Roman upper case letters

A	Area
$\mathbf{C}$	Damping matrix
E	Young's modulus
E_{cm}	Mean Young's modulus for concrete
E_{eq}	Equivalent Young's modulus
EI	Stiffness
E_k	Kinetic energy
$E_{k,tot}$	Kinetic energy after collision in the direction of body 2
$E_{k,0}$	Kinetic energy before collision
$E_{k,1}$	Kinetic energy for body 1 after collision
$E_{k,2}$	Kinetic energy for body 2 after collision
E_s	Young's modulus for steel
F	Force
F_b	Force acting on a beam
F_{sl}	Force acting on a slab
F_x	Force in x-direction
F_1	Force acting on body 1
F_2	Force acting on body 2
G	Shear modulus
I	Impulse
I	Moment of inertia
I_k	Characteristic impulse load
$\mathbf{K}$	Stiffness matrix
M	Moment
$\mathbf{M}$	Mass matrix
M_{Rd}	Bending moment capacity
M_f	Field moment
M_s	Support moment
N	Normal force
P	Pressure
Q	Equivalent static load
R	Internal resistance
R_b	Internal resistance of a beam
R_{sl}	Internal resistance of a slab
R_1	Internal resistance of body 1
$R_{1,max}$	Maximum internal resistance of body 1
R_2	Internal resistance of body 2
$R_{2,max}$	Maximum internal resistance of body 2

R_{sta}	Static internal resistance
$R_{sta,1}$	Static internal resistance of body 1
$R_{sta,2}$	Static internal resistance of body 2
R_{dyn}	Dynamic internal resistance
T	Torsional moment
T_I	Torsional moment of state I
T_{II}	Torsional moment of state II
V	Shear force
V_{Ed}	Design value of shear force
W	Work
W_e	External work
$W_{e,1}$	External work of body 1
$W_{e,2}$	External work of body 2
W_i	Internal work
$W_{i,1}$	Internal work of body 1
$W_{i,1}$	Internal work of body 2
X	Axis in global coordinate system
Y	Axis in global coordinate system
Z	Axis in global coordinate system

Roman lower case letters

a	Acceleration
c	Damping coefficient
c	Concrete cover
d	Effective height of the cross-section
d'	Distance from cross-section edge to compressed reinforcement
e	Coefficient of restitution
f	Frequency
f_y	Yield stress
$f_{y,mod}$	Modified yield stress
$\mathbf{f}$	Force vector
f_{cc}	Concrete compressive strength
f_{ct}	Concrete tensile strength
f_{sy}	Yield stress of reinforcing steel
f_{su}	Ultimate strength of reinforcing steel
f_1	Frequency of body 1
f_2	Frequency of body 2
h	Time step
h_b	Height of a beam
h_{cr}	Critical time step
k	Stiffness
k_b	Stiffness of a beam
k_{sl}	Stiffness of a slab
k_λ	Correction factor for plastic rotation capacity
k_1	Stiffness of spring 1
k_2	Stiffness of spring 2
k_2	Stiffness of body 2
l	Length
l_e	Element length

l_0	Distance between zero and maximum moment section
l_b	Length of a beam
m	Mass
m_b	Mass of a beam
m_1	Mass of body 1
m_2	Mass of body 2
n	An arbitrary positive integer
p	Momentum
p_0	Initial momentum
q	Distributed load
r	Axis in local coordinate system
r	Radius
s	Axis in local coordinate system
t	Axis in local coordinate system
t	Time
t	Thickness
t_0	Time at start
t_1	Time at unloading
Δt	Time increment
Δt_{cr}	Critical time increment
u	Displacement
u_c	Displacement in the centre of the slab
u_s	Displacement in the system point
u_1	Displacement of body 1
u_2	Displacement of body 2
u_{el}	Elastic deformation
u_{pl}	Plastic deformation
u_{tot}	Total deformation
$\dot{u}$	Velocity
$\ddot{u}$	Acceleration
$\ddot{u}_1$	Acceleration of body 1
$\ddot{u}_2$	Acceleration of body 2
Δu	Deformation of spring 1
Δu	Change of displacement
Δu_s	Change of displacement in the system point
$u''(x)$	Curvature of a beam
v	Velocity
v_{pl}	Velocity after plastic collision
v_0	Initial velocity
v_1	Velocity of body 1
v_2	Velocity of body 2
w_b	Width of a beam
x_u	Depth of the compression zone
x	Coordinate of horizontal length axis

Greek lower case letters

α	Angle
α	Displacement factor
α	Distance between loading and support in relation to the total length

α	Yield stress correction factor
β	Distance between loading and support in relation to the total length, 1 - α
β_{el}	Load factor
β_{shear}	Factor considering shear stress
γ	Factor for stiffness of a slab
γ_{sl}	Factor for stiffness of the quadratic slab at hand
γ_2	Factor for stiffness of an arbitrary quadratic slab
ε_{sfsu}	Strain corresponding to f_{su}
ε_{sy}	Yield strain of reinforcing steel
ε_{sh}	Strain at hardening of reinforcing steel
ε_{su}	Ultimate strain of reinforcing steel
θ	Rotation
θ_{pl}	Plastic rotation
$\theta_{pl,d}$	Plastic rotation capacity, design value
κ_F	Transformation factor for the load
κ_k	Transformation factor for the stiffness
κ_m	Transformation factor for the mass
κ_{mF}	Transformation factor for both mass and load
λ	Shear slenderness
υ	Poisson's ratio
ρ_c	Concrete density
φ	Angle between force and direction of displacement
φ	Twisting
ω	Angular frequency

Greek upper case letter

Φ	Diameter of reinforcement

1 Introduction

1.1 Background

During collisions between a moving object and a resisting structure, an impact load is obtained which can act very different from a static load. Examples of such collisions are when a structure is exposed to a vehicle crash, when an object is dropped on it during lifting, or if a strong wind throws an object at it.

These scenarios will create a dynamic response which can be of great importance for the behaviour of the structure. The methods that regard collision impact in Eurocode, CEN (2004), are very simplified and further studies of the subject are needed. Therefore, both simplified and advanced methods have to be developed.

This study is a continuation of a previous master's thesis, Asplund and Steckmest (2014).

1.2 Aim and objective

The aim of this thesis is to evaluate how the design with regard to collision impact between simply supported concrete members, mainly quadratic slabs, and incoming objects, can be carried out using both advanced and simplified methods. The simplified approach is made with a two degrees of freedom (2DOF) mass-spring model, which is compared to more advanced finite element (FE) models. The FE models are seen as reference models because they are supposed to describe the reality better than the 2DOF model. From this comparison it can be evaluated if and when the 2DOF model corresponds to the FE model and under which circumstances it is not.

It is also investigated how the response of the collision depends on the structural properties of the two objects involved. Even though it is the resisting concrete member that is of interest, the behaviour of the incoming object can change the overall behaviour of the collision.

In the previous master's thesis by Asplund and Steckmest, the behaviour of a linear elastic object colliding with a linear elastic simply supported concrete beam is evaluated. This is further developed in this thesis by introducing elastic and plastic non-linear (elasto-plastic) behaviour for both the incoming object and the resisting structure. The study is then extended to regard simply supported concrete slabs, which are of main interest, and it is evaluated whether similar concepts to that of beams can be used when making a 2DOF model. Different ways to model a concrete slab with an elasto-plastic behaviour are also studied, and it is checked if these models correspond to theory and hand calculations.

1.3 Limitations

In this thesis the damping effect of both the structure subjected to the impact load and the incoming object is neglected, since in most cases it has a small influence due to the relatively short duration of the applied load. This will be slightly on the safe side and unnecessary complicated calculations are avoided.

No long-term effects such as creep or shrinkage are considered, because it is only the parameters prior, during and after the collision impact that are of interest. For the same reason, thermal expansion is not considered because of that the temperature change during collision will not affect the structure sufficiently. When subjected to impulse loading, the reinforced concrete can obtain high strain rates. These higher strain rates can lead to a considerable increase in strength for the reinforced concrete, this is however neglected. Also, the influence of compressive membrane action is neglected.

A slab is significantly more complex than a beam, which gives a large number of combinations regarding geometry, boundary conditions and placement of the load. With regard to this, only a finite number of combinations will be investigated. To further limit the studied number of combinations, and to avoid unnecessary complexities, all investigated slabs and beams in this thesis will be simply supported and without subjection to normal force.

In this thesis, no physical tests are performed and the results from the 2DOF model are solely compared to the results from FE analysis, which is considered as describing reality better than the 2DOF model. To avoid numerical problems and long simulation times when modelling reinforced concrete in FE models in this thesis, the concrete and the reinforcement are not modelled separately, but as one single equivalent material. This equivalent material model will not give as accurate results as the separate material model during the collision, but it is deemed to be a good enough approximation for this study.

1.4   Method

A literature study is carried out covering the basic theory of dynamics and collisions, mass-spring systems and the structural response of reinforced concrete. A parametric study of several simplified dynamic 2DOF mass-spring models, that describes a collision between an incoming object and a concrete member, are made for the basic understanding of collision impact. These models are based on the fundamental equation of motion and are solved with a numerical integration method, called the Central Difference Method (CDM), in the commercial software MATLAB (2014). This 2DOF model is also verified and compared with classic impact theory.

The 2DOF model represents two bodies where one is the resisting structure. If this body is studied separately it is called a single degree of freedom (SDOF) model. To be able to use the SDOF as a representation of a slab or a beam, some of its parameters needs to be adjusted, which is done by multiplying the parameters with transformation factors. These transformation factors are derived using energy equations which are solved analytically for beams and numerically for slabs. The numerical derivation uses FE analysis with the commercial software ADINA 900 nodes version, ADINA (2014), to extract the displacement of a slab, and MATLAB to calculate the transformation factors with an algorithm that uses the derived equations.

Dynamic FE models are made in ADINA which are compared to the 2DOF model in a collision study. In this study, the FE analysis is considered to be describing the reality best. When comparing the results from 2DOF and FE models a number of parameters can be evaluated. One parameter that is of special interest is the displacement of the resisting structure over time, since it can be directly transferred to load bearing capacity. The evaluated collisions cover different parameters for the

incoming object and different impact locations for the resisting object so that more general results are gained and more conclusions can be drawn.

In the FE models, the concrete and reinforcement are modelled as one single material. The input parameters for this composite material are modified to approximately represent reinforced concrete using hand calculations in the commercial software Mathcad (2011).

Both beam elements and shell elements are tested for the modelling of a slab in the FE software ADINA. When modelling a slab with beam elements, a grid of beams is used where each beam represents one strip of the slab. These beams are created for both directions of the slab. For the elasto-plastic behaviour of the beam elements, moment-curvature and torsion-twisting relations and limits are manually implemented, which is done to better control the behaviour of each beam. This manually implemented behaviour is calculated using hand calculations in Mathcad. The beam grillage model is tested for different torsion-twisting relations to see how the torsional stiffness affects the slab.

In order to keep the 2DOF model regarding a slab with elasto-plastic behaviour simple, a hand calculated yield limit based on the moment capacity of the slab is needed, which is obtained using the strip method. The strip method is intended for distributed load and in this thesis, it is the point loads that are of interest. Therefore, yield lines of the slabs must be assumed and it is presumed that the yield lines go straight from the point load to the four corners of the slab.

1.5 Thesis outline

In Chapter 2, the basic theory used in this thesis is presented. This covers basic concepts of dynamics and impact theory, introduction to mass spring systems, the numerical integration method CDM, and how to treat the behaviour of reinforced concrete.

Chapter 3 contains a parametric study of different collision cases, with and without barrier, for a 2DOF model based on the theory of Chapter 2. The parametric study is made for the understanding of collisions and 2DOF systems and to decide which parameters are of importance. The results from the analysis are verified and compared to classic impact theory.

In Chapter 4, it is described how an elastic or plastic beam or slab, can be transformed into a SDOF system with the help of so called transformation factors. The theory of how to calculate these transformation factors and some of the derived factors is presented.

In Chapter 5, it is defined how the FE analysis of this thesis is carried out. It contains explanations of the equivalent Young's modulus, how to model elasto-plastic behaviour of the incoming object, different alternatives of how to model slabs and elasto-plastic behaviour of beam elements.

Chapter 6 covers a brief study of impact on simply supported beams and a more thoroughly study for simply supported slabs. This study handles both elastic and elasto-plastic behaviour of both the resisting structure and the incoming object. It also contains a thorough comparison between shell element modelling and beam grillage modelling for an elasto-plastic behaviour of the slab, and interesting discoveries for the SDOF transformation factors.

Chapter 7 is the concluding chapter of this thesis. Here, a final discussion is presented, which summarises the previous discussions and discoveries. A final conclusion is also presented in this chapter and some examples of further studies.

Chapter 7.2 contains the references used in this thesis. Additional information that is not presented in the main chapters is attached as appendices at the end.

2 Theory

2.1 Orientation

The structural behaviour of structures can differ depending on if the applied load is static or dynamic, especially if the dynamic load is an impact load. In many cases this different behaviour is not taken into consideration when designing structures. Instead, as an approximation, a static load is used which corresponds to a simplified version of the dynamic load, Johansson and Laine (2012). This simplified load is in the form of a static load which has a corresponding load configuration that does the same amount of work as the dynamic load. This is called an equivalent static load.

It is important to know that a specific equivalent static load depends on a specific dynamic load with its own conditions and the structural response of the loaded member. If these conditions are not fulfilled it is uncertain if the static load will be valid. This gives room for errors while trying to interpret the rules of Eurocode, CEN (2004). This along with unclear instructions in the rules on how to translate dynamic loads to static loads may make it difficult to make a reliable assessment for the structure at hand. Therefore it can be necessary to have a deeper understanding of the dynamic response of the structure.

In this chapter basic knowledge about structural dynamics, impact theory with corresponding mass-spring system and structural behaviour of reinforced concrete regarding impact is presented. This chapter is based on work presented in Johansson and Laine (2012), Craig and Kurdila (2006), Al-Emrani (2011) and Engström (2014).

2.2 Basic dynamics

2.2.1 Force and pressure

The term force can be described as the ability to accelerate the mass of a body. The relation between the force F, the mass m and its acceleration a is defined by Newton's second law of motion as

$$F = m \cdot a \tag{2.1}$$

The force per unit area is defined as pressure P

$$P = \frac{F}{A} \tag{2.2}$$

where F is the force acting on the area A.

2.2.2 Momentum and impulse

The momentum p of a body m is defined as

$$p = m \cdot v \tag{2.3}$$

where v is the velocity of the body.

If the body at hand has an initial velocity v_0 and is subjected to a force $F(t)$ during the time period $t_0 \leq t \leq t_1$, the final momentum will be

$$p = m \cdot v_1 = m \cdot v_0 + \int_{t_0}^{t_1} F(t)dt \tag{2.4}$$

where the change of momentum is defined as the transferred impulse I

$$I = \int_{t_0}^{t_1} F(t)dt = \int_{t_0}^{t_1} ma(t)dt = m\int_{t_0}^{t_1} a(t)dt = mv \tag{2.5}$$

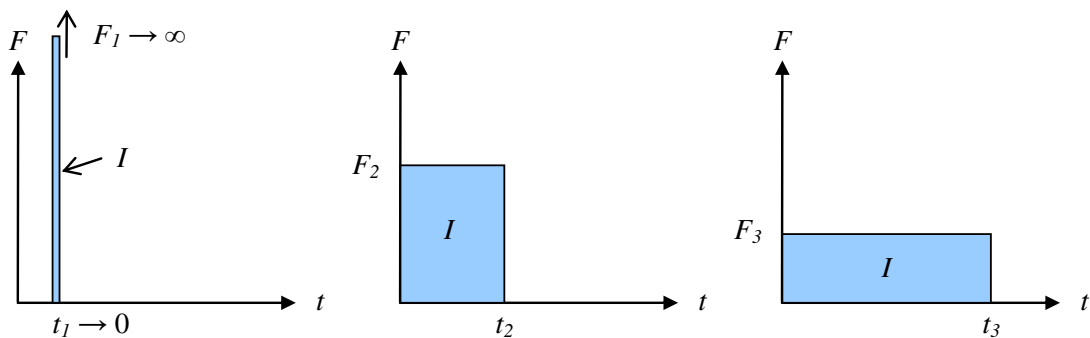and is equal to the area under the graph in a force-time diagram, see Figure 2.1.

Figure 2.1   The impulse I is of equal magnitude in all three cases even though the load F_i and time t_i differs.

2.2.3   Work and kinetic energy

If a force F acting on a body is causing a displacement u of the body it is said that the force has done the work W

$$W = F \cdot u \cdot \cos\varphi = F_x \cdot u \tag{2.6}$$

where φ is the angle between the force and the direction of the displacement. The work done is only dependent on the force F_x acting in the direction of the displacement, see Figure 2.2a. The work done by a variable load can be expressed as

$$W_x = \int_0^u F_x(x)dx \tag{2.7}$$

a)   b)
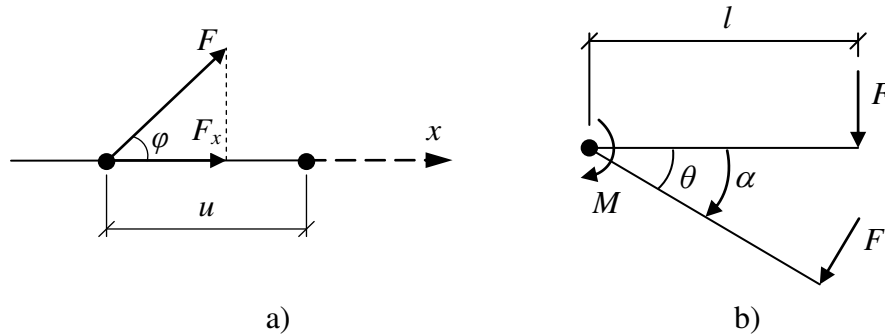
Figure 2.2   Work done by a) a force, and b) a moment.

A corresponding measurement is the work done by a moment *M*, defined in Figure 2.2b as

$$M = F \cdot l \tag{2.8}$$

for a given rotation θ

$$W = M \cdot \theta \tag{2.9}$$

This can be expressed more generally if the moment varies with the angle α, as

$$W = \int_0^\theta M(\alpha)d\alpha \tag{2.10}$$

The kinetic energy E_k for a body with mass *m* and the velocity *v* is defined as

$$E_k = \frac{m \cdot v^2}{2} \tag{2.11}$$

Work and kinetic energy are both a measure of energy and are often used to determine the total response in a collision analysis.

2.2.4   Dynamic equation of motion

By dividing the forces acting on a body into external forces *F(t)* and internal forces $R(u)_{sta}$ and $R(\dot{u})_{dyn}$, where the latter are referring to static respectively dynamic internal forces, a free body diagram can be obtained, see Figure 2.3. This free body can be expressed as a mass *m*, a spring with stiffness *k* and a damping *c*.
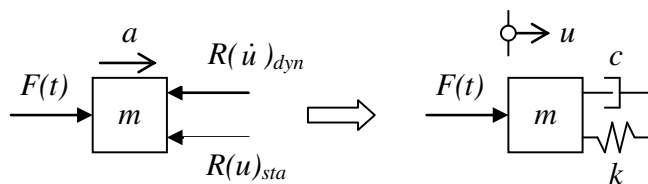

Figure 2.3   Schematic illustration of forces acting on an accelerating body.

Force equilibrium of the system in Figure 2.3 gives

$$F(t) - (R(u)_{sta} + R(\dot{u})_{dyn}) = ma \tag{2.12}$$

If the structural members are considered to behave linear elastically, the internal forces can be expressed as

$$R_{sta} = ku \tag{2.13}$$

$$R_{dyn} = c\dot{u} \tag{2.14}$$

where u is the displacement of the body, $\dot{u}$ is the velocity and the derivative of u with respect to time, k is the stiffness of the spring, and c is the damping factor. With equation (2.13) and (2.14) inserted in equation (2.12) the dynamic equation of motion can be expressed as

$$m\ddot{u} + c\dot{u} + ku = F(t) \tag{2.15}$$

where $\ddot{u} = a$ is the acceleration and the secondary derivative of u with respect to time.

2.3 Impact theory

2.3.1 Classic impact theory

To explain the behaviour of an impact, a simple model of two masses, where one of them collides with the other can be used. One such simple system is illustrated in Figure 2.4, where one body with mass m_1 and velocity v_0 collides with a second body with mass m_2 and no velocity. After the collision the first body has the velocity v_1 and the second body has the velocity v_2.
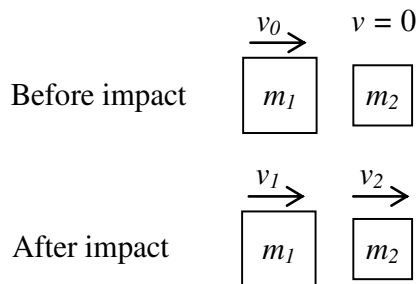

Figure 2.4   Example of an impact between one moving and one still body.

The momentum and kinetic energy before the collision is stated as the momentum and kinetic energy for the first mass

$$p_0 = m_1 \cdot v_0 \tag{2.16}$$

$$E_{k,0} = \frac{m_1 \cdot v_0{}^2}{2} \tag{2.17}$$

and after the collision they are

$$p = m_1 \cdot v_1 + m_2 \cdot v_2 \tag{2.18}$$

$$E_k = \frac{m_1 \cdot v_1^2}{2} + \frac{m_2 \cdot v_2^2}{2} \tag{2.19}$$

The impact procedure can be divided into two extreme cases named elastic collision and plastic collision. For an elastic collision both the momentum and the kinetic energy is preserved, which means that $E_{k,0} = E_k$ and $p_0 = p$, and the velocities after collision can be derived as

$$v_{1,el} = \frac{m_1 - m_2}{m_1 + m_2} \cdot v_0 \tag{2.20}$$

$$v_{2,el} = \frac{2m_1}{m_1 + m_2} \cdot v_0 \tag{2.21}$$

From this it can be noted that $v_{1,el} < 0$ if $m_1 < m_2$. The kinetic energy for the two bodies after collision is then

$$E_{k,1,el} = \frac{m_1 \cdot v_{1,el}^2}{2} = \frac{m_1}{2} \left(\frac{m_1 - m_2}{m_1 + m_2} \cdot v_0 \right)^2 = \left(\frac{m_1 - m_2}{m_1 + m_2} \right)^2 \cdot E_{k,0} \tag{2.22}$$

$$E_{k,2,el} = \frac{m_2 \cdot v_{2,el}^2}{2} = \frac{m_2}{2} \left(\frac{2m_1}{m_1 + m_2} \cdot v_0 \right)^2 = \frac{4m_1 \cdot m_2}{(m_1 + m_2)^2} \cdot E_{k,0} \tag{2.23}$$

From this, the total kinetic energy after collision $E_{k,el,tot}$ that is acting in the same direction as body 2 (positive direction) can be stated as

$$E_{k,el,tot} = \begin{cases} E_{k,1,el} + E_{k,2,el}, & m_1 \geq m_2 \\ E_{k,2,el}, & m_1 < m_2 \end{cases} \tag{2.24}$$

For a plastic collision only the momentum is preserved during the collision. The kinetic energy lost during the impact depends on the kinetic energy transformed to potential energy in body 1, when body 1 is doing a plastic work in the contact area towards body 2. The two bodies then have a common velocity which is stated as

$$v_{pl} = v_{1,pl} = v_{2,pl} = \frac{m_1}{m_1 + m_2} \cdot v_0 \tag{2.25}$$

Thus, the total kinetic energy after collision is

$$E_{k,pl,tot} = \frac{(m_1 + m_2) \cdot v_{pl}^2}{2} = \frac{m_1 + m_2}{2} \left(\frac{m_1}{m_1 + m_2} \cdot v_0 \right)^2 = \frac{m_1}{m_1 + m_2} \cdot E_{k,0} \tag{2.26}$$

To be able to describe elastic and plastic collisions, a coefficient of restitution e, is introduced. The coefficient of restitution is defined as

$$e = \frac{v_2 - v_1}{v_0} \tag{2.27}$$

If $e = 1$ it is an elastic collision and if $e = 0$ it is a plastic collision and if $0 < e < 1$ it is something in between. The velocities after collision when $0 \leq e \leq 1$ can be stated as

$$v_1 = \frac{m_1 - e \cdot m_2}{m_1 + m_2} \cdot v_0 \tag{2.28}$$

$$v_2 = \frac{(1+e) \cdot m_1}{m_1 + m_2} \cdot v_0 \tag{2.29}$$

and the corresponding kinetic energy for the two separate bodies are

$$E_{k,1} = \frac{m_1 \cdot v_1^2}{2} \tag{2.30}$$

$$E_{k,2} = \frac{m_2 \cdot v_2^2}{2} \tag{2.31}$$

The total kinetic energy can then for any e be stated as

$$E_{k,tot} = \begin{cases} E_{k,2}, & v_1 < 0 \\ E_{k,1} + E_{k,2}, & v_1 \geq 0 \end{cases} \tag{2.32}$$

An energy ratio $E_{k,tot} / E_{k,0}$ between the kinetic energy before and after the collision can be determined for different e and different mass ratios m_1 / m_2. This is illustrated in Figure 2.5, where it can be seen that the type of collision which depends on e and the mass ratio m_1 / m_2 plays a large role in how much of the kinetic energy in the positive direction is being preserved.

If $m_1 < m_2$ for an elastic collision, body 1 will move in the opposite direction compared to body 2, which means that $v_{1,el} < 0$. If the preserved kinetic energy in the positive direction for this elastic collision is divided with the preserved kinetic energy from the corresponding plastic collision, the following can be stated

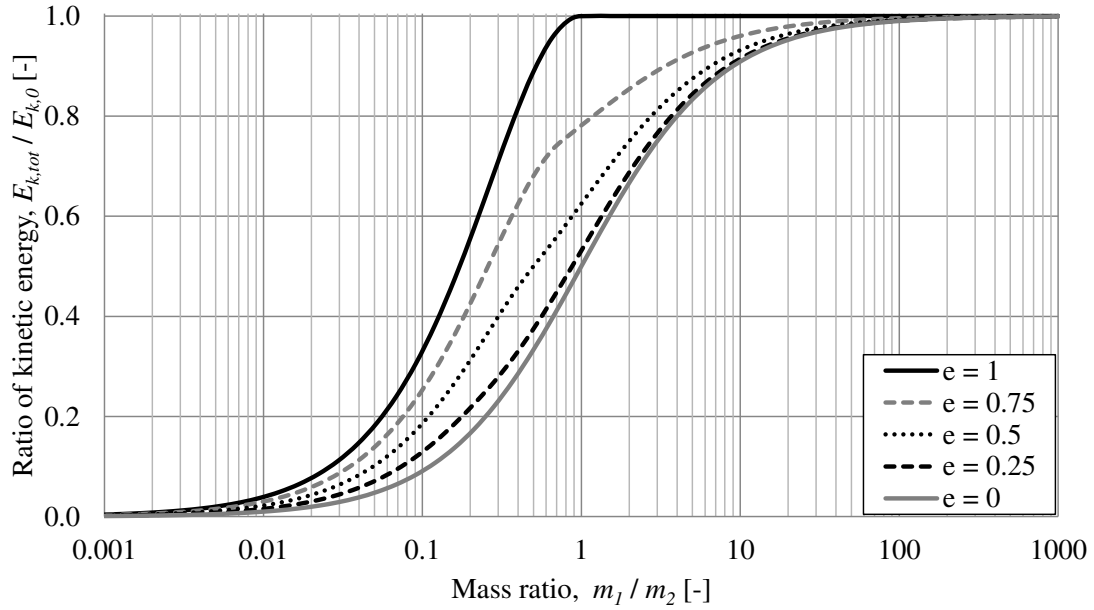$$\frac{E_{k,2,el}}{E_{k,pl,tot}} = \frac{4m_2}{m_1 + m_2} = \frac{4}{\dfrac{m_1}{m_2} + 1} \tag{2.33}$$

Figure 2.5   Energy ratio $E_{k,tot}$ / $E_{k,0}$ as a function of the mass ratio m_1 / m_2 for e = 1 (elastic), e = 0.25, e = 0.5, e = 0.75 and e = 0 (plastic).

So, when m_1 / $m_2 \rightarrow 0$, the elastic collision preserves a kinetic energy in the positive direction that is four times larger than the plastic collision. Also, when m_1 / $m_2 = 1$, the preserved kinetic energy in the elastic case is two times larger than for the plastic case. As illustrated in Figure 2.5, elastic and plastic collision preserve the same kinetic energy when m_1 / $m_2 \approx 100$ or larger.

From this it can be concluded that there may be a considerable difference between elastic and plastic collision. To assume elastic collision gives results on the safe side, though it can be excessive. On the contrary, the assumption of plastic collision can give results on the unsafe side.

2.3.2   Importance of mass

According to Section 2.2.2, the impulse *I* can be stated as

$$I = m \cdot v \tag{2.34}$$

and the kinetic energy for the same body is

$$E_k = \frac{m \cdot v^2}{2} \tag{2.35}$$

Using equation (2.34) and (2.35) the kinetic energy can be stated as a function of the impulse and the mass

$$E_k = \frac{I^2}{2m} \tag{2.36}$$

As can be seen, a higher mass gives a lower need for energy absorption. This can be compared with Newton's second law of motion

$$F = m \cdot a \tag{2.37}$$

where it can be seen that a higher mass generates a lower acceleration, and therefore also a lower response for the exposed body.

During a collision impact, a large load is acting during a very short time. In such a case, it may be more relevant to study the collision impulse, than the magnitude of the load. In Figure 2.6 a plastic collision is illustrated, where m_1 for example can be a simplification of a colliding vehicle, and m_2 the resisting structure.
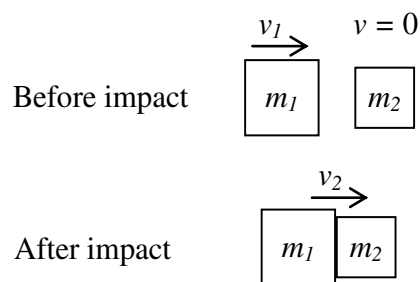
Figure 2.6   A schematic illustration of a plastic collision.

In Section 2.3.1, the preserved kinetic energy after a plastic collision is stated as

$$E_{k,pl,tot} = \frac{(m_1 + m_2) \cdot v_{pl}^{\,2}}{2} = \frac{m_1 + m_2}{2} \left(\frac{m_1}{m_1 + m_2} \cdot v_0 \right)^2 = \frac{m_1}{m_1 + m_2} \cdot E_{k,0} \tag{2.38}$$

which means that $E_{k,pl,tot} < E_{k,0}$. This can be explained by kinetic energy being transformed into potential energy within body 1. As can be seen in equation (2.38) a larger mass of body 2 m_2 generates a lower preserved kinetic energy and therefore a larger potential energy, which for collisions is seen as advantageous.

2.3.3   Energy absorption from deformation

Civil engineers are used to static models where a structure is supposed to withstand a load with limited deformations, Johansson and Laine (2012). In such static cases the stiffness and the load capacity are critical for design. However, when the structure is subjected to a large impulse load, the maximum static load capacity is often reached and it is therefore necessary to use the resilience of the structure in the design instead.

As can be seen in equation (2.6) the ability to absorb energy in a structure is a combination of force and deformation. This means that for a structural member subjected to an impulse load, it is often more important for the structure to be able to deform, than to have a high stiffness and load capacity, see Figure 2.7.
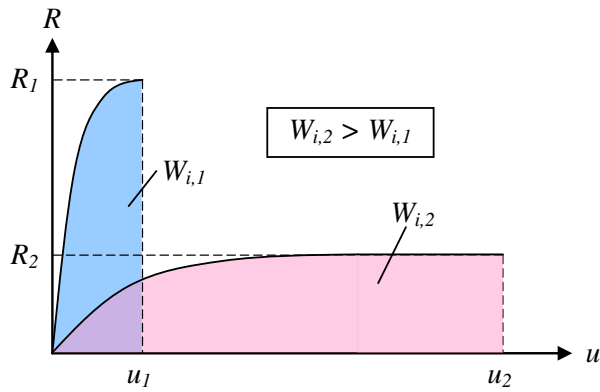
Figure 2.7   *Comparison in work absorption between a structure with low stiffness and high ability to deform, and a structure with high stiffness and low ability to deform.*

The structural response in this thesis is studied with three types of simplified responses: linearly elastic response (elastic response), ideal plastic response (plastic response) and a combination of elastic and plastic response (elasto-plastic response), see Figure 2.8. These simplifications are good approximations for many kinds of structures and are easily understood, Johansson and Laine (2012).
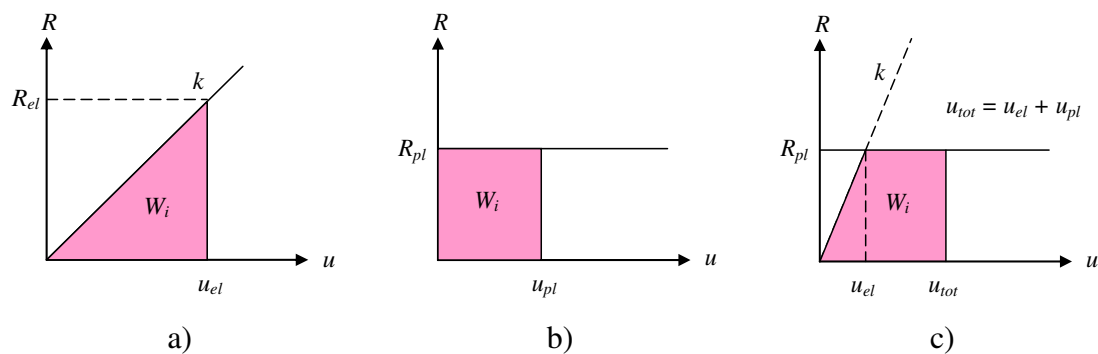
Figure 2.8   *Structural response with assumption of a) linear elastic response, b) ideal plastic response, and c) elasto-plastic response.*

2.4   Single degree of freedom systems

2.4.1   Orientation

When a simplified model for a dynamically loaded structure is requested, or as in this thesis a reinforced concrete member, a single degree of freedom (SDOF) system can often be used. In Figure 2.9 a SDOF model is illustrated where $F(t)$ is a load varying with time, $R(u)$ represents the static internal resistance and c is the damping coefficient. Damping reduces the amplitude of vibration over time. Usually when designing with regard to collision impact it is the maximum amplitude of vibration that is of interest. The influence of the damping effect is negligible for short collisions, and hence the damping will be neglected in this thesis.
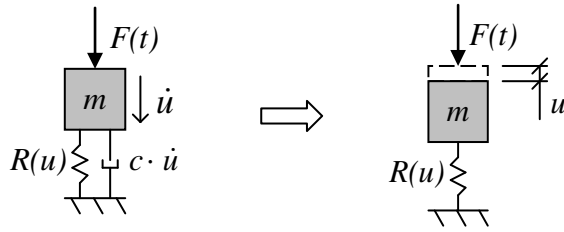
Figure 2.9   A SDOF system where the effect of damping c is neglected.

According to Johansson and Laine (2012) there are two extreme ways to describe dynamic loads, which are illustrated in Figure 2.10. The first is to use a characteristic impulse for an ideal impulse load, which means infinite high pressure acting at an infinitesimal short time. The second is to use a characteristic pressure load, with zero rise time, for an eternal shock wave.
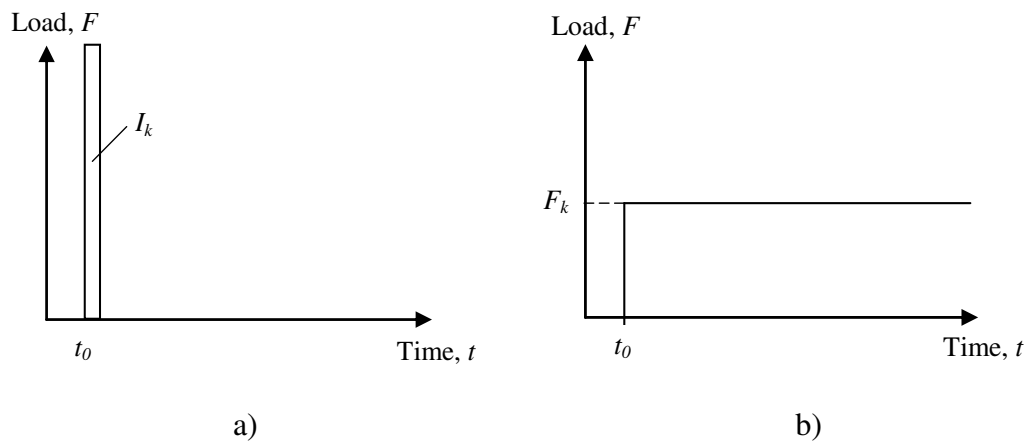

a)   b)

Figure 2.10   The two dynamic extreme cases where t_0 is the starting time a) characteristic impulse I_k, and b) characteristic pressure load F_k. In both cases, the load rise time is zero.

In this thesis only characteristic impulse load I_k is used because of the relatively short duration of the studied loads.

To stop the kinetic energy E_k, initiating the motion of a body, an equally large internal work W_i is needed. The kinetic energy E_k can be approximated as the external work W_e if there is no barrier. This means that

$$W_i = W_e \tag{2.39}$$

where

$$W_e = E_k \tag{2.40}$$

and as described in Section 2.3.2

$$W_e = E_k = \frac{I_k{}^2}{2m} \tag{2.41}$$

W_i is solved differently depending on whether elastic, plastic or elasto-plastic response is assumed.

2.4.2 Elastic response

For an elastic response, the stiffness k is constant, and the inner resistance $R(u)$ can be stated as

$$R(u) = ku \tag{2.42}$$

where u is the deformation. Using this, the internal work W_i can now be calculated as the marked area in Figure 2.11b.

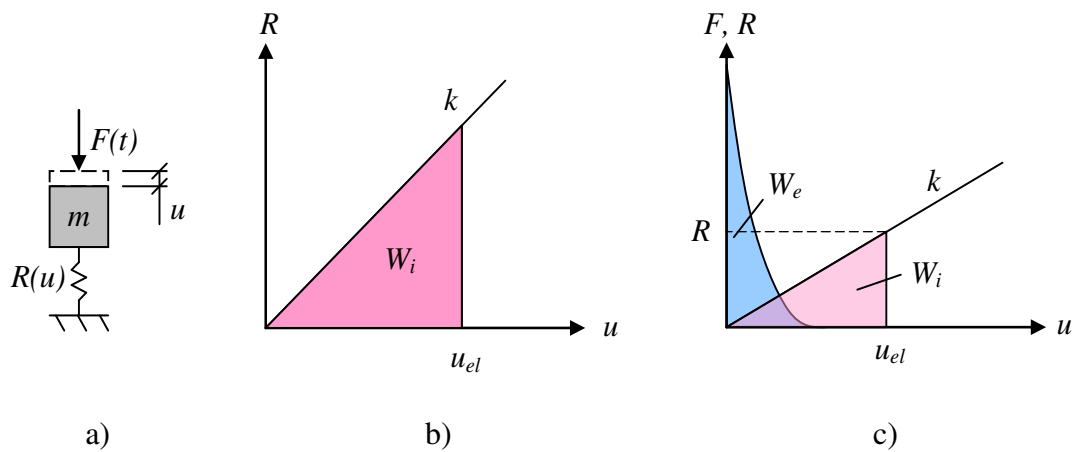$$W_i = \frac{R(u_{el}) \cdot u_{el}}{2} = \frac{ku_{el}^2}{2} \tag{2.43}$$

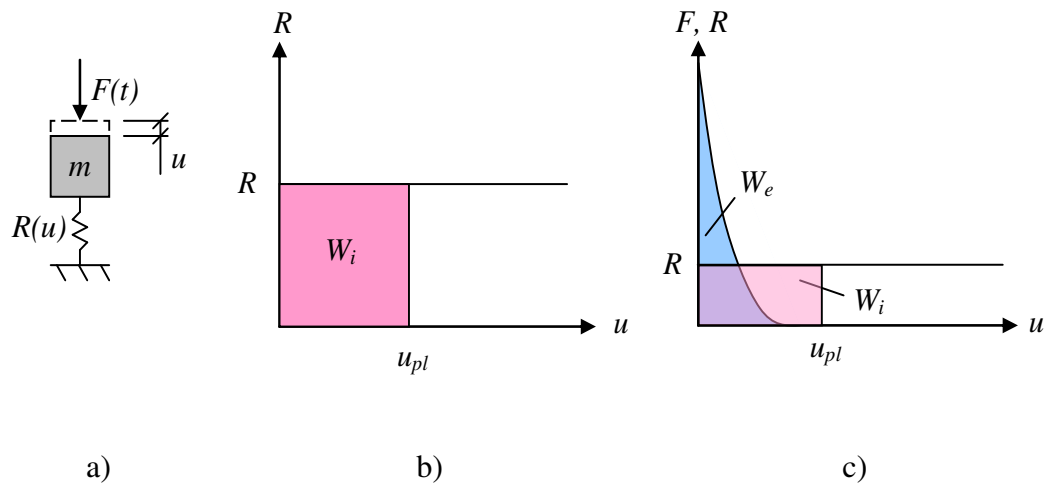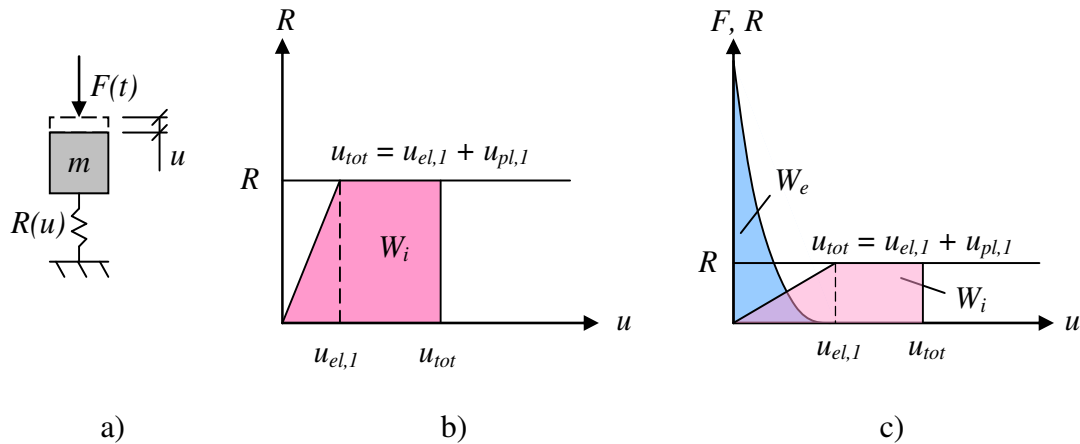a)   b)   c)

Figure 2.11   A SDOF system with elastic response a) dynamic SDOF system, b) force-deformation relation where the resistance force is linear, and c) energy balance between internal and external work.

A combination of $W_i = E_k$ and equation (2.43) gives the elastic deformation u_{el}

$$u_{el} = \frac{I_k}{m\omega} \tag{2.44}$$

where ω is the angular frequency defined as

$$\omega = \sqrt{\frac{k}{m}} \tag{2.45}$$

This gives the angular frequency in rad/s, but it can also be expressed in Hz as

$$f = \frac{\omega}{2\pi} = \frac{1}{2\pi}\sqrt{\frac{k}{m}} \tag{2.46}$$

2.4.3 Plastic response

For a plastic system $R(u)$ is constant, which is illustrated in Figure 2.12b. The internal work can thus be stated as

$$W_i = R(u_{pl}) \cdot u_{pl} = Ru_{pl} \tag{2.47}$$

Where u_{pl} is the plastic deformation that is needed for the system to absorb the external work W_e, see Figure 2.12c.

a)   b)   c)

Figure 2.12   A SDOF system with plastic response a) dynamic SDOF system, b) force-deformation relation where the resistance force is constant, and c) energy balance between inner and external work.

The plastic deformation can thus be derived by a combination of equation (2.41) and (2.47) as

$$u_{pl} = \frac{I_k^{\,2}}{2mR} \tag{2.48}$$

2.4.4 Elasto-plastic response

For an elasto-plastic system, a bilinear relation between resistance force and deformation is sought. This relation is stated as

$$R(u) = \begin{cases} ku, & u \leq u_{el,1} \\ R, & u > u_{el,1} \end{cases} \tag{2.49}$$

where $u_{el,1}$ is the limit for the elastic response. The internal work for the elasto-plastic response can be calculated as the area marked in Figure 2.13b, which is

$$W_i = \frac{R}{2}\left(u_{el,1} + 2u_{pl,1}\right) \tag{2.50}$$

where $u_{pl,1}$ is the required plastic response for an elasto-plastic system whereas u_{pl} is the pure plastic response for a plastic system.

Figure 2.13   A SDOF system with elasto-plastic response a) dynamic SDOF system, b) force-deformation relation where the resistance is bilinear, and c) energy balance between internal and external work.

The required plastic deformation can be stated by combining equation (2.41) with equation (2.50) as

$$u_{pl,1} = \frac{I_k^{\,2}}{2mR} - \frac{u_{el,1}}{2} \tag{2.51}$$

Because of the pure plastic deformation as in equation (2.48), and the total deformation as in Figure 2.13b, the total deformation can be stated as

$$u_{tot} = u_{pl} + \frac{u_{el,1}}{2} \tag{2.52}$$

2.5 Equivalent static load

2.5.1 Orientation

In many cases it is more convenient to work with static loads instead of dynamic loads. Hence there is an interest in translating the dynamic loads into an equivalent static load. This simplified equivalent static load is considering a static load which does the same amount of external work as the dynamic load Johansson and Laine (2012).

2.5.2 Elastic response

The equivalent static load Q is obtained, for an elastic system, by combining the relationship

$$W_e = \frac{Qu_{el}}{2} \tag{2.53}$$

with equation (2.43)

$$W_e = \frac{ku_{el}^2}{2} \tag{2.54}$$

Q can be written as

$$Q = ku_{el} \tag{2.55}$$

Combining equation (2.44), (2.45) and (2.55) gives

$$Q = I_k \sqrt{\frac{k}{m}} = I_k \omega \tag{2.56}$$

This is the static equivalent load Q which corresponds to the load that generates the same displacement as the impulse I_k.

2.5.3 Plastic response

For a case with plastic response the static equivalent load Q can be determined by setting the external work in equation (2.41) equal to

$$W_e = Qu_{pl} \tag{2.57}$$

This gives

$$Q = \frac{I_k^2}{2m \cdot u_{pl}} \tag{2.58}$$

which combined with equation (2.48) gives

$$Q = R \tag{2.59}$$

where R is the resisting force obtained from the maximum allowed displacement u_{pl}.

2.5.4 Elasto-plastic response

An elasto-plastic response is a combination of elastic and plastic response. This means that the equivalent static load is, as for the case with plastic response, determined by

$$Q = R \tag{2.60}$$

but here is R determined by the elastic stiffness k, via the resulting elastic deformation $u_{1,el}$ from equation (2.49) and the allowed plastic deformation $u_{1,pl}$ from equation (2.52).

2.6   Two degrees of freedom mass-spring systems

In this section, results from different collision scenarios using two degrees of freedom (2DOF) mass-spring systems are presented and evaluated. Additional results are also presented in Appendix B. The calculations are made using the Central Difference Method described in Section 2.7 in the commercial software MATLAB. For the code, see Appendix H.1. For more collision scenarios and additional studies and evaluation, see Asplund and Steckmest (2014).

A 2DOF system is a system where two separate displacements can occur. In this thesis is a 2DOF system referring to a mass-spring system consisting of two bodies with corresponding displacements which can be used as a simplified method to describe collisions, see Figure 2.14. The viscous damping forces are neglected as discussed in Section 2.4.1.
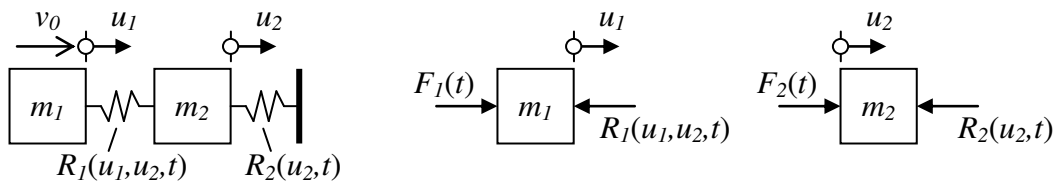
Figure 2.14   Illustration of a 2DOF mass-spring system which is used to analyse collisions in this thesis.

This system of two bodies and springs are able to express the behaviour of the bodies during the entire collision, compared to the classic impact theory described in Section 2.3.1, which only express the behaviour before and after the collision.

It is possible to derive the dynamic equation of motion, described in Section 2.2.4 for a SDOF system, of the mass-spring system in Figure 2.14 by applying Newton's second law of motion. A free body diagram of the mass-spring system is presented in Figure 2.15.
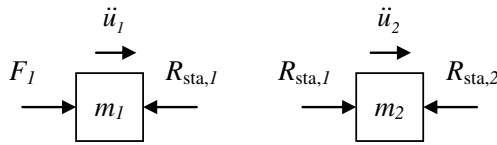
Figure 2.15   Free body diagram of a 2DOF mass-spring system.

Force equilibrium of the free body diagram gives

$$\rightarrow: F_1 - R_{sta,1} = m_1 \ddot{u}_1 \tag{2.61}$$

$$\rightarrow: R_{sta1} - R_{sta,2} = m_2 \ddot{u}_2 \tag{2.62}$$

If the structural members are considered having a linear elastic response the internal forces R_{sta} can be expressed as

$$R_{sta,1} = k_1 \left(u_1 - u_2 \right) \tag{2.63}$$

$$R_{sta,2} = k_2 u_2 \tag{2.64}$$

where u is the displacement of the body, $\ddot{u}$ is the acceleration, and the secondary derivative of u with respect to time, and k is the stiffness of the spring. By inserting equation (2.63) and (2.64) into equation (2.61) and (2.62) the dynamic equation of motion for the two bodies can be expressed as

$$m_1 \ddot{u}_1 - k_1 (u_1 - u_2) = F_1 \tag{2.65}$$

$$m_2 \ddot{u}_2 - k_1 u_1 + u_2 (k_1 + k_2) = 0 \tag{2.66}$$

which can be written on matrix form as

$$\begin{bmatrix} m_1 & 0 \\ 0 & m_2 \end{bmatrix} \begin{bmatrix} \ddot{u}_1 \\ \ddot{u}_2 \end{bmatrix} + \begin{bmatrix} k_1 & -k_1 \\ -k_1 & k_1 + k_2 \end{bmatrix} \begin{bmatrix} u_1 \\ u_2 \end{bmatrix} = \begin{bmatrix} F_1 \\ 0 \end{bmatrix} \tag{2.67}$$

and with symbolic matrix notations as

$$\mathbf{M\ddot{u}} + \mathbf{Ku} = \mathbf{f} \tag{2.68}$$

where $\mathbf{M}$ is the mass matrix, $\mathbf{K}$ is the stiffness matrix, $\mathbf{u}$ is the displacement vector, $\mathbf{\ddot{u}}$ is the acceleration vector and $\mathbf{f}$ is the load vector.

In this thesis, the mass in Figure 2.16a is referred to as body 1 and the mass in Figure 2.16b is referred to as body 2.
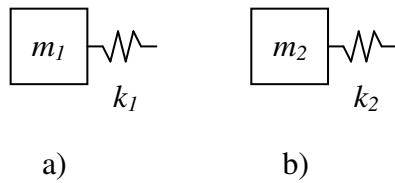
Figure 2.16   Illustration of a) body 1 with mass m_1 and stiffness k_1, and b) body 2 with mass m_2 and stiffness k_2.

The change of internal work dW_i of the bodies are defined as the internal resistance force R of the body times the change in displacement du, i.e.

$$dW_{i,1} = R_1 \cdot du_1 \tag{2.69}$$

$$dW_{i,2} = R_2 \cdot du_2 \tag{2.70}$$

In the same way, the change of external work dW_e of the bodies are defined as the external load F times the change in displacement du. In this thesis body 1 has an initial velocity v_0 and $F_1 = 0$ which means that the external energy is equal to the kinetic energy of body 1 $W_{e,1} = E_{k,1}$ before collision. The external force acting on body 2 is equal to the internal resistance force of body 1 $F_2 = R_1$ which gives

$$dW_{e,1} = 0 \tag{2.71}$$

$$dW_{e,2} = R_l \cdot du_2 \tag{2.72}$$

2.7 Central Difference Method

There are several methods that are used to numerically solve the dynamic equation of motion. The Central Difference Method (CDM) is one of the most fundamental of these and it is widely used because it is an exceedingly simple method to describe, and it is a second-order accurate algorithm. Experience in actual engineering problems suggests that second-order accurate techniques are required in many applications, see Craig and Kurdila (2006). If the dynamic equation of motion, equation (2.15), is written with symbolic matrix notations it becomes

$$\mathbf{M\ddot{u}} + \mathbf{C\dot{u}} + \mathbf{Ku} = \mathbf{f}(t) \tag{2.73}$$

If $\mathbf{u}(t_n) = \mathbf{u}_n$ is stated, where t_n is the time at iteration n, the velocity $\dot{\mathbf{u}}_n$ at the time t_n can be written as

$$\dot{\mathbf{u}}_n = \frac{\mathbf{u}_{n+1} - \mathbf{u}_{n-1}}{2h} \tag{2.74}$$

where h is the chosen time step. As can be seen, the derivative at time t_n in equation (2.74) is an approximation based on the slope of the line between $\mathbf{u}(t_{n-1})$ and $\mathbf{u}(t_{n+1})$, see Figure 2.17. To maintain this order of approximation the velocity can be written for step n + 1/2 as

$$\dot{\mathbf{u}}_{n+1/2} = \frac{\mathbf{u}_{n+1} - \mathbf{u}_n}{h} \tag{2.75}$$

and for step n - 1/2 as

$$\dot{\mathbf{u}}_{n-1/2} = \frac{\mathbf{u}_n - \mathbf{u}_{n-1}}{h} \tag{2.76}$$

The value of the acceleration $\ddot{\mathbf{u}}_n$, can then be stated as

$$\ddot{\mathbf{u}}_n = \frac{\dot{\mathbf{u}}_{n+1/2} - \dot{\mathbf{u}}_{n-1/2}}{h} = \frac{\mathbf{u}_{n+1} - 2\mathbf{u}_n + \mathbf{u}_{n-1}}{h^2} \tag{2.77}$$

which is illustrated in Figure 2.17.
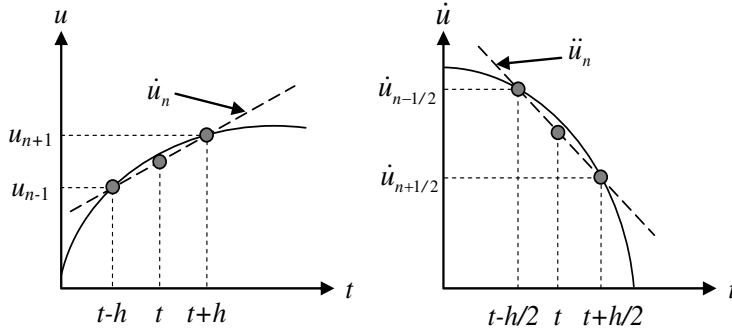
Figure 2.17   Illustration the approximate calculation of the velocity $\dot{u}_n$ and the acceleration $\ddot{u}_n$.

If equation (2.74) and (2.77) is inserted in equation (2.73) it can be formulated as

$$\left(\frac{\mathbf{M}}{h^2} + \frac{\mathbf{C}}{2h}\right)\mathbf{u}_{n+1} + \left(\mathbf{K} - \frac{2\mathbf{M}}{h^2}\right)\mathbf{u}_n + \left(\frac{\mathbf{M}}{h^2} - \frac{\mathbf{C}}{2h}\right)\mathbf{u}_{n-1} = \mathbf{f}(t) \tag{2.78}$$

which can be rewritten as

$$\mathbf{u}_{n+1} = \left(\frac{\mathbf{M}}{h^2} + \frac{\mathbf{C}}{2h}\right)^{-1}\left(\mathbf{f}(t) - \left(\mathbf{K} - \frac{2\mathbf{M}}{h^2}\right)\mathbf{u}_n - \left(\frac{\mathbf{M}}{h^2} - \frac{\mathbf{C}}{2h}\right)\mathbf{u}_{n-1}\right) \tag{2.79}$$

The damping is in this thesis neglected due to its small effect on the system during the studied time, as discussed in Section 2.4.1. Without the damping, equation (2.79) can be written as

$$\mathbf{u}_{n+1} = \left(\frac{\mathbf{M}}{h^2}\right)^{-1}\left(\mathbf{f}(t) - \left(\mathbf{K} - \frac{2\mathbf{M}}{h^2}\right)\mathbf{u}_n - \left(\frac{\mathbf{M}}{h^2}\right)\mathbf{u}_{n-1}\right) \tag{2.80}$$

When observing equation (2.80) it can be seen that the displacements $\mathbf{u}_{n-1}$ when $n = 0$ is needed. It can be stated as

$$\mathbf{u}_{-1} = \mathbf{u}_0 - h\dot{\mathbf{u}}_0 + \frac{h^2}{2}\ddot{\mathbf{u}}_0 \tag{2.81}$$

The CDM algorithm is conditionally stable, which in this case means that the method is stable provided that the time step h is selected to be smaller than a critical step size h_{cr}. According to Johansson and Laine (2012), the critical step size can be stated as

$$h_{cr} = \frac{2}{\omega} = 2\sqrt{\frac{m}{k}} \tag{2.82}$$

When solving a SDOF or 2DOF system, an even lower step size is most often needed, and a step size that is one hundredth of the load duration $t_1 - t_0$ is often valid, where t_0 is the time at the start of the loading. That is, the step size should fulfil

$$h \leq \begin{cases} h_{cr} \\ \dfrac{t_1 - t_0}{100} \end{cases} \qquad (2.83)$$

When deriving equation (2.80), constant stiffness matrix **K** is used. However, it is possible to use the CDM with these matrices varying over time. For the stiffness, this is done by letting the time varying $k(t)$ be a function of the current displacements $u(t)$, see Figure 2.18. This is a secant stiffness and it can be stated as ${}^t k = {}^t k({}^t u)$. In practice, the actual concern is not the stiffness, but the internal force ${}^t R$ which is defined as

$${}^t R = {}^t k \cdot {}^t u \qquad (2.84)$$
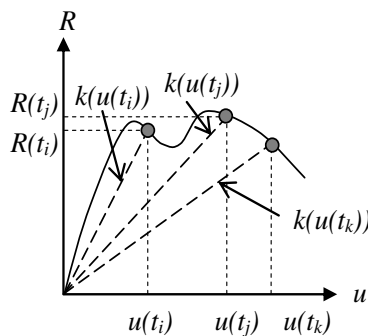
Figure 2.18   Secant stiffness k at time t for a system with an arbitrary response.

The stiffness at unloading can be modelled in the same way. For a plastic response, it is possible to model the loading and unloading with a desired linearly elastic stiffness, and then at a certain yield-stress, use the secant stiffness instead, see Figure 2.19.
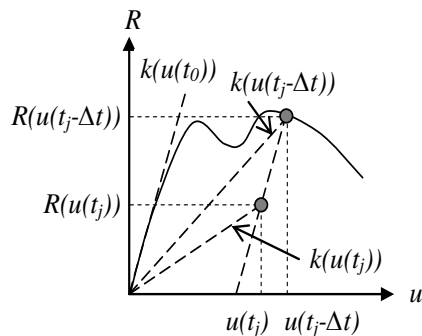
Figure 2.19   Stiffness at unloading for a system with plastic properties.

The CDM is an explicit numerical integration method, but in this thesis when using the commercial FE software ADINA (2014), implicit numerical integration is used. This decision is based on a study in Carlsson and Kristensson (2012) where the explicit and implicit integration methods in ADINA are compared to hand calculations. For a summarised step by step algorithm of how to use the Central Difference Method, see Appendix A.

2.8   Structural response of reinforced concrete

2.8.1   Orientation

A reinforced concrete member can be considered as a composite of concrete and reinforcement where concrete has a high compressive strength and the reinforcement has a high tensile strength, Al-Emrani (2011). For an impact loaded structure, the ductility is of great importance and the ductility of a composite is dependent on the properties of the involved materials. Concrete is a brittle material whereas reinforcement steel is ductile, see Figure 2.20 and Figure 2.21 respectively. Therefore the ability of reinforced concrete to show a ductile behaviour highly depends on the properties of the reinforcement steel.
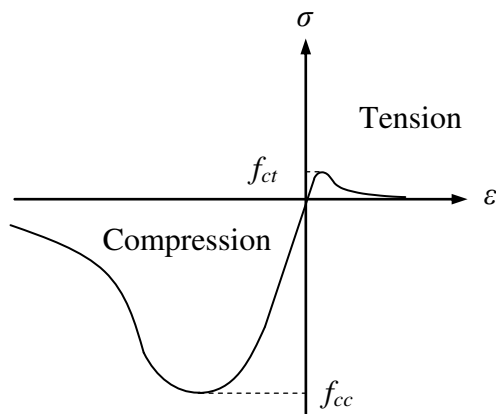
Figure 2.20   Stress-strain behaviour of concrete showing tensile strength f_{ct} and compressive strength f_{cc}.
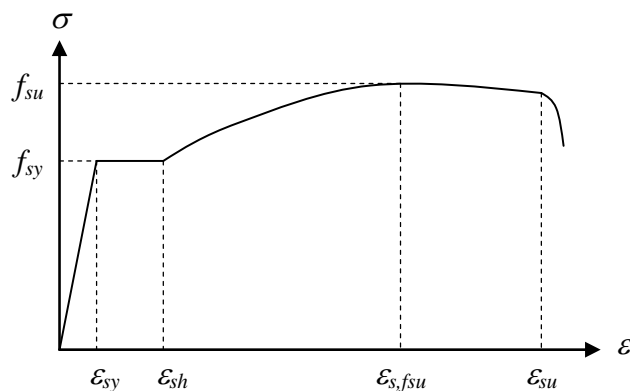
Figure 2.21   Stress-strain behaviour of reinforcement steel showing yield stress f_{sy}, ultimate strength f_{su}, yield strain ε_{sy}, strain at hardening ε_{sh}, and strain at ultimate strength $\varepsilon_{s,fsu}$.

2.8.2   Structural response of reinforced concrete beams

During increased loading of a reinforced concrete beam, different states are studied. State I is the uncracked state where no cracking has occurred and the beam has a linear elastic behaviour with primarily concrete properties. During state II the beam starts to crack and the reinforcement has an increasing importance for the behaviour. State III is the phase when the reinforcement starts to yield and the end of state III is the ultimate state for which the beam is designed. After state III the reinforcement of

the beam can be subjected to some strain hardening before the maximum capacity is reached. These states can be described using a simplified, bilinear, elasto-plastic model where the elastic part is based on a fully cracked beam and the elastic part on the ultimate state, see Figure 2.22.
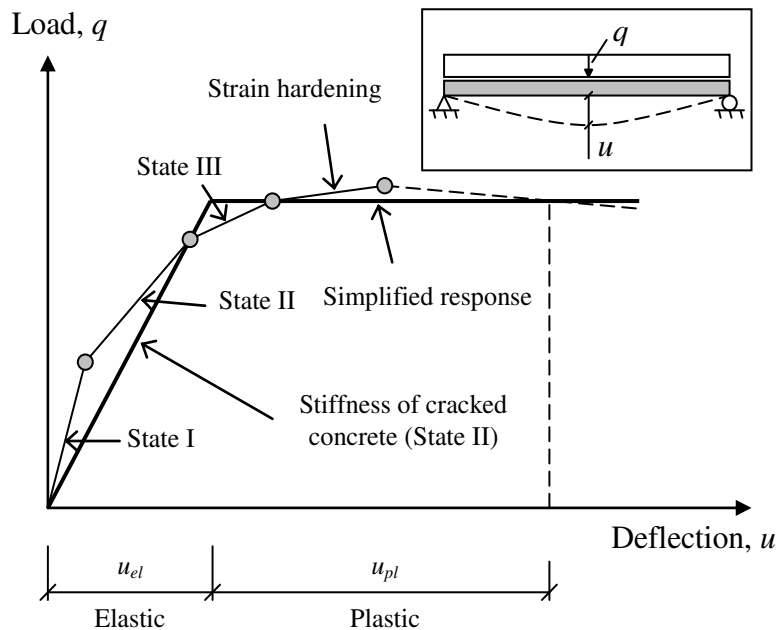
Figure 2.22   *Stress-strain behaviour of a simply supported reinforced concrete beam subjected to uniformly distributed load, illustrating the different response stages and a simplified response.*

2.8.3   Structural response of reinforced concrete slabs

A slab is a structural member with a thickness relatively small in relation to its length and width. In Eurocode 2, CEN (2004), it is stated that a slab has a ratio between width and thickness not smaller than five. There are three main types of slabs found in the literature: one-way slabs, two-way slabs and cantilever slabs. The first two slab types carries the load in one and two directions, respectively, and are supported on two or more edges. It is also possible with intermediate supports such as columns. The edges of slabs may be simply supported, partly fixed, fixed or free. Cantilever slabs also carry the load in one direction since they are only supported on one edge, Engström (2014). A slab is significantly more complex than a beam, which gives a large number of combinations regarding geometry, boundary conditions and placement of loads.

There are different methods of how to design according to moment distribution and deformations in the ultimate limit state. The strip method, which is a lower bound method, and the yield line method, which is an upper bound method, are two commonly used approaches, Engström (2014). Both methods are based on the plastic capacity of the slab.

The plastic capacity of a slab will first be reached in the most stressed point where a plastic hinge is formed. For a simply supported rectangular slab subjected to a uniformly distributed load the most stressed point is located in the centre and this is where the hinge will form. The hinge will spread along a yield line and branch off to

the corners and form a mechanism after which the slab cannot carry any increased loading, see Figure 2.23, Hultin (1994). For each slab a yield figure must be assumed and the capacities can be determined by equilibrium equations, which are different between the two methods.

Figure 2.23   Illustration of how a plastic hinge is formed in the centre of a simply supported rectangular slab subjected to uniformly distributed load and how the yield line develops towards the corners.

In this thesis the yield figure assumed for a slab subjected to a point load is based on the same principles as for a slab subjected to a uniformly distributed load, as illustrated in Figure 2.23, Johansson (2014).
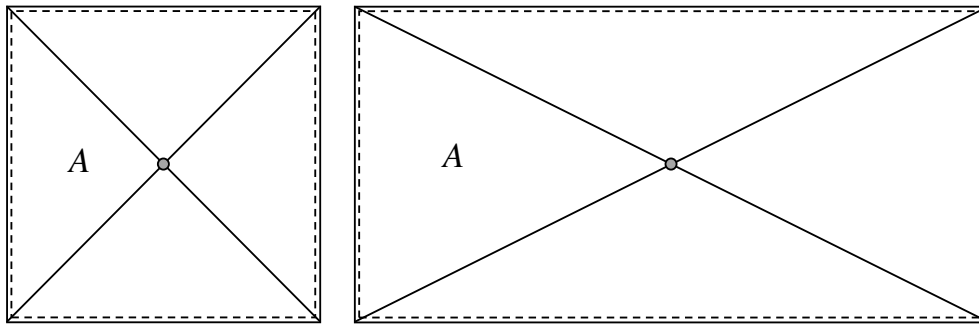
Figure 2.24   Illustration of how the yield lines are assumed to from at simply supported slabs subjected to a point load in the centre.

The hand calculated capacities of the slabs in this thesis are calculated with the principles of the strip method. But instead of calculating the required amount of reinforcement for a given load, the ultimate load capacity is calculated for a given reinforcement. The moment capacity M_x of the simply supported slab in Figure 2.24 is defined with the strip method in the same manner as for a slab subjected to a uniformly distributed load, as illustrated in Figure 2.25. The strip method is described in Engström (2014).
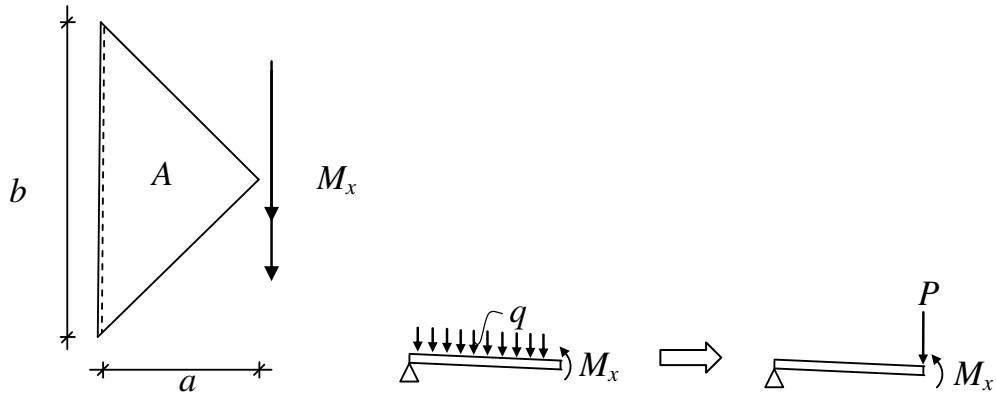
Figure 2.25   Illustration of how the moment capacity M_x for a slab subjected to a point load is defined in the same manner as for a slab subjected to a uniformly distributed load.

For all strip method calculations with point loads in this thesis, the yield lines are assumed to stretch from the point of loading to the corners, see Figure 2.26.
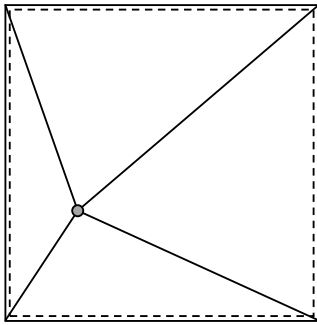
Figure 2.26   Illustration of how the yield lines are formed at a simply supported quadratic slab subjected to an arbitrary point load.

2.8.4   Rotational capacity

When the load capacity of a structure is evaluated with a plastic or elasto-plastic response it is often the allowed deformation u that is the governing factor. Hence it is needed to calculate the deformation u to find the structural capacity. It is also needed to calculate the deformation u to determine the equivalent load Q, as described in Section 2.5. It is possible to calculate the deformation with the rotational capacity θ of the structure, which is a measure of the structure's ability for plastic redistribution, see Figure 2.27. This rotational capacity is calculated in the point where a plastic hinge is formed. A plastic hinge is where a critical section experience substantial deformations when subjected to a bending moment, provided that the ductility of the reinforcing steel is sufficient, for a slab this critical section is along a yield line. It does not mean that the load bearing capacity in the structural member is reached. In fact, if the structural member is statically indeterminate it can carry more load until another plastic hinge is formed. A collapse mechanism in beams consists only of a critical number of plastic hinges, whereas for slabs a yield line is needed. When the number of critical plastic hinges is reached or a yield line is formed a collapse mechanism is formed, Johansson and Laine (2012).
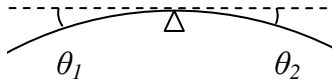
Figure 2.27   Plastic rotation θ_i of a continuous beam, where θ_i should not exceed the rotational capacity θ_{pl}.

A method to calculate the rotational capacity for dynamic load cases is stated in Eurocode 2 CEN (2004). The rotational capacity is here dependent on concrete and reinforcement class, see Figure 2.28.
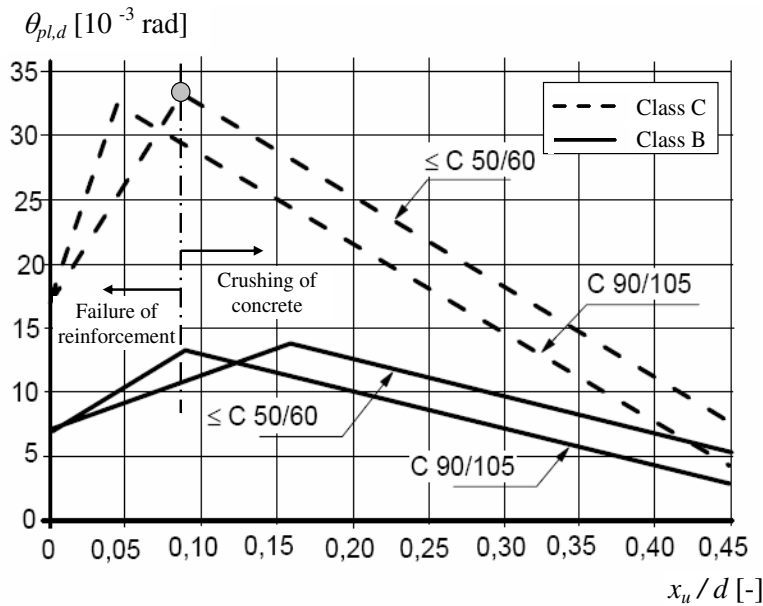

Figure 2.28   Design value for the plastic rotation capacity $\theta_{pl,d}$ for different concrete and reinforcement steel classes according to Eurocode 2 CEN (2004). The limit between reinforcement and concrete failure is visualized for concrete class C50/60 and reinforcement class C.

There is however a restriction regarding the reinforcement for the relationship presented in Figure 2.28 and for concrete classes $\leq$ C50/60 it is $x_u/d \leq 0.45$ and $x_u/d \leq 0.35$ for classes > C50/60.

The relationship presented in Figure 2.28 is only valid for shear slenderness $\lambda = 3.0$. For other values of the shear slenderness the plastic rotational capacity presented in Figure 2.28 should be multiplied by a correction factor k_λ

$$\theta_{pl,d} = k_\lambda \cdot \theta_{pl} \tag{2.85}$$

where

$$k_\lambda = \sqrt{\frac{\lambda}{3}} \tag{2.86}$$

and the shear slenderness is defined as

$$\lambda = \frac{l_0}{d} \tag{2.87}$$

where l_0 is the distance between the considered maximum moment section and the adjacent zero moment section after plastic redistribution, and d is the effective depth of the cross-section. As a simplification the shear slenderness λ may be estimated as

$$\lambda = \frac{M_{Ed}}{V_{Ed} \cdot d} \tag{2.88}$$

where M_{Ed} is the design value of the bending moment and V_{Ed} is the design value of the shear force, Engström (2011).

It is possible to calculate the maximum deformation $u_{pl,d}$ which the structural member can withstand with the plastic rotation presented in equation (2.85). According to Eurocode 2, for a simply supported beam that is subjected to either a uniformly distributed load or a point load in the mid-span, the maximum deformation can be calculated as

$$u_{pl,d} = \frac{\theta_{pl,d} \cdot l}{2} \tag{2.89}$$

where l is the length of the span.

There are other design codes that give recommendations for how to calculate rotational capacity. In Johansson and Laine (2012) a comparison between the recommendations given in Betonghandboken Cederwall (1990), Bk25:2 Fortifikationsförvaltningen (1973) and Eurocode 2 is made.

3 Study of 2DOF Collision Models

3.1 Orientation

This chapter covers a parametric study of collisions for a 2DOF model. This 2DOF model is used throughout this thesis and is made with the Central Difference Method in the commercial software MATLAB, see Appendix H.1.

In Section 3.2 are collisions without a barrier analysed, and in Section 3.3 are collisions with a barrier analysed. The barrier is in the form of an additional spring which is attached to body 2 at one side, and attached to a fixed support at the other side.

3.2 Without barrier

3.2.1 Orientation

In this section, elastic and plastic response will be studied for a 2DOF system where only body 1 has a spring; i.e. body 2 is free without any barrier preventing the movement. This system is then easily compared to a collision according to classic theory, see Figure 3.1. In Section 2.3.1, two bodies are studied before and after collision with classic impact theory.
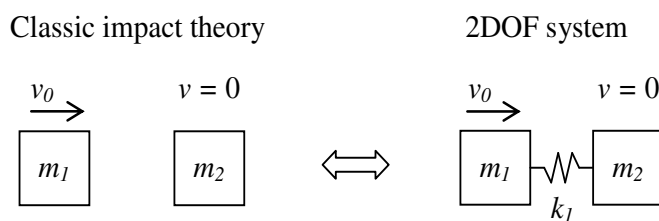
Figure 3.1   Schematic illustration of how the classic impulse theory can be modelled using a 2DOF mass-spring system.

An important difference between the two models is that the 2DOF system can describe the whole course of the collision, prior to, during and after the impact while the classic impact theory only is capable of describing the velocities before and after the collision. The response of a collision between two bodies, according to the classic impact theory is presented in Figure 3.2 for elastic cases, $e = 1$, and plastic cases, $e = 0$.

Two points on both the elastic and the plastic response curve are chosen to be further evaluated in this section. These points correspond to a mass ratio m_1 / m_2 of 0.2 and 2, see Figure 3.2. $E_{k,tot}$ and $E_{k,0}$ are defined as described in Section 2.3.1. The analyses are made with the 2DOF algorithm in Appendix H.1.
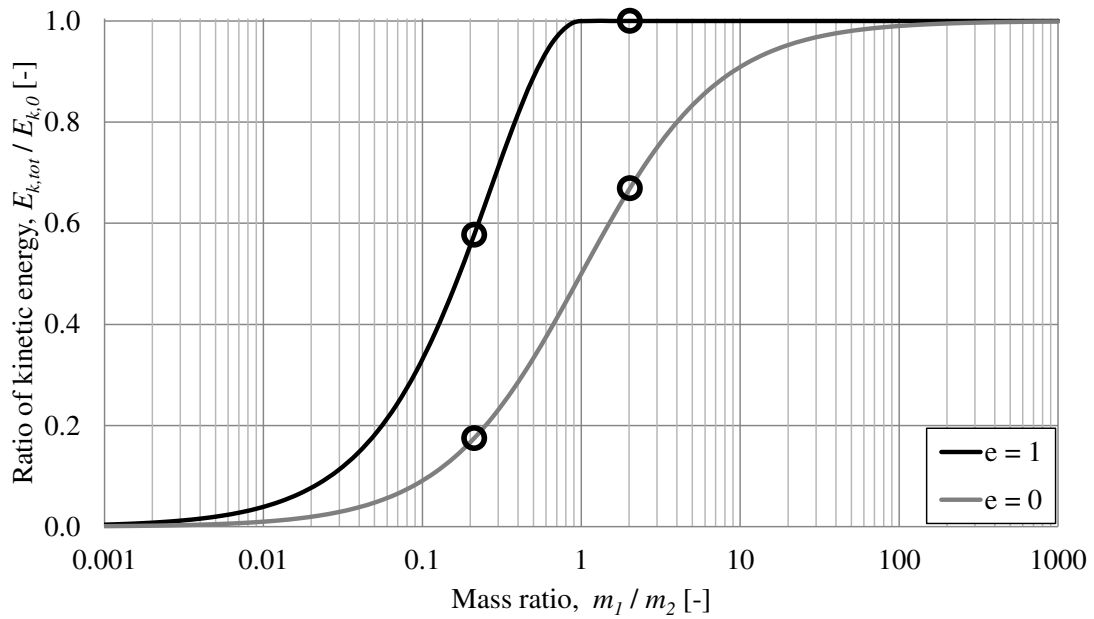
*Figure 3.2   Points of interest for the elastic and plastic cases in the classic impact
theory for further studies. Marked mass ratios m_1/m_2 are 0.2 and 2.*

3.2.2   Elastic collision

The parameters for the evaluation of the elastic response of a 2DOF system without
barrier are chosen so that the mass ratios m_1/m_2 are equal to the chosen points of
interest in Figure 3.2. The mass ratios are met by having a constant mass of body 2 m_2
and vary the mass of body 1 m_1. Here, $m_2 = 7\,500$ kg is symbolising a reinforced
concrete member, while $m_1 = 1\,500$ kg and $m_1 = 15\,000$ kg are symbolising a car and
a lorry, respectively. In addition to the difference in mass, a change in stiffness of
spring k_1 is also considered. The initial velocity v_0 is set to 27.8 m/s, which
corresponds to a velocity of 100 km/h. The input parameters of collision A1-A4 can
be seen in Table 3.1.

*Table 3.1   Input parameters for collision A1-A4 with elastic response for the
2DOF system.*

Case	v_0 [m/s]	k_1 [kN/m]	m_1 [kg]	m_2 [kg]
Collision A1	27.8	100	1 500	7 500
Collision A2	27.8	100	15 000	7 500
Collision A3	27.8	1 000	1 500	7 500
Collision A4	27.8	1 000	15 000	7 500

The two bodies involved in the collision should only interact when there is a
compressive force in the spring, which means that the tensile response of the spring
must be excluded. This is done by setting a linear elastic response of the spring when

the deformation $\Delta u = u_1 - u_2$ is positive and a stiffness of zero when the deformation is negative, see Figure 3.3.
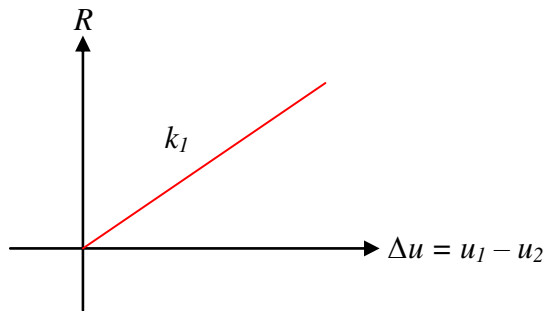
Figure 3.3   Illustration of how the spring stiffness k_1 varies with the deformation Δu for an elastic case.

In Table 3.2 the 2DOF analysis of collision A1-A4 are compared to calculations according to classic impact theory described in Section 2.3.1. After testing different time steps h for the 2DOF model it is concluded that smaller time steps give results closer to the classic impact theory. In this section, a time step of $h = 1$ ms is used for the 2DOF model which gives identical results between the two theories. As can be observed in Table 3.2 collision A1 and A3 give the same results. This is due to the fact that the stiffness k does not affect the final velocities v after the collision, but only the behaviour during the collision. This is also the case for collision A2 and A4. For collision A1 and A3, $I_1 < 0$, which means that body 1 moves in the negative direction after the collision and that body 2 has a larger impulse than the initial impulse, $I_2 > I_0$. For all four collisions is the total impulse preserved.

Table 3.2   Comparison of results between the 2DOF system and the classic impact theory with elastic response, collision A1-A4.

	Collision A1 and A3		Collision A2 and A4	
	2DOF	Classic theory	2DOF	Classic theory
v_0 [m/s]	27.80	27.80	27.80	27.80
v_1 [m/s]	-18.53	-18.53	9.27	9.27
v_2 [m/s]	9.3	9.3	37.1	37.1
$E_{k,0}$ [kJ]	580	580	5 796	5 796
$E_{k,tot}$ [kJ]	322	322	5 796	5 796
I_0 [kNs]	41.70	41.70	417	417
I_1 [kNs]	-27.80	-27.80	139.05	139.05
I_2 [kNs]	69.75	69.75	278.25	278.25

The displacement u, velocity v, internal resistance R and impulse I as a function of time for collision A1 are illustrated in Figure 3.4. In collision A1, the mass of body 1

is less than the mass of body 2, i.e. $m_1 < m_2$. As discussed in Section 2.3.1 body 1 will move in the opposite direction after the collision, as can be seen by the negative displacement in Figure 3.4a. This is also shown in Figure 3.4b where body 1 receives a negative velocity after the collision while body 2 moves in the positive direction. The duration of collision A1 is about 0.35 s as seen in Figure 3.4c where the internal force in the spring is illustrated. Here it is clear that the spring is only active when there is a compressive force and that the tensile response is excluded. Figure 3.4d illustrates how the impulse, or momentum, is transferred from body 1 to body 2 and as the two curves are mirrored it is clear that the momentum is preserved during the collision. In Figure 3.4 it can be seen that the displacement u during the collision reaches 3.5 m for body 1, which might seem to be unreasonably large. The reason that the displacement is large is due to the combination of low spring stiffness k_1 and high initial velocity v_0.

a)

b)

c)

d)
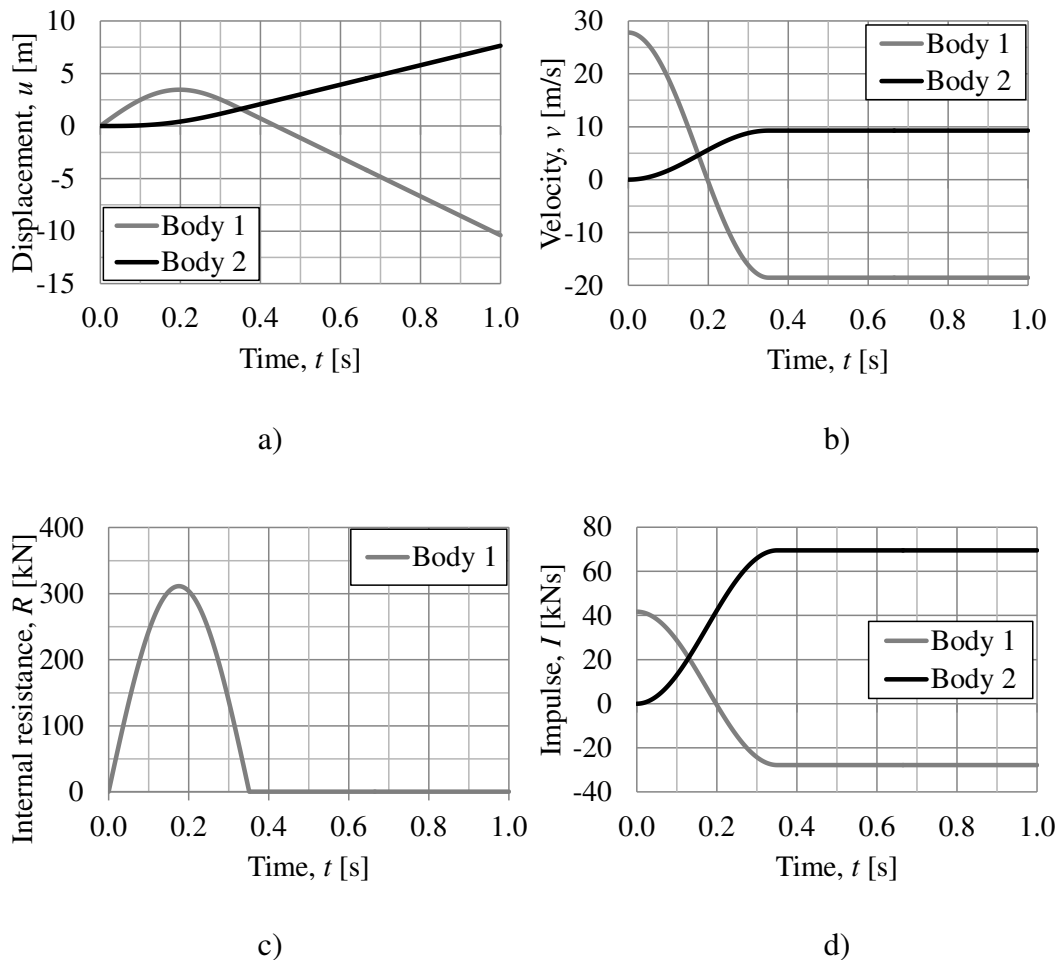
Figure 3.4   Response for collision A1 a) displacement u, b) velocity v, c) internal resistance R, and d) impulse I.

The displacement u, velocity v, internal resistance R and impulse I as a function of time for collision A3 are illustrated in Figure 3.5. As can be observed the duration of the impact for collision A3 is approximately 0.1 s, which is shorter than collision A1. However, the shape of the response curves is the same for both collision A1 and A3. This demonstrates that the stiffness k_1 has a great influence on the duration of the impact. Greater stiffness gives shorter duration of impact and vice versa. For corresponding results for collisions A2 and A4, see Appendix B.1.
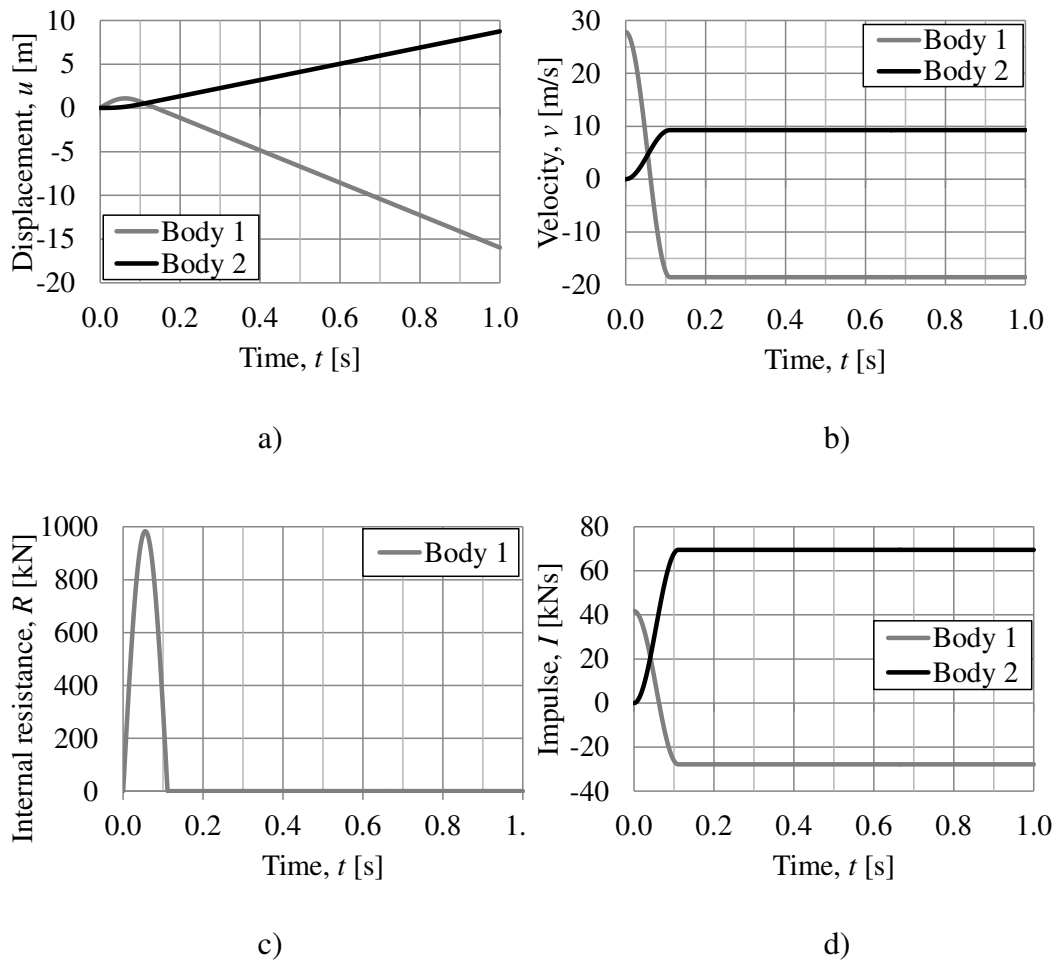
Figure 3.5   Response for collision A3 a) displacement u, b) velocity v, c) internal resistance R, and d) impulse I.

In Figure 3.6 the kinetic energy in the positive direction of body 2 $E_{k,tot}$ is illustrated as a function of time for collision A1-A4. For collision A2 and A4 the mass of body 2 is lower than the mass of body 1, i.e. $m_1 > m_2$, and this is seen as there is no loss in kinetic energy after the collision. However, for collision A1 and A3 there is a loss in the kinetic energy after the collision since $m_1 < m_2$, i.e. body 1 bounce back and get a negative velocity after impact. This is the same response as calculated with the classic impact theory presented in Table 3.2. As can be seen in Figure 3.6 the time of the collisions is varying between the collisions which have different spring stiffness k_1. This means that a higher stiffness gives shorter collision time and vice versa.
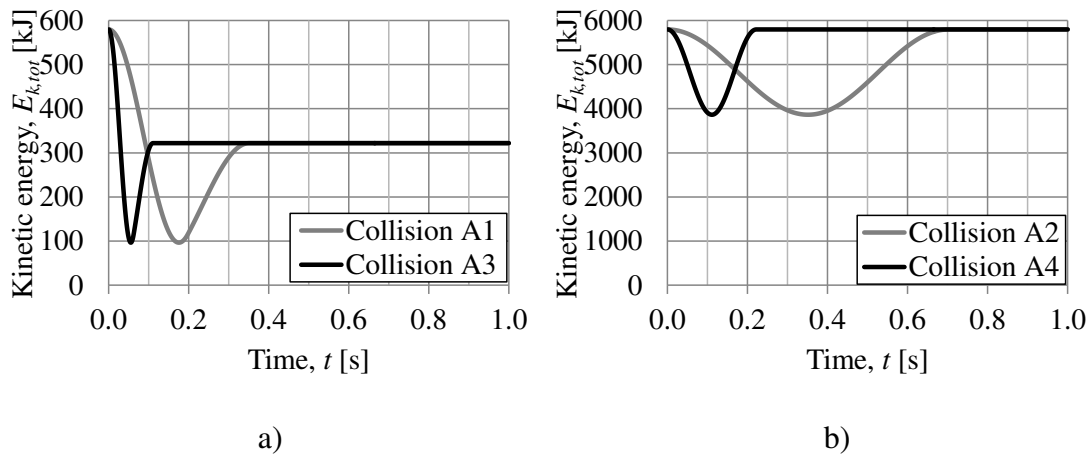
Figure 3.6   Change in kinetic energy $E_{k,tot}$ in the positive direction of body 2 during a) collision A1 and A3, and b) collision A2 and A4.

In Figure 3.7 the internal work W_i of the spring is illustrated as a function of time t for collision A1-A4. As can be observed in Figure 3.7a, body 1 moves in the opposite direction compared to body 2 after the collision, and therefore a loss in internal work W_i in the final phase of the collision. As can be observed in Figure 3.7b, in collision A2 and A4 both bodies are moving in the same direction after the collision. It can also be observed that collision A1 and A2 has lower stiffness k_1 than collision A3 and A4 since the durations of the collisions are larger.
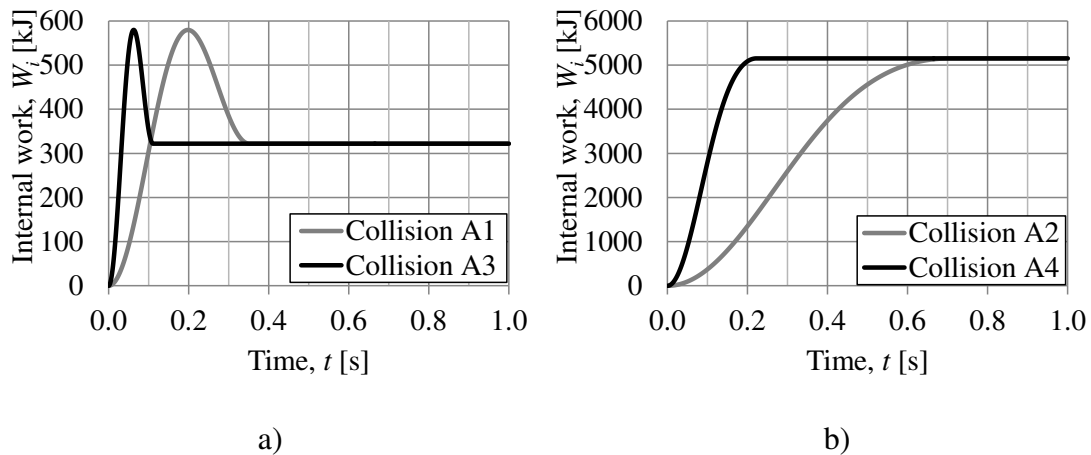
Figure 3.7   Change in internal work W_i during a) collision A1 and A3, and b) collision A2 and A4.

3.2.3   Plastic collision

The plastic response of a 2DOF system without barrier is now studied for the same collisions as in Section 3.2.2, with the exception that in these cases, two different internal resistances $R_{1,max}$ are considered instead of two separate stiffness k_1. The reason for this is that for a plastic collision, the internal resistance of body 1 R_1 is constant and there is no stiffness k_1. Four plastic collisions are analysed in this section, see Table 3.3 for the input parameters.

Table 3.3   *Input parameters for collision B1-B4 with plastic response for the 2DOF system.*

Case	v_0 [m/s]	$R_{1,max}$ [kN]	m_1 [kg]	m_2 [kg]
Collision B1	27.8	250	1 500	7 500
Collision B2	27.8	250	15 000	7 500
Collision B3	27.8	500	1 500	7 500
Collision B4	27.8	500	15 000	7 500

As discussed in Section 3.2.2 for the elastic collisions, the two bodies involved in the collision interact only when there is a compressive force in the spring, and the tension response of the spring is excluded. This is done by using a constant internal resistance R_1 when the deformation Δu is positive and no resistance when the deformation is negative, see Figure 3.8.
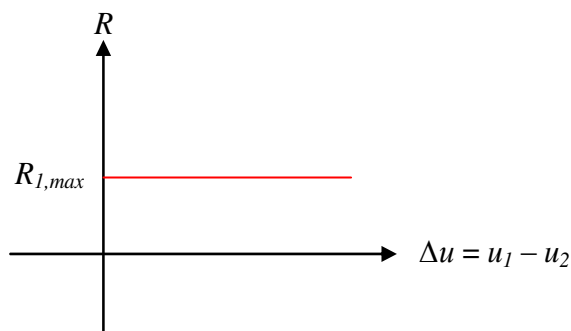
Figure 3.8   *Illustration of how the internal resistance R_1 is constant for the deformation Δu for a plastic case.*

In Table 3.4 the 2DOF analysis of collision B1-B4 are compared to calculations according to classic impact theory described in Section 2.3.1. As can be observed in Table 3.4, the results for plastic collision B1-B4 is not fully identical between the 2DOF and the classic theory, as they are for the elastic collision A1-A4 in Table 3.2. This is due to the fact that it is difficult to obtain a fully plastic collision with a 2DOF system, as can be seen in Table 3.4 where the coefficient of restitution is $e \neq 0$ for the 2DOF systems. The coefficient of restitution e is for the 2DOF system calculated according to equation (2.27), whereas for the classic impact theory it is one of the input data. In this section is a time step $h = 0.1$ ms used, however, the results are relatively close but can be improved further by using a smaller time step.

Table 3.4   *Comparison of results between the 2DOF system and the classic impact theory with plastic response, collision B1-B4.*

Case		e [-]	v_0 [m/s]	v_1 [m/s]	v_2 [m/s]	$E_{k,0}$ [kJ]	$E_{k,tot}$ [kJ]
Collision B1	2DOF	0.001	27.80	4.61	4.64	580	97
Collision B1	Classic theory	0	27.80	4.63	4.63	580	97
Collision B2	2DOF	0.001	27.80	18.52	18.55	5 796	3 864
Collision B2	Classic theory	0	27.80	18.53	18.53	5 796	3 864
Collision B3	2DOF	0.001	27.80	4.44	4.67	580	97
Collision B3	Classic theory	0	27.80	4.63	4.63	580	97
Collision B4	2DOF	0.001	27.80	18.52	18.55	5 796	3 864
Collision B4	Classic theory	0	27.80	18.53	18.53	5 796	3 864

In Figure 3.9, displacement u, velocity v, internal resistance R and impulse I are illustrated as a function of time t for collision B1. From Figure 3.9a and Figure 3.9b it can be confirmed that the collision is plastic since $v_1 \approx v_2$ and the curves for u_1 and u_2 are more or less parallel. There is a small difference between v_1 and v_2 which can be reduced further by a reduced time step h. In Figure 3.9c it can be observed that the spring works plastically because R_1 holds a constant value of $R_{1,max}$ during the whole collision, and then after the collision, the spring stops to act and $R_1 = 0$. In Figure 3.9d, the transfer of impulse from body 1 to body 2 can be confirmed. It is also possible to see that the total impulse is conserved and holds a constant value for $I_1 + I_2$. All four graphs of Figure 3.9 show that the collision lasts for approximately 0.14 s. For corresponding results for collision B2-B4, see Appendix B.2.

a)

b)

c)

d)
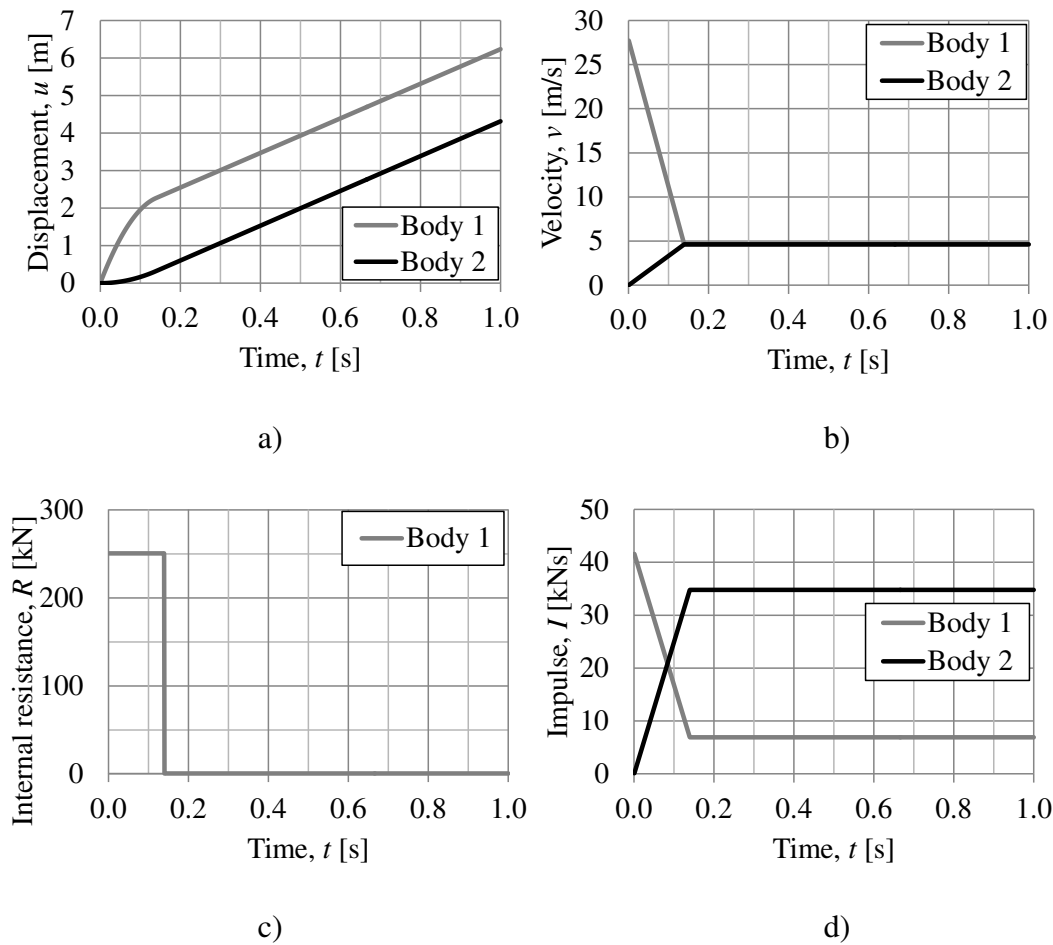
Figure 3.9   Response for collision B1 with a time step of h = 1 ms a) displacement u,   b) velocity v,   c) internal   resistance R,   and d) impulse I.

In Figure 3.10 the total kinetic energy $E_{k,tot}$ in the positive direction is illustrated as a function of time t for collision B1-B4. As can be seen, the initial kinetic energy is ten times larger for collision B2 and B4 than for collision B1 and B3, which is correct since the mass of body 1 is ten times larger for the former two. The reason that collision B2 and B4 takes a longer time than collision B1 and B3 is also due to the difference in mass, and the reason that collision B2 takes a longer time than collision B4 is the lower maximum internal resistance $R_{1,max}$ for collision B2. It is also possible to observe that a large portion of the kinetic energy is transformed into potential energy during the collision, as it should for a plastic collision.
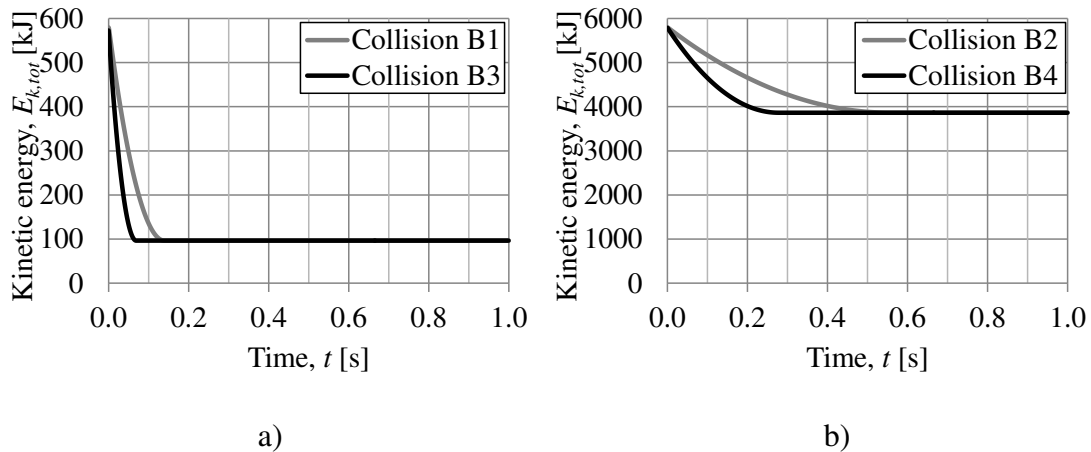
Figure 3.10   Change in kinetic energy $E_{k,tot}$ in the positive direction of body 2 during a) collision B1 and B3, and b) collision B2 and B4.

In Figure 3.11 the internal work W_i of the spring is illustrated as a function of time t for collision B1-B4. As can be observed in Figure 3.11a, body 1 do not move in the opposite direction compared to body 2 after the collision since there is no loss in internal work W_i during the final phase of the collision. This happens despite body 1 has a lower mass than body 2, and indicates a plastic collision. It can also be observed that collision B1 and B2 has lower stiffness k_1 than collision B3 and B4 since the durations of the collisions are greater.
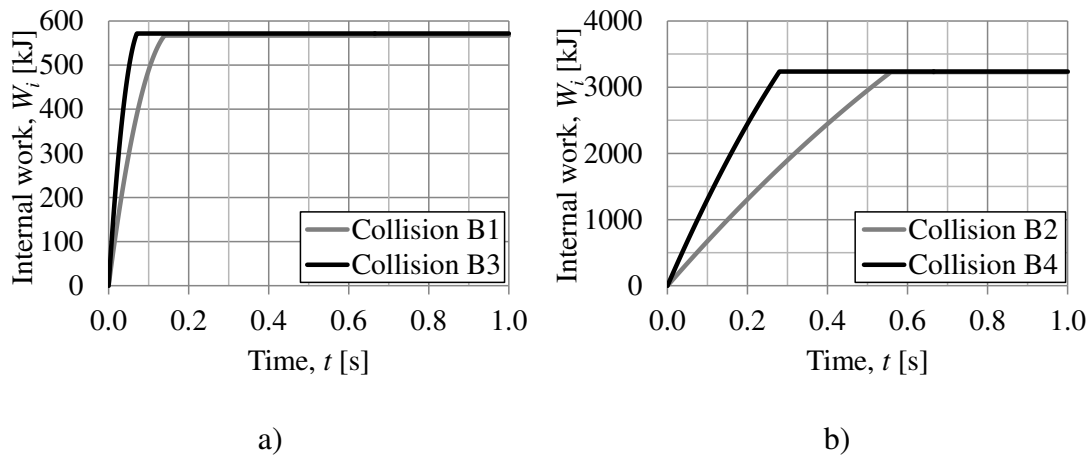
Figure 3.11   Change in internal work W_i during a) collision B1 and B3, and b) collision B2 and B4.

As for the elastic analysis, smaller time steps h for the numerical integration gives results closer to the classic impact theory and here a time step of $h = 1$ ms is used. The importance of a valid time step is even more noticeable for the plastic collisions than for the elastic collisions, because when larger time steps are used, a large difference between the velocities v_1 and v_2 is received, but for a plastic collision v_1 should be equal to v_2 after the collision. Figure 3.12a shows a displacement of body 2 that is greater than the displacement of body 1, i.e. $u_2 > u_1$ after the collision. It can also be observed in Figure 3.12b that the velocity v_1 and v_2 are far from equal after the collision when a time step of $h = 25$ ms is used. These type of errors can occur when a to large time step h is used. The graphs in Figure 3.12 where a time step of $h = 25$ ms

is used can be compared to the more accurate results presented in Figure 3.9 where a time step of $h = 1$ ms is used.

a)   b)
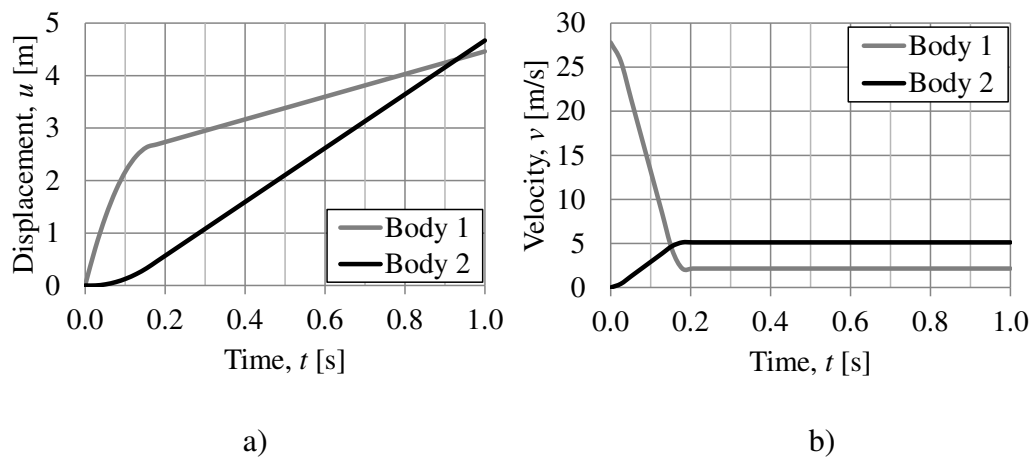
Figure 3.12   Response for collision B1 with a to large time step of h = 25 ms a) displacement u, and b) velocity v.

3.2.4   Elasto-plastic collision

As for the elastic and plastic 2DOF collision analysis without barrier in Section 3.2.2 and 3.2.3, the corresponding elasto-plastic study is also carried out for different collision cases. Two different collision cases based on input data that gives the most interesting elasto-plastic responses, from the previous collisions in Section 3.2.2 and 3.2.3, are analysed here. The input data for the two collisions is presented in Table 3.5 where collision C1 has the same stiffness k_1 as collision A1, the same internal resistance force R_1 as collision B1, and the same masses as both. Collision C2 gains its input data from collision A2 and B2 in a corresponding way.

Table 3.5   Input parameters for collision C1 and C2 with elasto-plastic response for the 2DOF system.

Case	v_0 [m/s]	$R_{1,max}$ [kN]	k_1 [kN/m]	m_1 [kg]	m_2 [kg]
Collision C1	27.8	250	100	1 500	7 500
Collision C2	27.8	250	100	15 000	7 500

As for the corresponding elastic and plastic analysis, the two bodies involved in the collision only interact when there is a compressive force in the spring, which means that the tension response of the spring is excluded. This is done by using $R_1 = k \cdot \Delta u$ until $R_1 = R_{1,max}$ and then a constant internal resistance R_1 when the deformation Δu is positive, and no resistance when the deformation is negative, see Figure 3.13.
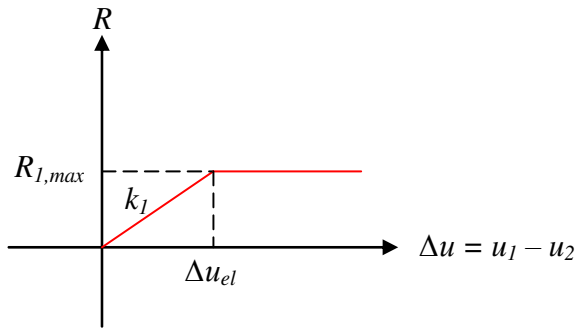
Figure 3.13   Illustration of a case with elasto-plastic response which is a combination of an elastic case with a spring stiffness k_1 that varies with the deformation Δu and a plastic case where the internal resistance R_1 is constant for the deformation Δu.

The two collisions are analysed with a 2DOF elasto-plastic model and the coefficient of restitution e is calculated with equation (2.27). The different e is then used with the classic impact theory, and the results in Table 3.6 are obtained. As for the elastic and plastic analysis, smaller time steps h for the numerical integration gives results closer to the classic impact theory, therefore a time step of $h = 1$ ms is used.

Table 3.6   Comparison of results between the 2DOF system and the classic impact theory with elasto-plastic response, collision C1 and C2.

	Collision C1		Collision C2	
	2DOF	Classic theory	2DOF	Classic theory
e [-]	0.804	0.804	0.402	0.402
v_0 [m/s]	27.80	27.80	27.80	27.80
v_1 [m/s]	-14.00	-13.99	14.81	14.81
v_2 [m/s]	8.36	8.36	25.99	25.99
$E_{k,0}$ [kJ]	580	580	5 796	5 796
$E_{k,tot}$ [kJ]	262	262	4 177	4 177

In Figure 3.14, displacement u, velocity v, internal resistance R and impulse I are illustrated as a function of time t for collision C2. Collision C2 has a coefficient of restitution of $e \approx 0.4$, which means that it has 40 % elastic behaviour and 60 % plastic behaviour. In Figure 3.14a and Figure 3.14b it is hard to see that the collision acts more in a plastic than in an elastic manner. But it can be observed that the collision is not elastic because in that case, a much larger difference between v_1 and v_2 would have been obtained and it is not plastic since then v_1 and v_2 would have had the same value. Figure 3.14c shows that the two bodies respond in an elasto-plastic manner since the response follows Figure 3.13 as

$$\begin{cases} R_1 = k_1 \cdot \Delta u, & \Delta u \leq u_{el} \\ R_1 = R_{1,max}, & \Delta u > u_{el} \end{cases} \qquad (3.1)$$

In Figure 3.14d, the transfer of impulse from body 1 to body 2 can be confirmed. It is possible to observe that the total impulse is conserved and holds a constant value for $I_1 + I_2$. All four graphs of Figure 3.14 show that the collision lasts for approximately 0.95 s. For corresponding results for collision C1, see Appendix B.3.
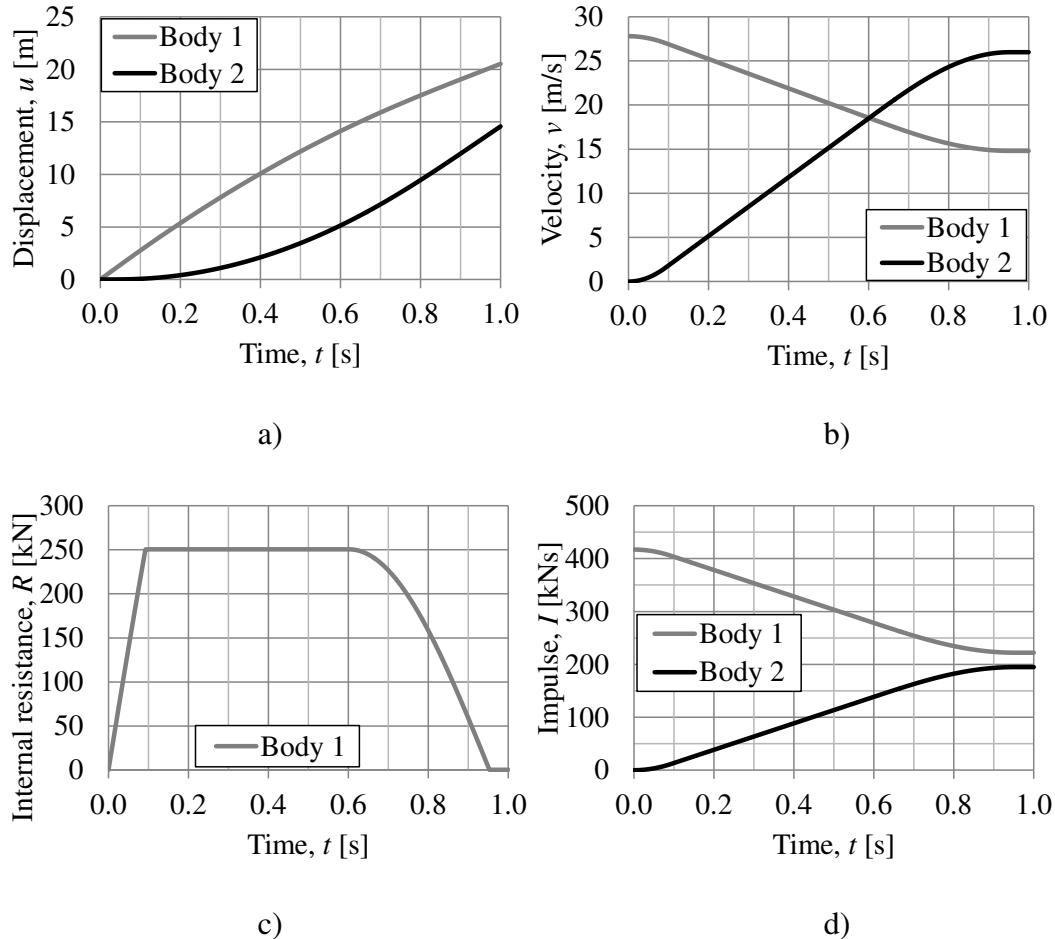
Figure 3.14   Response for collision C2 a) displacement u, b) velocity v, c) internal resistance R, and d) impulse I.

In Figure 3.15 the total kinetic energy $E_{k,tot}$ in the positive direction is illustrated as a function of time t for collision C1 and C2. Similarly to the elastic and plastic analysis, the initial kinetic energy is ten times larger for collision C2 than for collision C1, which is correct since the mass of body 1 is ten times larger in collision C2 than in collision C1. The difference in mass is also one reason that collision C2 has a longer duration than collision C1, another reason is the difference in coefficient of restitution e.

For collision C1, a large portion of the total kinetic energy $E_{k,tot}$ is lost before the minimum value in Figure 3.15 is reached. After the minimum value of the total kinetic energy is reached, the collision regains a portion of its kinetic energy again. This proves that it is a mixture of elastic and plastic response. The same could be said of collision C2, but in this case, not all of the kinetic energy in the positive direction is

transferred to internal energy W_i, but also to kinetic energy in the negative direction, see Figure 3.15, Figure 3.16 and Table 3.6.
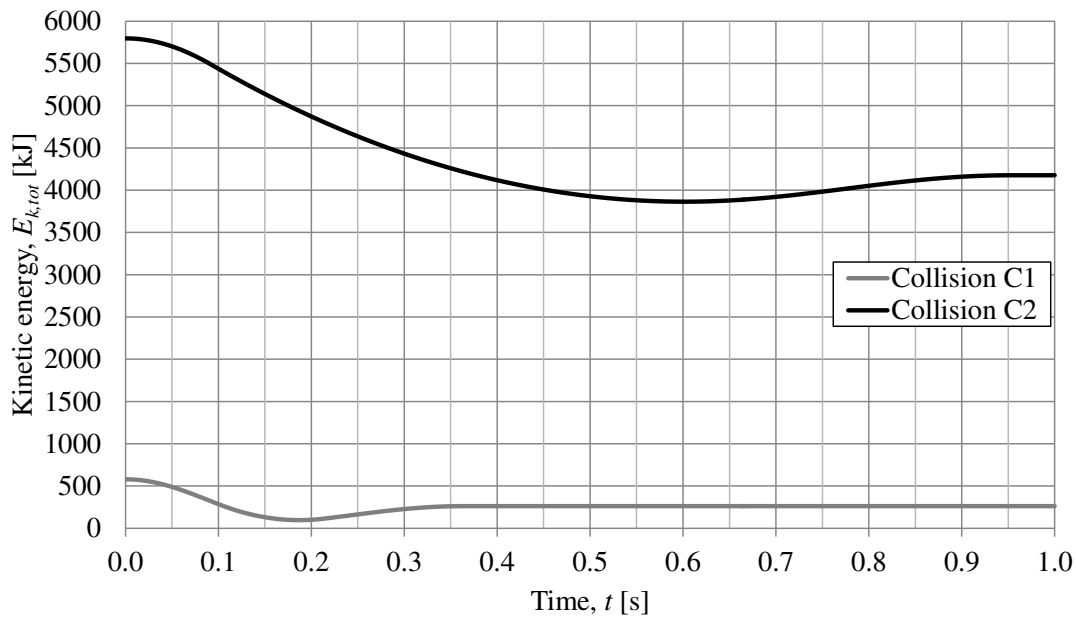
Figure 3.15   Change in kinetic energy $E_{k,tot}$ in the positive direction of body 2 during collision C1 and C2.

In Figure 3.16 the internal work W_i of the spring is illustrated as a function of time t for collision C1 and C2. As can be observed for collision C1, body 1 loses internal energy in the final phase of the collision, this means that body 1 is moving in the opposite direction of body 2 after the collision, which indicates that the collision is not fully plastic.
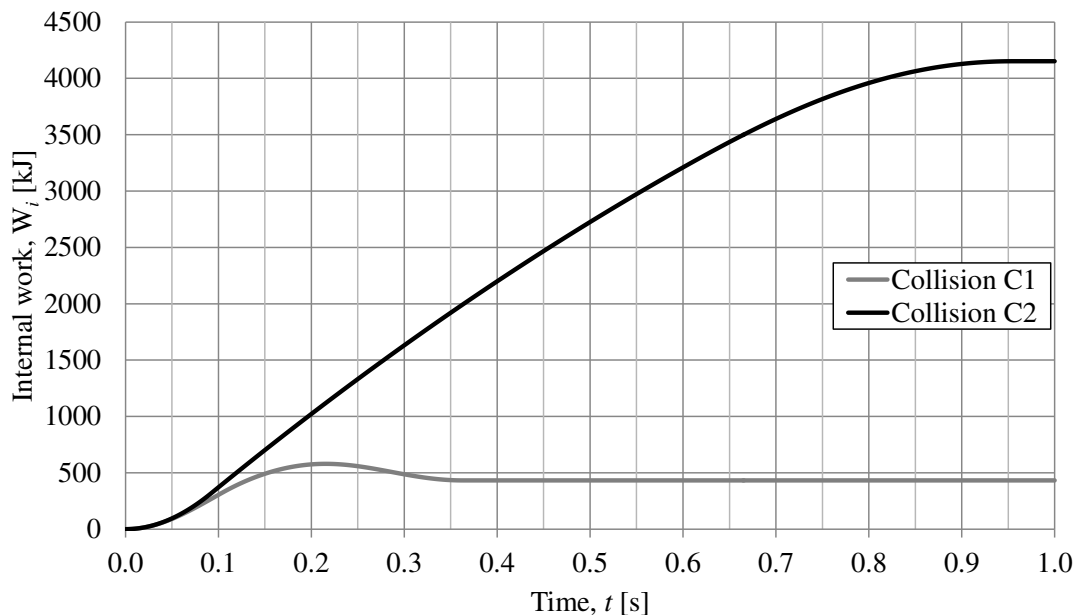
Figure 3.16   Change in internal work W_i during collision C1 and C2.

3.3 Elastic collision with barrier

In the collision impacts that are of interest in this thesis, the structural member which is symbolized by body 2, is attached to a larger system. Therefore, a barrier in the form of an additional spring attached to body 2 at one side and fixed at the other is introduced, as illustrated in Figure 3.17.
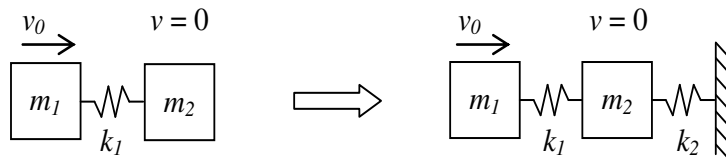
Figure 3.17   Illustration of how a 2DOF system without barrier is transformed into a system with a barrier.

The structural response of body 1 during a collision, is significant for what kind of load $F_2(t)$ that is acting on body 2, and therefore also what type of dynamic response that can be expected from body 2. The two extremes are as in Section 3.2 elastic and plastic response, with elasto-plastic response in between.

If an elasto-plastic analysis is considered, a very large number of collision scenarios may be obtained, even if only one of the bodies is studied with elasto-plastic response. This can be complicated to describe thoroughly and it demands more input data in the form of stiffness k and internal resistance R. Hence, in this section only an elastic response for both bodies is considered. The elasto-plastic response of reinforced concrete structures, is instead treated in Chapter 6.

The shape of the load acting on body 2 $F_2(t)$ that is created when body 1 collides with body 2 can have a great importance for the response of body 2. How this shape affects the resulting response is complex and depends on the properties of both the involved bodies. As an example, it is not only the mass ratio m_1 / m_2 and the load $F_2(t)$ that affects the structural response in form of the internal resistance for spring 2 R_2, but also the frequency ratio f_1 / f_2, Johansson (2014).

The two bodies involved in the collision interact only when there is a compressive force in the spring of body 1, which means that the tensile response of the spring must be excluded. Hence, the stiffness of spring 1 k_1 has a linear elastic response while the deformation Δu is positive and no stiffness when the deformation is negative. The response of spring 2 depends solely on the displacement of body 2 u_2 and has a linear elastic response for both the positive and the negative displacement. The reason for this is that body 2 corresponds to a structural member that is connected to a larger structural system and therefore strives to return to its original state, see Figure 3.18.
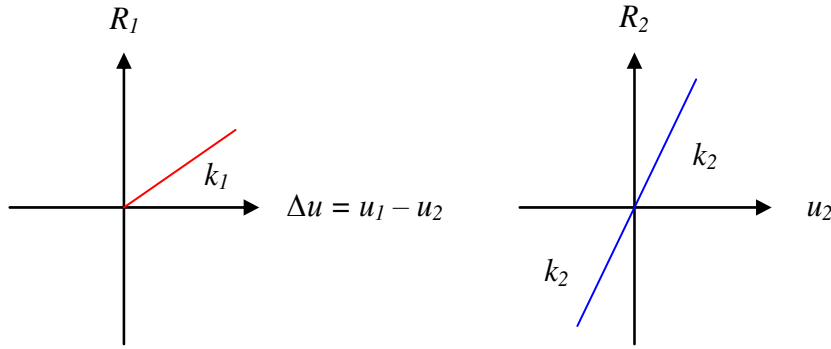
Figure 3.18   Illustration of how the spring stiffness k_1 varies with the deformation Δu and how the spring stiffness k_2 varies with the deformation u_2 for an elastic case.

The method used here is based on converting the dynamic load to an equivalent static load $F_{2,sta}$. An advantageous tool is to determine a load factor β_{el} which describes the relation between the dynamic load $F_{2,dyn}$ and the equivalent static load $F_{2,sta}$ as

$$F_{2,sta} = \beta_{el} \cdot F_{2,el} \tag{3.2}$$

$F_{2,el}$ is the maximum dynamic load, derived for a collision with a fully stiff member, so called hard impact, and it is determined by setting internal work and the kinetic energy that acts on body 1 equal to $E_{k,0} = W_{i,el,1}$, where the kinetic energy is

$$E_{k,0} = \frac{mv_0^2}{2} \tag{3.3}$$

The area under the curve in Figure 3.19 is the internal work

$$W_{i,el,1} = \frac{k_1 u_{1,el}^2}{2} = \frac{R_{1,el}^2}{2k_1} \tag{3.4}$$
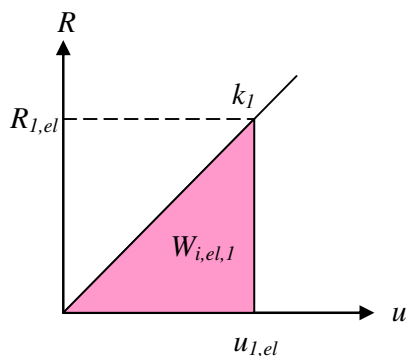
Figure 3.19   Force-displacement relation showing the internal work $W_{i,el,1}$ as the area under the curve.

By putting the dynamic load equal to the internal resistance $F_{2,el} = R_{1,el}$, the maximum dynamic load can be expressed as

$$F_{2,el} = v_0 \sqrt{k_1 \cdot m_1} \tag{3.5}$$

The equivalent static load $F_{2,sta}$ also corresponds to the internal resistance of body 2 R_2, described as

$$F_{2,sta} = R_2 = k_2 u_{el,2} \tag{3.6}$$

The load factor β_{el} in equation (3.2) can therefore be expressed as

$$\beta_{el} = \frac{R_2}{F_{2,el}} \tag{3.7}$$

The relation between the load factor β_{el} and the frequency ratio f_1 / f_2 for different mass ratio m_1 / m_2 can be seen in Figure 3.20. The input values for the curves based on data from Johansson (2014), are presented in Appendix E.
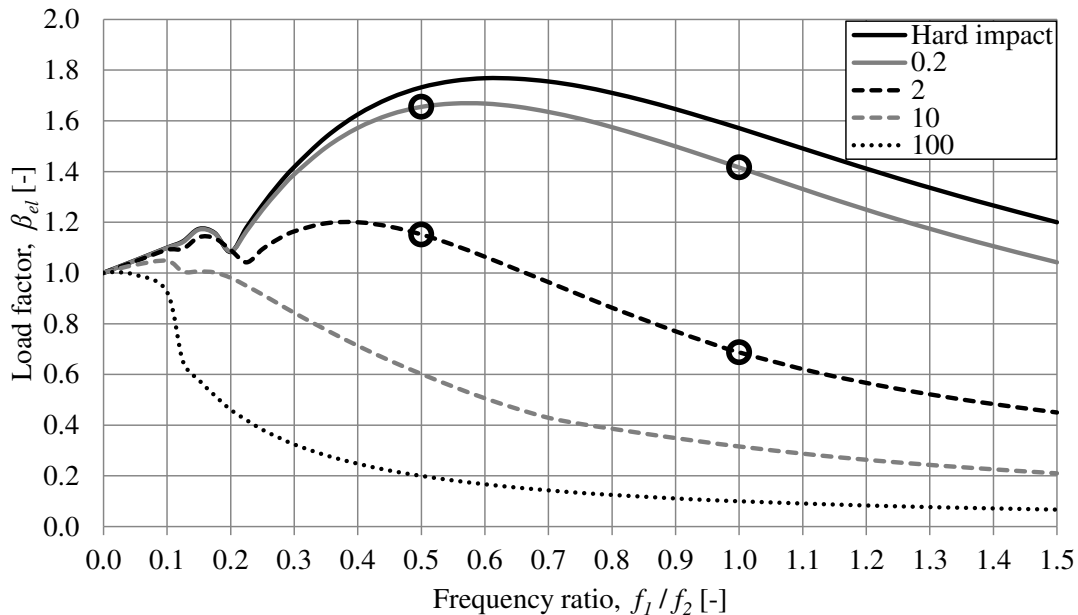
Figure 3.20   Relationship between load factor β_{el} and frequency ratio f_1 / f_2 for different mass ratio m_1 / m_2, based on Johansson (2014). Circles in diagram mark cases that are further studied in this section.

The marked cases in Figure 3.20 are selected mass ratios m_1 / m_2 which are further investigated in this section. The input values for the selected ratios are listed in Table 3.7. These collisions are based on the collisions in Section 3.2.2, with the same initial velocity $v_0 = 27.8$ m/s and the same masses, but with a different stiffness k_1 and now also k_2.

If the collision cases in Table 3.7 are compared to the more practical collision cases studied in Chapter 6, the stiffness k_1 and k_2 in this section can seem to be of a very small magnitude and large displacements are obtained. However, from the results in this section, one can still gain the understanding of elastic collisions with barriers.

Table 3.7   Input parameters for collision D1-D4 with elastic response for the 2DOF system with initial velocity $v_0 = 27.8$ m/s.

	Collision D1	Collision D2	Collision D3	Collision D4
k_1 [kN/m]	100	1 000	400	4 000
k_2 [kN/m]	2 000	2 000	2 000	2 000
m_1 [kg]	1 500	15 000	1 500	15 000
m_2 [kg]	7 500	7 500	7 500	7 500
Mass ratio m_1 / m_2 [-]	0.2	2	0.2	2
Frequency ratio f_1 / f_2 [-]	0.5	0.5	1	1
Load factor β_{el} [-]	1.65	1.15	1.42	0.69

The displacement u, velocity v, impulse I and internal resistance R for both bodies during collision D4 is presented in Figure 3.21. From Figure 3.21c it can be seen that the impact duration is approximately 0.3 s. Spring 2 has an elastic response at tension, as shown in Figure 3.18, which is why the response of body 2 after the impact is a wave motion, see Figure 3.21. Accordingly, body 2 will sway back and forth with no reduced effect since no damping effect is regarded. As can be seen from the internal resistance R for body 1 in Figure 3.21c, spring 1 endures two separate collisions, a phenomenon which happens due to k_1 and m_1 being much larger than k_2 and m_2. This double collision is also observable in Figure 3.21a where $u_1 - u_2 \leq 0$ at $t \approx 0.15$ s.

In Figure 3.21c, the dynamic load $F_{2,el}(t)$ from a hard impact is added to the graph to illustrate the difference compared to $R_1(t)$ for collision D4.
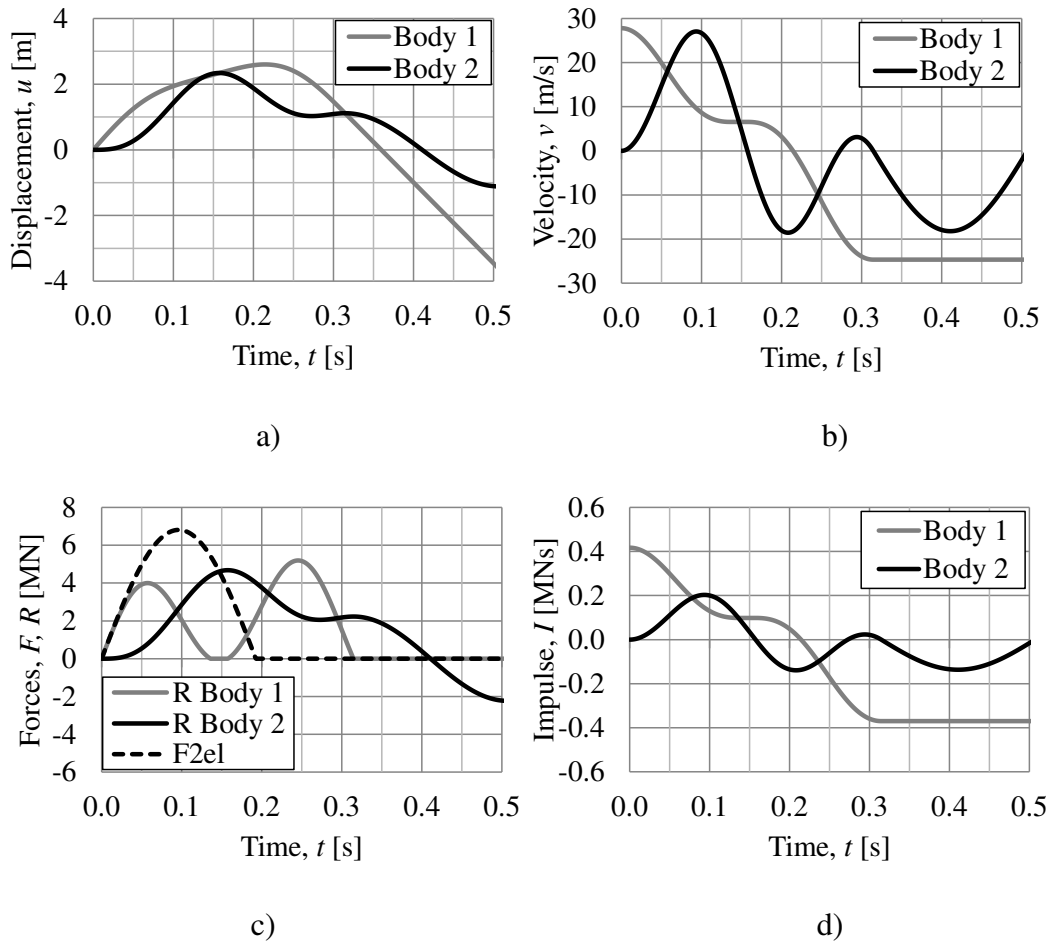
Figure 3.21 Response for collision D4 a) displacement u, b) velocity v, c) internal resistance R and dynamic load $F_{2,el}$, and d) impulse I.

The change in internal energy W_i and kinetic energy E_k for both bodies during collision D4 is presented in Figure 3.22. The wave motion which appears for body 2 after the impact is clearly seen in Figure 3.22b, where the internal work $W_{i,2}$ is zero when the kinetic energy $E_{k,2}$ is maximum and vice versa.
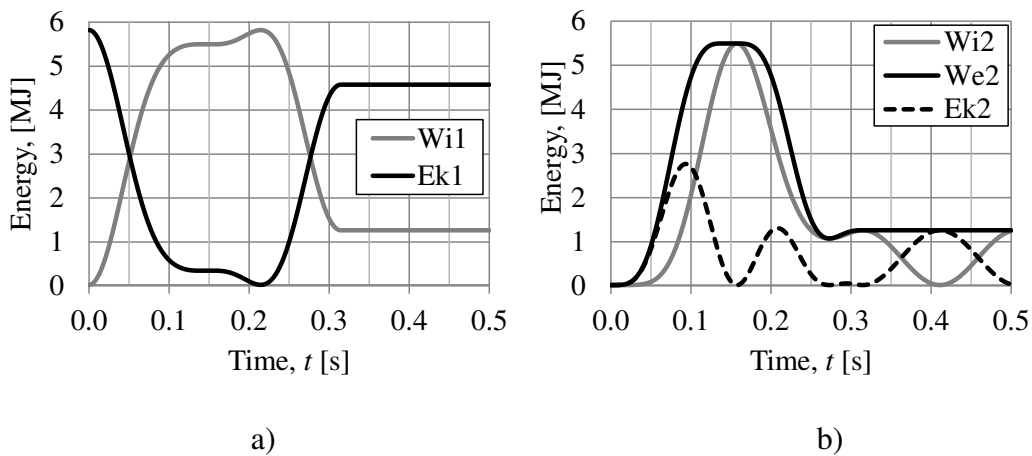
Figure 3.22 Response for collision D4 a) internal work $W_{i,1}$ and kinetic energy $E_{k,1}$ for body 1, and b) internal work $W_{i,2}$, external work $W_{e,2}$ and kinetic energy E_k for body 2.

The phenomena seen from collision D4 due to spring 1 being fully compressed before spring 2 starts to compress is also seen in Figure 3.23. There is a tendency for the same phenomena for collision D2, but not as clear. Collision D1 and D3 shows no such thing and this are due to the relatively low stiffness of spring 1 k_1 and low mass m_1. The time of the four impacts are clearly shown in Figure 3.23, where it can be observed that the internal resistance of body 1 R_1 is zero after the collision.

a)   b)
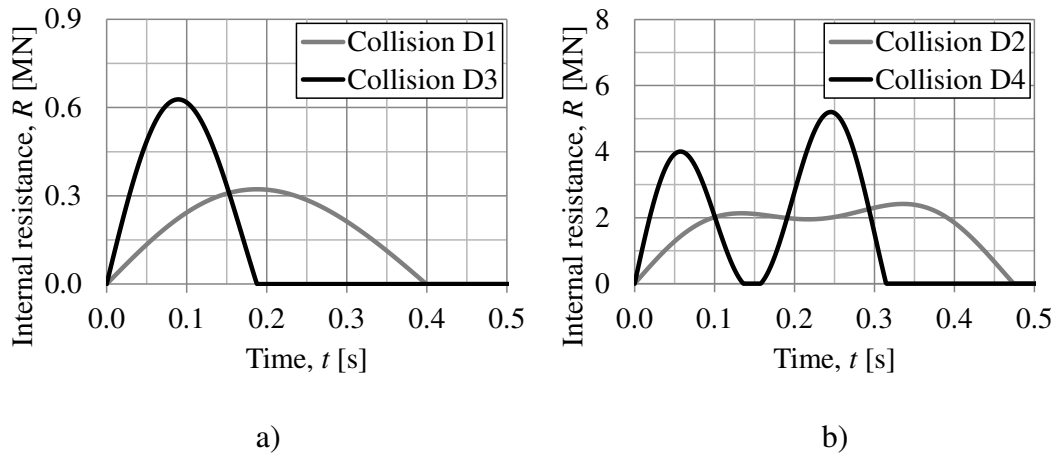
Figure 3.23   Internal resistance of body 1 R_1 for a) collision D1 and D3, and b) collision D2 and D4.

The internal resistance of body 2 for collision D1-D4 is presented in Figure 3.24. After the collision all four collisions shows a wave motion for body 2.
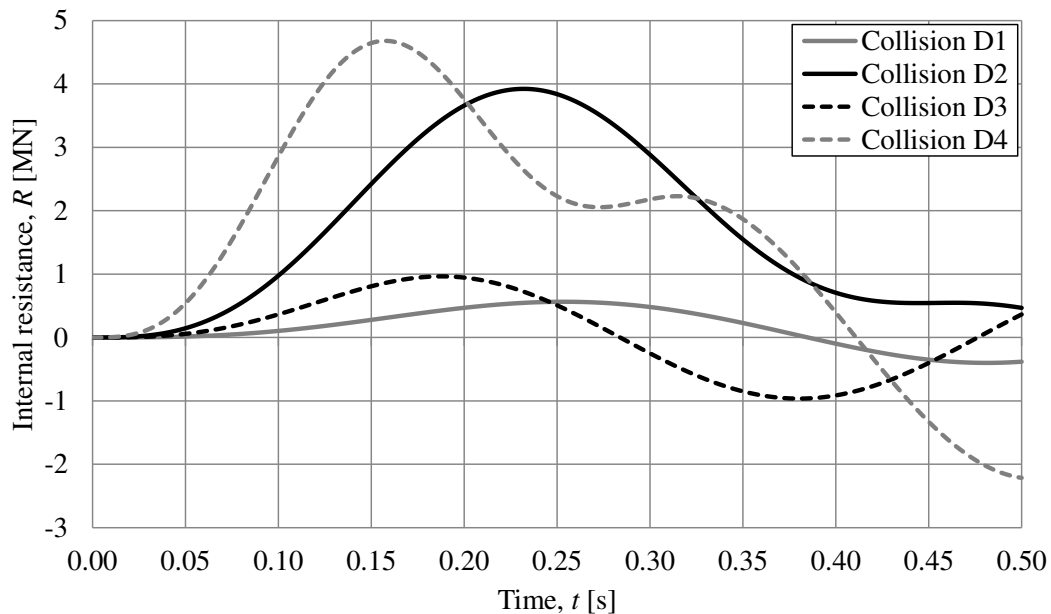
Figure 3.24   Internal resistance of body 2 R_2 for collision D1-D4.

For corresponding diagrams for collision D1-D3, see Appendix B.4.

4 Transformation of Structural Member to SDOF System

4.1 Transformation of beams to SDOF systems

4.1.1 Orientation

In Chapter 3, collisions and impacts are analysed using 2DOF-models. However, if these mass-spring models should be valid, they must first be transformed from the real structure that is of interest.

If a beam with linear elastic material properties and retained boundary conditions is loaded with a point or distributed static load, the displacement shape of the beam is always the same no matter what the magnitude of the load is. This enables the possibility to describe the displacement along the entire beam with only one displacement u_s in a certain location of the beam, see Figure 4.1. A beam with plastic material properties can be described in the same way even though the displacement shape is different.
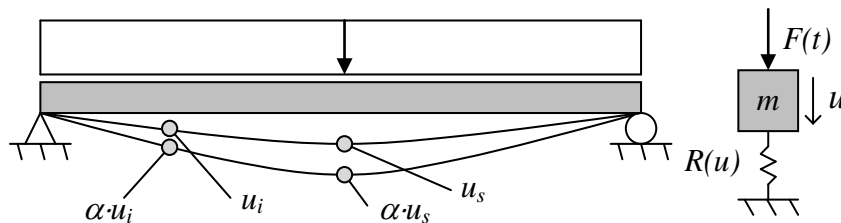
Figure 4.1   A change in displacement of a beam with a factor α means that the constant shape of displacement is scaled along the whole beam with this factor.

This location of the beam is called the system point and the properties of the SDOF-model should be adjusted so that

$$u_{SDOF} = u_s \tag{4.1}$$

It is common to have the system point located at the point where the displacement is the largest, or at the centre of the beam, Johansson and Laine (2012). In this thesis point loads are of interest and the system point is chosen to be at the point of loading. The transformation to a SDOF system from a beam is made through applying a mass m, a resisting force $R(u)$, and an external load $F(t)$, see Figure 4.2. As discussed in Section 2.4, the damping effect is neglected in this thesis.
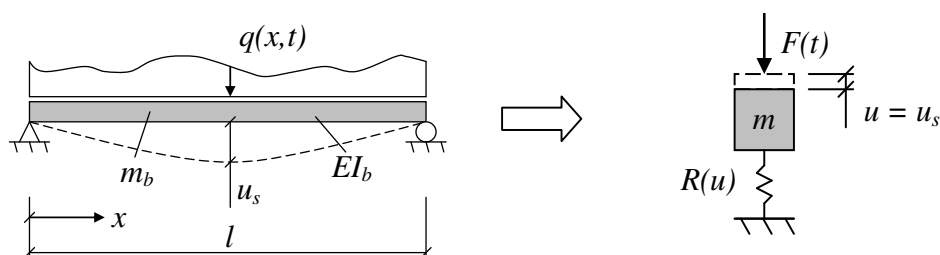
Figure 4.2   Illustration of how to transform a beam to an equivalent SDOF system.

For linear elastic response with $R(u) = k \cdot u$, a relation between the equivalent SDOF system and the beam can be made using different transformation factors κ

$$m = \kappa_m \cdot m_b \qquad (4.2)$$

$$k = \kappa_k \cdot k_b \qquad (4.3)$$

$$F = \kappa_F \cdot F_b \qquad (4.4)$$

where m_b, k_b and F_b is the mass, stiffness and external load of the beam. By using this, the dynamic equation of motion, equation (2.15), can be written as

$$\kappa_m m_b \ddot{u} + \kappa_k k_b u = \kappa_F F_b(t) \qquad (4.5)$$

For a system with plastic or elasto-plastic response, it can instead be written as

$$\kappa_m m_b \ddot{u} + \kappa_k R_b(u) = \kappa_F F_b(t) \qquad (4.6)$$

where $R_b(u)$ describes the static response of the beam. The transformation factors κ are derived on the basis of the theory of energy conservation where the kinetic energy of the mass m, the work done by the external force $F(t)$ and the internal resistance R should be equal between the two systems, Johansson and Laine (2012).

4.1.2 Conservation of kinetic energy

To conserve the kinetic energy E_k between the two systems illustrated in Figure 4.2 the energy can be written as

$$E_k = \frac{m \cdot v_s^2}{2} = \int_{x=0}^{x=l} \frac{m'(x) \cdot v(x)^2}{2} dx \qquad (4.7)$$

where v_s is the velocity at the system point, $m'(x)$ is the mass per unit length and $v(x)$ is the velocity per unit length. By using that

$$v_s = \frac{\Delta u_s}{\Delta t} \qquad (4.8)$$

and

$$v(x) = \frac{\Delta u(x)}{\Delta t} \qquad (4.9)$$

where Δu_s and $\Delta u(x)$ are the displacements at the system point and along the beam, equation (4.7) for a beam with constant mass per unit length $m'(x) = m'$, can be expressed as

$$m \cdot u_s{}^2 = \frac{m_b}{l} \int\limits_{x=0}^{x=l} u(x)^2 \, dx \qquad (4.10)$$

The transformation factor κ_m can be derived by combining equation (4.2) and (4.10)

$$\kappa_m = \frac{1}{l} \int\limits_{x=0}^{x=l} \frac{u(x)^2}{u_s{}^2} \, dx \qquad (4.11)$$

4.1.3 Conservation of external work

To conserve the external work W_e between the two systems illustrated in Figure 4.2 the energy can be written as

$$W_e = F \cdot u_s = \int\limits_{x=0}^{x=l} q(x) \cdot u(x) \, dx \qquad (4.12)$$

where $q(x)$ is the load per unit length. The external force for a beam F_b with constant uniformly distributed load $q(x) = q$ can be expressed as

$$F_b = \int\limits_{x=0}^{x=l} q(x) \, dx = \int\limits_{x=0}^{x=l} \frac{F_b}{l} \, dx \qquad (4.13)$$

With this inserted in equation (4.12) and by using equation (4.4), the transformation factor κ_F can be expressed as

$$\kappa_F = \frac{1}{l} \int\limits_{x=0}^{x=l} \frac{u(x)}{u_s} \, dx \qquad (4.14)$$

For an arbitrary distributed load which acts at $x = x_1$ to $x = x_2$ the transformation factor κ_F can be expressed as

$$\kappa_F = \frac{1}{x_2 - x_1} \int\limits_{x=x_1}^{x=x_2} \frac{u(x)}{u_s} \, dx \qquad (4.15)$$

In the case of a beam subjected to a point load, equation (4.12) can be rewritten as

$$W_e = F \cdot u_s = F_b \cdot u_s \qquad (4.16)$$

and the transformation factor κ_F will, with equation (4.4), become

$$\kappa_F = \frac{u}{u_s} = 1 \qquad (4.17)$$

4.1.4 Conservation of internal work

The internal work W_i for a linear elastic material can be written as

$$W_i = \frac{ku_s^2}{2} = \frac{1}{2} \int\limits_{x=0}^{x=l} \left(\frac{N(x)^2}{EA} + \frac{\beta_{shear}V(x)^2}{GA} + M(x) \cdot u''(x) \right) dx \qquad (4.18)$$

where E is the Young's modulus, G is the shear modulus, β_{shear} is a factor to consider the shear stress, A is the sectional area, $N(x)$ is the normal force, $V(x)$ is the shear force, $M(x)$ is the moment and $u''(x)$ is the curvature of the beam, Johansson and Laine (2012). The contribution from the normal and shear forces are in general small and can be neglected, and equation (4.18) can thus be simplified to

$$W_i = \frac{ku_s^2}{2} = \frac{1}{2} = \int\limits_{x=0}^{x=l} M(x) \cdot u''(x) dx \qquad (4.19)$$

By combining this with equation (4.3) the transformation factor κ_k can be written as

$$\kappa_k = \int\limits_{x=0}^{x=l} \frac{M(x) \cdot u''(x)}{k_b \cdot u_s^2} dx \qquad (4.20)$$

The stiffness of a beam with elastic response can be determined in the same way as for a spring, which means using the elastic correlation between load and displacement. For an elastic beam subjected to a point load the correlation can be written as

$$F_b = k_b \cdot u_s \qquad (4.21)$$

which combined with equation (4.20) gives

$$\kappa_k = \int\limits_{x=0}^{x=l} \frac{M(x) \cdot u''(x)}{F_b \cdot u_s} dx \qquad (4.22)$$

where F_b is derived from equation (4.13).

4.1.5 Summary

According to Biggs (1964), the transformation factors for internal and external work are equal, i.e.

$$\kappa_k = \kappa_F \qquad (4.23)$$

If using equation (4.23) and dividing equation (4.6) by the transformation factor κ_F, the dynamic equation of motion can be written as

$$\frac{\kappa_m}{\kappa_F} m_b \ddot{u} + \frac{\kappa_k}{\kappa_F} k_b u = F_b(t) \qquad (4.24)$$

By introducing a combined transformation factor κ_{mF}

$$\kappa_{mF} = \frac{\kappa_m}{\kappa_F} \tag{4.25}$$

equation (4.24) can be rewritten as

$$\kappa_{mF} m_b \ddot{u} + k_b u = F_b(t) \tag{4.26}$$

This means that it is only the mass of the beam m_b that is affected by a transformation factor κ_{mF} when transforming a beam to a SDOF system.

In the case of a beam subjected to a point load the transformation factor κ_{mF} according to equation (4.17) can be expressed as

$$\kappa_{mF} = \kappa_m \tag{4.27}$$

4.2 Determination of transformation factors for a beam

4.2.1 Orientation

Derivation of the transformation factors κ_m and κ_F for beams for different load cases with elastic response is done in Johansson (2014) and in Asplund and Steckmest (2014). The transformation factors used in this thesis for beams are presented in Appendix D.1.

4.2.2 Elastic response for a point load

The displacement $u(x)$ of a simply supported beam with an elastic response subjected to a point load is defined according to Lundh (2000) as

$$u(x) = \begin{cases} \dfrac{F_b \beta}{6EI_b} ((1-\beta^2)l^2 x - x^3), & 0 \le x \le \alpha l \\[2mm] \dfrac{F_b \alpha}{6EI_b} ((1-\alpha^2)l^2 (l-x) - (l-x)^3), & \alpha l \le x \le l \end{cases} \tag{4.28}$$

where x, l, α, β, F_b and EI_b are illustrated in Figure 4.3.
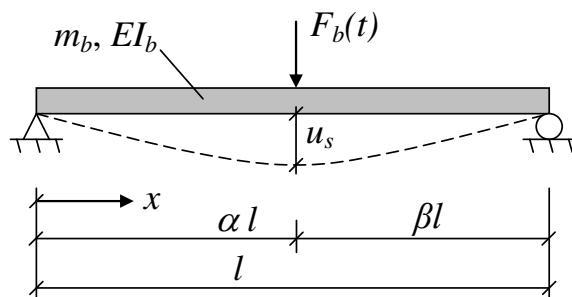
Figure 4.3   Illustration of a simply supported beam with elastic response subjected to a point load.

The displacement at the system point $u_s = u(\alpha \cdot l)$ can be written as

$$u_s = \frac{F_b l^3}{3EI_b} \alpha^2 \beta^2 \qquad (4.29)$$

By inserting equation (4.28) and (4.29) in equation (4.11) and using the fact that the transformation factor $\kappa_{F,el}$ is equal to one for cases with a beam subjected to a point load, the following $\kappa_{mF,el}$ can be derived as

$$\kappa_{mF,el} = \frac{1}{l} \int_{x=0}^{x=\alpha l} \frac{\left(\frac{F_b \beta}{6EI_b} ((1-\beta^2)l^2 x - x^3) \right)^2}{\left(\frac{F_b l^3}{3EI_b} \alpha^2 \beta^2 \right)^2} dx +$$

$$+ \frac{1}{l} \int_{x=\alpha l}^{x=l} \frac{\left(\frac{F_b \alpha}{6EI_b} ((1-\alpha^2)l^2 (l-x) - (l-x)^3) \right)^2}{\left(\frac{F_b l^3}{3EI_b} \alpha^2 \beta^2 \right)^2} dx = \qquad (4.30)$$

$$= \frac{\alpha^3}{28\beta^2} + \frac{(23\alpha^2 + 10\alpha + 2)\beta}{105\alpha^2} + \frac{\beta^2 - 2}{12\alpha} - \frac{\alpha}{10\beta^2} + \frac{1}{12\alpha\beta^2} + \frac{\alpha}{10}$$

If equation (4.21) and (4.29) is combined, the beam stiffness k_b can be written as

$$k_b = \frac{3EI_b}{l^3 \alpha^2 \beta^2} \qquad (4.31)$$

As can be seen from equation (4.31), a smaller length of the beam l gives a much higher stiffness and vice versa, since it is to the power of three. The stiffness also increases rapidly when the load acts closer to the supports, when either α or β is close to zero, see Asplund and Steckmest (2014).

4.2.3 Plastic response for a point load

For a simply supported beam with plastic response the displacement $u(x)$ varies linearly when subjected to a point load, see Figure 4.4.
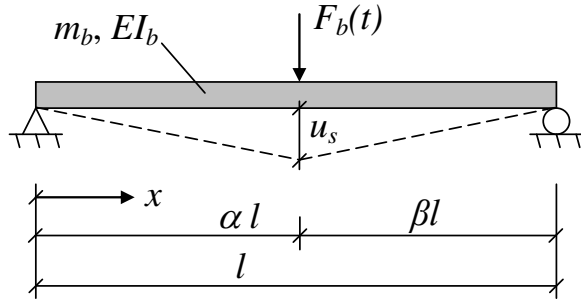
Figure 4.4   Illustration of a simply supported beam with plastic response subjected to a point load.

If the displacement $u(x)$ is stated as a function of u_s instead of the force F_b, it can be written as

$$u(x) = \begin{cases} u_s \dfrac{x}{\alpha l}, & 0 \le x \le \alpha l \\[2mm] u_s \dfrac{l-x}{\beta l}, & \alpha l \le x \le l \end{cases} \tag{4.32}$$

By inserting equation (4.32) in equation (4.11) and using the fact that the transformation factor $\kappa_{F,pl}$ is equal to one for a case with a beam subjected to a point load, $\kappa_{mF,pl}$ can be written as

$$\kappa_{mF,pl} = \frac{1}{l}\int_{x=0}^{x=\alpha l}\frac{\left(u_s\dfrac{x}{\alpha l}\right)^2}{u_s^{\,2}}dx + \frac{1}{l}\int_{x=\alpha l}^{x=l}\frac{\left(u_s\dfrac{l-x}{\beta l}\right)^2}{u_s^{\,2}}dx =$$

$$= \frac{\alpha}{3} + \frac{1}{\beta^2}\left(\frac{1}{3} - \alpha + \alpha^2 - \frac{\alpha^3}{3}\right) = \frac{1}{3} \tag{4.33}$$

4.3   Transformation of slabs to SDOF systems

4.3.1   Orientation

The transformation of a slab into a SDOF system is done similarly to the transformation of beams done in Section 4.1. The equation of motion can be written according to equation (4.26) as

$$\kappa_{mF} m_{sl}\ddot{u} + k_{sl}u = F_{sl}(t) \tag{4.34}$$

where

$$\kappa_{mF} = \frac{\kappa_m}{\kappa_F} \tag{4.35}$$

is the transformation factor handling both the mass and the force. The transformation factor for one-way slabs is the same as for beams. Whilst the properties for beams and one-way slabs can vary in the longitudinal direction, the properties for two-way slabs can vary in both longitudinal and transversal direction. This means that the derivation of the transformation factors for two-way slabs must be done for two directions.

4.3.2 Conservation of kinetic energy

To conserve the kinetic energy E_k between a slab and a 2DOF system, the energy can be written as

$$E_k = \frac{m \cdot v_s^2}{2} = \int_{y=0}^{y=l_y} \int_{x=0}^{x=l} \frac{m'(x, y) \cdot v(x, y)^2}{2} \, dxdy \tag{4.36}$$

where v_s is the velocity at the system point, $m'(x,y)$ is the mass per unit length and $v(x,y)$ is the velocity per unit length. By using that

$$v_s = \frac{\Delta u_s}{\Delta t} \tag{4.37}$$

and

$$v(x, y) = \frac{\Delta u(x, y)}{\Delta t} \tag{4.38}$$

where Δu_s and $\Delta u(x,y)$ are the displacements at the system point and along the slab, equation (4.36) for a slab with constant mass $m'(x,y) = m'$, can be expressed as

$$m \cdot u_s^2 = \frac{m_e}{l_x \cdot l_y} \int_{y=0}^{y=l_y} \int_{x=0}^{x=l_x} u(x, y)^2 \, dxdy \tag{4.39}$$

By combining

$$m = \kappa_m \cdot m_{sl} \tag{4.40}$$

and equation (4.39) it is possible to express the transformation factor κ_m as

$$\kappa_m = \frac{1}{l_x \cdot l_y} \int_{y=0}^{y=l_y} \int_{x=0}^{x=l_x} \frac{u(x, y)^2}{u_s^2} \, dxdy \tag{4.41}$$

4.3.3 Conservation of external work

To conserve the kinetic energy W_e between a slab and a 2DOF system the energy can be written as

$$W_e = F \cdot u_s = \int\limits_{y=0}^{y=l_y} \int\limits_{x=0}^{x=l_x} q(x, y) \cdot u(x, y) dx dy \qquad (4.42)$$

where $q(x,y)$ is the load per unit length. The external force F_{sl} for a slab with constant uniformly distributed load $q(x,y) = q$ can be expressed as

$$F_{sl} = \int\limits_{y=0}^{y=l_y} \int\limits_{x=0}^{x=l_x} q(x, y) dx dy = \int\limits_{y=0}^{y=l_y} \int\limits_{x=0}^{x=l_x} \frac{F_{sl}}{l \cdot w} dx dy \qquad (4.43)$$

By combining

$$F = \kappa_F \cdot F_{sl} \qquad (4.44)$$

with equation (4.42) and (4.43) it is possible to express the transformation factor κ_F as

$$\kappa_F = \frac{1}{l_x \cdot l_y} \int\limits_{y=0}^{y=l_y} \int\limits_{x=0}^{x=l_x} \frac{u(x, y)}{u_s} dx dy \qquad (4.45)$$

For a constant distributed load $q(x,y) = q$, with an arbitrary area of distribution which acts at $x = x_1$ to $x = x_2$, and $y = y_1$ to $y = y_2$, the transformation factor κ_F can be expressed as

$$\kappa_F = \frac{1}{(x_2 - x_1)(y_2 - y_1)} \int\limits_{y=y_1}^{y=y_2} \int\limits_{x=x_1}^{x=x_2} \frac{u(x, y)}{u_s} dx dy \qquad (4.46)$$

As for a beam subjected is the transformation factor $\kappa_F = 1$ for a slab subjected to a point load.

4.3.4 Conservation of internal work

As for beams the transformation factors regarding internal and external work are equal, according to Biggs (1964)

$$\kappa_k = \kappa_F \qquad (4.47)$$

4.4 Derivation of transformation factors for a slab

4.4.1 Orientation

A slab is significantly more complex than a beam, which gives a multitude of combinations regarding geometry, boundary conditions and placement of the load. With regard to this, only a limited number of combinations are investigated and only for a quadratic slab. Three load cases are chosen for further evaluation and the slab is modelled as simply supported on all four sides. The slab and the three load cases are presented in Figure 4.5. Unlike for beams, the transformation factors for slabs cannot be as easily derived analytically and a numerical FE analysis is therefore used instead.
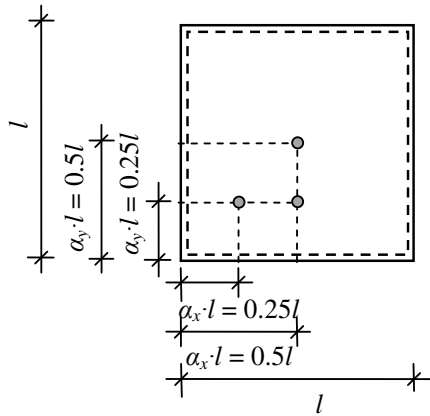
Figure 4.5   Illustration of the points for the applied point load at the reinforced concrete slab which is used for derivation of the transformation factors κ_{mF}. The points are defined using the length factors α_x and α_y and the simply supported quadratic slab has the side length l.

4.4.2   Elastic response for a point load

The FE analysis for the evaluation of the transformation factors in this thesis for cases with elastic response uses shell elements and is described more thoroughly in Chapter 5. Because of the shell elements being sensitive to stress concentrations, the point load is distributed over a small area, which is described more in detail in Section 5.4. This will influence the value of the transformation factor κ_F to a value less than one, i.e. $\kappa_F < 1$. The transformation factors are numerically derived according to Section 4.3 from FE analyses, see Appendix H.2. The derived transformation factors for the three load cases are presented in Table 4.1. The length factors α_x and α_y are defined as illustrated in Figure 4.5. Load case 1-3 is used for the remaining slab analysis conducted in this thesis.

Table 4.1   Transformation factors κ_m, κ_F, κ_{mF}, slab stiffness k_{sl} and displacement at the system point u_s for load case 1-3 with a load of 100 kN.

	Load case 1	Load case 2	Load case 3
α_x [-]	0.5	0.5	0.25
α_y [-]	0.5	0.25	0.25
κ_m [-]	0.200	0.231	0.236
κ_F [-]	0.987	0.982	0.977
κ_{mF} [-]	0.203	0.235	0.241
k_{sl} [MN/m]	10.79	15.94	22.02
u_s [mm]	9.27	6.27	4.54
γ_{sl} [m/GN]	655.5	655.5	655.5

It should be noted that these transformation factors are unique for these load cases and only for quadratic slabs with elastic response. The values of the transformation factors are also unique for the length-thickness ratio l / t of the slab. In this thesis, a quadratic slab with length $l = 5.6$ m and thickness $t = 0.2$ m is used which gives a length-

thickness ratio $l / t = 28$. In fact, the values of the transformation factors are valid for an arbitrary slab with the same length-thickness ratio, Johansson (2014).

In Johansson (2014), transformation factors and slab stiffness are derived and presented for different load cases and different slabs. The values of κ_{mF} in Table 4.1 differ a bit from the corresponding values in Johansson, where a length-thickness ratio of 20 is used. However, the difference between the transformation factor κ_{mF} presented in Table 4.1 and in Johansson is approximately 0.4 %, 1.4 % and 3.2 % for load case 1-3 and can arguably be considered negligible. This difference can also be a result of the difference in the number of element used in each model.

As for the beam, κ_{mF} and k_{sl} grows larger when the load and the system point are closer to the support, as can be seen in Table 4.1. It should be noted that k_{sl} is unique for these set of properties and load cases. However, it is possible to express any slab stiffness without having to do a FE analysis for cases with an elastic response of the slab, Johansson (2014). The equivalent stiffness k_2 of an arbitrary slab can be calculated as

$$k_2 = \frac{\gamma_{sl}}{\gamma_2} \cdot k_{sl} \tag{4.48}$$

where

$$\gamma = \frac{l^2}{E \cdot t^3} \tag{4.49}$$

is a factor which considers the length of the slab l, the Young's modulus E and the slab thickness t. The factor γ_{sl} is the ratio for the slab which k_{sl} is calculated for while γ_2 is the ratio for an arbitrary quadratic slab.

4.4.3 Theoretical plastic response for a point load

For a simply supported slab with plastic response, the displacement $u(x,y)$ varies linearly when subjected to a point load as handled in Section 2.8.3, see Figure 4.6.
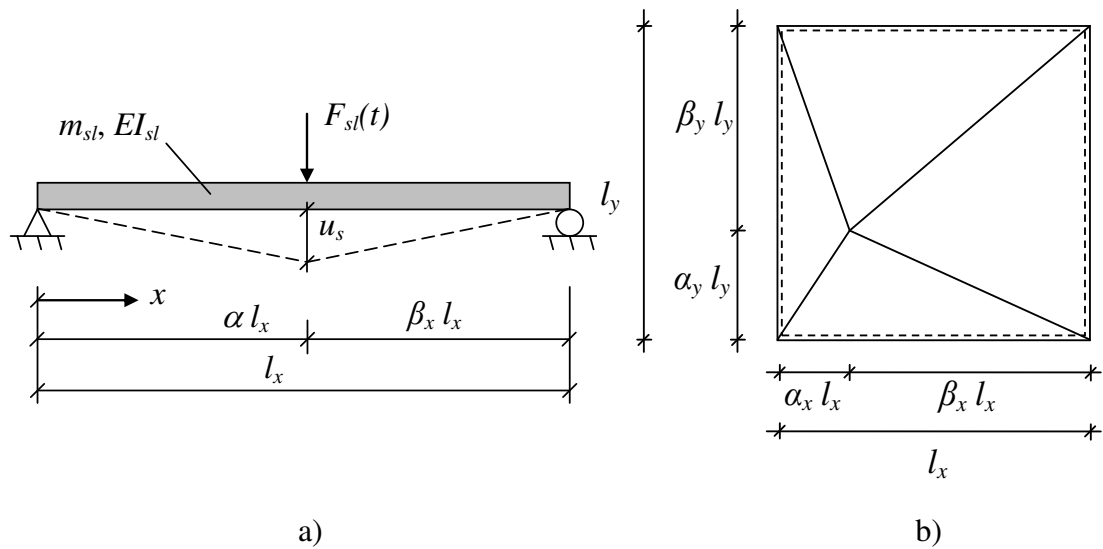
Figure 4.6   Illustration of a simply supported slab with plastic response subjected to a point load a) section, and b) plane.

The plastically deformed slab illustrated in Figure 4.6 has the shape of a pyramid and $\kappa_{m,pl}$ can be derived analytically with equation (4.41). To be able to solve the integral in this equation, the slab is divided into four parts according to Figure 4.7.
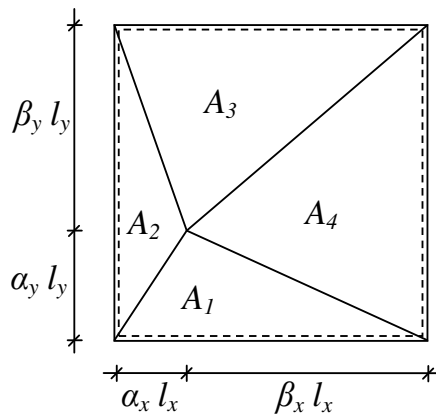
Figure 4.7   Illustration of a simply supported slab with plastic response divided into four areas A_1, A_2, A_3 and A_4.

If the displacement $u(x,y)$ is stated as a function of u_s instead of the force F_{sl}, it can be written as

$$u(x,y) = \begin{cases} \dfrac{y}{\alpha_y \cdot l_y} \cdot u_s, & A_1 \\[2ex] \dfrac{x}{\alpha_x \cdot l_x} \cdot u_s, & A_2 \\[2ex] \left(1 - \dfrac{y}{l_y}\right) \cdot \dfrac{u_s}{\beta_y}, & A_3 \\[2ex] \left(1 - \dfrac{x}{l_x}\right) \cdot \dfrac{u_s}{\beta_x}, & A_4 \end{cases} \qquad (4.50)$$

By inserting equation (4.50) into equation (4.41) and using the fact that the transformation factor $\kappa_{F,pl} = 1$ for a case with a slab subjected to a point load, $\kappa_{mF,pl}$ can be written as

$$\kappa_{mF,pl} = \frac{1}{l_x \cdot l_y \cdot u_s^2} \cdot \left(\begin{array}{l} \iint\limits_{A_1} \left(\frac{y}{\alpha_y \cdot l_y} \cdot u_s \right)^2 dA + \iint\limits_{A_2} \left(\frac{x}{\alpha_x \cdot l_x} \cdot u_s \right)^2 dA + \\ + \iint\limits_{A_3} \left(\left(1 - \frac{y}{l_y} \right) \cdot \frac{u_s}{\beta_y} \right)^2 dA + \iint\limits_{A_4} \left(\left(1 - \frac{x}{l_x} \right) \cdot \frac{u_s}{\beta_x} \right)^2 dA \end{array} \right) \tag{4.51}$$

The integral for part A_1 becomes

$$\frac{1}{l_x \cdot l_y \cdot u_s^2} \cdot \left(\int\limits_{y=0}^{y=\alpha_y \cdot l_y} \int\limits_{x=\frac{\alpha_x \cdot l_x}{\alpha_y \cdot l_y} \cdot y}^{x=l_x - \frac{\beta_x \cdot l_x}{\alpha_y \cdot l_y} \cdot y} \left(\frac{y}{\alpha_y \cdot l_y} \cdot u_s \right)^2 dxdy \right) =$$

$$\frac{1}{l_x \cdot \alpha_y^2 \cdot l_y^3} \cdot \left(\int\limits_{y=0}^{y=\alpha_y \cdot l_y} \int\limits_{x=\frac{\alpha_x \cdot l_x}{\alpha_y \cdot l_y} \cdot y}^{x=l_x - \frac{\beta_x \cdot l_x}{\alpha_y \cdot l_y} \cdot y} y^2 dxdy \right) = \dots = \frac{\alpha_y}{12} \tag{4.52}$$

Area 2, 3 and 4 are calculated in the same fashion and by using the fact that $\alpha_x + \beta_x = \alpha_y + \beta_y = 1$, $\kappa_{mF,pl}$ becomes

$$\kappa_{mF,pl} = \frac{\alpha_y}{12} + \frac{\alpha_x}{12} + \frac{\beta_y}{12} + \frac{\beta_x}{12} = \frac{1}{12} \cdot (1+1) = \frac{1}{6} \tag{4.53}$$

5 FE Modelling

5.1 Orientation

This chapter covers how the incoming object and the resisting structure are modelled with FE software for this thesis. It is the FE software ADINA (2014) 900 Nodes Version 9.0 that is used and as the name implies, a maximum of 900 nodes can be used. The slab geometry and element size examined is largely based on this limit.

During the uncracked state, state I, of the reinforced concrete behaviour the reinforcement has a small influence on the total stiffness and the beam can be simplified to a solid concrete beam. However, in the cracked state, state II, the reinforcement has a large influence on the stiffness and must therefore be considered. In this thesis, the focus is not on modelling each state of the concrete behaviour thoroughly, thus the more roughly estimated elasto-plastic behaviour discussed in Section 2.8 is enough.

Based on this, it is sufficient to model the elastic part of the reinforced concrete as one equivalent material based on state II, instead of modelling the reinforcement and concrete separately in the commercial software ADINA. In this thesis, the equivalent material is modelled with an equivalent Young's modulus when shell elements are used, and manually implemented moment-curvature and torsion-twisting relations when beam elements are used.

For the FE slab models of this thesis, both a shell element model and a beam grillage model are evaluated. The beam grillage model uses a grid with beams in two directions, where the beams are modelled with beam elements. The usage of shell and beam elements for slabs is more thoroughly described in Section 5.4 and Section 5.5.

5.2 Equivalent Young's modulus

The cross-section defined in ADINA is the cross-section of state I, hence the moment of inertia I that is calculated by ADINA is I_I. Therefore, the input value for the Young's modulus in ADINA is a reduced equivalent Young's modulus E_{eq} so that the stiffness of state II is used. The equivalent Young's modulus is calculated as

$$E_{eq} = \frac{I_{II}}{I_I} E_{cm} \tag{5.1}$$

where E_{cm} is the mean Young's modulus of the concrete and I_I and I_{II} are the moments of inertia for state I and state II, respectively. The stiffness used by ADINA is then

$$EI_b = E_{eq} I_I = \frac{I_{II}}{I_I} E_{cm} I_I = E_{cm} I_{II} \tag{5.2}$$

where EI_b is the stiffness of the beam in state II. However, Young's modulus is not an input to ADINA when using moment-curvature relations, which is explained further in Section 5.5.2. Hence, the equivalent Young's modulus E_{eq} is only used for FE models modelled with shell elements.

5.3 Elasto-plastic response for the incoming object

As described in Section 3.2.4, body 1 should have an elasto-plastic response in compression and no tensile stiffness. However, no element type in the commercial software ADINA (2014) can account for this. It is possible to model a non-linear elastic spring element in ADINA. A comparison between the response of body 1 modelled with a 2DOF and a FE model using non-linear elastic spring element, is illustrated in Figure 5.1. In both Figure 5.1a and Figure 5.1b it can be observed that there has not occurred any plastic deformation, where the shape of the loading and the unloading stage is the same. The 2DOF model and the FEM model are giving identical results.

a)   b)
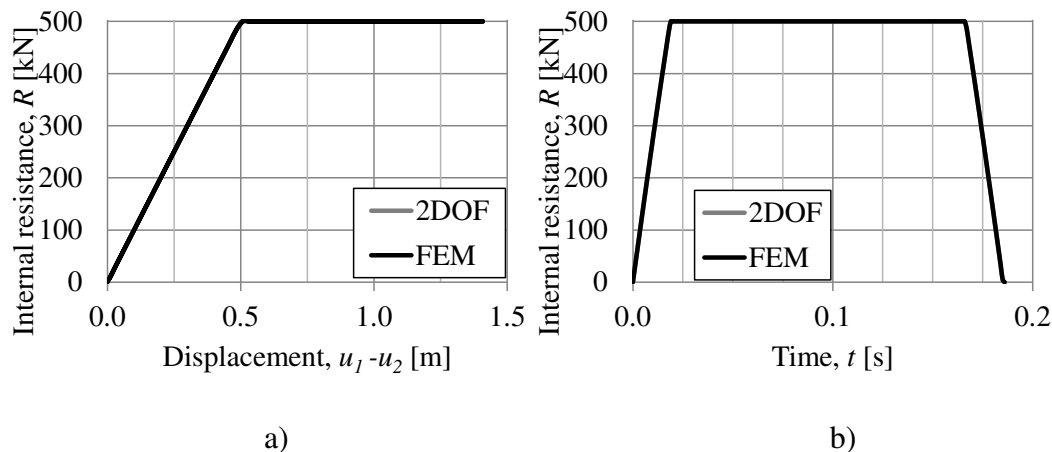
Figure 5.1   *Comparison between a 2DOF model and the corresponding FE model with a non-linear spring for the same case as the elasto-plastic case. a) Internal resistance R as a function of difference in displacement $u_1 - u_2$, and b) internal resistance R as a function of time t.*

To account for plastic deformations, a spring element cannot be used. For the plastic deformations, a truss element can instead be used, but it requires the same compressive and tensile properties. In order to be able to model the elasto-plastic response, and have different properties in compression and tension, a spring element is combined with a truss element. The spring element acts as a non-linear elastic member until the plastic limit is reached, whilst the truss element acts as an elasto-plastic member, which account for plastic deformations, see Figure 5.2.
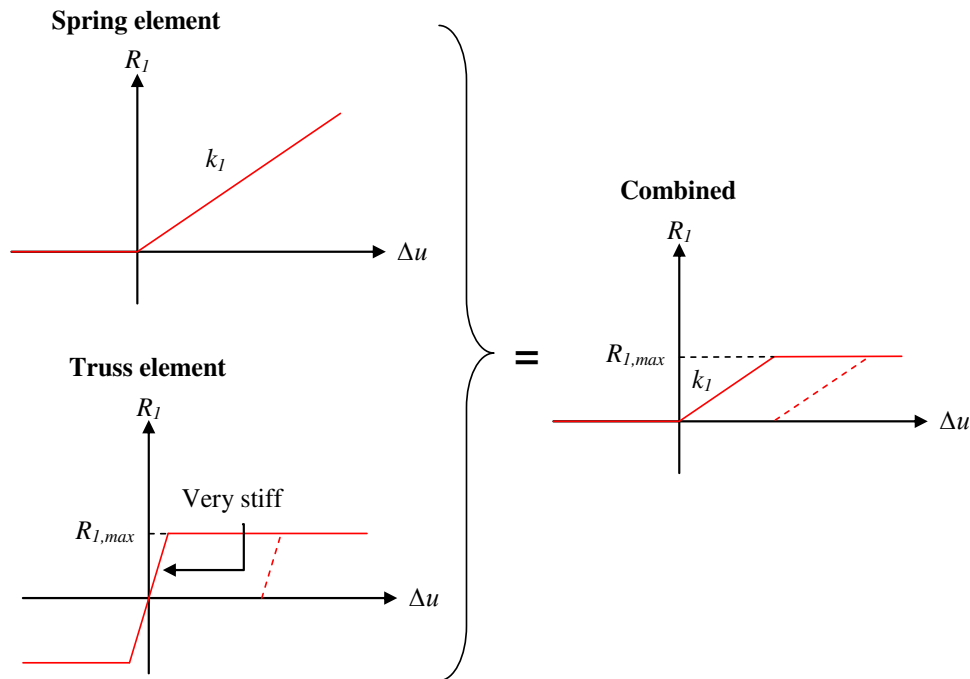
Figure 5.2   Illustration of how the properties of a spring and truss element are combined to simulate the elasto-plastic behaviour of body 1.

In Figure 5.3b it can be observed that there has indeed occurred a plastic deformation, where there is a different shape between the loading and the unloading stage. In Figure 5.3 the elasto-plastic response of the 2DOF and the FEM model can be observed and both models have identical response.

a)   b)
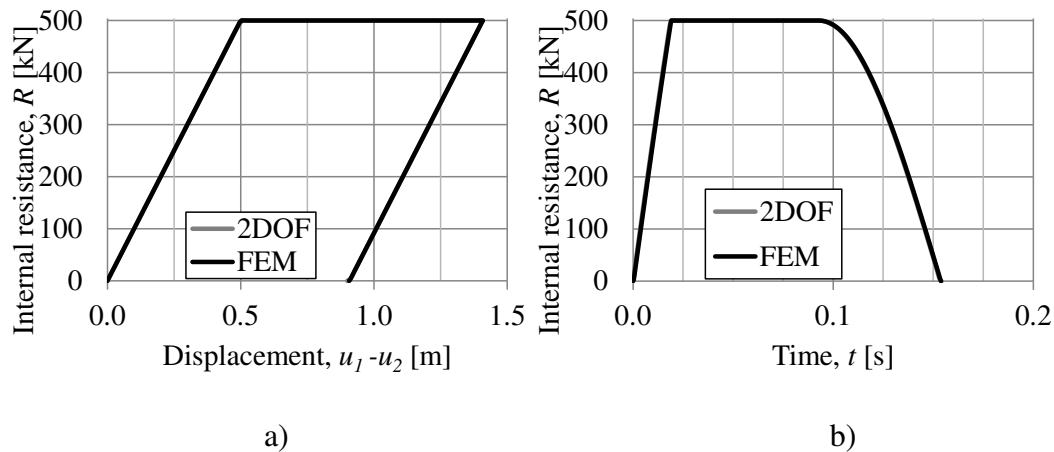
Figure 5.3   Comparison between a 2DOF model and the corresponding FE model with elasto-plastic response of body 1 and elastic response of body 2 with a time step of h = 0.3 ms. a) Internal resistance R as a function of difference in displacement $u_1 - u_2$, and b) internal resistance R as a function of time t.

The truss element in ADINA is not fully plastic but rather elasto-plastic. It has a stiffness *k* which is chosen to be as large as possible for the model to be stable. Which is found to be approximately 1 GN/m for the cases in this thesis, which gives satisfying results as observed in Figure 5.3.

The choice of time step in ADINA is critical and can result in major differences. By using a time step of $h = 0.3$ ms, no visible difference between the 2DOF and the FE analysis will be seen, as can be observed in Figure 5.3. Whilst a time step of $h = 1$ ms will result in a noticeable difference between the two analyses as illustrated in Figure 5.4. The results even suggest that the FE analysis is modelled with an initial internal resistance, which of course is false.
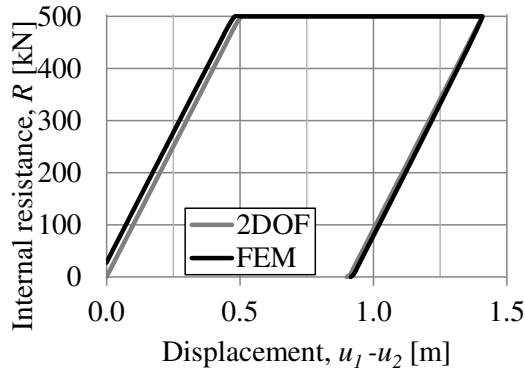
Figure 5.4   Comparison between a 2DOF model and the corresponding FE model with elasto-plastic response of body 1 and elastic response of body 2 with a time step of h = 1 ms.

The model with a non-linear elastic spring element without a truss element does not account for the plastic deformations and when compared to the elasto-plastic model there is a difference in the response of body 2. The displacement of body 2 u_2 as a function of time for both models is illustrated in Figure 5.5. As can be observed, the main difference between the two models is during the unloading stage and after the collision. However, if the purpose of the analysis is to find the maximum value or the response after collision, it might be sufficient to model the incoming object with a non-linear elastic spring element. Although, it is uncertain if this model is valid if body 2 is subjected to multiple collisions after each other, since the plastic deformation then will have a larger influence. The model with a non-linear elastic spring element without a truss element is therefore not further used in this thesis.
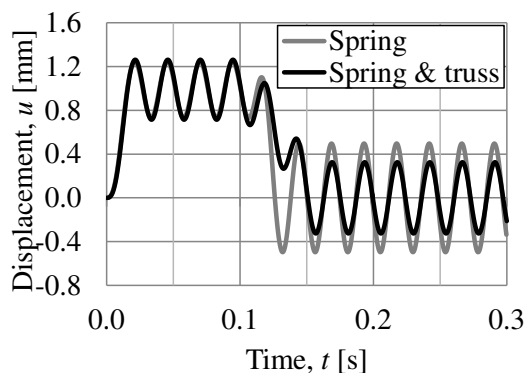
Figure 5.5   Comparison between the displacement of body 2 u_2 for the FE model with a non-linear spring and the elasto-plastic case modelled with a spring and a truss.

5.4 Shell elements

It is possible to model slabs with shell elements in the commercial software ADINA (2014) and it is shell elements that are used when deriving the transformation factors in Section 4.4. In this thesis, for all the FE models with shell elements, 28 x 28 4-node shell elements are used together with a length-thickness ratio of $l / t = 28$ for the slab. Normally a Poisson's ratio of $v = 0.2$ is used for reinforced concrete. However, since beams deform only in one direction, $v = 0$ is chosen throughout this thesis for better consistency between the shell element and beam grillage model which is treated in Section 5.5.1.

However, there are some issues when using shell elements that must be taken into account. When applying a point load to a slab modelled with shell elements, an unreasonable large deformation will occur at the node where the load is applied, because of the shell elements being sensitive to high stress concentrations. To avoid this error the point load can be distributed over a small area as illustrated in Figure 5.6. In this thesis the area in which the point load is distributed over is chosen to have a side length of twice the element length $c = 2l_e = 0.4$ m. This is the smallest area that can be used if the centre of the distributed load should remain in the same point as where the point load is applied.
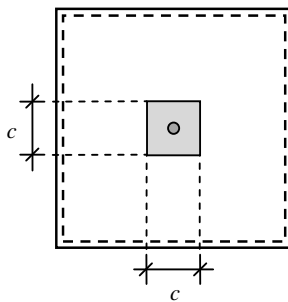
Figure 5.6 Illustration of how a point load can be distributed over an area with a side length c.

The difference in displacement at the system point u_s between applying the load as a static point load and as a static distributed point load is illustrated in Figure 5.7. Even though the difference seems to be small, it will have an influence of large magnitude since the displacement at the system point u_s is squared in the derivation of the transformation factor κ_m, see Section 4.1.2. For the models subjected to dynamic loads, the load is distributed in the same manner because otherwise a local instability in the node where the load is applied will occur for slabs with elasto-plastic response.

a)   b)
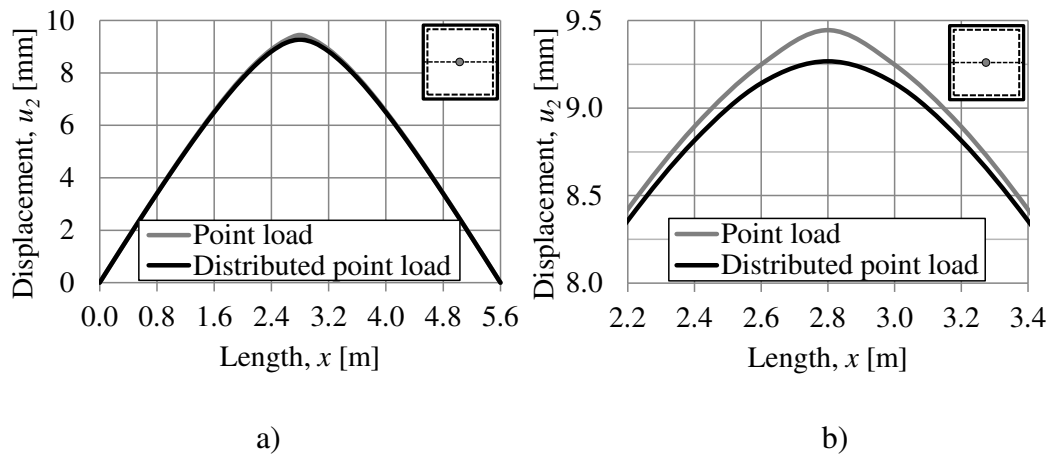
Figure 5.7   *Comparison of the displacement u_2 along a line described in the upper right hand corner, between a point load and a distributed point load. The maximum displacement illustrated is at the system point. For a) the whole slab, and b) magnified.*

When modelling slabs with plastic or elasto-plastic response in ADINA using shell elements, there will be an unintended increase of the moment capacity. This is due to that ADINA uses von Mises plastic theory and thereby automatically uses a Poisson's ratio of $v = 0.5$ during the plastic phase, no matter what input value that is given, Augustsson and Härenstam (2010). However, this phenomenon will not appear when using a beam grillage model, which is further discussed in Section 5.5.1.

To be able to verify the beam grillage model, an elasto-plastic shell element model is made for comparison even though the problem with $v = 0.5$ during the plastic phase still exists. In ADINA, the stress distribution is described by a polynomial of order six as illustrated in Figure 5.8b, Augustsson and Härenstam (2010).

a)   b)
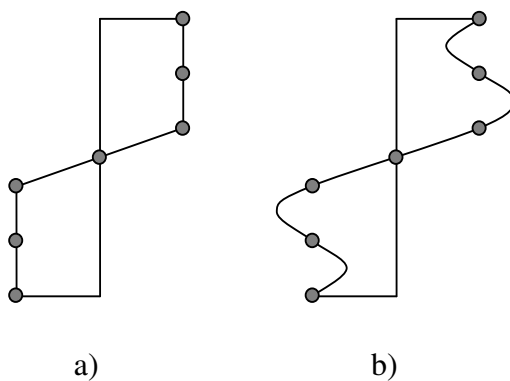
Figure 5.8   *Illustration of the a) expected stress distribution with seven integration points, and b) stress distribution with seven integration points used by ADINA.*

The stress distribution in Figure 5.8b will result in a lower section modulus W and therefore a lower bending moment resistance than the stress distribution in Figure 5.8a, since $M_{Rd} = W \cdot f_y$. To gain the same bending moment resistance as the stress distribution in Figure 5.8a, a modified yield stress $f_{y,mod}$ is used in ADINA. This modified yield stress can be expressed for rectangular homogenous cross section as

$$f_{y,mod} = \frac{1}{\alpha} f_y \qquad (5.3)$$

where α is a correction factor. In this thesis is $\alpha = 0.231$ used, which is derived in Augustsson and Härenstam (2010).

5.5 Beam elements

5.5.1 Beam grillage

A grillage of beams using beam elements can be used when studying an elasto-plastic response of a slab. This simplified method uses a grid with beams in two directions, where the width of each beam w_b is equal to the spacing between the beams as illustrated in Figure 5.9.
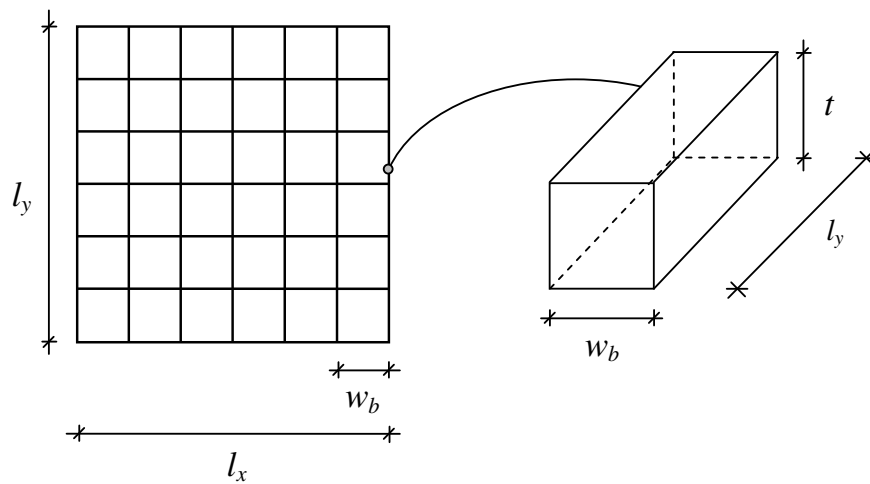
Figure 5.9   Illustration of the beam grillage model with evenly distributed beams in two directions creating a slab.

It should be noted that this grid will cause the beams to overlap in each intersection of the nodal points. Hence, the beam grillage will have a mass which is twice the intended. The solution which is used in this thesis to solve this issue is to reduce the density ρ to half of the intended value. However, this will change the velocity of the propagating impulse wave c in the material, see equation (5.4), Carlsson and Kristensson (2012). However, the frequencies will remain unchanged and this solution will therefore be sufficient.

$$c = \sqrt{\frac{E}{\rho}} \qquad (5.4)$$

An important advantage with the beam grillage model is that the behaviour of the beam elements can be manually controlled by using moment-curvature and torsion-twisting relations, which are treated in Section 5.5.3. This means that the problem during the plastic phase with shell elements, discussed in Section 5.4 with a Poisson's ratio of $v = 0.5$, will not exist. Another advantage with a beam grillage model is that, orthotropic behaviour, different reinforcement arrangement in different sections, and

different amount of reinforcement in top and bottom can be modelled. In this thesis the properties of the studied slab is equal for both directions and in all sections.

The problem with stress concentration occurring when applying a point load using shell elements discussed in Section 5.4 can be avoided by using a beam grillage model. Therefore, the load for both the static analysis and the dynamic analysis are acting in one point for the beam grillage model, and does not need to be distributed.

Beam elements with the beam width w_b equal to the slab thickness t will give the best results for the FE analysis using beam grillage, Lim (2013). A reinforced concrete slab with a thickness of $t = 0.2$ m is used in this thesis, hence the beam width in the beam grillage model $w_b = 0.2$ m. However, this can be seen as a disadvantage since it limits the width of the elements to the thickness of the slab.

In Figure 5.10, the local coordinate system of the beam elements and the global coordinate system used by ADINA (2014) are illustrated. As can be observed, the local coordinate system uses r, s and t and the global uses X, Y and Z directions. The main local axes that are used for the beam grillage are r and s. It is around the s axis that the main bending occurs and it is around the r axis that torsion occurs.
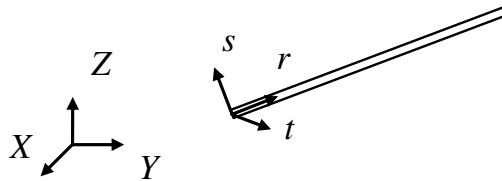
Figure 5.10   Illustration of the global and local coordinate system for beam elements.

5.5.2   Moment-curvature relation

To ensure that the model behaves as intended, the behaviour of the resisting structure can be modelled with moment-curvature and torsion-twisting relations, that are directly implemented in the commercial software ADINA (2014). This is only done for beams and slab models using beam elements.

For the elasto-plastic cases, the moment-curvature relation used in ADINA is based on the principle which is discussed in Section 2.8 and illustrated in Figure 2.22. This means that the beam elements have linear elastic response with the stiffness of state II until the moment capacity of state III is reached, M_{Rd}. The corresponding curvature at this point is calculated as

$$\left(\frac{1}{r}\right)_{pl} = \frac{M_{Rd}}{EI_b} \tag{5.5}$$

and for larger curvatures, the beam has a plastic response with no limit in curvature. This is illustrated in Figure 5.11.
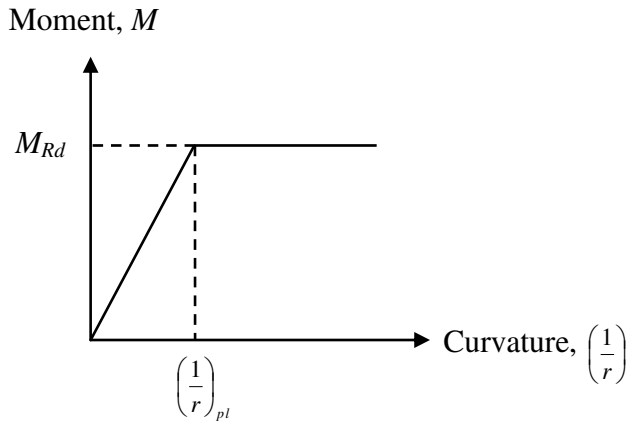
Figure 5.11   Illustration of an ideal moment-curvature relation.

In ADINA, it may be difficult to obtain convergence in the analysis if the inclination of the moment-curvature relation in the plastic region is zero. Therefore, a small inclination in this part is used which can be changed depending on how stable the model is. In Figure 5.12a, an applied load-displacement curve is presented from the results of an ADINA model for a beam where moment-curvature relation is used. This relation curve can be used to check if the beam behaves as it should and that the moment-curvature relation is valid. In Figure 5.12b the same applied load-displacement curve is presented but with a longer displacement range. For such a relation curve it can also be observed how stable the model is by seeing how large the displacement can be before the model stops to work. If the model cannot handle a sufficiently large plastic displacement, a steeper plastic inclination can be used for the moment-curvature relation. As can be seen in Figure 5.12b, a small inclination is used for the plastic part.

a)

b)
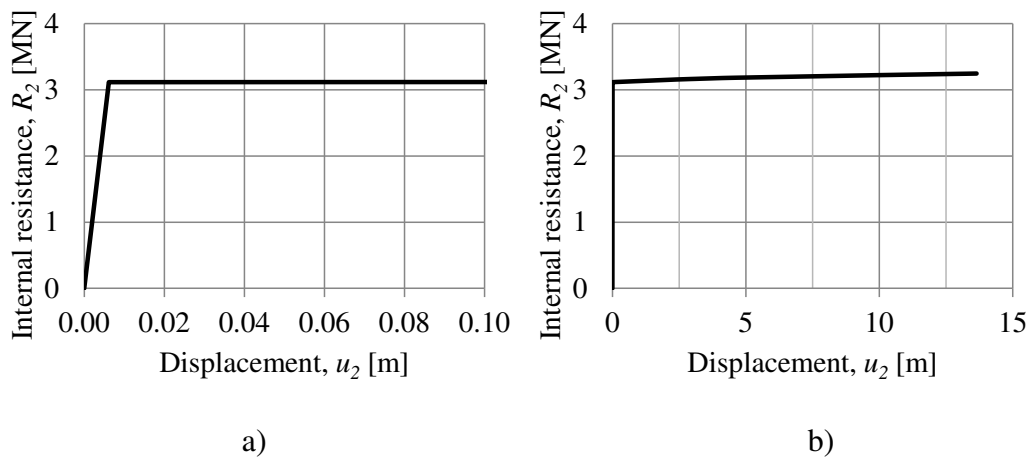
Figure 5.12   Illustration of the load-displacement relation used in the FE analysis a) curve illustrating elastic and plastic part, and b) same curve illustrating the full range of the displacement until the model collapses.

The inclination of the plastic part of the moment-curvature relation which is used in this thesis is illustrated in Figure 5.13. This inclination results in a small error, but this is deemed to be small and negligible. When modelling slabs with beam elements the moment-curvature is used in a corresponding way.

Moment, M

$1.05M_{Rd}$

M_{Rd}

Curvature, $\left(\frac{1}{r}\right)$

$\left(\frac{1}{r}\right)_{pl}$

100 m^{-1}
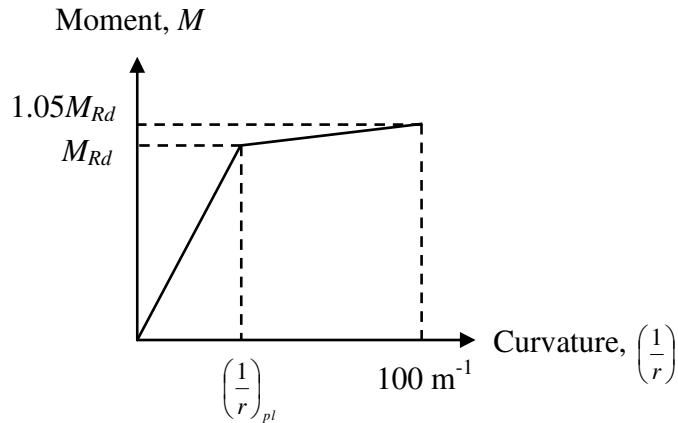
Figure 5.13   Illustration of the inclination of the plastic part of the moment-curvature relation used in the FE analyses.

In this thesis, the yield curvature is $(1/r)_{pl} = 2.56\cdot10^{-3}$ m^{-1} for the beam and $(1/r)_{pl} = 17\cdot10^{-3}$ m^{-1} for the beams in the beam grillage model.

5.5.3   Torsion-twisting relation

As for moment-curvature relation, a torsion-twisting relation for the beam elements is manually added to the FE model in the commercial software ADINA (2014). The torsion-twisting relation is added as a fully linear relation that represents the cracked cross-section of state II. Torsional moments do not matter when analysing two dimensional beams, but for the beam grillage model it is essential. The torsional stiffness and its corresponding torsion-twisting relation is calculated and presented in Appendix G. A torsional stiffness which corresponds to the stiffness of a cracked cross-section $T_{II}(\varphi)$, is used in this thesis. The torsional stiffness can be expressed as

$$T_{II}(\varphi) = \frac{I_{II}}{I_{I}} T_{I}(\varphi) \qquad (5.6)$$

where $T_{I}(\varphi)$ is the torsional stiffness of an uncracked cross-section and $T_{II}(\varphi)$ is the torsional stiffness of a cracked cross-section.

In Table 5.1 the results for different ways to model the torsional stiffness are presented, where model 1 and 2 uses the torsional stiffness calculated by ADINA. For model 3 to 6 the torsion-twisting relation is manually inserted and the torsion used in the current model is defined as $T(\varphi)$. The values in Table 5.1 are calculated from the reinforced concrete slab used in this thesis, where the moment of inertia ratio is $I_{II} / I_{I} = 0.181$, see Appendix G. The input data of the studied slab is more thoroughly presented in Section 6.2.1.

Table 5.1   *Comparison between different methods to model the torsional stiffness $T(\varphi)$. The values are based on the slab used in this thesis, presented in Section 6.2.1, where the moment of inertia ratio is $I_{II} / I_I = 0.181$.*

Model	κ_{mF} [-]	k_{sl} [MN/m]	u_s [mm]	f [Hz]
Model 1: Shell element	0.203	10.79	9.27	8.98
Model 2: Beam grillage with default moment-curvature and torsion-twisting	0.197	10.35	9.67	8.87
Model 3: Beam grillage with $T(\varphi) = T_{II}(\varphi) = 0.181T_I(\varphi)$	0.196	10.31	9.70	8.87
Model 4: Beam grillage with $T(\varphi) = T_I(\varphi)$	0.168	28.77	3.48	15.44
Model 5: Beam grillage with $T(\varphi) = 0.1T_I(\varphi)$	0.203	8.27	12.10	7.87
Model 6: Beam grillage with $T(\varphi) = 0.001T_I(\varphi)$	0.212	5.68	17.60	6.45

As can be observed from Table 5.1, the transformation factor κ_{mF}, the stiffness k_{sl} and the fundamental eigenfrequency f of the beam grillage model is highly dependent on the torsional stiffness, especially for model 4 where the torsional stiffness of an uncracked section is used. The results of model 6 are also relatively different compared to the other models, but model 6 uses a torsional stiffness $T(\varphi)$ that is far from $T_{II}(\varphi)$, compared to model 4 which uses a $T(\varphi)$ that is relatively close to $T_{II}(\varphi)$. It is not uncommon to have a moment of inertia ratio I_{II} / I_I lower than the one used in this thesis. For such cases, a model using the torsional stiffness of an uncracked section will be even more deviant.

The displacement u_2 along a straight line is presented in Figure 5.14a and in Figure 5.14b, where the line is presented in each figure. In Figure 5.14a it can be noted that model 4 has a deviant shape and it can be the reason why the transformation factor κ_{mF} differs so much for this model. The difference between model 3 and model 4 is greater in Figure 5.14b than in Figure 5.14a which means that the beam grillage model corresponds to shell elements better in the centre of the slab than closer to the supports.
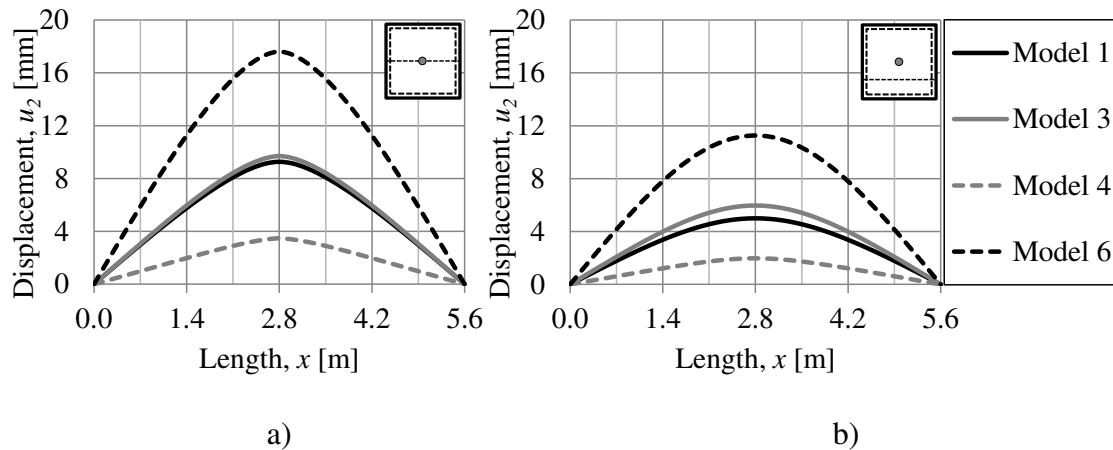
Figure 5.14 *Comparison between four methods to model the torsional stiffness T(φ) for a load of 100 kN, a) displacement u_2 along a straight line described in the upper right hand corner, and b) displacement u_2 along a straight line described in the upper right hand corner.*

When calculating the moment distribution in a slab by hand with either strip method or yield line method, see Section 2.8.3, the slab is considered to have lost all its torsional stiffness, therefore the stiffness is set to zero, Engström (2014). However in reality some torsional stiffness still exists even though the slab is in state II.

The importance of torsional stiffness is not further analysed in this thesis, and a torsional stiffness of $T(φ) = T_{II}(φ)$ is chosen. This is because the torsional stiffness T_{II} corresponds well to the stiffness which is used by ADINA when analysing slabs with shell elements and a comparison between the two FE models can be conducted.

6 Comparison between 2DOF and FE Models

6.1 Comparison for a beam

6.1.1 Orientation

In the FE analysis a simply supported reinforced concrete beam is analysed, which can be compared to a 2DOF model with a barrier. For simplicity the reinforcement is placed symmetrically in equal amounts at the top and bottom of the beam as illustrated in Figure 6.1. The FE analysis is carried out with the commercial software ADINA (2014).
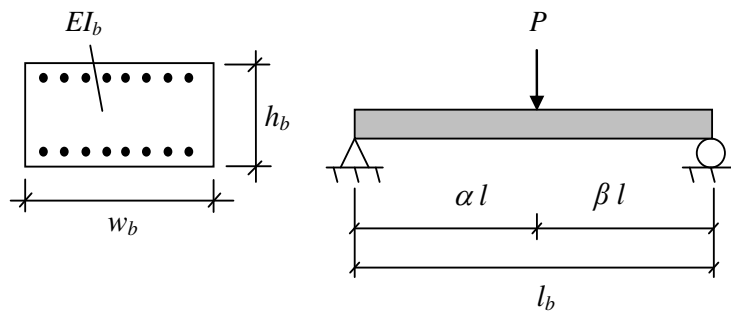
Figure 6.1   The simply supported reinforced concrete beam with stiffness EI_b, width w_b, length l_b, height h_b and the load placement factors α and β.

The geometry and parameters of the beam used in the FE model are presented in Table 6.1. The material and cross-sectional properties presented are calculated in the same manner as the calculations presented in Appendix G, where the properties of the beams in the beam grillage model are calculated. The properties in Table 6.1 are used for both elastic and elasto-plastic beams, but for elastic cases the moment-curvature relation continues to be linear elastic after the moment capacity is reached.

The chosen beam presented in Table 6.1 is very large and has therefore a very large mass m_b of 15 000 kg. The reason for this is that the beam, which in the 2DOF model represents body 2, should have a mass after multiplication with the transformation factor κ_{mF} that is approximately equal to 7 500 kg, which is the mass m_2 used earlier in this thesis.

The comparison for beams is conducted for elastic body 1 and body 2, elasto-plastic body 1 and elastic body 2 and finally, elastic body 1 and elasto-plastic body 2. Not so many collisions are analysed for beams, since the main interest of this thesis is slabs.

Table 6.1 *Properties of the simply supported reinforced concrete beam, with corresponding input parameters to ADINA.*

Length l_b	5 m
Height h_b	1 m
Width w_b	1.25 m
Mass m_b	15 000 kg
Density ρ_c	2 400 kg/m^3
Concrete class	C30/37
Concrete Young's modulus E_{cm}	33 GPa
Reinforcement	B500B Φ16 s200
Reinforcement Young's modulus E_s	200 GPa
Concrete cover c	40 mm
Moment capacity M_{Rd}	519 kNm
Yielding curvature $\left(\dfrac{1}{r}\right)_{pl}$	$2.56 \cdot 10^{-3}$ m^{-1}

The stiffness of body 2 k_2, used in the 2DOF model, is calculated for a beam according to equation (4.31), as

$$k_b = \frac{3EI_b}{l^3 \alpha^2 \beta^2} \tag{6.1}$$

6.1.2 Elastic body 1 and body 2

To be able to perform valid comparisons between 2DOF and FEM for slab and beam collisions with elasto-plastic response, the 2DOF and FEM models are verified for an elastic beam collision case. This is evaluated more thoroughly in the precedent master's thesis Asplund and Steckmest (2014).

A collision with elastic response for both involved bodies is evaluated and the bodies have properties according to Table 6.1 and Table 6.2.The position of the point load is represented by the factor α and is illustrated in Figure 4.3.

Table 6.2 *2DOF input parameters for collision E1 with an elastic response for both body 1 and body 2.*

Case	α [-]	κ_{mF} [-]	k_1 [MN/m]	k_2 [MN/m]	m_1 [kg]
Collision E1	0.5	0.486	1.0	77.8	1 500

The parameters are chosen so that they approximately correspond to the collision examples presented in Chapter 3. The parameters m_2, E_{eq}, EI_b and k_b for the 2DOF model are calculated according to Section 4.2.2.

The displacement for body 2 u_2 and the internal resistance of body 1 R_1 for the 2DOF and FE model are illustrated in Figure 6.2. In Figure 6.2b it is observed that the duration of the collision is approximately 0.12 s. As can be observed, the two models are quite comparable, though there are some differences. The two models are showing the same response until the unloading stage and after the collision there is a slight shift in the phase of the beam oscillation. These shifts can origin from a slight difference in eigenfrequency.
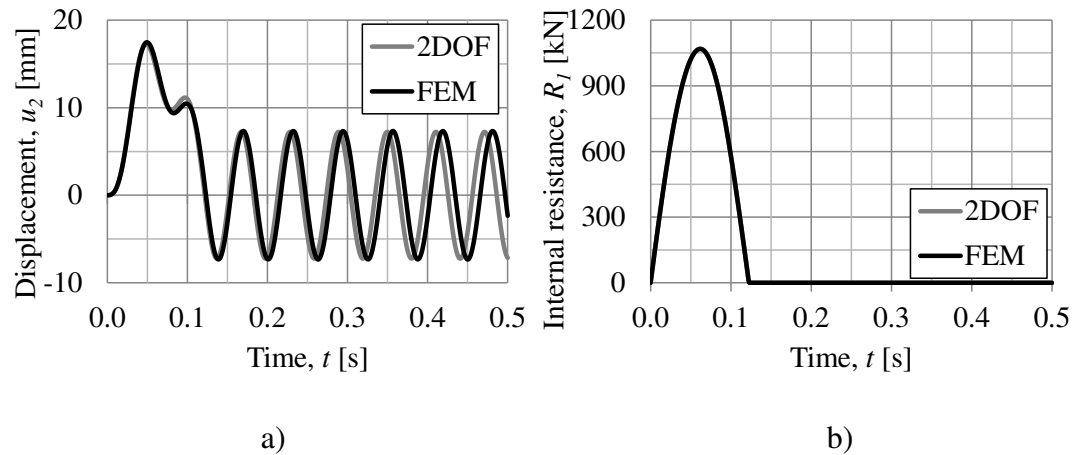
Figure 6.2   Comparison between the 2DOF model and the FE model for collision E1, a) displacement of body 2 u_2, and b) internal resistance of body 1 R_1.

The transformation factor κ_{mF} is calculated from the results achieved from the corresponding static FE analysis according to equation (4.27). The factor κ_{mF} is calculated to 0.485 which is close to the theoretically derived factor $\kappa_{mF} = 0.486$, see Appendix D.1.

As can be observed in Appendix D.1, where elastic collisions are presented for the 2DOF system studied in Section 3.2.2, collision E1 corresponds well to earlier studied impacts.

6.1.3   Elasto-plastic body 1 and elastic body 2

In reality the bodies involved in a collision may have more of an elasto-plastic response. In this section, a series of four different collisions with elasto-plastic response of body 1 and elastic response of body 2 are evaluated. The studied beam and the colliding object have properties according to Table 6.1 and Table 6.3. The position of the point load is represented by the factor α and is illustrated in Figure 6.1.

Table 6.3   *2DOF input parameters for collision F1-F4 with elasto-plastic response of body 1 and elastic response of body 2.*

Case	α [-]	κ_{mF} [-]	k_1 [MN/m]	k_2 [MN/m]	m_1 [kg]	$R_{1,max}$ [kN]
Collision F1	0.5	0.486	1.0	77.8	1 500	500
Collision F2	0.5	0.486	1.0	77.8	1 500	250
Collision F3	0.25	0.774	1.0	138.4	1 500	500
Collision F4	0.25	0.774	1.0	138.4	1 500	250

The parameters are chosen so that they approximately correspond to the collision examples presented in Chapter 3. The parameters m_2, E_{eq}, EI_b and k_2 for the 2DOF model are calculated according to Section 4.2.3.

The displacement of body 1 for collision F1 for both the 2DOF and FE model are illustrated in Figure 6.3a and as can be observed, the 2DOF and FE models generate identical results. Figure 6.3b illustrates the internal resistance of body 1 and it can be observed that the duration of the collision is approximately 0.15 s. However, when comparing the displacement and velocity of body 2 between the two methods, there are some very small differences as can be observed in Figure 6.3c and Figure 6.3d. The two models are showing the same response until the unloading stage and after the collision there is a slight shift in the phase. It is due to the same reason as for collision E1 in Section 6.1.2.

The maximum displacement of body 2 u_2 for collision F1 is not similar to that of collision E1 in Figure 6.2a, even if these two collisions have the same input data, except for the maximum internal resistance of body 1 $R_{1,max}$. The elasto-plastic collision F1 causes a smaller maximum displacement of body 2 u_2 than the elastic collision E1. This is due to the fact that an elastic body 1 creates a larger internal resistance R_1, which means a larger load on body 2.

Note that the duration of the collision is 0.15 s, but the difference in displacement $u_1 - u_2 = 0$ at the time 0.22 s. This difference is due to the fact that body 1 has endured plastic deformations.
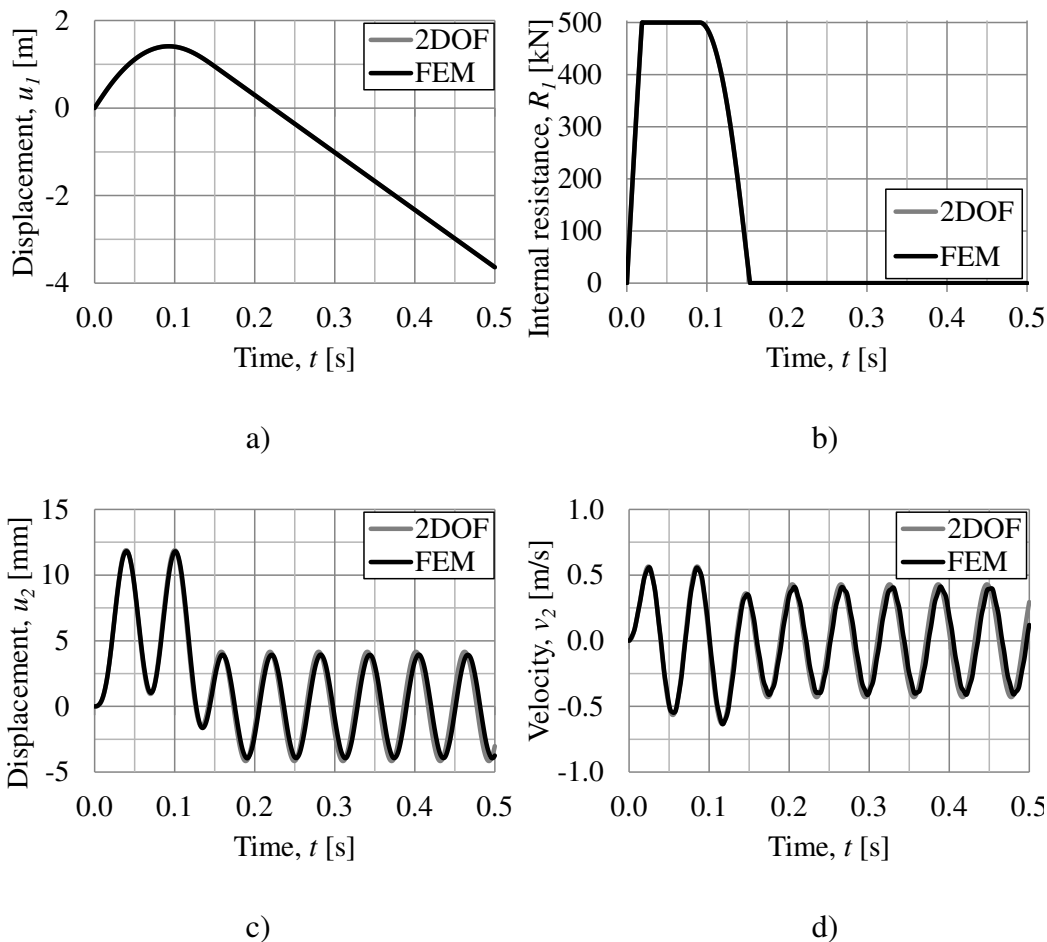
Figure 6.3 Illustration of the response for collision F1, a) displacement of body 1 u_1, b) internal resistance of body 1 R_1, c) displacement of body 2 u_2, and d) velocity of body 2 v_2.

The displacement of body 1 for collision F3 for both the 2DOF and FE model are illustrated in Figure 6.4a and as can be observed, the two models generate identical results. Figure 6.4b illustrates the internal resistance of body 1 and it can be observed that the duration of the collision is approximately 0.15 s. This is the same as for collision F1 which is expected since they both have the same maximum internal resistance $R_{1,max}$. However, there are some differences when comparing the displacement and velocity of body 2 between the two methods, as can be observed in Figure 6.4c and Figure 6.4d. The differences are larger than for collision F1 and it is due to the change in the position of the point load. However, the maximum displacement for body 2 is corresponding.

The transformation factor κ_{mF} is derived from static load cases which correspond well to the dynamic load cases if the load is applied in the centre of the span. However, the closer to the supports the point load is applied the larger the difference between static and dynamic cases. This is discussed more thoroughly in both Asplund and Steckmest (2014) and Johansson (2014).
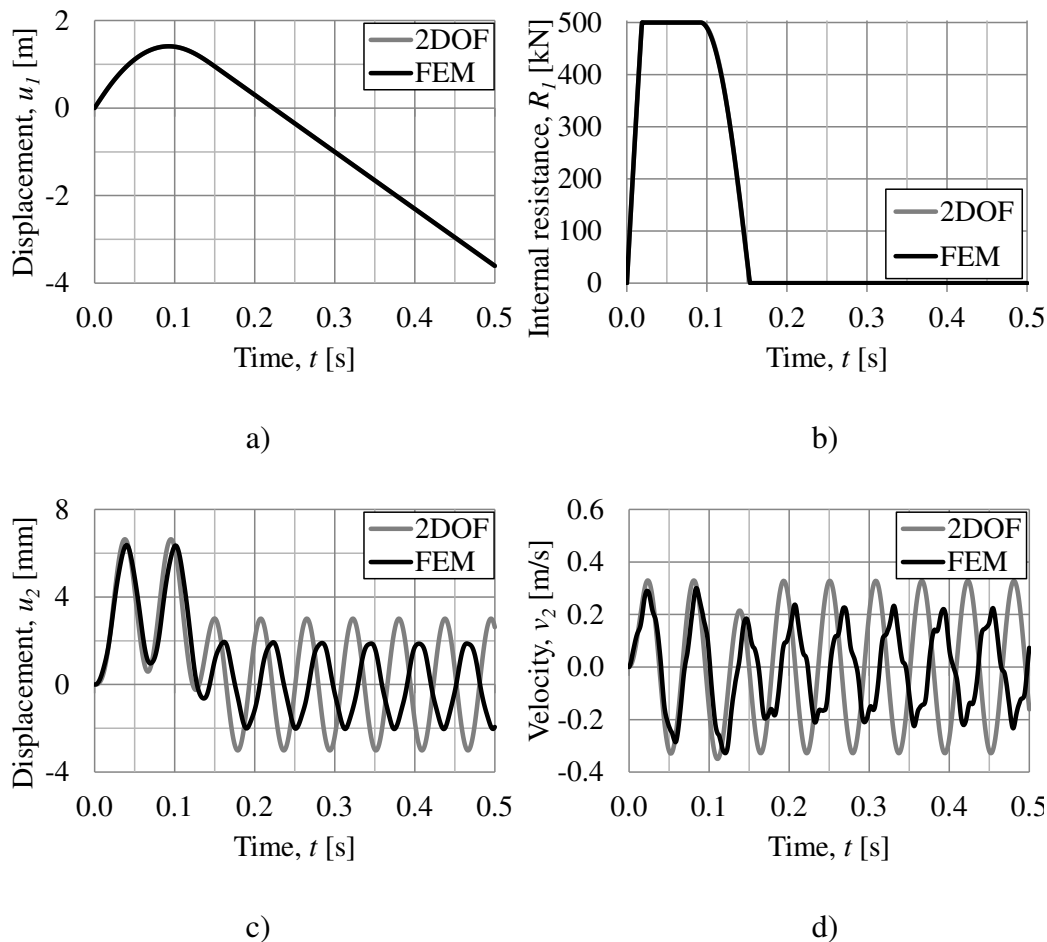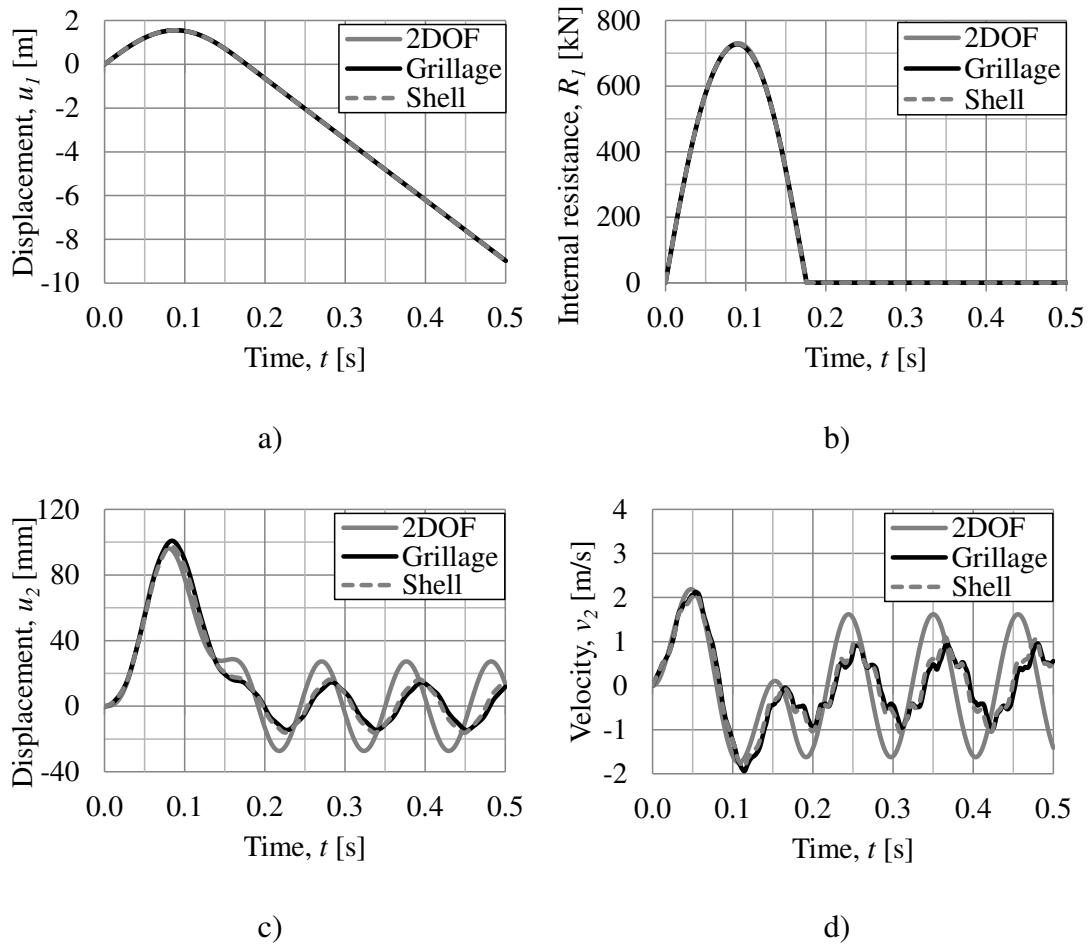
Figure 6.4 Illustration of the response for collision F3, a) displacement of body 1 u_1, b) internal resistance of body 1 v_1, c) displacement of body 2 u_2, and d) velocity of body 2 v_2.

For corresponding response diagrams for collision F2 and F4, see Appendix C.2.

6.1.4   Elastic body 1 and elasto-plastic body 2

To model a realistic behaviour for the structure, an elasto-plastic response of the beam is used. However, the transformation factor κ_{mF} is dependent on both elastic and plastic response and is unique for each set of properties. For a beam with the impact applied in the centre, three cases with different transformation factors are evaluated further. The further evaluated transformation factors are fully elastic $\kappa_{mF} = 0.486$, fully plastic $\kappa_{mF} = 0.333$ and one in between $\kappa_{mF} = 0.410$. These cases are presented in Table 6.4, where M_{Rd}, α and l_b is described in Table 6.1 and Figure 6.1.

Body 1 is modelled with elastic response for all three cases. The studied beam has properties according to Table 6.1. The position of the point load is represented by the factor α as illustrated in Figure 4.3. Collision G1a-G1c are all identical except for the transformation factor κ_{mF}, i.e. only the 2DOF model varies between the three cases.

The maximum internal resistance of body 2 $R_{2,max}$ is calculated with moment equilibrium as

$$R_{2,max} = \frac{M_{Rd}}{\alpha(1-\alpha)l_b} \tag{6.2}$$

where M_{Rd}, α and l_b is described in Table 6.1 and Figure 6.1.

Table 6.4   2DOF   input   parameters   for   collision G1a-G1c   with   different transformation factor κ_{mF} and with elastic response of body 1 and elasto-plastic response of body 2.

Case	α [-]	κ_{mF} [-]	k_1 [MN/m]	k_2 [MN/m]	m_1 [kg]	$R_{2,max}$ [kN]
Collision G1a	0.5	0.486	0.5	77.8	1 500	415
Collision G1b	0.5	0.410	0.5	77.8	1 500	415
Collision G1c	0.5	0.333	0.5	77.8	1 500	415

The displacement of body 1 for collision G1a for both the 2DOF and FE model are illustrated in Figure 6.5a and as can be observed, the two models generates similar results Even though the transformation factor κ_{mF} differs between the three cases, the displacement of body 1 for the 2DOF model is very similar. This is due to the fact that the internal resistance R_1 is the same for all three cases and that the magnitude of the displacement u_1 and the velocity v_1 is so large in comparison to the difference between the transformation factors κ_{mF}. The reason u_1 and v_1 are large is because the stiffness ratio k_1 / k_2 is small. As illustrated in Figure 6.5b the duration of the collision is approximately 0.16 s.

However, when comparing the displacement and velocity of body 2 for the two methods, there are some differences as can be observed in Figure 6.5c and Figure 6.5d. It shows that the response of the collision modelled in ADINA is not corresponding to the case modelled with a fully elastic κ_{mF}, collision G1a. This is expected since it is an elasto-plastic model.
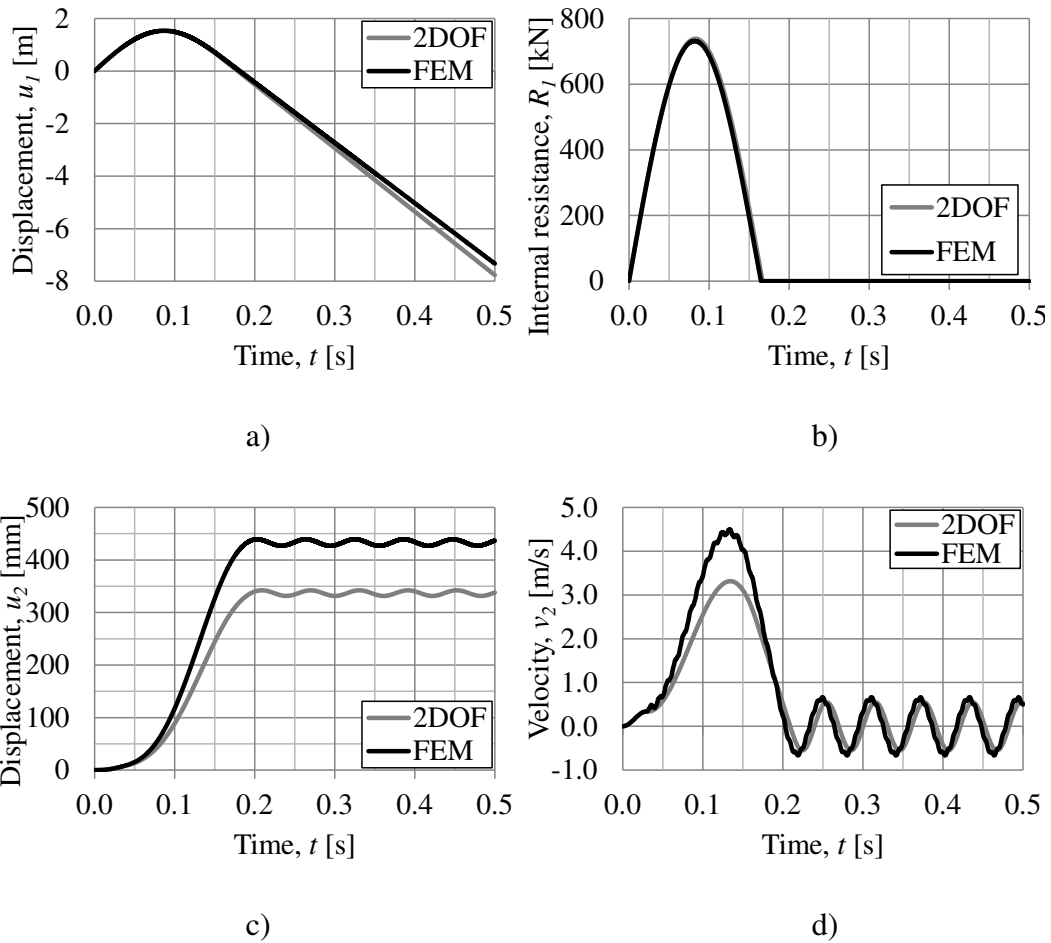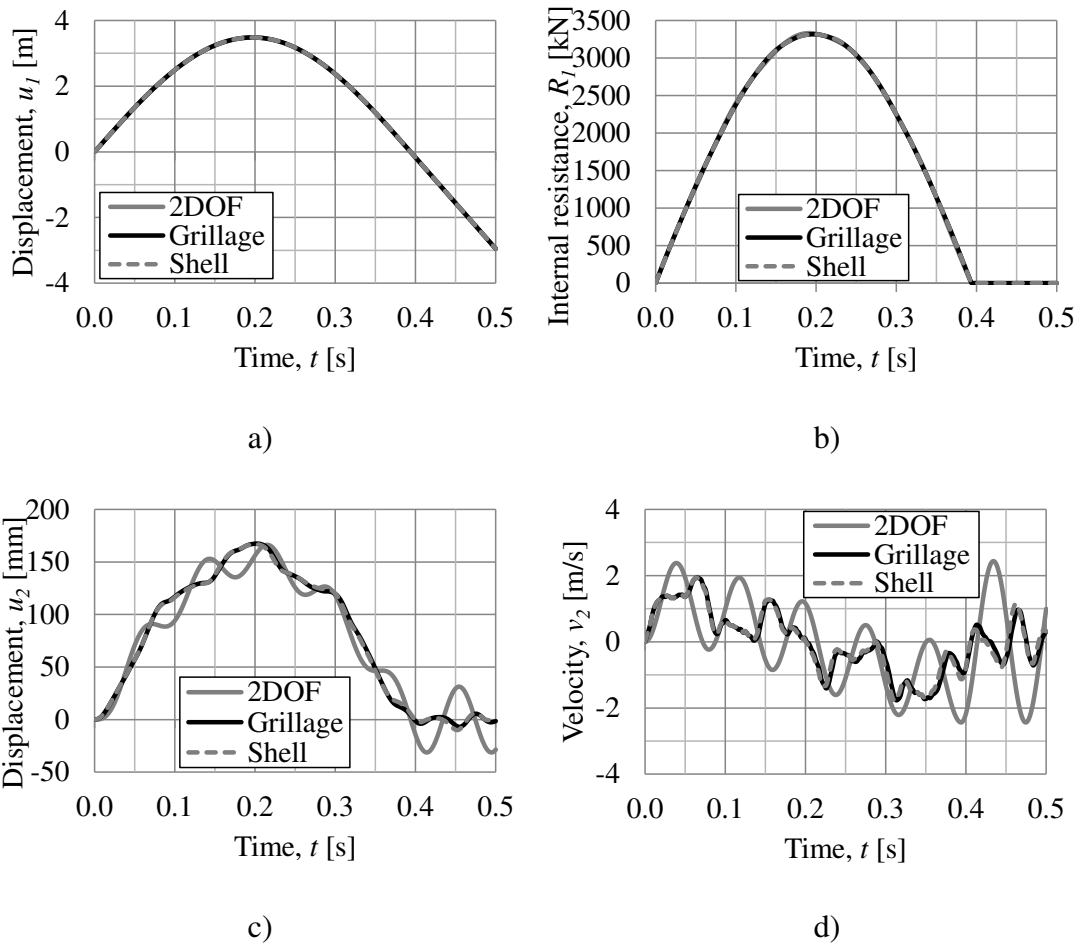
Figure 6.5   Illustration of the response for collision G1a, a) displacement of body 1 u_1, b) internal resistance of body 1 R_1, c) displacement of body 2 u_2, and d) velocity of body 2 v_2.

When comparing the displacement and velocity of body 2 for the two methods, there are some differences as can be observed in Figure 6.6a and Figure 6.6b. It shows that the response of the collision modelled in ADINA is not directly in between the fully elastic and fully plastic case. However, it is closer than for collision G1a, which shows that it is closer to the fully plastic case.
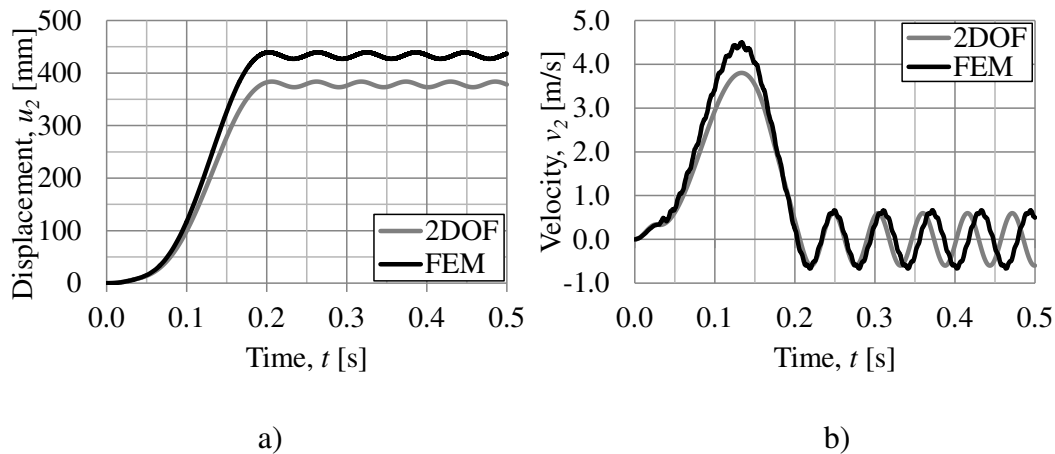
Figure 6.6   Illustration of the response for collision G1b, a) displacement of body 2 u_2, and b) velocity of body 2 v_2.

When comparing the displacement and velocity of body 2 between the two models for collision G1c there are some minor differences as can be observed in Figure 6.7a and Figure 6.7b. It clearly shows that the response of the collision modelled in ADINA is very close to fully plastic. However, this result is unique for this specific beam and incoming object, since the response is highly dependent on the properties of the two bodies.
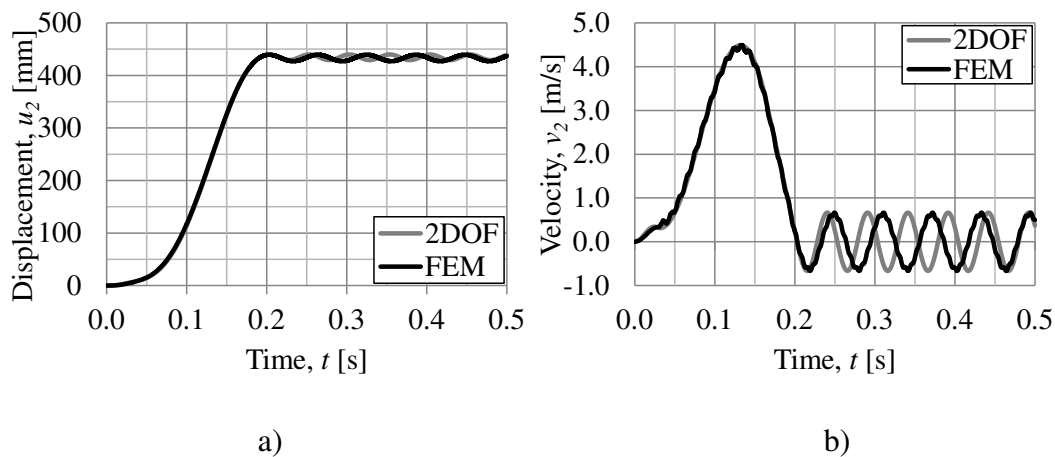
Figure 6.7   Illustration of the response for collision G1c, a) displacement of body 2 u_2, and b) velocity of body 2 v_2.

6.1.5   Discussion

The 2DOF has good correspondence with the FE model when body 2 has a fully elastic response, the correspondence is however better the closer the impact is to the centre of the beam. When comparing the response of the displacement of body 2 u_2 for collision E1 in Figure 6.2a, with u_2 for collision F1 in Figure 6.3c, the results are different. The elasto-plastic collision F1 causes a smaller maximum displacement of body 2 than the elastic collision E1, which means that there is a large difference if body 1 is elastic or elasto-plastic. However, it is on the safe side to assume an elastic behaviour of body 1, which agrees with the theory given in Section 2.3.1.

The elasto-plastic behaviour of body 2 has good correspondence between the 2DOF and the FE model for beams subjected to an impact in the centre of the beam, if a correct transformation factor κ_{mF} is chosen. The usage of κ_{mF} can be improved by finding an approach that calculates an optimised κ_{mF} for each collision. This approach could be based on calculation of the elastic displacement u_{el} and plastic displacement u_{pl} of the beam. If $u_{pl} \approx 0$, an elastic κ_{mF} is used, if $u_{pl} \gg u_{el}$ a plastic κ_{mF} is used, and if $u_{pl} \approx u_{el}$ a mean value of an elastic and plastic κ_{mF} is used.

The response for both elastic and elasto-plastic behaviour for body 1 is the same for both the FE model and the 2DOF model, which validates that ADINA handles a mass and a spring similar to the 2DOF model using the Central Difference Method.

This section handles beams subjected to collisions, however if further conclusions should be drawn, more collision cases need to be analysed. This is not treated in this thesis since the main focus is collision impact at slabs.

6.2 Comparison for a slab

6.2.1 Orientation

In the FE analysis a simply supported reinforced concrete slab is used which is compared to a 2DOF model with a barrier. For simplicity is the reinforcement placed symmetrically in equal amounts at the top and at the bottom of the slab, as illustrated in Figure 6.8. The FE analyses are carried out with the commercial software ADINA (2014).
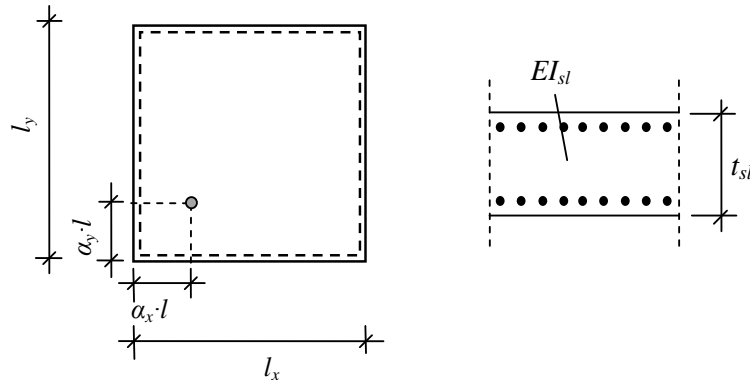
Figure 6.8   The simply supported reinforced concrete slab with stiffness EI_{sl}, length l_x, length l_y, thickness t_{sl} and the load placement factors α_x and α_y.

The geometry and the parameters of the slab modelled with shell elements are presented in Table 6.5. The length, width and thickness ratios of the slab is chosen so that 28 x 28 elements can be used and a length thickness ratio $l/t = 28$ is gained as discussed in Section 4.4.2. The magnitude of the length, width and thickness of the slab is chosen so that the mass of the slab m_{sl} becomes approximately the same as the mass of the beam in Section 6.1, i.e. 15 000 kg. The reinforcement arrangement and the concrete class are chosen to represent a standard, but quite stiff slab. In this chapter, more collisions are analysed than for beams in Section 6.1 since the main interest of this thesis is slabs.

Table 6.5   Properties of the concrete slab used in the shell element model and for hand calculations.

Length x-direction l_x	5.6 m
Length y-direction l_y	5.6 m
Thickness t_{sl}	0.2 m
Mass m_{sl}	15 052.8 kg
Density ρ_c	2 400 kg/m^3
Concrete class	C30/37
Concrete Young's modulus E_{cm}	33 GPa
Reinforcement	B500B Φ16 s200
Reinforcement Young's modulus E_s	200 GPa
Concrete cover c	30 mm
Equivalent Young's modulus E_{eq}	5.98 GPa
Moment capacity $m_{Rd,m}$	67.2 kNm/m

The geometry and the parameters of the beams used in the beam grillage model which is used for further analysis are presented in Table 6.6. The material and cross-sectional properties for the two slab models presented in the tables are calculated according to Appendix G.

Note that there is a difference in the density ρ between the two slab models, this is discussed more thoroughly in Section 5.5.1.

Table 6.6   Properties of the concrete beams used in the beam grillage model.

Length l_b	5.6 m
Height h_b	0.2 m
Width w_b	0.2 m
Density ρ_c	1 200 kg/m^3
Concrete class	C30/37
Concrete Young's modulus E_{cm}	33 GPa
Reinforcement	B500B Φ16 s200
Steel Young's modulus E_s	200 GPa
Concrete cover c	30 mm
Moment capacity $M_{Rd,b}$	13.4 kNm
Yield curvature $\left(\dfrac{1}{r}\right)_{pl}$	$17 \cdot 10^{-3}$ m^{-1}
Torsional stiffness relation $\dfrac{T_{II}}{\varphi}$	674.4 kNm^2

6.2.2 Elastic body 1 and body 2

To be able to perform valid comparisons between 2DOF and FEM for slab collisions with elasto-plastic response, the 2DOF and FE models are confirmed for a series of twelve collisions with an elastic response for both body 1 and body 2. The input parameters for these collisions are presented in Table 6.7. The transformation factor κ_{mF} and the stiffness of the slab k_{sl} used for these collisions are the corresponding factors derived in Section 4.4.2, for a slab modelled with shell elements. The length factors α_x and α_y are defined as illustrated in Figure 6.8.

Table 6.7   2DOF and FE input parameters for collision H1-H12 with initial velocity $v_0 = 27.8$ m/s.

Case	α_x [-]	α_y [-]	κ_{mF} [-]	k_1 [MN/m]	m_1 [kg]	k_{sl} [MN/m]
Collision H1	0.5	0.5	0.203	0.5	1 500	10.79
Collision H2	0.5	0.25	0.235	0.5	1 500	15.94
Collision H3	0.25	0.25	0.241	0.5	1 500	22.02
Collision H4	0.5	0.5	0.203	1	1 500	10.79
Collision H5	0.5	0.25	0.235	1	1 500	15.94
Collision H6	0.25	0.25	0.241	1	1 500	22.02
Collision H7	0.5	0.5	0.203	0.5	15 000	10.79
Collision H8	0.5	0.25	0.235	0.5	15 000	15.94
Collision H9	0.25	0.25	0.241	0.5	15 000	22.02
Collision H10	0.5	0.5	0.203	1	15 000	10.79
Collision H11	0.5	0.25	0.235	1	15 000	15.94
Collision H12	0.25	0.25	0.241	1	15 000	22.02

A comparison between the responses for the 2DOF and the FE models modelled with both shell elements and as a beam grillage, for collision H1, can be seen in Figure 6.9. As can be observed, the response for the two FE models is almost the same. The response of body 1 is identical between the 2DOF and the FE models. However, there is a difference in the response for body 2 between the 2DOF and the FE models.

As can be seen from the internal resistance of body 1 R_1 in Figure 6.9b, the collision has a duration of approximately 0.17 s. In Figure 6.9c, the correspondence between the displacements of body 2 u_2 is approximately the same for the first 0.13 s between the models, but after that it differs a bit. The small difference seen in Figure 6.9c during the rebound is believed to cause the phase shift and difference in amplitude after the collision. The overall behaviour during the collision seems to be good, and it is this response that is of main interest.

Figure 6.9　*Illustration of collision H1, a) displacement of body 1 u_1, b) internal resistance of body 1 R_1, c) displacement of body 2 u_2, d) velocity of body 2 v_2.*

In Figure 6.10, collision H1 is compared with collision H4 for the shell element model. When comparing these collisions, it is only the stiffness of body 1 k_1 that is different and it is collision H4 that has a stiffer body 1. The duration of the collision is shorter with a larger k_1 as seen in Figure 6.10b, and discussed in Chapter 3. To be noted is that a larger stiffness also gives larger maximum displacement of body 2 u_2, as seen in Figure 6.10a.
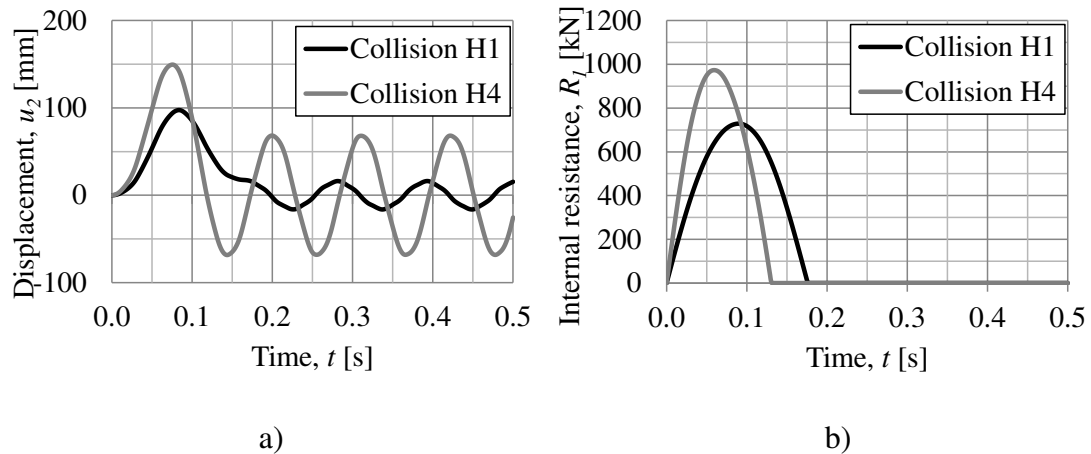
Figure 6.10 Comparison in response between collision H1 and collision H4 for the shell element model, a) displacement of body 2 u_2, and b) internal resistance of body 1 R_1.

A comparison between the responses for the 2DOF and the FE models modelled with both shell elements and as a beam grillage, for collision H12, can be seen in Figure 6.11. As can be observed, the response for the two FE models is almost the same. The response of body 1 is identical between the 2DOF and the FE models. However, there is a difference in the response for body 2 between the 2DOF and the FE models.

As can be seen from the internal resistance of body 1 R_1 in Figure 6.11b, the collision has a duration of approximately 0.39 s. In Figure 6.11c, the maximum displacements of body 2 u_2 is approximately the same even though the 2DOF model has a slightly different response. Even though there is a difference after the collision, is the overall behaviour during the collision good, and it is this response that is of main interest.

a)

b)

c)

d)

Figure 6.11   Illustration of collision H12, a) displacement of body 1 u_1, b) internal resistance of body 1 R_1, c) displacement of body 2 u_2, and d) velocity of body 2 v_2.

In Figure 6.12, collision H9 is compared with collision H12 for the shell element model. When comparing these collisions, it is only the stiffness of body 1 k_1 that is different and it is collision H12 that has a stiffer body 1. The duration of the collision is shorter with a larger k_1 as seen in Figure 6.12b. To be noted is that a larger stiffness also gives larger maximum displacement of body 2 u_2, as seen in Figure 6.12a.
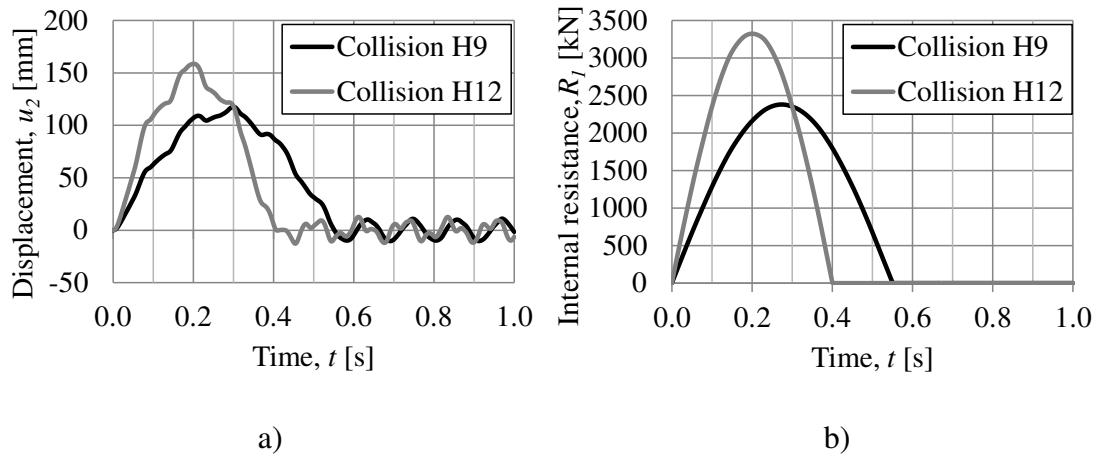
Figure 6.12   Comparison in response between collision H9 and collision H12 for the shell element model, a) displacement of body 2 u_2, and b) internal resistance of body 1 R_1.

The overall correspondence between the 2DOF and FE models are in this section good. However, this is probably not the case for all property combinations of body 1 and body 2.

For response diagrams for collision H2-H11, see Appendix C.4.

6.2.3   Elasto-plastic body 1 and elastic body 2

In reality, the involved bodies in a collision may have more of an elasto-plastic response. In this section a series of eight collisions is evaluated, where body 1 is modelled with an elasto-plastic response and body 2 is modelled with elastic response. The input parameters for the studied cases are presented in Table 6.8. To avoid a large number of collision cases, the point load is applied in the centre of the slab for all collisions, i.e. $\alpha_x = \alpha_y = 0.5$, $\kappa_{mF} = 0.203$ and $k_{sl} = 10.79$ MN/m.

Table 6.8   2DOF and FE input parameters for collision I1-I8 with initial velocity $v_0 = 27.8$ m/s. The point load is applied in the centre of the slab, i.e. $\alpha_x = \alpha_y = 0.5$, $\kappa_{mF} = 0.203$ and $k_{sl} = 10.79$ MN/m.

Case	k_1 [MN/m]	m_1 [kg]	$R_{1,max}$ [MN]
Collision I1	0.5	1 500	0.3
Collision I2	0.5	1 500	0.6
Collision I3	1	1 500	0.3
Collision I4	1	1 500	0.6
Collision I5	0.5	15 000	1
Collision I6	0.5	15 000	2
Collision I7	1	15 000	1
Collision I8	1	15 000	2

A comparison between the responses for the 2DOF and the FE model modelled with both shell elements and as a beam grillage, for collision I1 can be seen in Figure 6.13.

As can be observed, the response for the two FE models is almost the same. The response of body 1 is identical between the 2DOF and the FE models. However, there is a difference in the response for body 2 between the 2DOF and the FE models.

As for collision H1 presented in Figure 6.9, the response of u_2 in Figure 6.13c is quite similar between the models during, but not after the collision, which has the duration of approximately 0.24 s according to Figure 6.13b. However, it is the response during the collision that is of main interest.

a)

b)

c)

d)
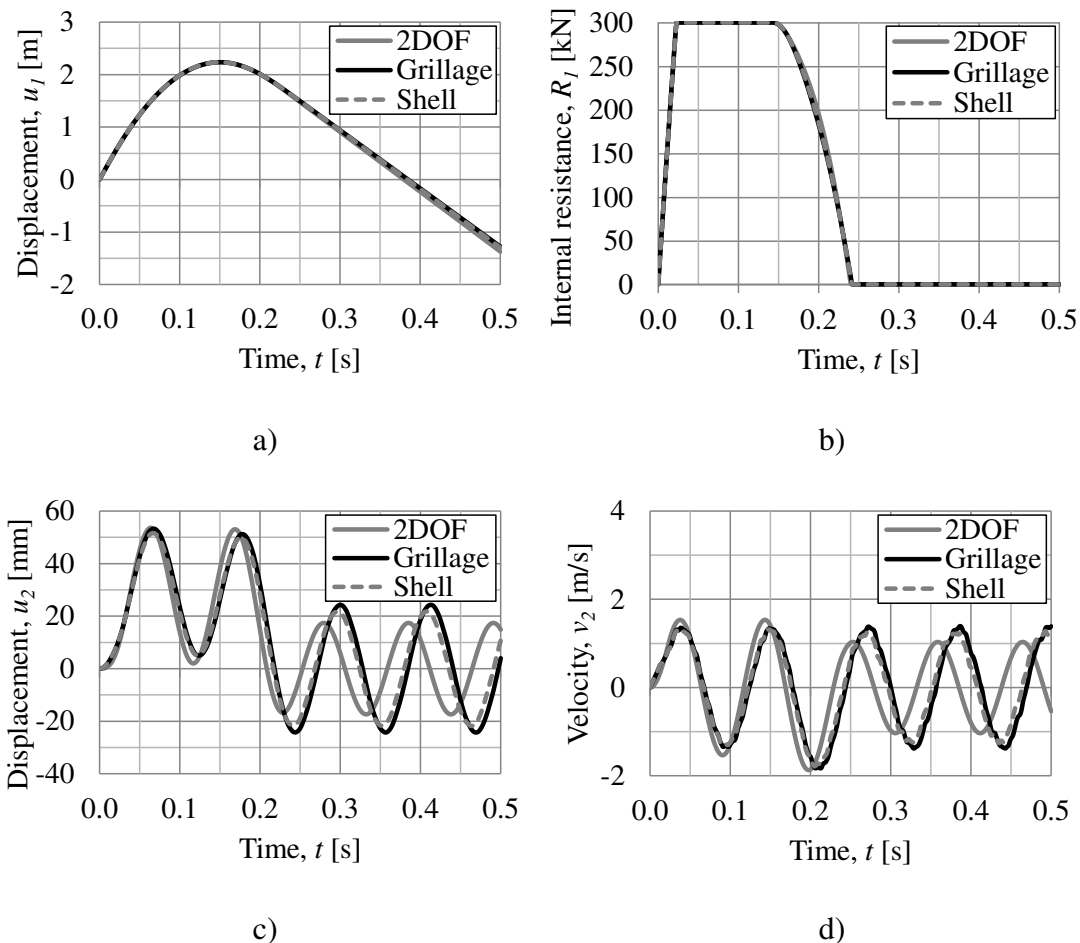
Figure 6.13 *Illustration of collision I1, a) displacement of body 1 u_1, b) internal resistance of body 1 R_1, c) displacement of body 2 u_2, d) velocity of body 2 v_2.*

In Figure 6.14, collision I1 is compared with collision I3 for the shell element model. When comparing these collisions, it is only the stiffness of body 1 k_1 that is different and it is collision I3 that has a stiffer body 1. The duration of the collision is shorter with a larger k_1 as seen in Figure 6.14b, but the responses of body 1 are similar. As illustrated in Figure 6.14a, the responses of body 2 are also similar in this comparison, even though k_1 is twice as large for collision I3 as for collision I1. That the responses are similar is due to that both collisions has the same maximum internal resistance of body 1 $R_{1,max}$, and this parameter is more dominant than k_1 for these collisions. However, a larger stiffness still gives larger maximum displacement of body 2 u_2.

a)   b)
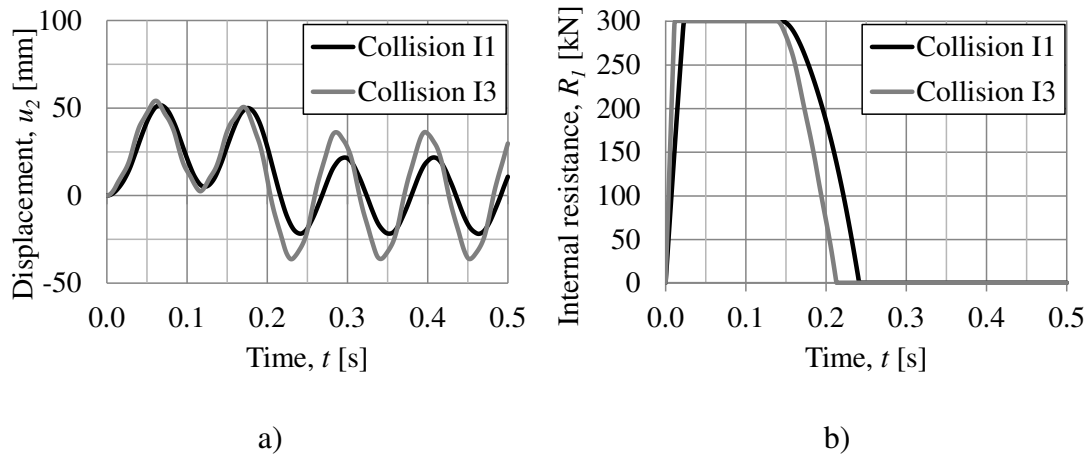
Figure 6.14   Comparison in response between collision I1 and collision I3 for the shell element model, a) displacement of body 2 u_2, and b) internal resistance of body 1 R_1.

A comparison between the responses for the 2DOF and the FE model modelled with both shell elements and as a beam grillage, for collision I8 can be seen in Figure 6.15. As can be observed, the response for the two FE models is almost the same. The response of body 1 is identical between the 2DOF and the FE models. However, there is a difference in the response for body 2 between the 2DOF and the FE models.

As for collision I1 presented in Figure 6.13, the response of u_2 in Figure 6.15c is quite similar between the models during, but not after the collision, which has the duration of approximately 0.42 s according to Figure 6.15b. However, it is the response during the collision that is of main interest.

a)

b)

c)

d)
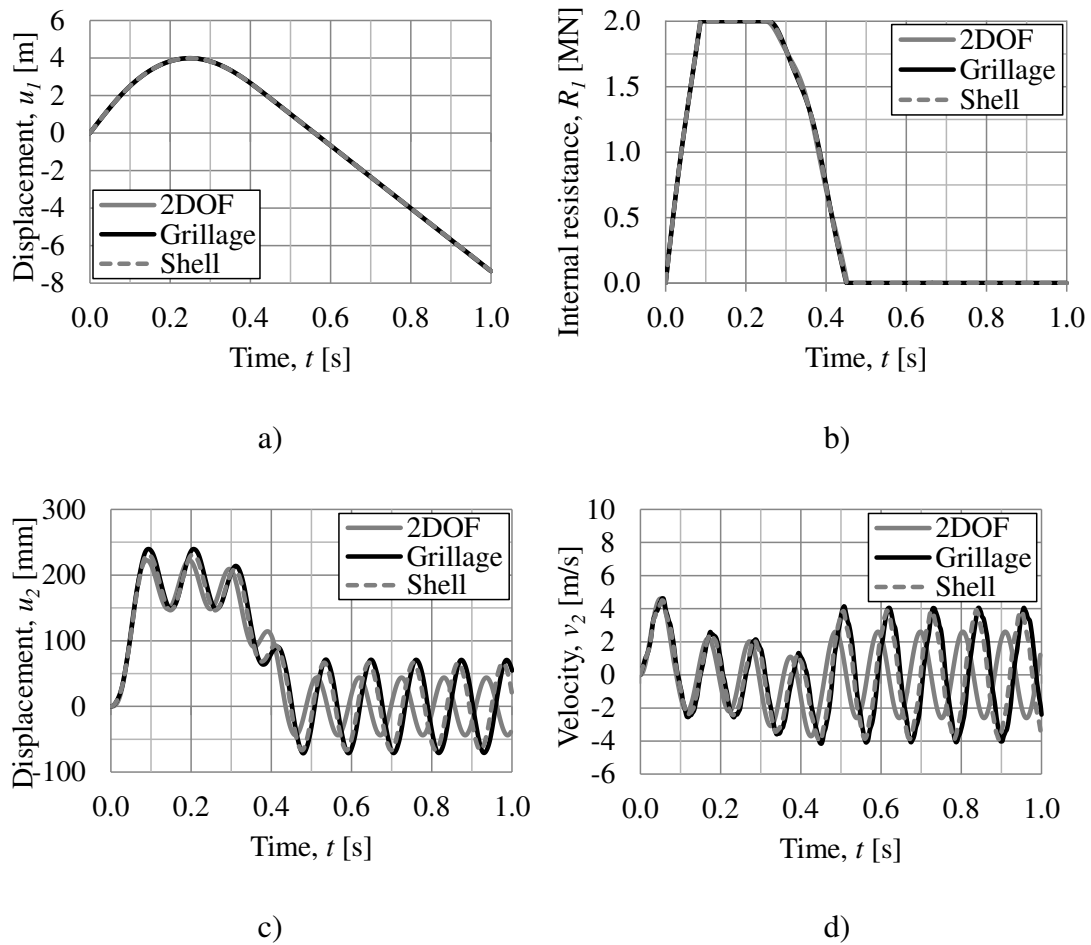
Figure 6.15   Illustration of collision I8, a) displacement of body 1 u_1, b) internal resistance of body 1 R_1, c) displacement of body 2 u_2, and d) velocity of body 2 v_2.

In Figure 6.16, collision I6 is compared with collision I8 for the shell element model. When comparing these collisions, it is only the stiffness of body 1 k_1 that is different and it is collision I8 that has a stiffer body 1. The duration of the collision is shorter with a larger k_1 as seen in Figure 6.16b. A larger stiffness also gives larger maximum displacement of body 2 u_2, as seen in Figure 6.16a. In this comparison however, there is a small difference in maximum displacements of body 2 u_2 between collision I6 and collision I8, this is due to the influence of the maximum internal resistance of body 1 $R_{1,max}$.

a)   b)
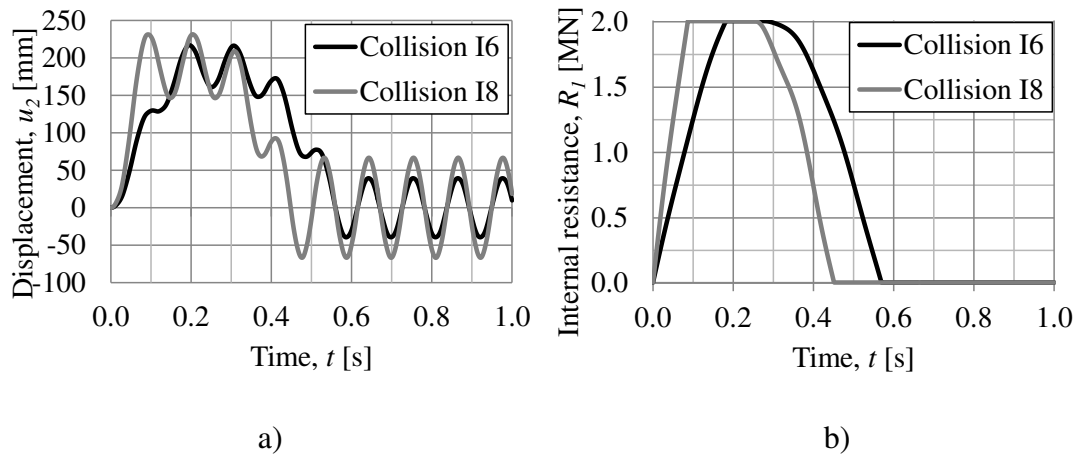
Figure 6.16   Comparison in response between collision I6 and collision I8 for the shell element model, a) displacement of body 2 u_2, and b) internal resistance of body 1 R_1

In Figure 6.17, a comparison between collision H1, I1 and I2 is presented for the responses of the shell element analysis. The response of u_2 for collision I1 is not similar at all with the response of u_2 for collision H1, even if these two collisions have the same input data, except for the maximum internal resistance of body 1 $R_{1,max}$. The elasto-plastic collision I1 causes a smaller maximum displacement of body 2 u_2 than the elastic collision H1. However, collision I2 has a higher $R_{1,max}$ than collision I1 and is therefore closer to the fully elastic collision H1.

a)   b)
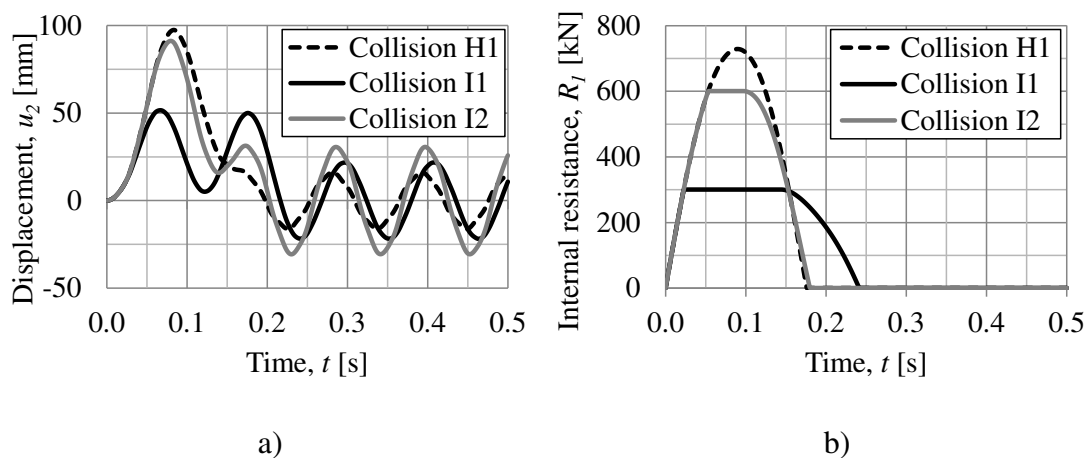
Figure 6.17   Comparison in response between collision H1, collision I1 and collision I2 for the shell element model, a) displacement of body 2 u_2, and b) internal resistance of body 1 R_1.

The overall correspondence between the 2DOF and FE models are in this section good. However, this is probably not the case for all property combinations of body 1 and body 2.

For response diagrams for collision I2-I7, see Appendix C.5.

6.2.4 Elastic body 1 and elasto-plastic body 2

6.2.4.1 Orientation

For the collision analysis with an elasto-plastic slab, some issues exist. Firstly, it is of interest to examine the collision impact at an elasto-plastic slab using a beam grillage model. However, it is concluded in Section 6.2.4.2 that the elasto-plastic beam grillage model does not have a sufficiently good behaviour. Therefore, shell elements are used instead for the elasto-plastic slab.

Secondly, it is discovered that the transformation factor κ_{mF}, has a lower value than expected for elasto-plastic slabs modelled with shell elements. This is more thoroughly evaluated in Section 6.2.4.3.

6.2.4.2 Static study of the elasto-plastic slab model

The concrete slab can be modelled as a beam grillage according to Section 5.5.1. One way to verify the model is to show the response during loading in a load-displacement diagram. An increasing prescribed displacement is applied in the system point of the slab $u_s = u_2$ to create an internal resistance force R_2 in the system point. This response is illustrated in Figure 6.18 for torsional stiffness model 3 to 6, which are presented in Section 5.5.3, together with the load capacity calculated with strip method according to Appendix G.

The analysis shows that a local inaccuracy in the model occurs at the node where the prescribed displacement is applied, which causes the sharp stop in load capacity for model 3 to 5 as illustrated in Figure 6.18. The local inaccuracy occurs in one node which deflects at a much faster rate than the other nodes after a certain point. For model 6, which is modelled with no torsional stiffness, this local inaccuracy is not occurring. The reason for this is that model 6 does not reach a load level which is as high as for model 3 to 5, because model 6 is limited by its moment capacity. Whereas model 3 to 5 have no load limit since they have no limit in torsional stiffness.

Since the strip method is on the safe side and does not account for torsional stiffness, it is expected to have the lowest load capacity. Model 6 is showing a load capacity which is about half the load capacity obtained with the strip method, according to Appendix G. This indicates that the response of the beam grillage model used is non-viable.
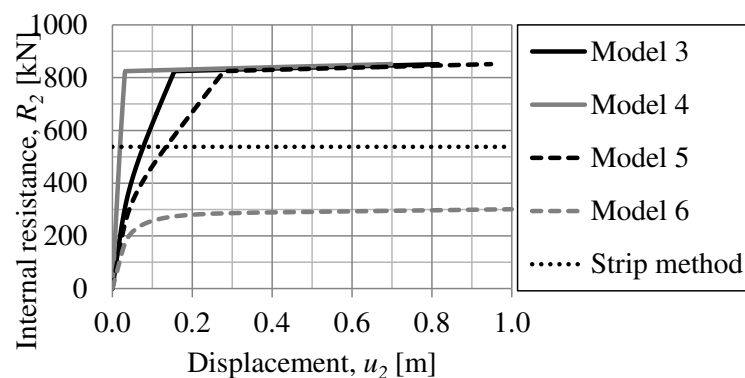
Figure 6.18   Illustration of the load-displacement response for torsional stiffness model 3 to 6, see Section 5.5.3, for load case 1 and the load capacity calculated with the strip method.

The local inaccuracy is believed to happen due to a stress concentration which is caused by the fact that the torsion-twisting relation is modelled with linear response and has no limit. Hence, the concrete slab will continue to carry load after the bending moment capacity of the beam grillage has been reached. A new test where the beam elements also yield in torsion is conducted, with the yield limit presented in Table 6.9. The torsion-twisting relation is modelled with a bilinear curve, in the same manner as the moment-curvature relation for model 3, see Appendix G for the calculation of this yield limit for the torsional moment.

Table 6.9   Properties for the bilinear torsional stiffness used in the beam grillage model.

Yield twist φ	4.165 km^{-1}
Torsional moment T_{II}	2.80 kNm

The response is illustrated in Figure 6.19 and as can be observed, the local inaccuracy phenomenon is now gone. However, the load capacity is still far below the load capacity obtained with the strip method, which suggests that this beam grillage model is also non-viable. For corresponding load-displacement relations for load case 2 and 3 and for a rectangular slab, see Appendix F.2.
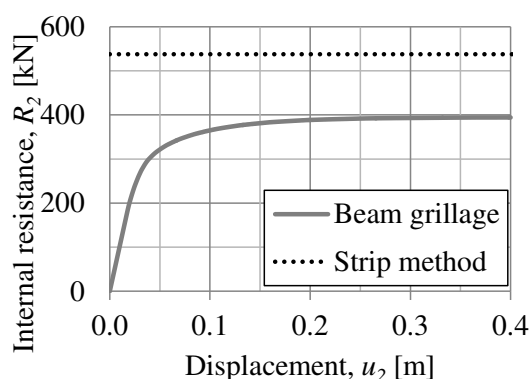
Figure 6.19   Illustration of the load-displacement response of a beam grillage model based on torsional stiffness model 3 for load case 1, but with a bilinear torsion-twisting response.

The response of the same slab modelled with shell elements, according to Section 5.4, is illustrated in Figure 6.20. Even though the shell elements show a load capacity which is slightly lower than the load obtained from the strip method, it has a much more satisfactory response than the response from the beam grillage model. To obtain a load-displacement curve for the beam grillage model which is somewhat close to the response from the shell element model, both the moment-curvature and the torsion-twisting limits needs to be increased with a factor of square root of two. The beam grillage model with increased strength is illustrated in Figure 6.20.
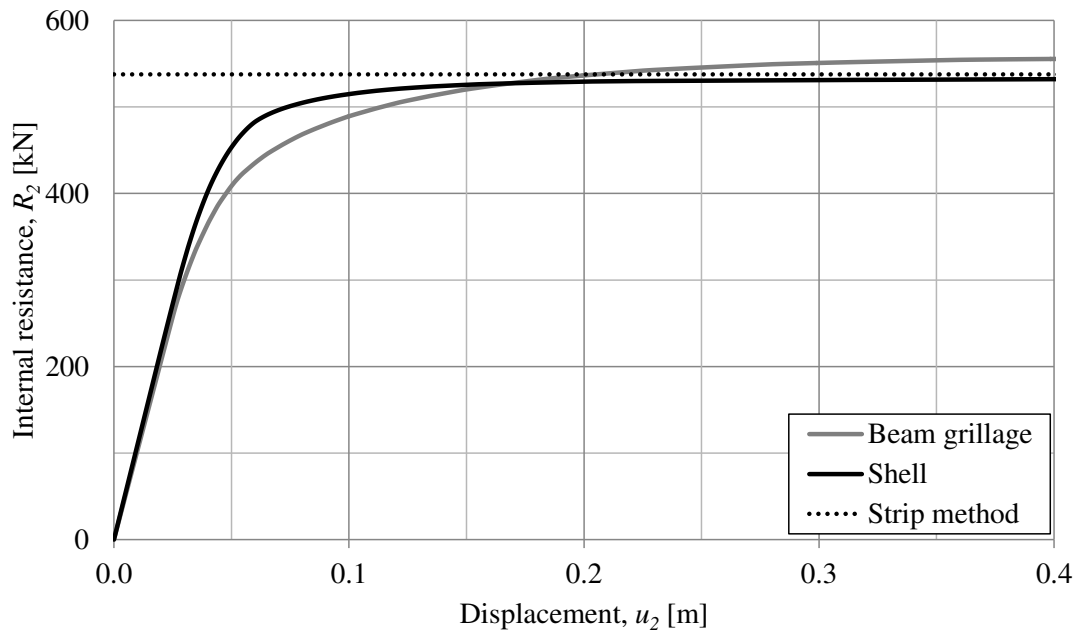
Figure 6.20   Illustration of the load-displacement response of the slab modelled with shell elements and the slab modelled as a beam grillage with torsion-twisting and moment-curvature limits increased with a factor of $\sqrt{2}$.

It is believed that the reason why the beam grillage model generates a load capacity which is far below both what the strip method and what the shell element model suggests, is that the beam grillage model is having trouble distributing the load once the yield limit is reached in a local beam element. To verify this, the displacement along a line which goes through the point of loading is plotted for both the beam grillage and the shell element model. The response between the two failure modes should be similar with a peak in the centre. As illustrated in Figure 6.21, this is also the case when compared to the theoretical displacement, discussed in Section 4.4.3.
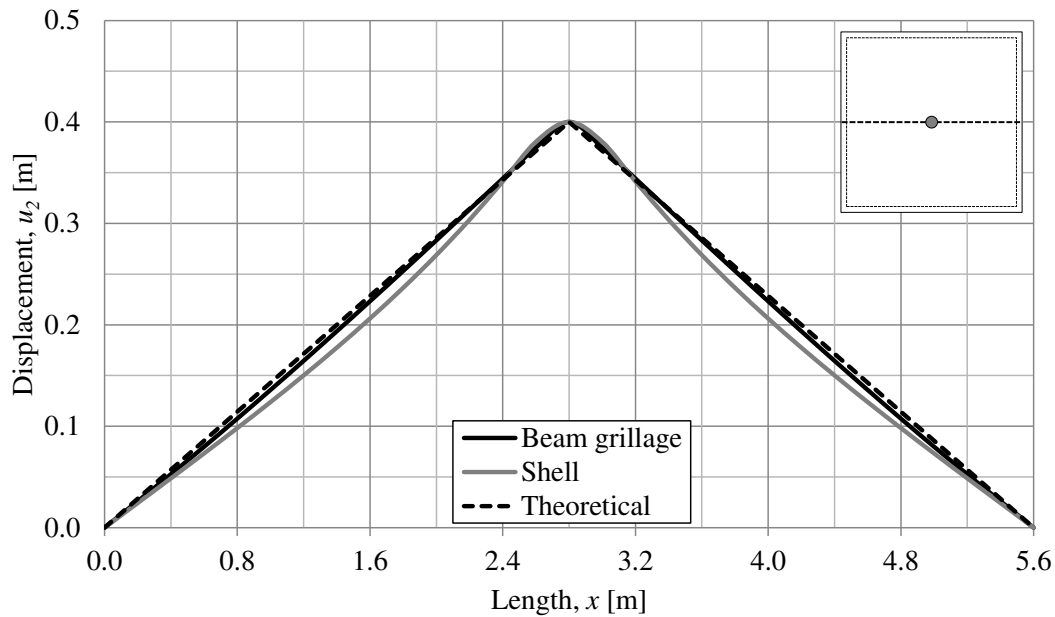
Figure 6.21   Illustration of the displacement of body 2 u_2 on a quadratic slab along a line for the theoretical assumed model, the beam grillage and the shell element model. The line and the point of loading are presented in the upper right hand corner.

The expected failure mode is that there will be a plateau between the yield lines, as illustrated by the theoretical displacement illustrated in Figure 6.22. It is possible to observe that the shell element model is having a response which vaguely reminds of a plateau-in contrast to the beam grillage model which instead has a response which is similar to the one observed in Figure 6.21. Even though the shell element is showing a plateau like behaviour, none of the two models is close to the theoretically assumed displacement, which clearly indicates that there is a major difference between the assumed failure mode and the obtained. The beam grillage and shell element model are corresponding better in the centre of the slab, when the load is applied at the centre of the slab, which agrees with the results obtained in Section 5.5.3.
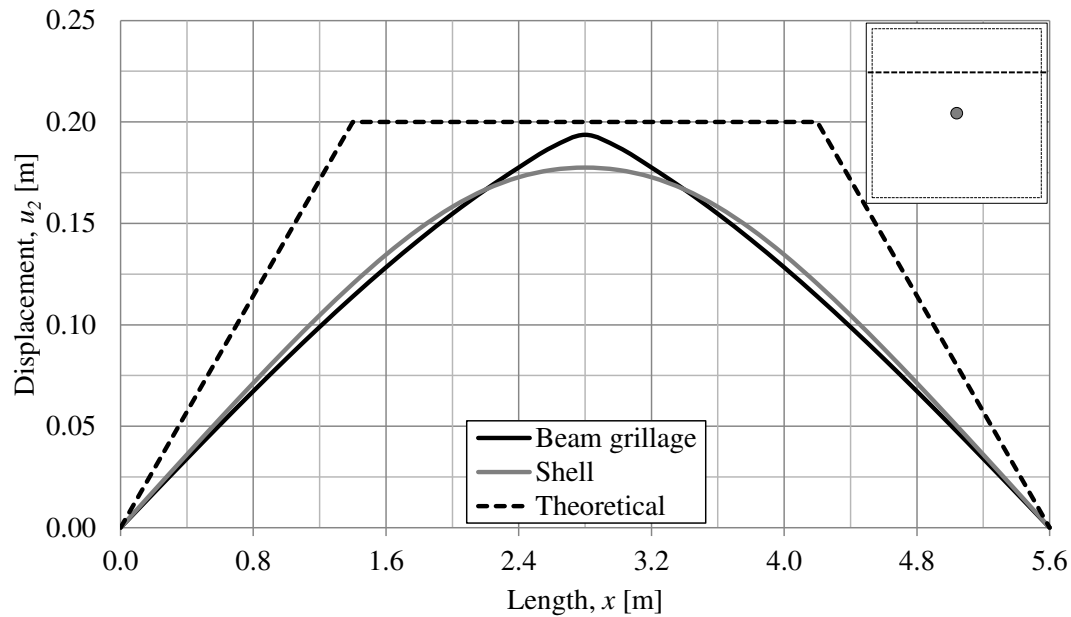
Figure 6.22   Illustration of the displacement of body 2 u_2 on a quadratic slab along a line for the theoretical assumed model, the beam grillage and the shell element model. The line and the point of loading are presented in the upper right hand corner.

In Figure 6.23, the deformation of the whole beam grillage model is illustrated from different angles of view. From this, the results of Figure 6.21 and Figure 6.22 can be confirmed, and it can also be stated that the areas close to the corners of the slab is not deforming as expected.
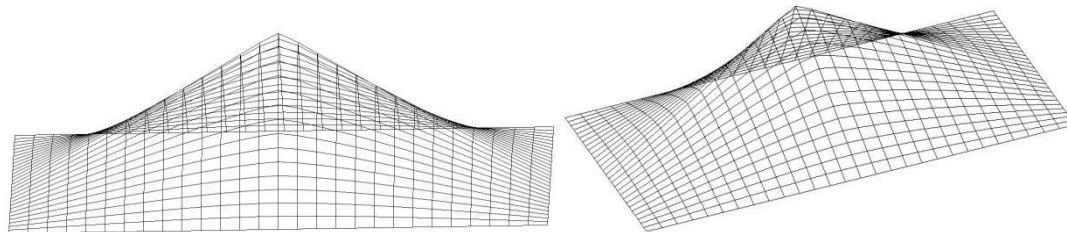
Figure 6.23   Illustration of the element grid and the deformation of the beam grillage model in ADINA from two different angles of view.

Based on Figure 6.21, Figure 6.22 and Figure 6.23, the failure mode for the beam grillage model is believed to be according to Figure 6.24a. This means that the area in which the moment is distributed at is reduced to half of the area in the expected failure mode used in the strip method calculations, as schematically illustrated in Figure 6.24b. This is believed to be the reason why the load capacity for the beam grillage model without torsional resistance is half of the load capacity according to the strip method in Figure 6.18.

a)   b)
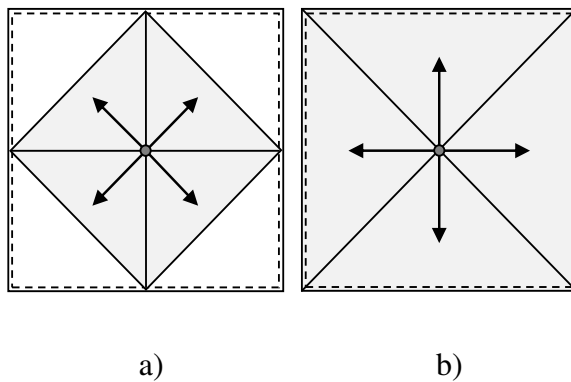
Figure 6.24   Illustration of the suggested failure modes for a simply supported reinforced concrete slab for load case 1, modelled a) as a beam grillage, and b) with shell elements. The marked area is the load carrying part of the slab.

Since the beam grillage model is having trouble distributing the load to the corners of the slab, a beam grillage model with diagonally placed beams is analysed, see Figure 6.25. To still have a quadratic cross section of the beams, the distance between the nodes in *x*- and *y*-direction is increased to 0.28 m, which gives a width of the beams that is $0.28 / \sqrt{2} = 0.198$ m ≈ 0.2 m. Therefore, the same moment-curvature and torsion-twisting relations as the normal beam grillage model are used.
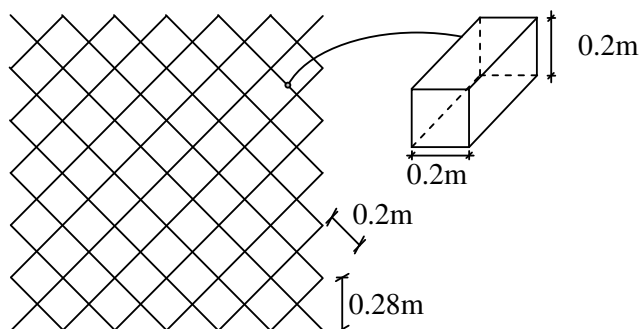
Figure 6.25   Illustration of the diagonal beam grillage model and the cross-section of the beams.

This model with diagonal beams, is having the expected failure mode and almost the expected load capacity for a load placed in the centre, see Figure 6.26.
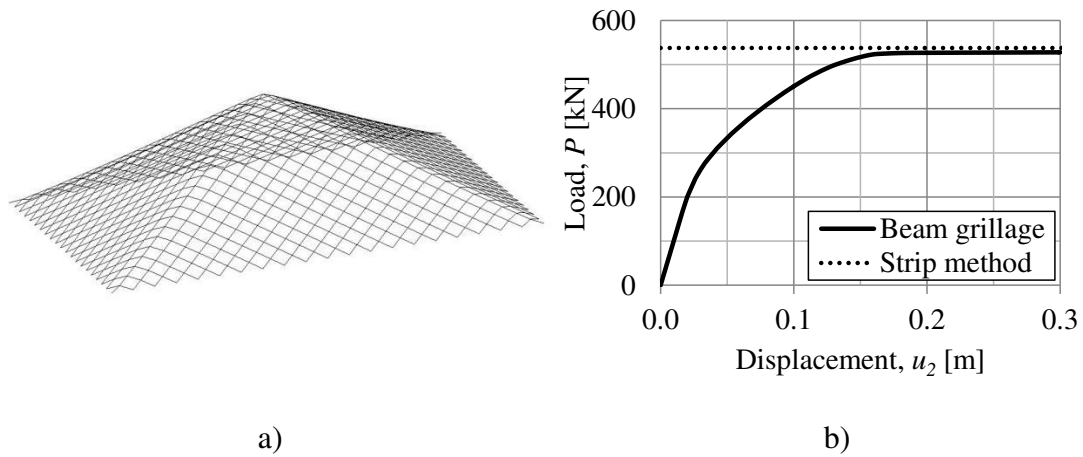
Figure 6.26   *Study of diagonal beam grillage model for load case 1, a) element grid and the deformation of the model in ADINA, and b) load-displacement response.*

However, the failure mode and load capacity for a load placed unsymmetrically is not as expected for the diagonal beam grillage model, see Figure 6.27. Hence, this type of modelling is non-viable.
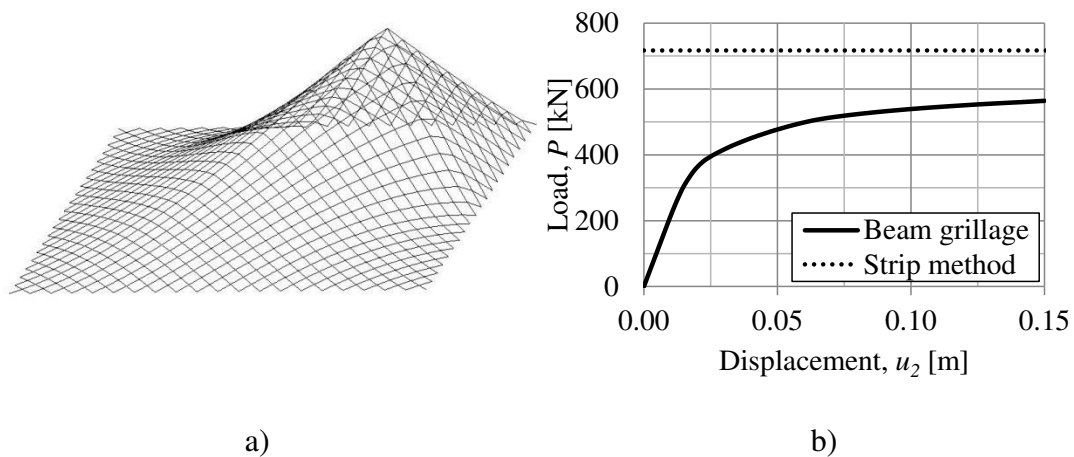
Figure 6.27   *Study of diagonal beam grillage model for load case 3, a) element grid and the deformation of the model in ADINA, and b) load-displacement response.*

Finally, a beam grillage model with both a normal grid of beams and a diagonal grid of beams is analysed, see Figure 6.28. The node positions of this model are the same as for the diagonal beam grillage model. Therefore, the beams in the normal directions have a width of 0.28 m and the diagonal beams have a width of 0.2 m. The beams with a width of 0.28 m have moment-curvature and torsion-twisting relations which are calculated in the same manner as for the normal beam grillage model, see Appendix G. Since this model now has beams in four directions, whereas the normal beam grillage model has in two directions, the moment capacity and torsional stiffness capacity is divided by two. The density is divided by four since it is divided by two for the normal beam grillage model.
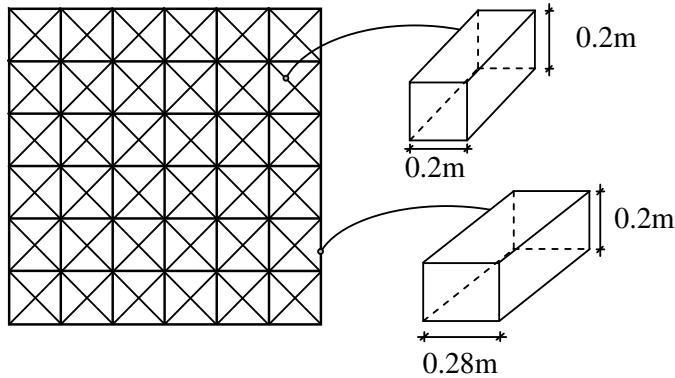
Figure 6.28   Illustration of the beam grillage model with both a normal grid of beams and a diagonal grid of beams and the cross-section of the beams.

This model has a quite good plastic deformation shape, as illustrated in Figure 6.29. However, this model is unstable and cannot handle large displacements and therefore no distinct load capacity can be found. The response indicates that there are two different yield limits. The reason for this is believed to be that there are both normal and diagonal beams with different capacities. It is also difficult to use correct input data since both normal and diagonal directions are used. This makes it hard to utilise the advantages of the beam grillage model, i.e. moment-curvature, torsion-twisting, orthotropic behaviour and different reinforcement arrangement in different sections. This model can therefore be considered as non-viable as well.

a)   b)
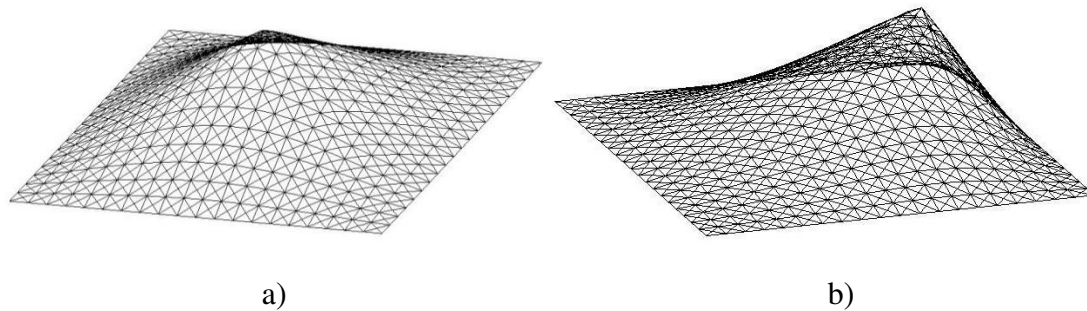
Figure 6.29   Illustration of how the element grid and the deformation of the beam grillage model with both a normal grid of beams and a diagonally grid of beams. For a) load case 1, and b) unsymmetrical load case.

Based on this, the elasto-plastic slab used for the analyses in this thesis is modelled with shell elements. This despite that ADINA (2014) will set the Poison's ratio to $v = 0.5$ when the shell elements yields, which causes an unintended increase of the moment capacity, as discussed in Section 5.4.

The failure mode for a slab modelled with shell elements is not completely as expected and has a smoother deformation shape than expected, as seen in Figure 6.22. This is believed to depend on the fact that the failure mode for a slab subjected to a point load cannot be derived from the same principles used for a uniformly distributed load. Hence, the obtained failure mode is different from the expected one. This is believed to be the reason why the load capacity for a slab modelled with shell elements is slightly lower than the expected load capacity obtained from the strip method, as illustrated in Figure 6.20.

In Figure 6.30 the plastic strain distribution is illustrated for load case 1 and 3, were purple and blue indicates that the strain is low or around the yield limit and red and

pink indicates a very high plastic strain. The plastic strain can be interpreted as yielding in the reinforcement, which means that the yield strain can be seen as an illustration of the yield lines. For load case 1 in Figure 6.30a, it can be observed that the failure mode reminds of the expected one, which explains why the load capacity obtained is close to that calculated with the strip method. However, for load case 3 the failure mode is different from the expected, as illustrated in Figure 6.30b. The same goes for load case 2 and for load cases on rectangular slabs, which are presented with corresponding illustrations in Appendix F.2.

a)   b)
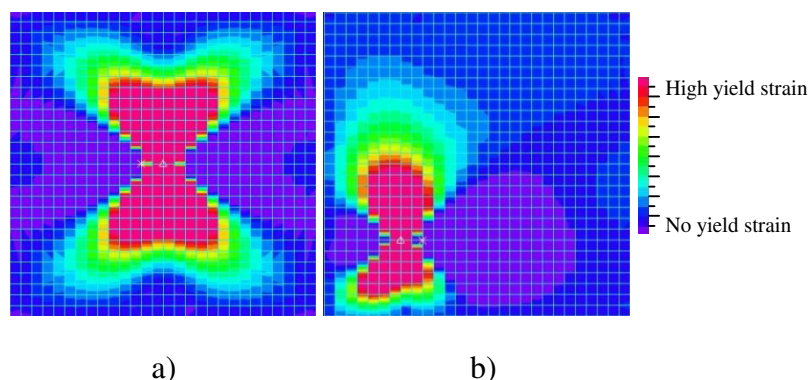
Figure 6.30   Illustration of the distribution of the plastic strain in x-direction for a) load case 1, and b) load case 3.

In Figure 6.31a, the load-displacement response for load case 1 is illustrated. It can be stated that the strip method calculations has very similar load capacity to that of the shell element model. This is probably a result of that the failure mode reminds of the expected one, as seen in Figure 6.30a. However, the load capacity calculated with the strip method is not on the safe side for load case 1, even if it is close. In Figure 6.31b, the load-displacement response for load case 3 is illustrated. The load capacity calculated with the strip method is in this case clearly overestimated if compared to that from the FE analysis. This is probably a result of that the failure mode is far from the expected one, as seen in Figure 6.30b.

a)   b)
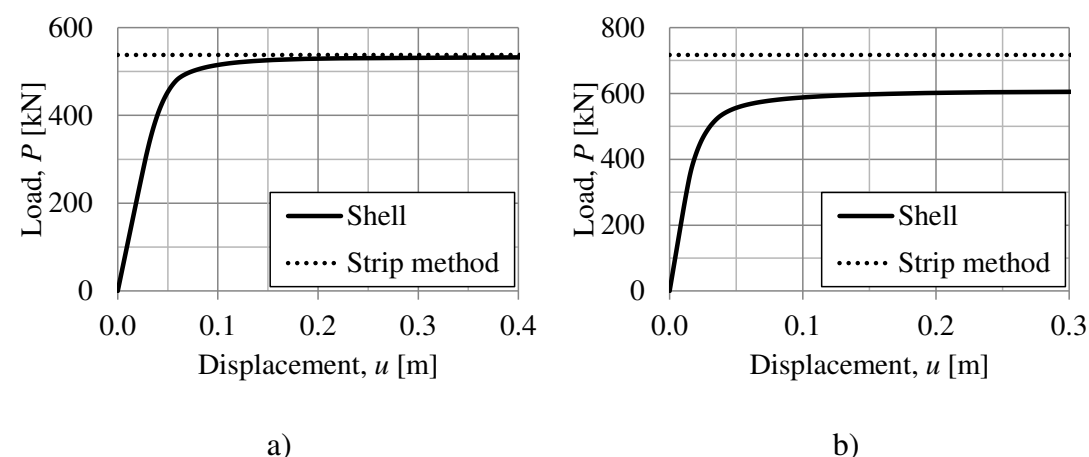
Figure 6.31   Illustration of the load-displacement response of the shell element model for a slab subjected to a point load a) load case 1, and b) load case 3.

To verify that the shell element model is valid, a uniformly distributed load is applied on the same quadratic slab and on a rectangular slab with side length $l_x = 2l_y$. As can

be observed in Figure 6.32 the failure mode is the same as the expected one as discussed in Section 2.8.3. Purple and blue indicates that the strain is low or around the yield limit and red and pink indicates a very high plastic strain.

a)   b)
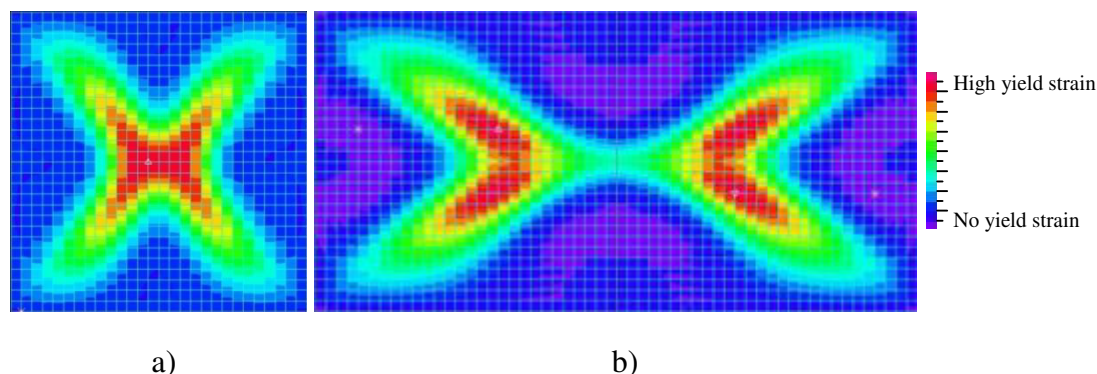
Figure 6.32   *Illustration of the distribution of the plastic strain in x-direction for a) quadratic slab subjected to a uniformly distributed load, and b) rectangular slab with side length $l_x = 2l_y$ subjected to a uniformly distributed load.*

The load capacity is calculated with the strip method according to Appendix G for both of the cases with uniformly distributed load. As can be observed in Figure 6.33, the load capacity obtained with the strip method is below the load obtained from the shell element model, hence the strip method is on the safe side as expected. This means that the shell element model is valid. However, this also means that it is not possible to directly translate the analogy of the strip method used for slabs subjected to uniformly distributed loads, onto slabs subjected to point loads.

a)   b)
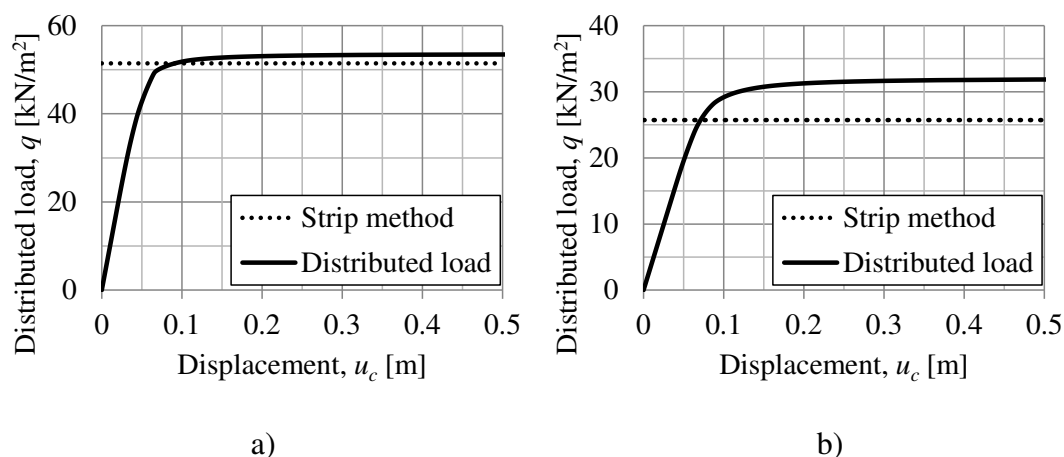
Figure 6.33   *Illustration of the load-displacement response, where the displacement u_c is measured in the centre of the slab, of the shell element model for a slab subjected to a uniformly distributed load a) quadratic slab, and b) rectangular slab with side length $l_x = 2l_y$.*

To further verify the shell element model for a quadratic slab with a uniformly distributed load, its displacement lines are compared to the theoretical displacement lines, see Figure 6.34. From this comparison it can be concluded that the displacements are also close to the expected, just as the strains illustrates in Figure 6.32.

a)   b)
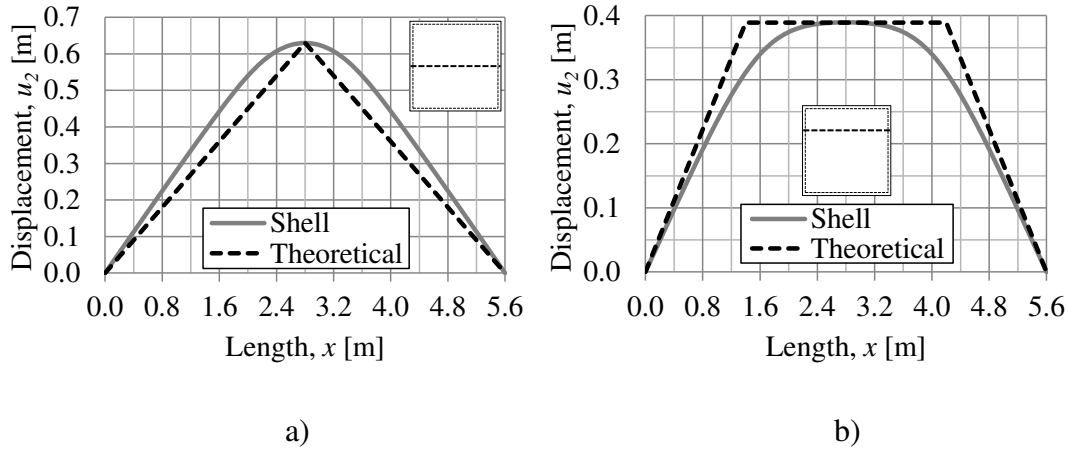
Figure 6.34   Displacement of body 2 u_2, on a quadratic slab subjected to a uniformly distributed load, along a line for the shell element model and the theoretical assumed model. For a) a line through the centre, and b) a line between the centre and the edge.

For additional plastic strain distribution diagrams for load case 2 and for a rectangular slab with side length $l_x = 2l_y$ subjected to a point load in the centre, see Appendix F.3.

6.2.4.3   Reduction of the plastic transformation factor $\kappa_{mF,pl}$

The slab modelled with shell elements subjected to a point load, does not have the shape of a pyramid when having elasto-plastic behaviour, as illustrated in Figure 6.21 and Figure 6.22. More figures illustrating this phenomenon is shown in Appendix F.1. This result do not agree with Section 4.4.3, where a pyramid like deformation shape of the slab is assumed when $\kappa_{mF,pl}$ is derived. The displacement in the system point u_s, is larger than for a pyramid shaped yield response, if this is compared to the mean displacements for all the nodes of the slab. This leads to a lower $\kappa_{m,pl}$, and thereby a lower $\kappa_{mF,pl}$ according to equation (6.3) derived in Section 4.1.2.

$$\kappa_m = \frac{1}{l} \int_{x=0}^{x=l} \frac{u(x)^2}{u_s^2} \, dx \tag{6.3}$$

In Figure 6.35, κ_{mF} is plotted as a function of the displacement at the system point u_s, for the static load cases 2 and 3 presented in Section 4.4.2. As can be seen, κ_{mF} do not have one single value for the plastic part. Instead κ_{mF} seems to decrease with increasing displacement in the system point u_s. It can also be observed that κ_{mF} is lower than the derived $\kappa_{mF,pl} = 1/6$ in Section 4.4.3. For corresponding diagrams for κ_m and κ_F, see Appendix D.2.

In Figure 6.35, it can also be seen that the curve for κ_{mF} depends on the actual load case. Load case 2 has a value for κ_{mF} of approximately 0.10 when the displacement in the system point u_s of the slab is 0.6 m. Load case 3 on the other hand has a value of approximately 0.07 for κ_{mF} when the displacement in the system point u_s of the slab is 0.6 m.
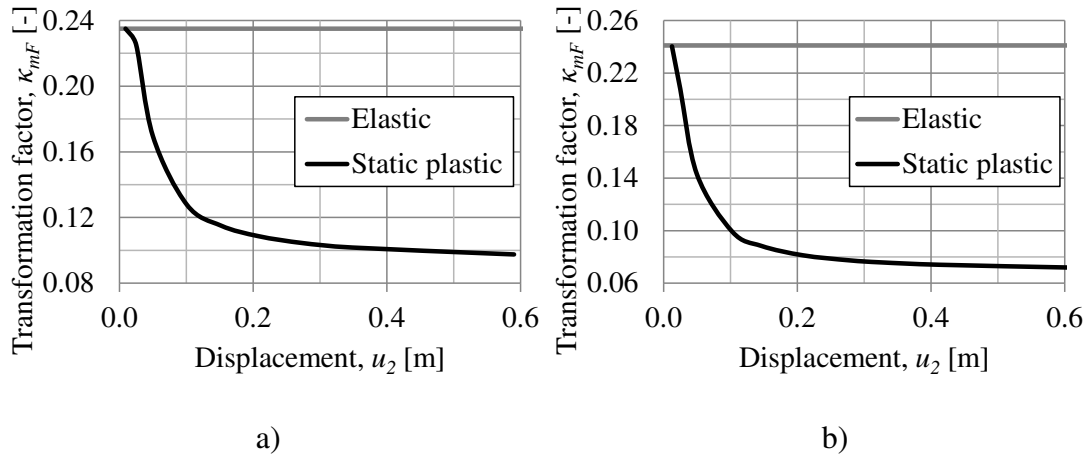
Figure 6.35 Illustration of the transformation factor κ_{mF} plotted as a function of the displacement at the system point of body 2 u_2 for a) load case 2, and b) load case 3.

Since of the transformation factors being different for different static load cases and different plastic displacements, it can be suspected that κ_{mF} does not have the same curve for a dynamic case, where the load duration is short and load magnitude is high, as for a static case where the load is stepwise applied. Figure 6.36a shows κ_{mF} as a function of the displacement of body 2 u_2 for the static load case 1 and the corresponding curve for a dynamic case. The dynamic case is a collision impact with properties of body 1 according to collision H10 in Table 6.7 but with an initial velocity of $v_0 = 10$ m/s. The displacement of body 2 u_2 as a function of time for the dynamic case is illustrated in Figure 6.36b. The values of κ_{mF} for the dynamic case are derived during the first 0.27 s of the collision, until the maximum displacement u_2 has occurred.

Figure 6.36a clearly shows that the values for κ_{mF} are not the same for static and dynamic cases. The dynamic case has lower values for κ_{mF} than the static case, which means that the dynamic case has a more locally shaped deformation around the load application area according to equation (6.3). The reason for this is believed to be that the slab does not have the time to distribute the deformation completely, because of the relatively short duration of the collision impact. However, the dynamic case will have a κ_{mF} which is the same as for a static case when the deformation has reached its maximum value.

CHALMERS, *Civil and Environmental Engineering*, Master's Thesis 2015:87
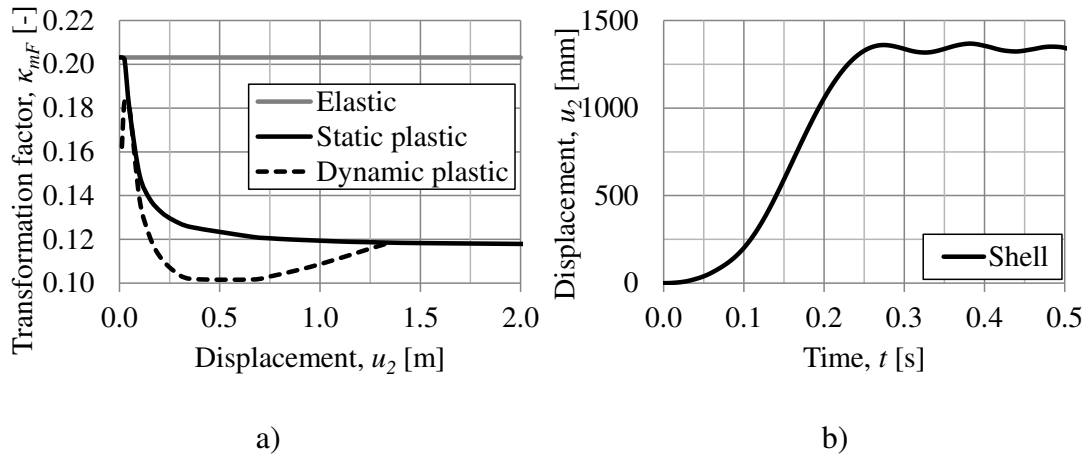
Figure 6.36   *Illustration of a) the transformation factor κ_{mF} plotted as a function of the displacement at the system point of body 2 u_2 for load case 1, and the first 0.25 s of a dynamic case based on collision H10 but with an initial velocity $v_0 = 10$ m/s, and b) the displacement at the system point u_s as a function of time for the current dynamic case.*

In Figure 6.37, the static displacement is compared to the dynamic case used in Figure 6.36. These plots further confirms that slabs subjected to an impact load can have more local displacements around the load application area than slabs subjected to static point loads.
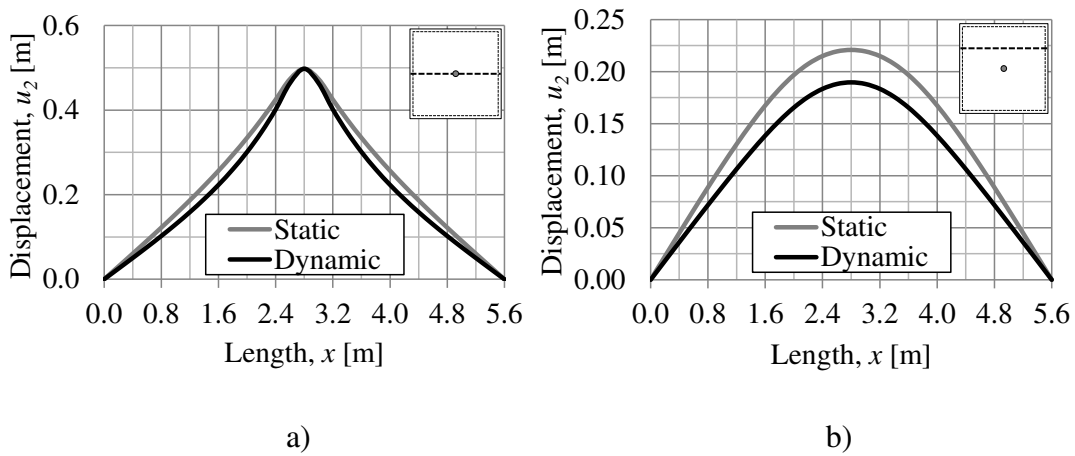
Figure 6.37   *Displacement of body 2 u_2, on a quadratic slab subjected to a static point load and a dynamic case 0.14 s into the collision used in Figure 6.36. For a) a line through the centre, and b) a line between the centre and the edge.*

Based on this, it can be stated that κ_{mF} can have a lower value than the theoretically derived value of 1/6, and especially for dynamic cases. Therefore, when analysing an elasto-plastic slab with 2DOF in Section 6.2.4.4, $\kappa_{mF} = 0.1$ is tested.

6.2.4.4   Comparison between 2DOF and shell element model

To model a more realistic behaviour for the simply supported reinforced concrete slab, an elasto-plastic response is used, as discussed in Section 6.2.4.3. A series of twelve collisions with an elastic response of body 1 and an elasto-plastic response of

body 2 is conducted with input parameters according to Table 6.10. As described in Section 6.2.4.3, only shell element models are used for the FE analysis in this section.

Table 6.10   FE and 2DOF input parameters for collision J1-J12.

Case	α_x [-]	α_y [-]	k_1 [MN/m]	m_1 [kg]	v_0 [m/s]	2DOF k_2 [MN/m]	2DOF $R_{2,max}$ [kN]
Collision J1	0.5	0.5	0.5	1 500	27.8	10.79	537.7
Collision J2	0.5	0.25	0.5	1 500	27.8	15.94	537.7
Collision J3	0.25	0.25	0.5	1 500	27.8	22.02	716.9
Collision J4	0.5	0.5	1	1 500	27.8	10.79	537.7
Collision J5	0.5	0.25	1	1 500	27.8	22.02	537.7
Collision J6	0.25	0.25	1	1 500	27.8	22.02	716.9
Collision J7	0.5	0.5	0.5	15 000	10	10.79	537.7
Collision J8	0.5	0.25	0.5	15 000	10	15.94	537.7
Collision J9	0.25	0.25	0.5	15 000	10	22.02	716.9
Collision J10	0.5	0.5	1	15 000	10	10.79	537.7
Collision J11	0.5	0.25	1	15 000	10	15.94	537.7
Collision J12	0.25	0.25	1	15 000	10	22.02	716.9

The reason for having the lower value of $v_0 = 10$ m/s, or 36 km/h, for collision J6-J12 instead of $v_0 = 27.8$ m/s, as in the previous parts of this thesis, is that $v_0 = 27.8$ m/s gives extremely large displacements in the slab. The stiffness of body 2 in the 2DOF model is taken from the stiffness of the slab k_{sl} presented in Table 4.1, and the maximum internal resistance of body 2 $R_{2,max}$ is derived using the strip method explained in Section 2.8.3. The length factors α_x and α_y are defined as illustrated in Figure 6.8.

Similarly to the beam with elasto-plastic response in Section 6.1.4 the transformation factor κ_{mF} now depends on both elastic and plastic response and is unique for each set of properties. In Section 6.2.4.3, it is also shown that κ_{mF} can be lower than the theoretically derived value of 1/6 during plastic response, for the slab model used in this thesis. Because of this uncertainty, different κ_{mF} are tested in the 2DOF model for collision J1-J12. The κ_{mF} used in the 2DOF are, the elastic κ_{mF} presented in Table 4.1 for different load cases, the theoretically derived plastic $\kappa_{mF} = 1/6$ from Section 4.4.3, and $\kappa_{mF} = 0.1$ as discussed in Section 6.2.4.3.

In Figure 6.38, the load-displacement relation for load case 1 and 3 are illustrated for both the shell element model and the 2DOF model. As can be seen in Figure 6.38b, the maximum internal resistance of body 2 $R_{2,max}$, is very different in the 2DOF model compared to the shell element model for load case 3. The reason for this is that the strip method gives a load capacity that is approximately 18 % higher than the load capacity obtained by the shell element model. It is believed that the assumed failure mode used in the strip method is not correct. See Appendix F.2 for more load-displacement diagrams.

The load-displacement relations would have been better if $R_{2,max}$ in the 2DOF model had been based on the load capacity of the shell element model. However, the strip method is still used to calculate $R_{2,max}$ for the 2DOF model so that the input data for the 2DOF model can be based on hand calculations.

a)   b)
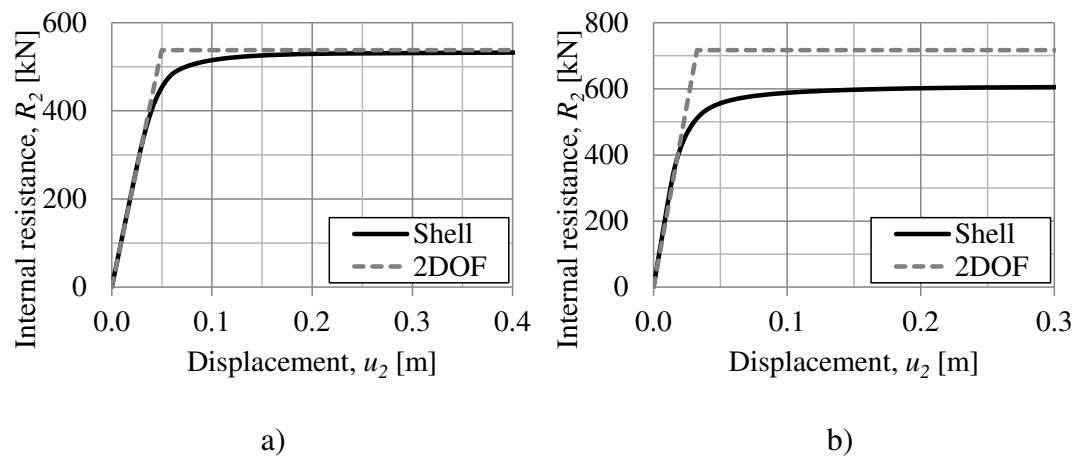
Figure 6.38   Illustration of the load-displacement relation for the shell element and the 2DOF model for a) load case 1, and b) load case 3.

A comparison between the responses for the 2DOF system and the FE model with shell elements for collision J1 can be seen in Figure 6.39. The internal resistance of body 1 R_1 is plotted as a function of time in Figure 6.39b. In this diagram, all the 2DOF model curves and the shell element model correspond well and it can be stated that the collision has a duration of approximately 0.17 s. However, in contrast to the analysis carried out with a slab modelled with an elastic response there is now a slight difference after the collision for the displacement of body 1 u_1 as seen in Figure 6.39a.

In Figure 6.39c, the displacement of body 2 u_2 as a function of time is illustrated. It can be seen that the 2DOF closest to the shell element model is the one using $\kappa_{mF} = 0.1$, which has a maximum displacement quite close to shell elements, but not on the safe side.

The response after 0.17 s is not corresponding well between the 2DOF and the shell element model. A part of this difference is believed to be a result of the difference in load-displacement relations for load case 1, where the 2DOF model has a sharper curve than the shell element model, see Figure 6.38. In addition, the load-displacement relation for the shell element model may be different for dynamic cases compared to the static cases presented in Figure 6.38. The fact that the actual transformation factor κ_{mF} from the shell element model varies so much is also believed to affect the correspondence.
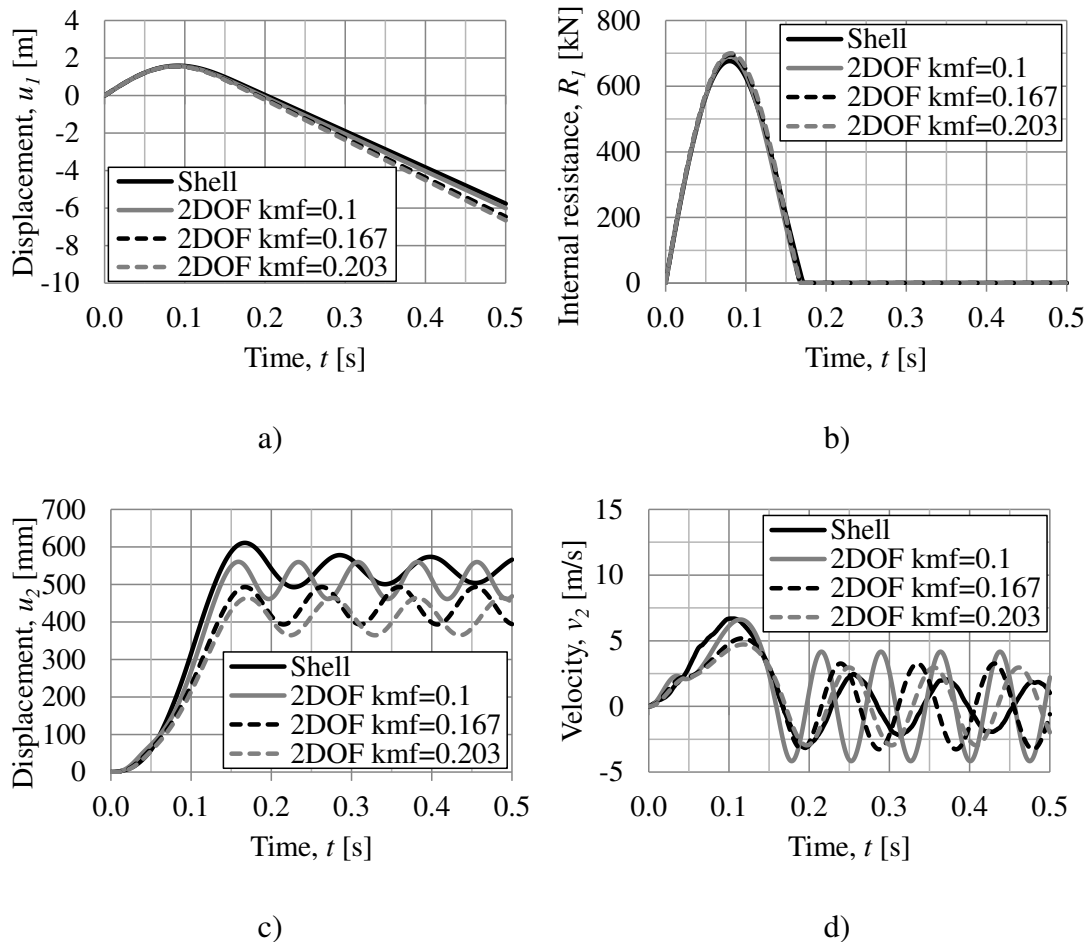
Figure 6.39   Illustration of collision J1, a) displacement of body 1 u_1, b) internal resistance of body 1 R_1, c) displacement of body 2 u_2, and d) velocity of body 2 v_2.

A comparison between the responses for the 2DOF and the FE model with shell elements for collision J3 can be seen in Figure 6.40. The internal resistance of body 1 R_1 is plotted as a function of time in Figure 6.40b. In this diagram, the 2DOF and the shell element model do not correspond as well as for body 1 in previous sections of this thesis. But all models seem to have the same collision duration of approximately 0.17 s. However, in contrast to the analysis carried out with a slab modelled with an elastic response there is now a slight difference after the collision for the displacement of body 1 u_1 as seen in Figure 6.40a.

In Figure 6.40c, the displacement of body 2 u_2 as a function of time is illustrated. It can be seen that the 2DOF and the shell element model do not correspond at all. One reason for this is believed to be the great difference in the maximum internal resistance of body 2 $R_{2,max}$ between the models for load case 3, see Figure 6.38b.
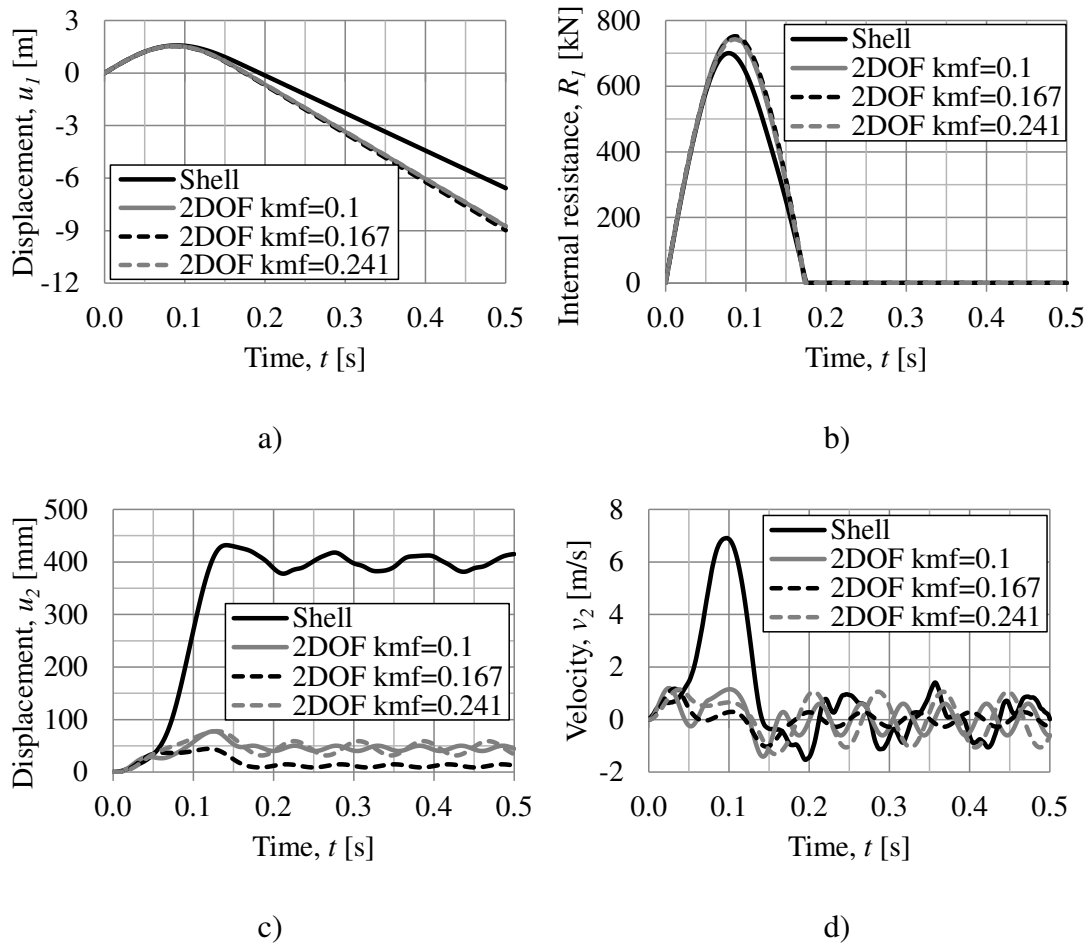
Figure 6.40   Illustration of collision J3, a) displacement of body 1 u_1, b) internal resistance of body 1 R_1, c) displacement of body 2 u_2, and d) velocity of body 2 v_2.

To decrease the large difference observed in Figure 6.40, the maximum internal resistance of body 2 $R_{2,max}$ obtained from the FE analysis is used as input data for the 2DOF model instead of the hand calculated $R_{2,max}$. This is illustrated in Figure 6.41 were it can be observed that the difference between the 2DOF and shell element model is smaller than in Figure 6.40, but still large.
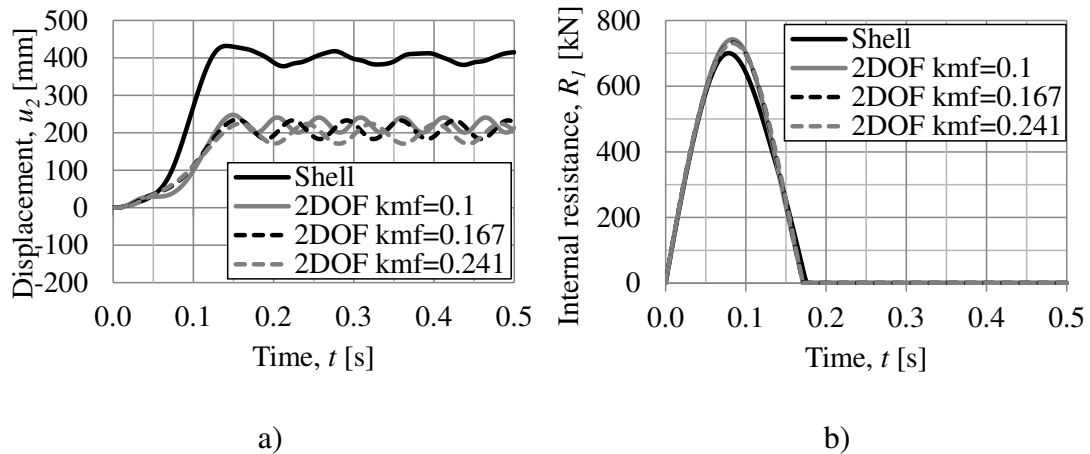
Figure 6.41   Illustration of the response for collision J3 with $R_{2,max}$ obtained from the FE analysis as input data, a) displacement of body 2, and b) internal resistance of body 1 R_1.

A comparison between the responses for the 2DOF and the FE model with shell elements for collision J7 can be seen in Figure 6.42. The internal resistance of body 1 R_1 is plotted as a function of time in Figure 6.42b. In this diagram, the 2DOF and the shell element model do not correspond as well as for body 1 in previous sections of this thesis. The models have a collision duration of about $0.55 - 0.6$ s. However, in contrast to the analysis carried out with a slab modelled with an elastic response there is now a slight difference after the collision for the displacement of body 1 u_1 as seen in Figure 6.42a.

In Figure 6.42c, the displacement of body 2 u_2 as a function of time is illustrated. It can be seen that the 2DOF model closest to the shell element model is the one using $\kappa_{mF} = 0.1$, and that all 2DOF model curves maximum displacements are close to the shell element models.

When comparing collision J7 with collision J10, which is presented in Appendix C.6, it is only the stiffness of body 1 k_1 that is different. As seen the duration of the collision is shorter with a larger k_1 and a larger stiffness gives slightly larger displacement of body 2 u_2.
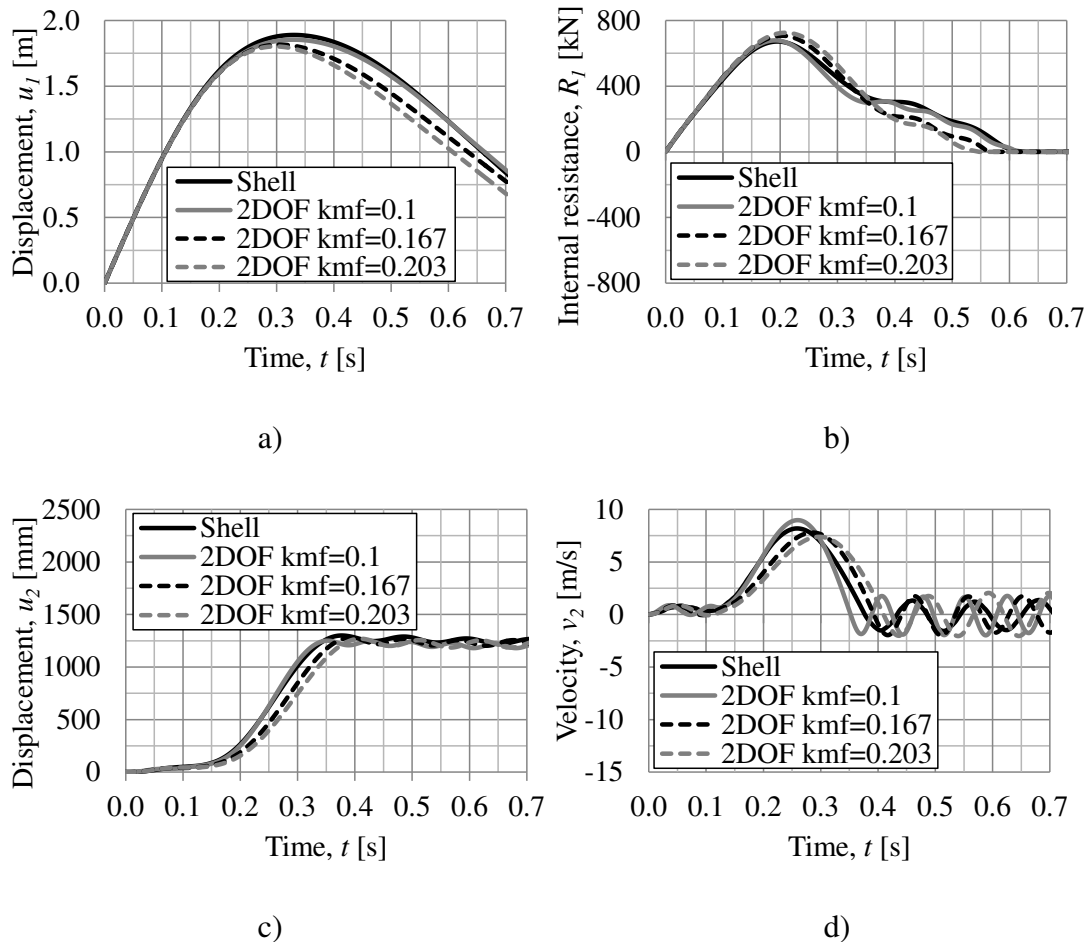
Figure 6.42   Illustration of collision J7, a) displacement of body 1 u_1, b) internal resistance of body 1 R_1, c) displacement of body 2 u_2, and d) velocity of body 2 v_2.

A comparison between the responses for the 2DOF and the FE model with shell elements for collision J9 can be seen in Figure 6.43. The internal resistance of body 1 R_1 is plotted as a function of time in Figure 6.43b. In this graph, the 2DOF and the shell element model do not correspond as well as for body 1 in previous sections of this thesis. The models have a collision duration of about $0.55 - 0.6$ s. However, in contrast to the analysis carried out with a slab modelled with an elastic response there is now a difference after the collision for the displacement of body 1 u_1 as seen in Figure 6.43a.

In Figure 6.43c, the displacement of body 2 u_2 as a function of time is illustrated. It can be seen that the 2DOF and the shell element model do not correspond at all, just as for collision J3. This too is believed to partly depend on the great difference in the maximum internal resistance of body 2 $R_{2,max}$ between the models for load case 3, see Figure 6.38b.
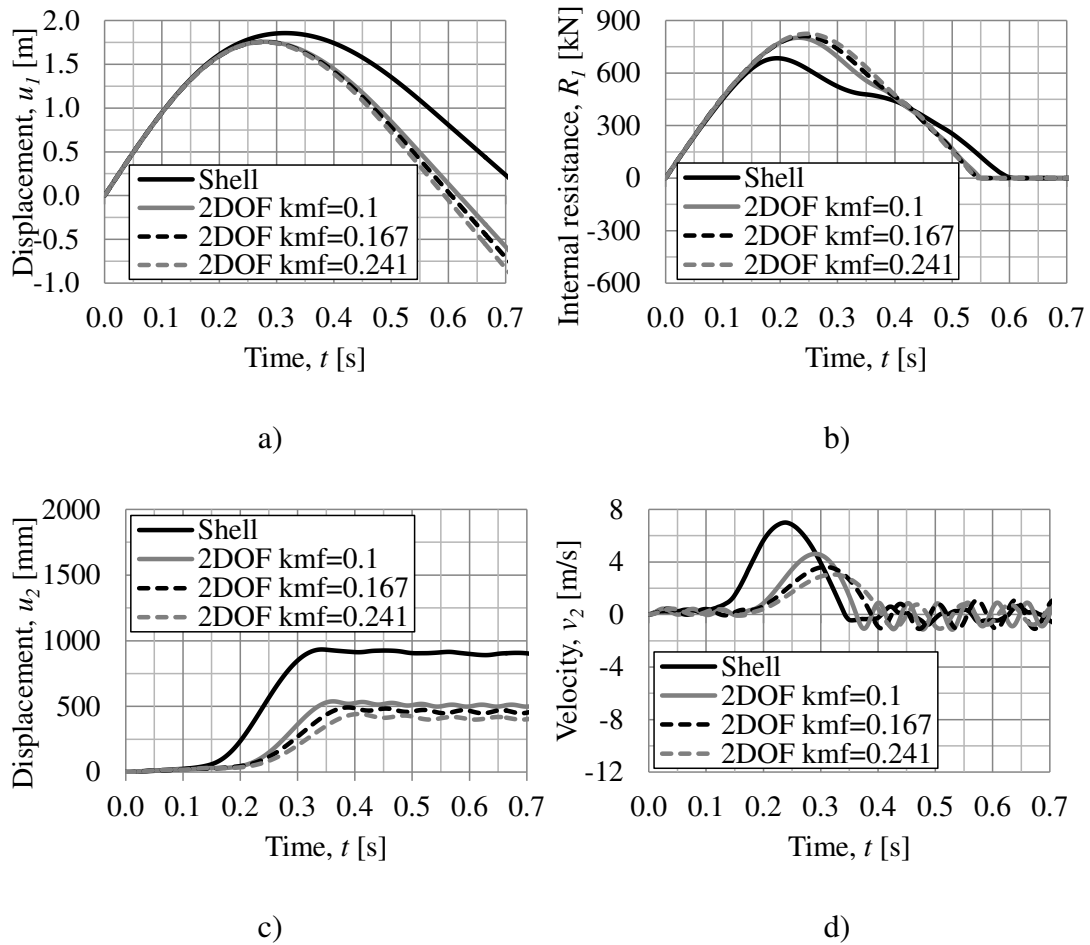
Figure 6.43   Illustration of collision J9, a) displacement of body 1 u_1, b) internal resistance of body 1 R_1, c) displacement of body 2 u_2, and d) velocity of body 2 v_2.

To decrease the large difference observed in Figure 6.43, the maximum internal resistance of body 2 $R_{2,max}$ obtained from the FE analysis is used as input data for the 2DOF model instead of the hand calculated $R_{2,max}$. This is illustrated in Figure 6.44 were it can be observed that the difference between the 2DOF and shell element model is much smaller than in Figure 6.43. As illustrated in Figure 6.44a, the maximum displacement of body 2 u_2 is not so different between the 2DOF and FE model. This can however be a coincidence.
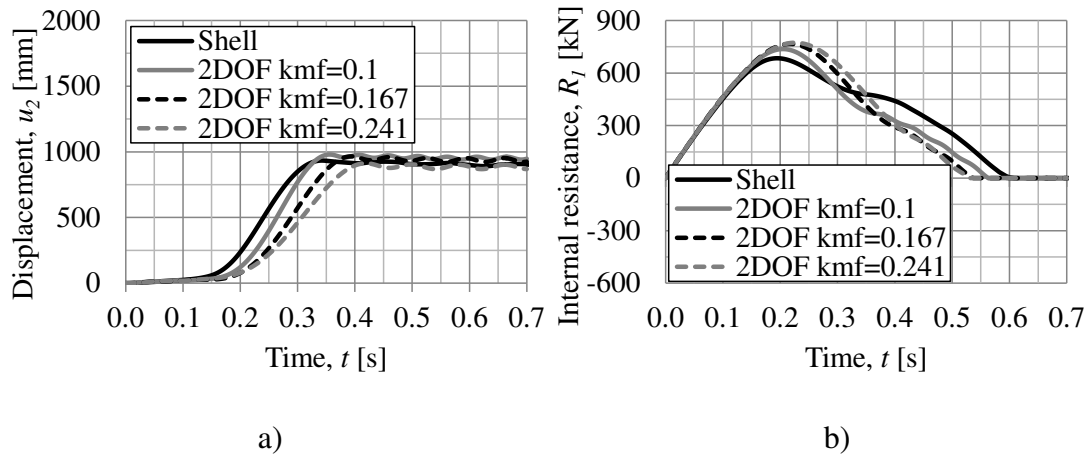
Figure 6.44   Illustration of the response for collision J9 with $R_{2,max}$ obtained from the FE analysis as input data, a) displacement of body 2, and b) internal resistance of body 1 R_1.

The overall correspondence between the 2DOF and FE models are in this section good when the collision impact is located in the centre of the slab. However, when the collision impact is not located at the centre of the slab, the correspondence is not so good.

See Appendix C.6 for the corresponding response diagrams regarding collision J1-J12.

6.2.5   Discussion

The 2DOF has an overall good correspondence compared to both of the FE models when body 2 has a fully elastic response, the correspondence is however better the closer the impact is to the centre of the slab. Whether body 1 has elastic or elasto-plastic response, does not seem to be of high importance for the correspondence of body 2 between the 2DOF and FE models. However, when comparing the response of the displacement of body 2 u_2 for collision H1 in Figure 6.9c, with u_2 for collision I1 in Figure 6.13c, the results are different. The elasto-plastic collision I1 causes a much smaller maximum displacement of body 2 than the elastic collision H1, i.e. there is a large difference if body 1 is elastic or elasto-plastic. However, it is on the safe side to assume an elastic behaviour of body 1, which agrees with the theory in Section 2.3.1.

The shell element model and the beam grillage model have almost the exact same behaviour for an elastic response of body 2. However, when the slab is yielding in the FE models, the shell element model and the beam grillage model do not have the same behaviour at all, and it is decided that the shell element model has the better behaviour of the two, see Section 6.2.4.2. However, it can be discussed whether the shell element model produce results close to that expected in a reinforced concrete slab, since it does not have the expected failure mode. How to model an elasto-plastic reinforced concrete slab with shell elements needs to be further studied.

The shell element model have the disadvantages that moment-curvature and torsion-twisting relations cannot be manually implemented, and that the Poisson's ratio is set to $v = 0.5$ during yielding. It is also hard to have orthotropic behaviour, different reinforcement arrangement in different sections, and different amount of reinforcement in top and bottom when shell elements are used. When studying a beam

in Section 6.1, the beam elements have good elasto-plastic behaviour and it is first when the beam elements are used in a beam grillage, it starts to have problems with the stress distribution.

The correspondence is not good at all if the maximum internal resistance of body 2 $R_{2,max}$ differs to much between the models, which is expected. As an example, for load case 3, the difference between the hand calculated $R_{2,max} = 717$ kN, and the $R_{2,max} = 608$ kN obtained from FEM, is almost 20 %. Also, the correspondence between the models is good when the impact is located in the centre of the slab, but not otherwise.

The correspondence between the 2DOF model and the shell element model for body 1 is less good for collision J7 in Figure 6.42, than for collision tests in earlier sections. On the other hand, the correspondence between the two models is quite good for body 2 in this case. The reason for this is believed to be the difference in the load-displacement relations illustrated in Figure 6.38a.

It can be stated that the 2DOF model with an elasto-plastic response of body 2 can be improved by having more accurate ways to calculate $R_{2,max}$ and by having a multi-linear k_2 function so that it corresponds to the load-displacement diagram in Figure 6.38. It is believed that a more accurate stiffness k_2 is resulting in an overall better correspondence between the FE and 2DOF model.

The usage of the transformation factor κ_{mF} can also be improved, either by finding an approach that calculates an optimised κ_{mF} for each collision, or by having a varying κ_{mF}. In this section, guessed and constant values for κ_{mF} are used, but as discussed in Section 6.2.4.3, the behaviour of κ_{mF} is complex.

By increasing the stiffness of body 1 k_1 the duration of the collision is decreased but most important, the load on body 2 is increased and therefore also the displacement, as seen in Section 6.2.2, 6.2.3 and 6.2.4.4. This means that by choosing a stiffness which is larger than expected, a result which is on the safe side is obtained. This is also more thoroughly discussed in the precedent master's thesis by Asplund and Steckmest (2014).

7 Final Remarks

7.1 Conclusions

This thesis is evaluating how the design with regard to collision impact between simply supported reinforced concrete members and incoming objects, can be carried out using both FE analysis and a 2DOF model. The studies evaluate elastic and elasto-plastic response for both the incoming object and the resisting structure. Quadratic slabs are of main interest but beams are also evaluated. When slabs are evaluated, the 2DOF model is compared to both a shell element model and a beam grillage model. The FE and 2DOF models have good correspondence for beams with both elastic and elasto-plastic behaviour and for quadratic slabs with elastic behaviour.

If body 1 has elastic or elasto-plastic response is not of greater importance for the correspondence between the 2DOF and FE models for body 2. However, a body 1 with elastic behaviour gives larger displacement in the resisting structure than a body 1 with elasto-plastic behaviour for the same collision, which means that an elastic body 1 gives results on the safe side. Also, a higher stiffness k_1 of body 1 gives a higher displacement in the resisting structure, and therefore it is on the safe side to assume a higher stiffness than expected for the incoming object.

When comparing the 2DOF and FE models the latter are seen as reference models because they are supposed to describe the reality better than the 2DOF model. However, the beam grillage model with elasto-plastic behaviour does not give the expected response, even though single beams modelled in the same way have the correct behaviour. It is therefore concluded that a shell element model better represent the real behaviour of an elasto-plastic reinforced concrete slab than the case using a beam grillage model.

For a quadratic slab with elasto-plastic behaviour, the 2DOF and FE model shows good correspondence when the load is applied at the centre of the slab. One reason for this is the fact that the hand calculated maximum slab resistance is quite similar to that from the FE model in this case. However, the hand calculated resistance is not always on the safe side, as expected when using the strip method.

When the impact location is not located at the centre of the slab, the hand calculated resistance is not similar to that achieved from the FE model. This because the failure modes assumed in the hand calculations, do not correspond to those obtained in the FE model. That is one of the reasons that there is not so good correspondence between the 2DOF and FE model for these cases. On the other hand, the correspondence is better if the resistance used in the 2DOF is based on the results from the FE analysis. However, if the resistance needs to be derived for each case with FE software, then the collision can be analysed with FE software instead of a 2DOF model. It is believed that the 2DOF model can be improved if a more accurate way of deriving the maximum slab resistance is found.

When comparing different values for the transformation factor κ_{mF} in the 2DOF model with the FE model, for a quadratic slab with an elasto-plastic behaviour, there is a large difference. The result shows that the obtained value of κ_{mF} is lower than the theoretical plastic value of $\kappa_{mF} = 1/6$, which gives an underestimated value of the displacement of the slab. This is due to the fact that the theoretical plastic failure mode is different from the obtained failure mode in the FE model.

In addition, the analysis shows that κ_{mF} derived from collision cases is even lower than that derived from static cases. Since the main interest is the response during the collision, this phenomenon may be of great importance. The fact that κ_{mF} can have a lower value during collision leads to an even more underestimated value of the slab displacement.

7.2 Further studies

In this thesis simply supported quadratic concrete slabs are studied and with limited load cases. To further extend the study, other boundary conditions, different slab geometries and more load cases should be evaluated.

To get improved results with the 2DOF model for slabs with elasto-plastic behaviour, hand calculations approaches for the load capacity that gives more accurate results and on the safe side need to be found. It is believed that the failure mode obtained from the FE model is different from the failure mode assumed in the hand calculations, where the yield lines goes straight from the point of loading to the corners of the slab. To improve the response further in the 2DOF model it is possible to use a multi-linear stiffness of the slab for better correspondence with the load-displacement relation of the FE model.

The reality of a slab with elasto-plastic behaviour is in this thesis represented by a FE model using shell elements. This model could be compared to physical tests or a more detailed FE model with concrete and reinforcement modelled separately, to verify that the behaviour of the model is sufficient. Also, the shell element model in this thesis is made in the commercial FE software ADINA, and can be verified and compared to models made in other FE software.

The beam grillage model with elasto-plastic response can be further evaluated. Even though the beam grillage model does not have a good response in this thesis, it has a large theoretical advantage since manually implemented moment-curvature and torsion-twisting relations can be used, which gives more control of the slab behaviour than what is possible using the shell element model. Hence, using a beam grillage model, orthotropic behaviour, different reinforcement arrangement in different sections, and different amount of reinforcement in top and bottom can be modelled. Further studies of how torsion-twisting relations should be handled in a FE model of a slab can also be done for a beam grillage model. The beam grillage model in this thesis is made in the commercial FE software ADINA, and it may be possible that this way of modelling works different in other FE software.

It is discovered in this thesis that the transformation factor κ_{mF} is varying when the slab is yielding and can decrease to a value well below the theoretical derived plastic value $\kappa_{mF} = 1/6$, especially for dynamic cases. Therefore, κ_{mF} needs to be derived for different load cases and for different slabs and if necessary, even for different incoming objects with altering velocities. It is of special interest to evaluate if κ_{mF} differ more between static and dynamic cases when the slab is large, due to local displacements. It could also be evaluated if it is best to use a constant or a varying transformation factor κ_{mF} during the 2DOF analyse.

8   References

ADINA R and D, Inc., 2014. *ADINA System 9.0 Release Notes,* Watertown: s.n.

Al-Emrani, M., Engström, B., Johansson, M. and Johansson, P., 2011. *Bärande Konstruktioner, del 1,* Göteborg: Chalmers University of Technology.

Asplund, E. and Steckmest, D., 2014. *Design with Regard to Collision Impact,* Göteborg: Chalmers University of Technology.

Augustsson, R. and Härenstam, M., 2010. *Design of reinforced concrete slab with regard to explosion,* Göteborg: Chalmers University of Technology.

Biggs, J. M., 1964. *Introduction to Structural Dynamics.* Boston: McGraw-Hill Inc..

Carlsson, M. and Kristensson, R., 2012. *Structural Response with Regard to Explosions,* Lund: Lund University.

Cederwall, K., Lorentsen, M. and Östlund, L., 1990. *Betonghandboken - Konstruktion.* 2nd ed. Stockholm: Svensk byggtjänst.

CEN, 2004. Eurocode 2: Design of concrete structures Part 1-1, Stockholm: SIS Förlag AB.

Craig Jr., R. R. and Kurdila, A. J., 2006. Fundamentals of Structural Dynamics. 2nd ed. Hoboken: John Wiley & Sons, Inc..

Engström, B., 2011. Design and analysis of continous beams and columns, Göteborg: Chalmers University of Technology.

Engström, B., 2014. Design and analysis of slabs and flat slabs, Göteborg: Chalmers University of Technology.

Fortifikationsförvaltningen, 1973. Provisoriska anvisningar för dimensionering av armerade betongkonstruktioner som skydd mot verkan av konventionella vapen inom närmissområde. Bk 25:2 ed. Stockholm: Fortifikationsförvaltningen - Befästningsavdelningen.

Hultin, E., 1994. Betongplattor, Göteborg: Chalmers University of Technology.

Johansson, M., 2014. Beräkningsmetodik, transportmissöden och trombgenererade missiler, Göteborg: Reinertsen Sverige AB.

Johansson, M. and Laine, L., 2012. Bebyggelsens motståndsförmåga mot extrem dynamisk belastning, Delrapport 3: Kapacitet hos byggnader, Göteborg: Reinertsen Sverige AB.

Lim, S., 2013. Redistribution of force concentrations in reinforced concrete cantilever slab using 3D non-linear FE analyses, Göteborg: Chalmers University of Technology.

Lundh, H., 2000. Hållfasthetslära, Stockholm: Royal Institute of Technology.

Parametric Technology Corporation, 2011. Mathcad 15.0, Needham, MA: Parametric Technology Corporation.

The Mathworks Inc., 2014. MATLAB r2015b, Natick, MA: The Mathworks Inc..

Appendix A   Central Difference Method

In this appendix, the Central Difference Method presented in Section 2.7 is summarised step by step, based on the algorithm in Craig and Kurdila (2006).

Table A.1   *Algorithm to solve Newton's second law of motion with the Central Difference Method based on Craig and Kurdila (2006).*

Step	Action
0	(0.1) Input the mass, damping and stiffness matrices $\mathbf{M}$, $\mathbf{C}$, $\mathbf{K}$ (0.2) Calculate the LU factorization of $\mathbf{M}$ (0.3) Input the initial conditions $\mathbf{u}_0$ and $\mathbf{v}_0$ (0.4) Set the simulation parameters, including the time step h (0.5) Calculate the initial acceleration from the equations of motion $$\ddot{\mathbf{u}}_0 = \mathbf{M}^{-1}\left(\mathbf{f}(0) - \mathbf{C}\mathbf{v}_0 - \mathbf{K}\mathbf{u}_0\right)$$ (0.6) Calculate the LU-factorization of $$\frac{\mathbf{M}}{h^2} + \frac{\mathbf{C}}{2h}$$ (0.7) Calculate the starting displacement value from the equation $$\mathbf{u}_{-1} = \mathbf{u}_0 - h\dot{\mathbf{u}}_0 + \frac{h^2}{2}\ddot{\mathbf{u}}_0$$
1	Loop for each time step, $n = 1 \ldots, t_n = t_1 \ldots$
2	Solve the displacements for the next time step $$\mathbf{u}_{n+1} = \left(\frac{\mathbf{M}}{h^2} + \frac{\mathbf{C}}{2h}\right)^{-1}\left(\mathbf{f}(t) - \left(\mathbf{K} - \frac{2\mathbf{M}}{h^2}\right)\mathbf{u}_n - \left(\frac{\mathbf{M}}{h^2} - \frac{\mathbf{C}}{2h}\right)\mathbf{u}_{n-1}\right)$$
3	Evaluate the set of velocities and accelerations, as needed $$\dot{\mathbf{u}}_n = \frac{\mathbf{u}_{n+1} - \mathbf{u}_{n-1}}{2h}$$ $$\ddot{\mathbf{u}}_n = \frac{\mathbf{u}_{n+1} - 2\mathbf{u}_n + \mathbf{u}_{n-1}}{h^2}$$
4	set $n = n+1$ and continue to the next time step

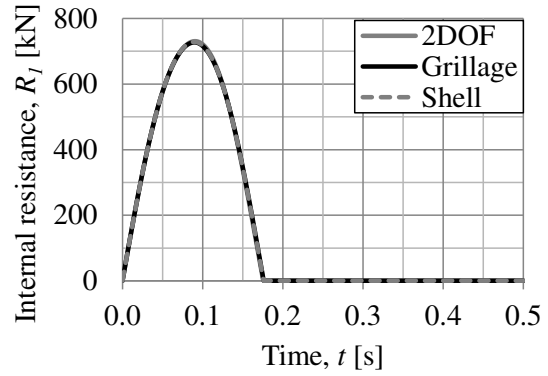# Appendix B   Results from 2DOF Analysis

B.1   Elastic response without barrier

In this section, results for collision A1-A4 are presented according to the analysis discussed in Section 3.2.2.

Table B.1   Input parameters for collision A1-A4 with elastic response for the 2DOF system.

Case	v_0 [m/s]	k_1 [kN/m]	m_1 [kg]	m_2 [kg]
Collision A1	27.8	100	1 500	7 500
Collision A2	27.8	100	15 000	7 500
Collision A3	27.8	1 000	1 500	7 500
Collision A4	27.8	1 000	15 000	7 500

a)

b)

c)

d)
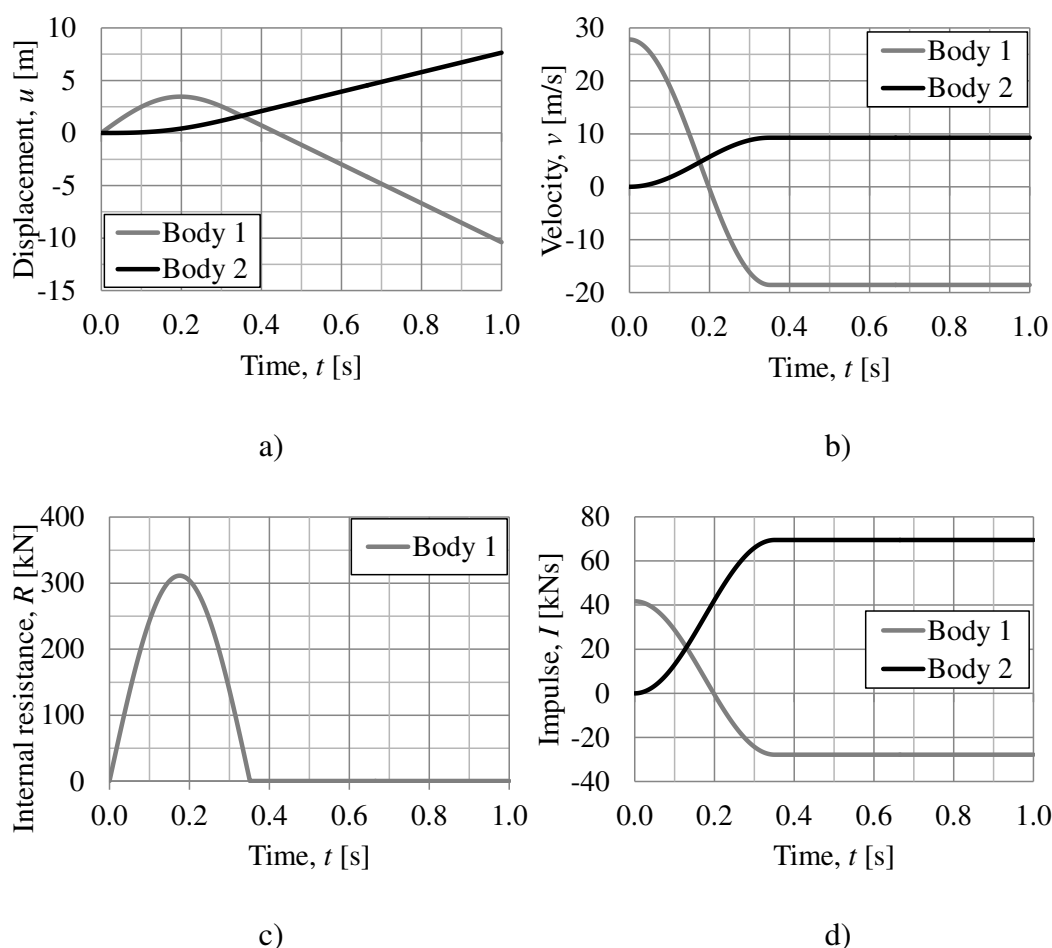
Figure B.1   Response for collision A1 a) displacement u, b) velocity v, c) internal resistance R, and d) impulse I.
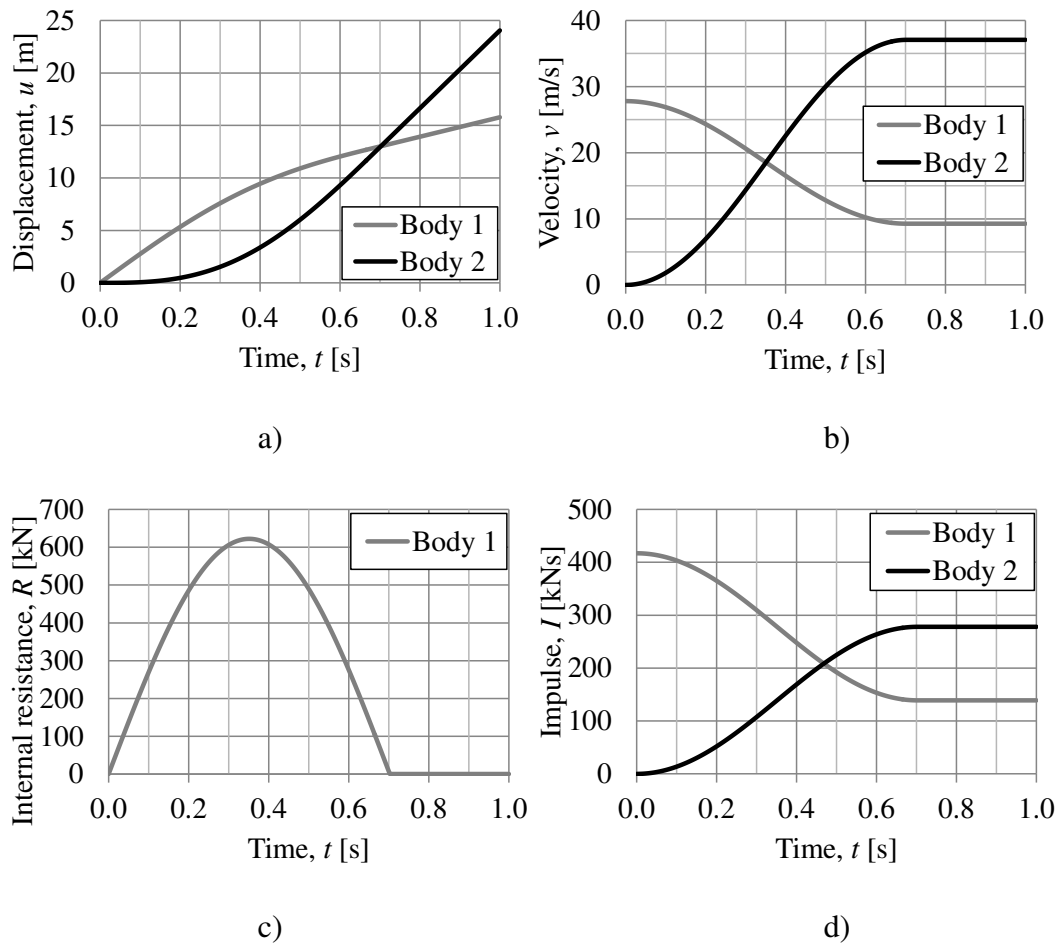
Figure B.2   Response for collision A2 a) displacement u, b) velocity v, c) internal resistance R, and d) impulse I.
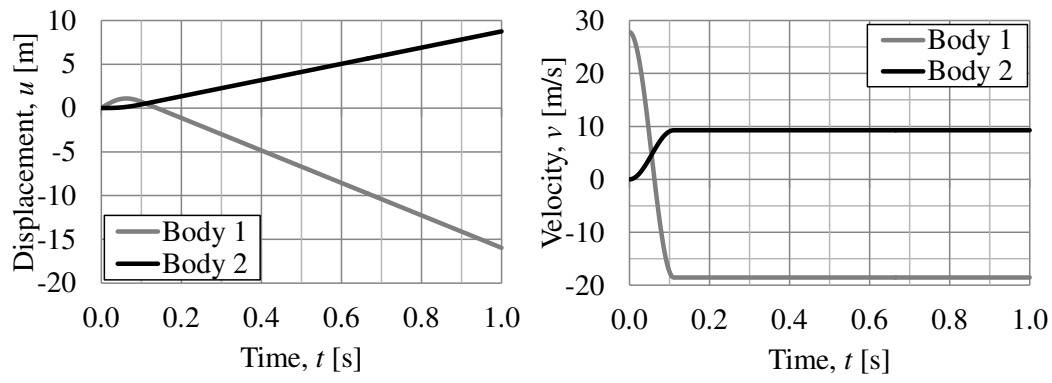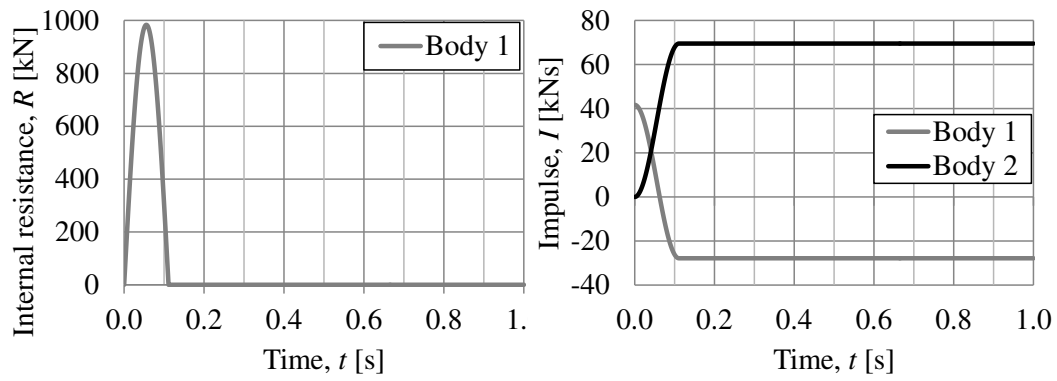
Figure B.3   Response for collision A3 a) displacement u, b) velocity v, c) internal resistance R, and d) impulse I.
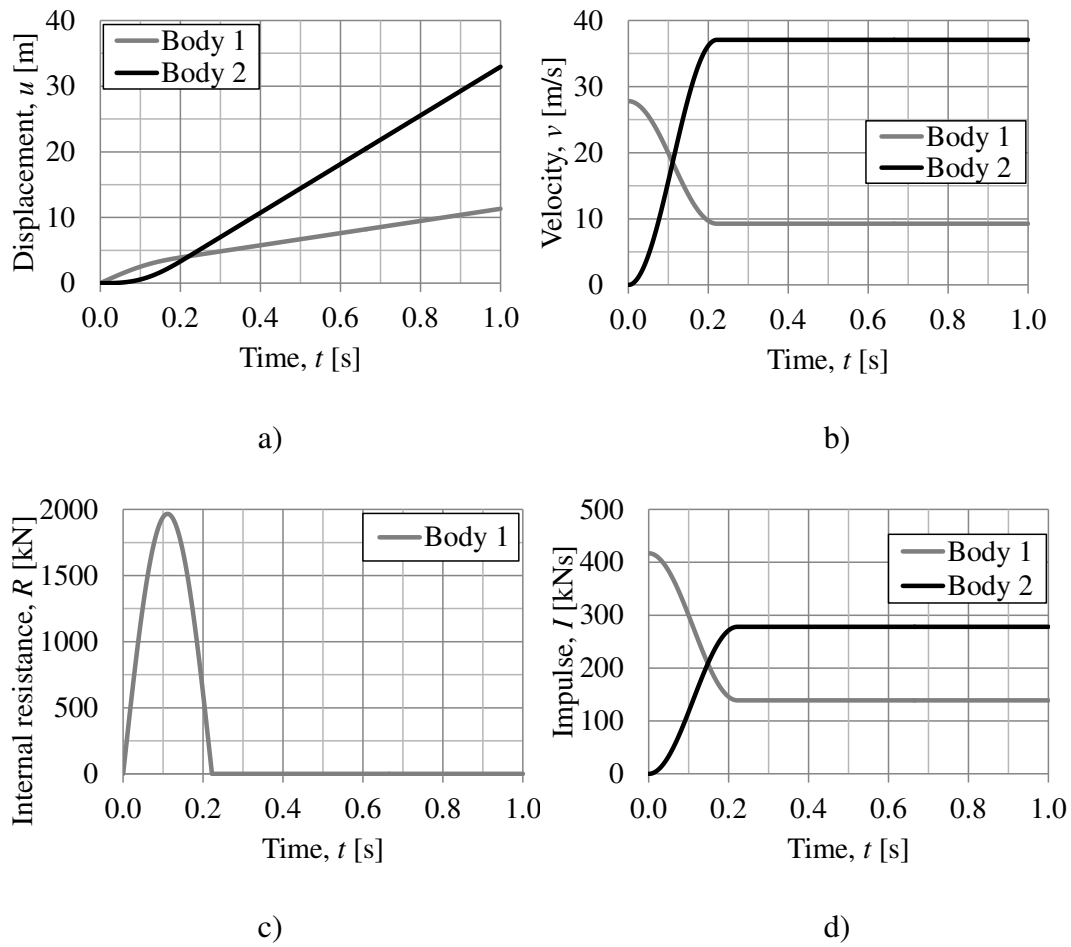
Figure B.4   *Response for collision A4 a) displacement u, b) velocity v, c) internal resistance R, and d) impulse I.*
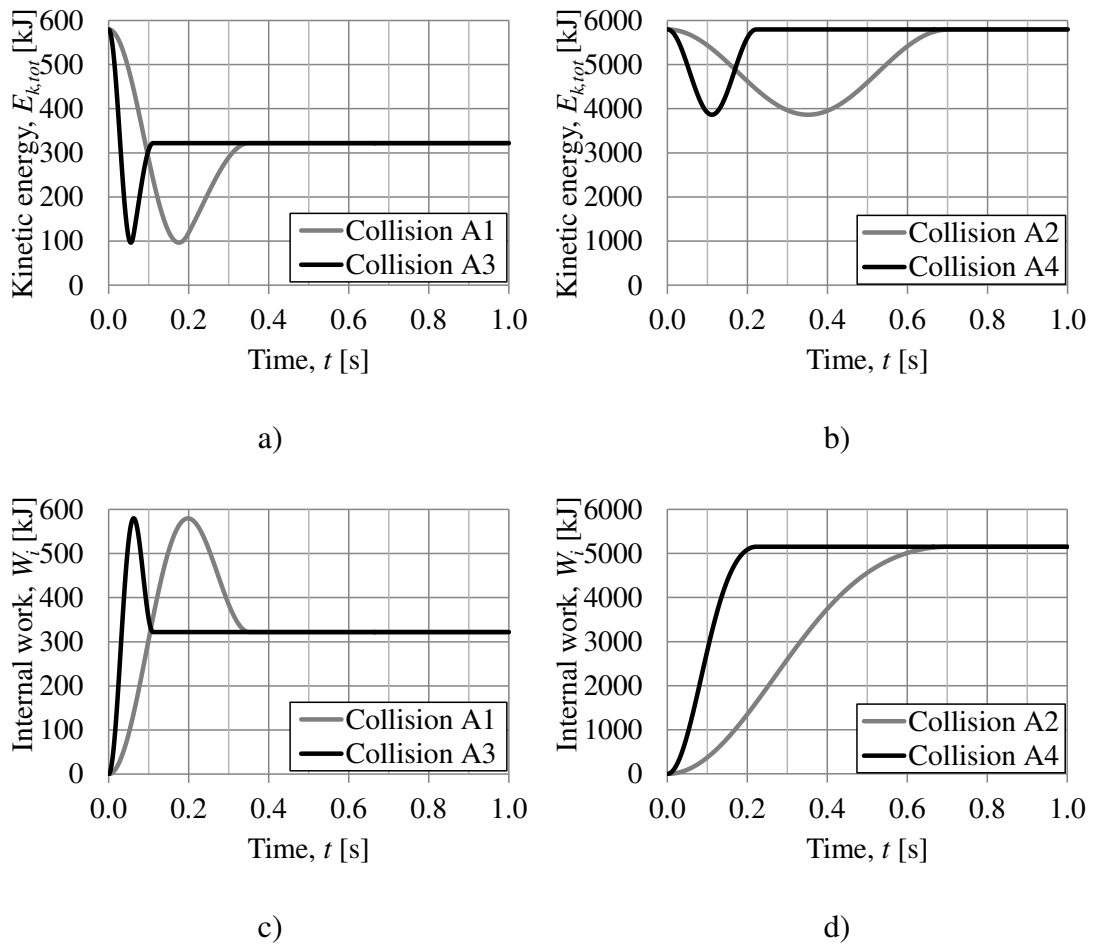
Figure B.5 *Response for collision A1-A4 a) kinetic energy $E_{k,tot}$ for collision A1 and A3, b) kinetic energy $E_{k,tot}$ for collision A2 and A4, c) internal work W_i for collision A1 and A3, and d) internal work W_i for collision A2 and A4.*

B.2 Plastic response without barrier

In this section, results for collision B1-B4 are presented according to the analysis discussed in Section 3.2.3.

Table B.2   Input parameters for collision B1-B4 with plastic response for the 2DOF system.

Case	v_0 [m/s]	$R_{1,max}$ [kN]	m_1 [kg]	m_2 [kg]
Collision B1	27.8	250	1 500	7 500
Collision B2	27.8	250	15 000	7 500
Collision B3	27.8	500	1 500	7 500
Collision B4	27.8	500	15 000	7 500
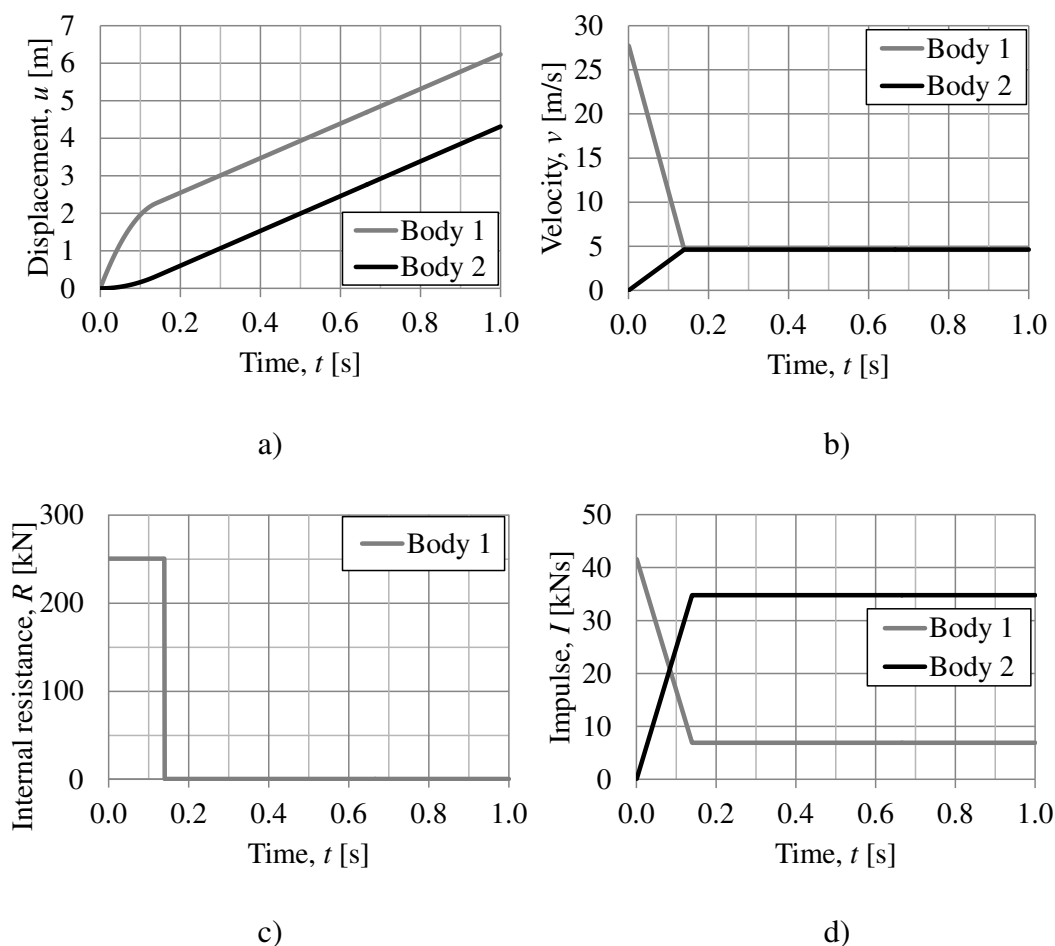
Figure B.6   Response for collision B1 a) displacement u, b) velocity v, c) internal resistance R, and d) impulse I.
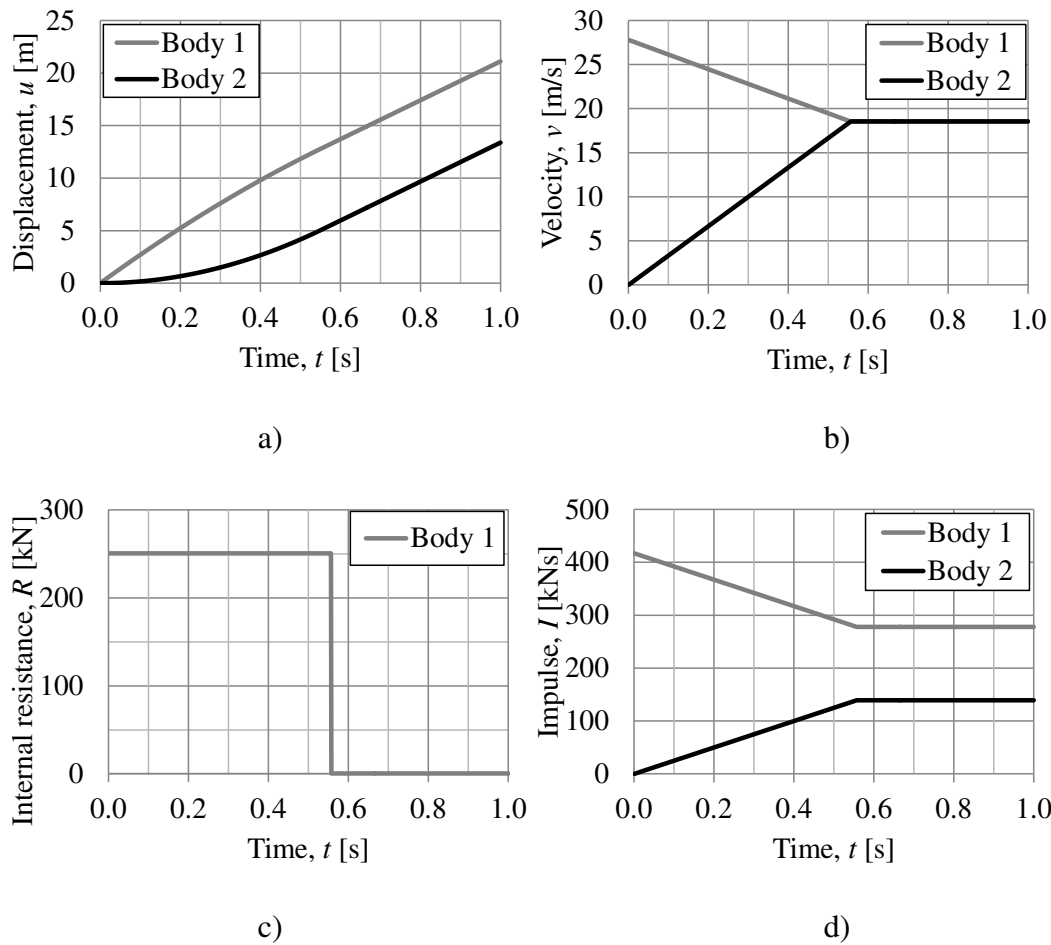
Figure B.7   Response for collision B2 a) displacement u, b) velocity v, c) internal resistance R, and d) impulse I.
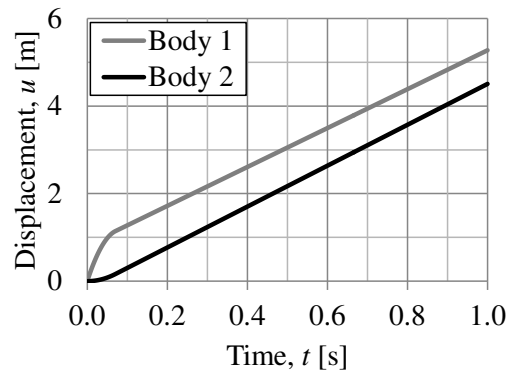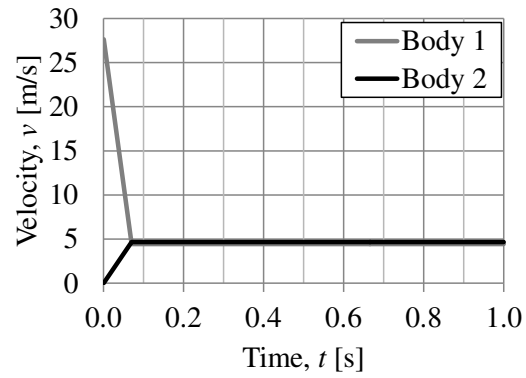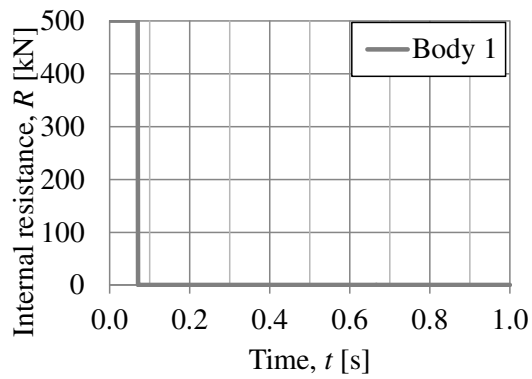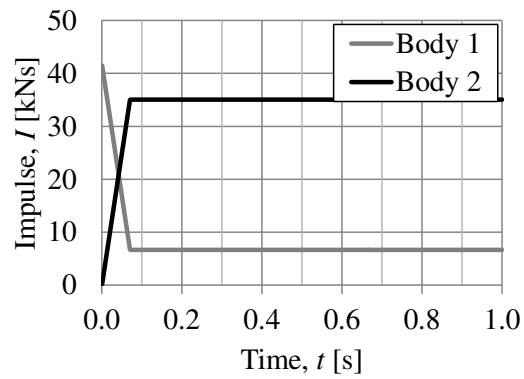
Figure B.8   Response for collision B3 a) displacement u, b) velocity v, c) internal resistance R, and d) impulse I.
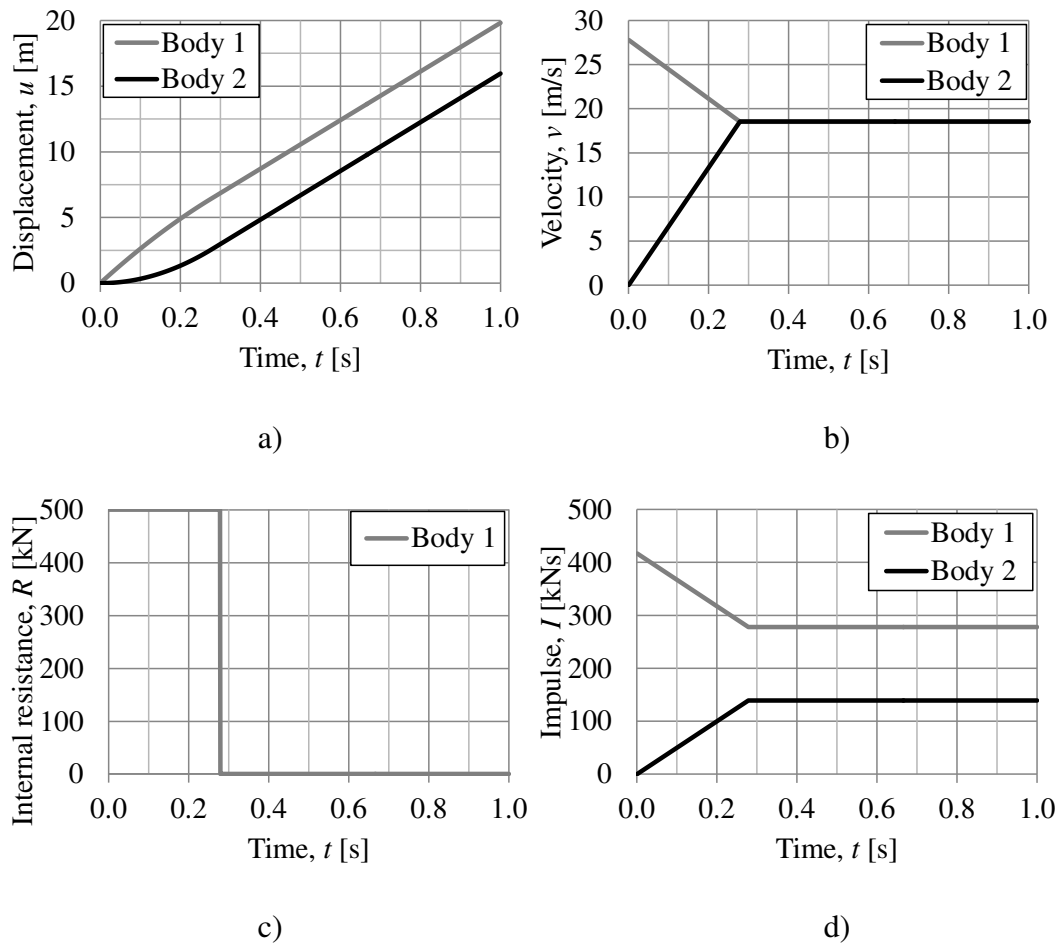
Figure B.9 Response for collision B4 a) displacement u, b) velocity v, c) internal resistance R, and d) impulse I.

a)

b)

c)

d)
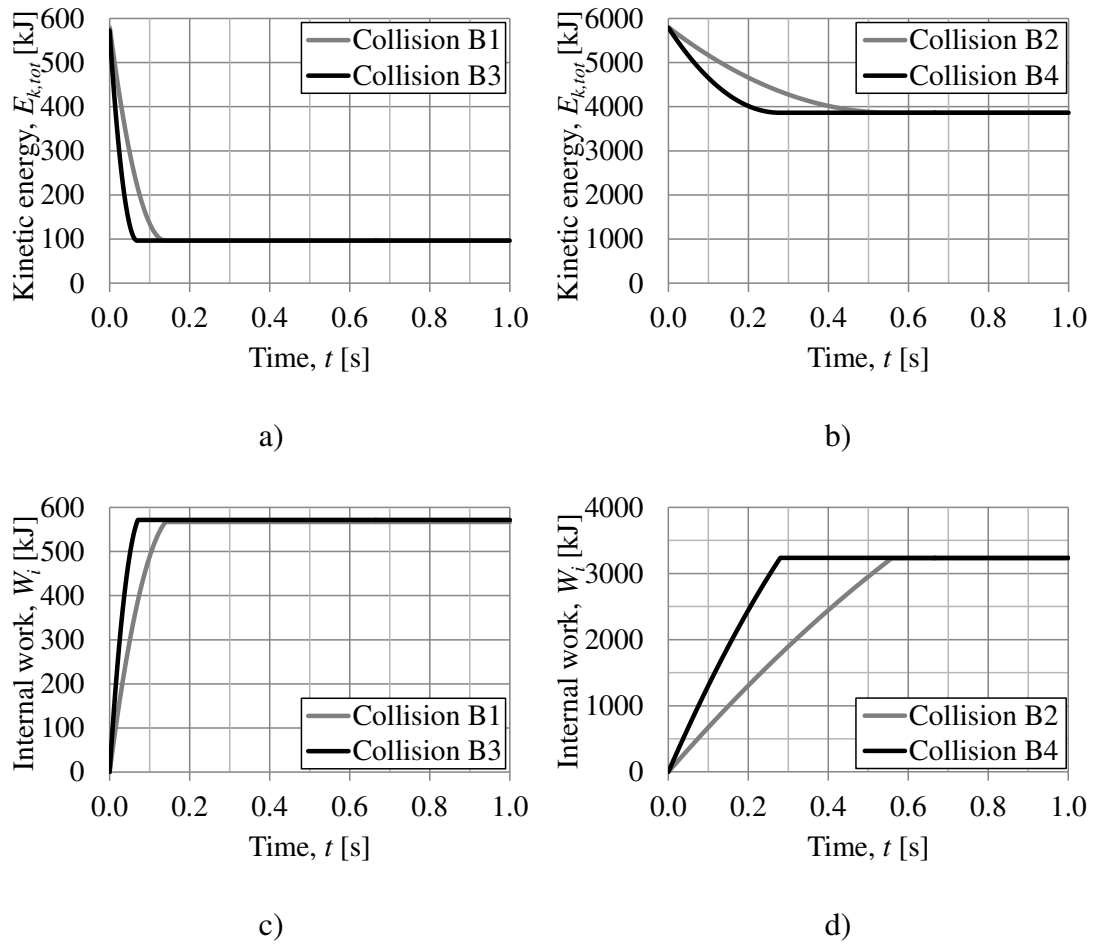
Figure B.10   Response for collision B1-B4 a) kinetic energy $E_{k,tot}$ for collision B1 and B3, b) kinetic energy $E_{k,tot}$ for collision B2 and B4, c) internal work W_i for collision B1 and B3, and d) internal work W_i for collision B2 and B4.

CHALMERS, *Civil and Environmental Engineering*, Master's Thesis 2015:87

B.3 Elasto-plastic response without barrier

In this section, results for collision C1 and C2 are presented according to the analysis discussed in Section 3.2.4.

Table B.3   Input parameters for collision C1 and C2 with elasto-plastic response for the 2DOF system.

Case	v_0 [m/s]	$R_{1,max}$ [kN]	k_1 [kN/m]	m_1 [kg]	m_2 [kg]
Collision C1	27.8	250	100	1 500	7 500
Collision C2	27.8	250	100	15 000	7 500
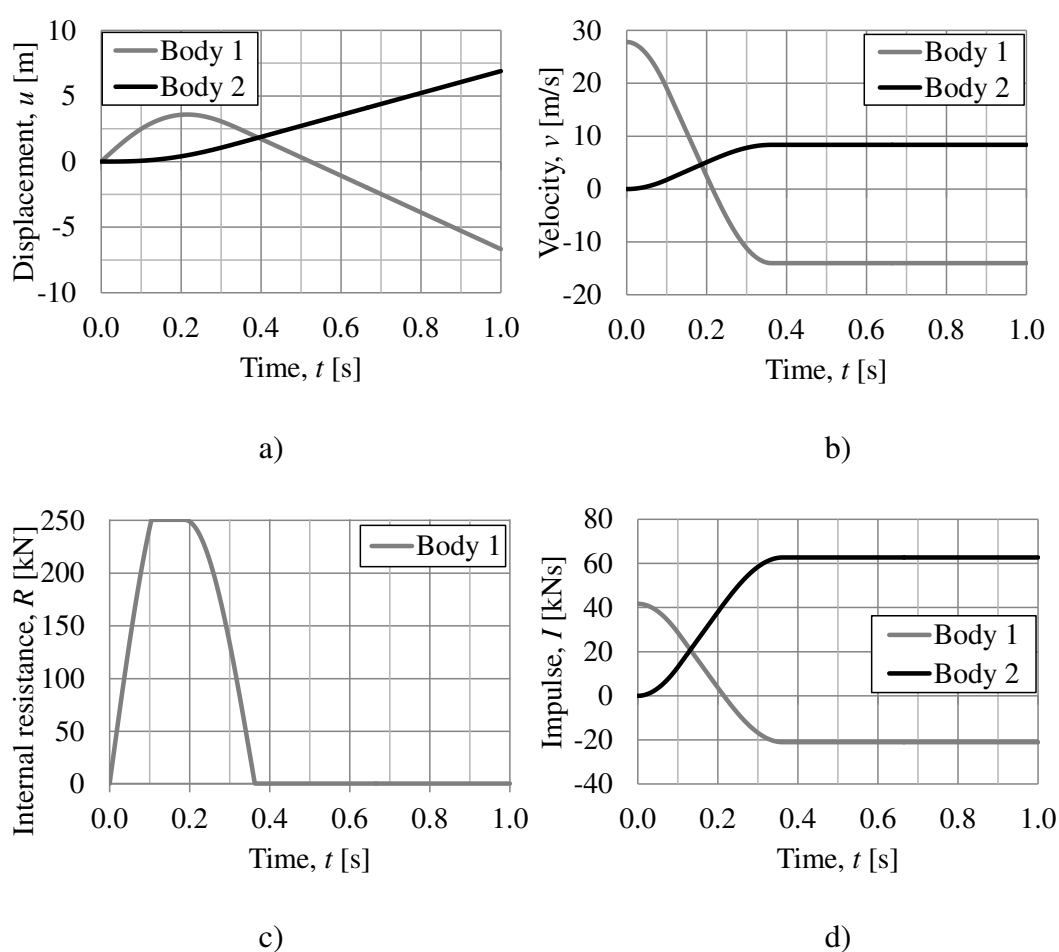
Figure B.11   Response for collision C1 a) displacement u, b) velocity v, c) internal resistance R, and d) impulse I.
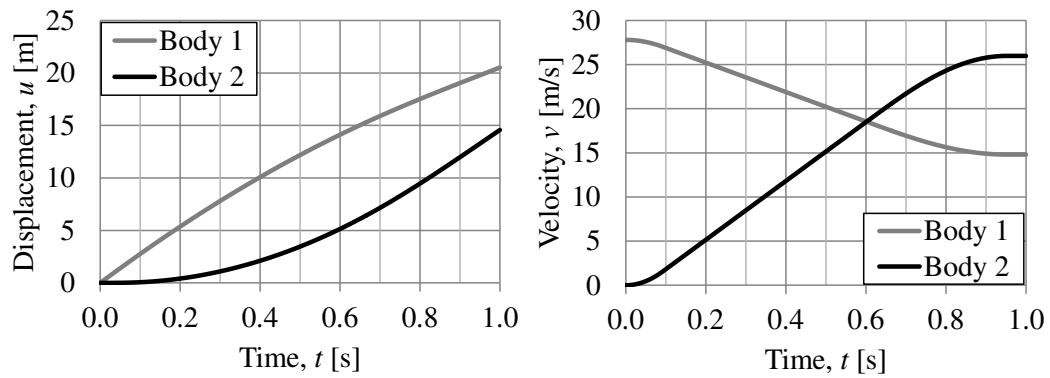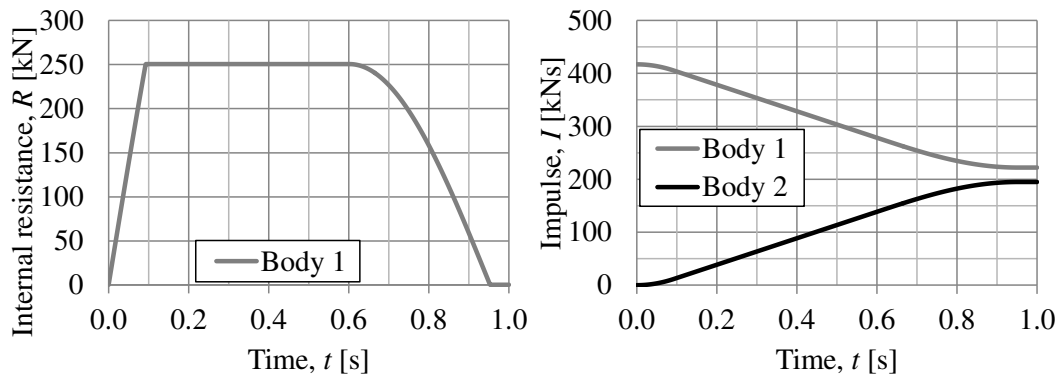
Figure B.12 *Response for collision C2 a) displacement u, b) velocity v, c) internal resistance R, and d) impulse I.*
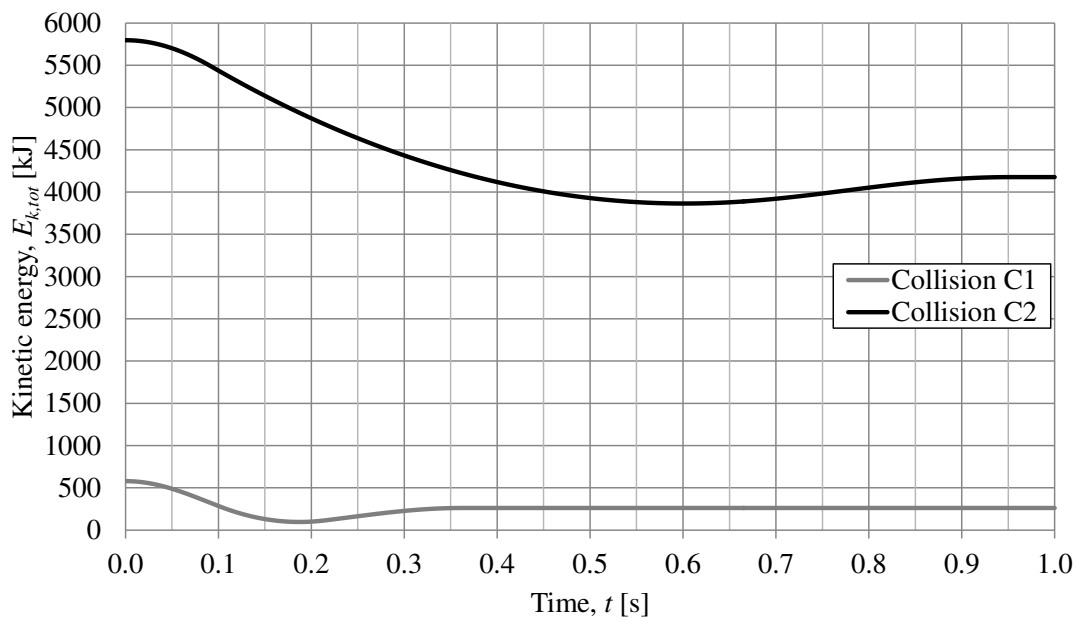
Figure B.13 *Change in kinetic energy $E_{k,tot}$ in the positive direction of body 2 during collision C1 and C2.*

CHALMERS, *Civil and Environmental Engineering*, Master's Thesis 2015:87
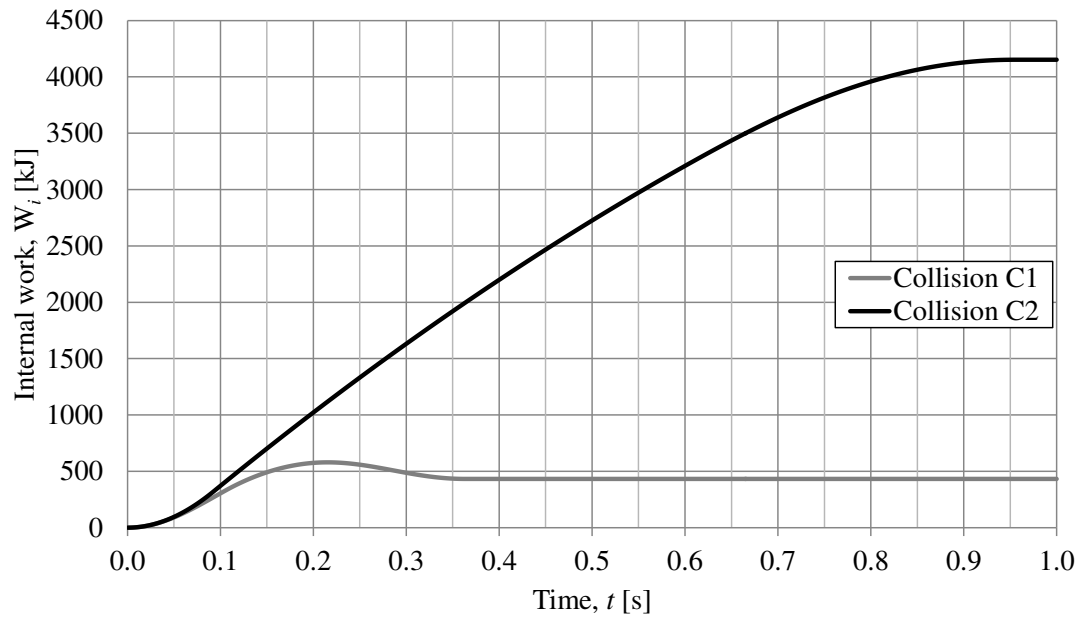
Figure B.14   Change in internal work Wᵢ during collision C1 and C2.

B.4 Elastic response with barrier

In this section, results for collision D1-D4 are presented according to the analysis discussed in Section 3.3.

Table B.4 *Input parameters for collision D1-D4 with elastic response for the 2DOF system with initial velocity $v_0 = 27.8$ m/s.*

	Collision D1	Collision D2	Collision D3	Collision D4
k_1 [kN/m]	100	1 000	400	4 000
k_2 [kN/m]	2 000	2 000	2 000	2 000
m_1 [kg]	1 500	15 000	1 500	15 000
m_2 [kg]	7 500	7 500	7 500	7 500
Mass ratio m_1 / m_2 [-]	0.2	2	0.2	2
Frequency ratio f_1 / f_2 [-]	0.5	0.5	1	1
Load factor β_{el} [-]	1.65	1.15	1.42	0.69

CHALMERS, *Civil and Environmental Engineering*, Master's Thesis 2015:87

a)   b)

c)   d)

Figure B.15   Response for collision D1 a) displacement u, b) velocity v, c) internal resistance R, and d) impulse I.
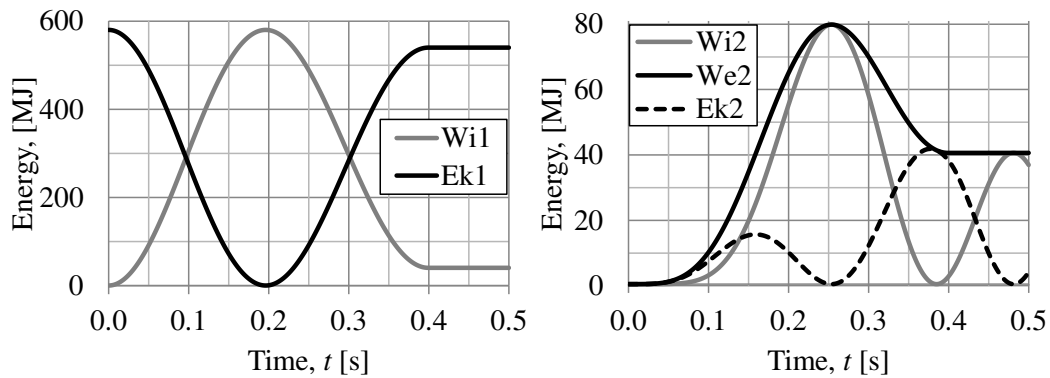
a)   b)

Figure B.16   Response for collision D1 a) internal work $W_{i,1}$ and kinetic energy $E_{k,1}$ for body 1, and b) internal work $W_{i,2}$, external work $W_{e,2}$ and kinetic energy E_k for body 2.
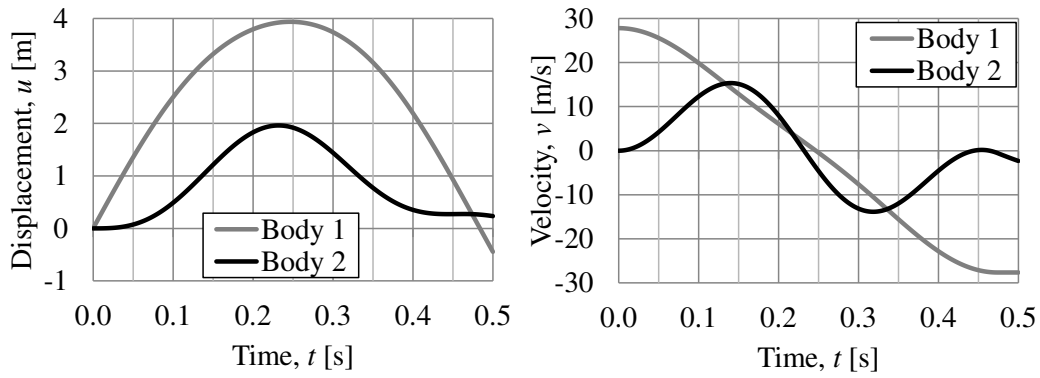
a)

b)
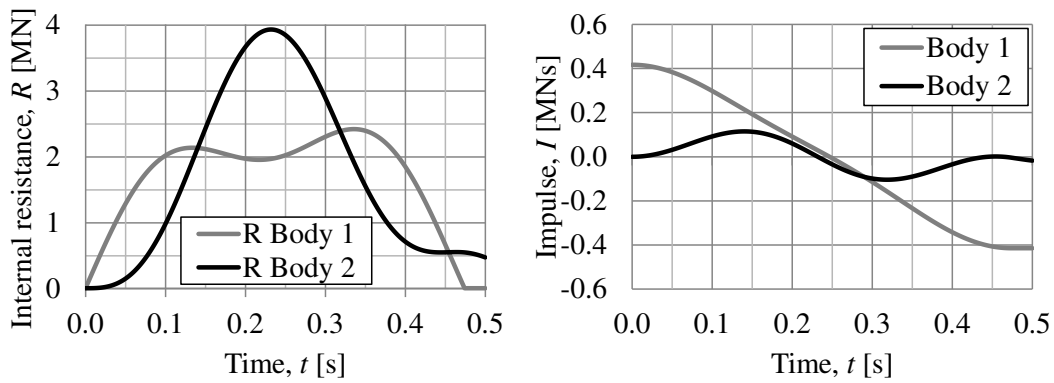
c)

d)

Figure B.17 Response for collision D2 a) displacement u, b) velocity v, c) internal resistance R, and d) impulse I.
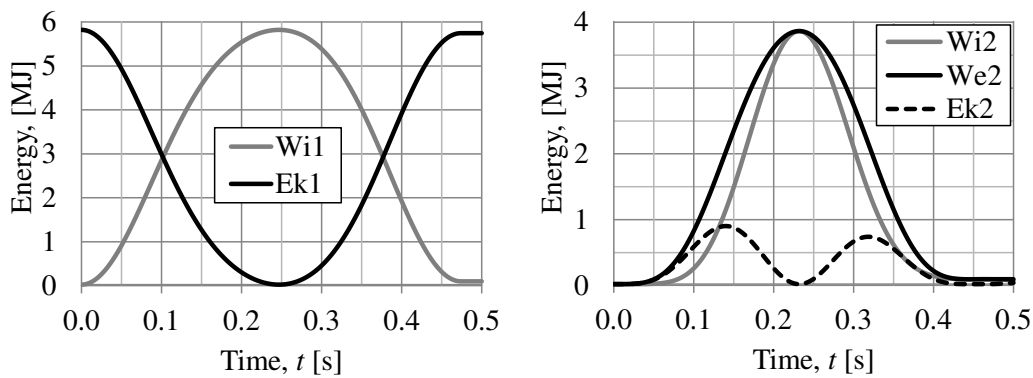
a)

b)

Figure B.18 Response for collision D2 a) internal work $W_{i,1}$ and kinetic energy $E_{k,1}$ for body 1, and b) internal work $W_{i,2}$, external work $W_{e,2}$ and kinetic energy E_k for body 2.

CHALMERS, *Civil and Environmental Engineering*, Master's Thesis 2015:87

a)

b)
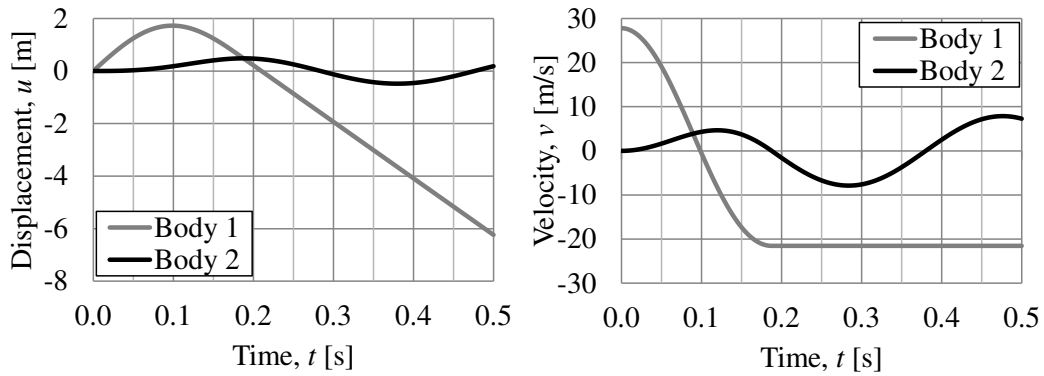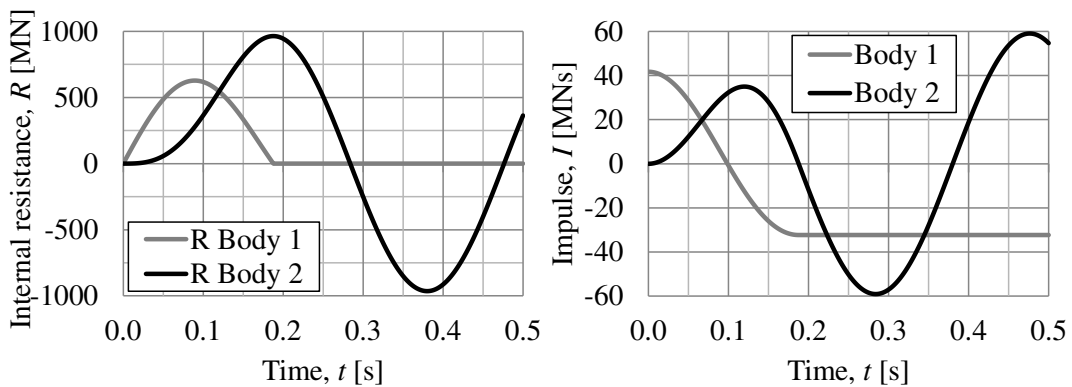
Figure B.19 Response for collision D3 a) displacement u, b) velocity v, c) internal resistance R, and d) impulse I.
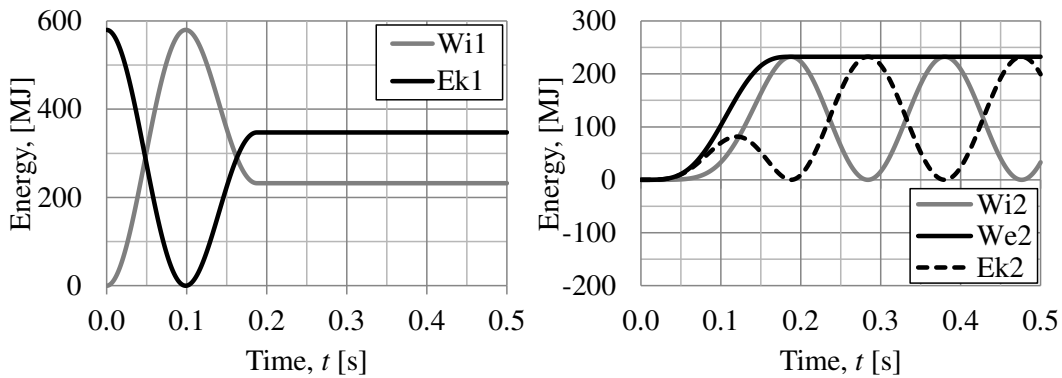
a)

b)

Figure B.20 Response for collision D3 a) internal work $W_{i,1}$ and kinetic energy $E_{k,1}$ for body 1, and b) internal work $W_{i,2}$, external work $W_{e,2}$ and kinetic energy E_k for body 2.
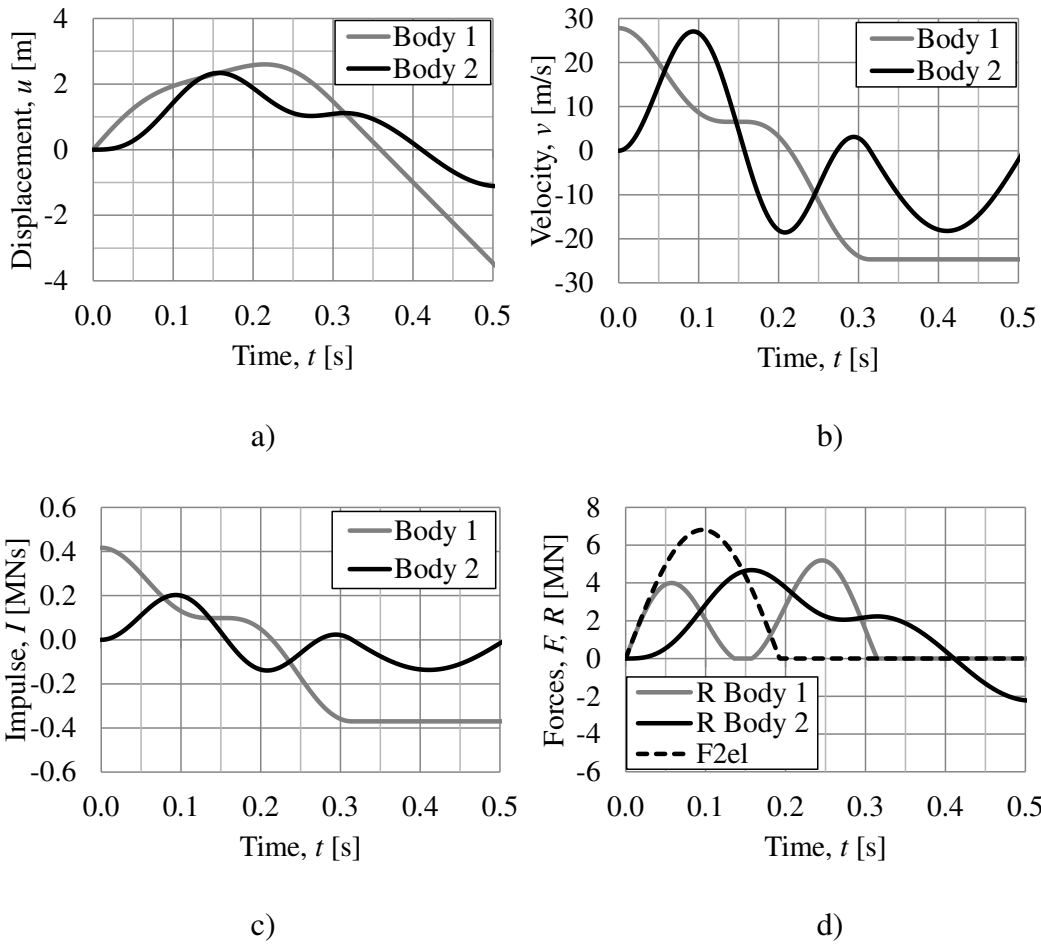
Figure B.21 Response for collision D4 a) displacement u, b) velocity v, c) internal resistance R and dynamic load $F_{2,el}$, and d) impulse I.
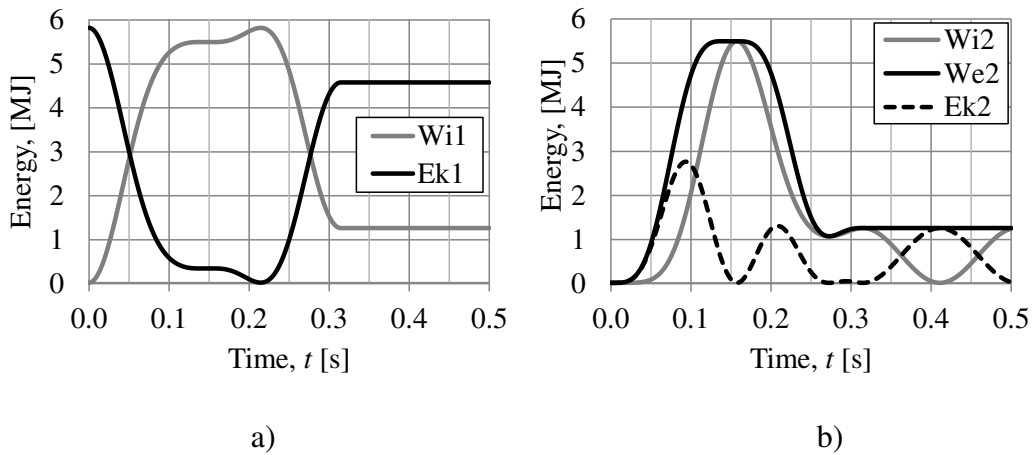
Figure B.22 Response for collision D4 a) internal work $W_{i,1}$ and kinetic energy $E_{k,1}$ for body 1, and b) internal work $W_{i,2}$, external work $W_{e,2}$ and kinetic energy E_k for body 2.

CHALMERS, *Civil and Environmental Engineering*, Master's Thesis 2015:87
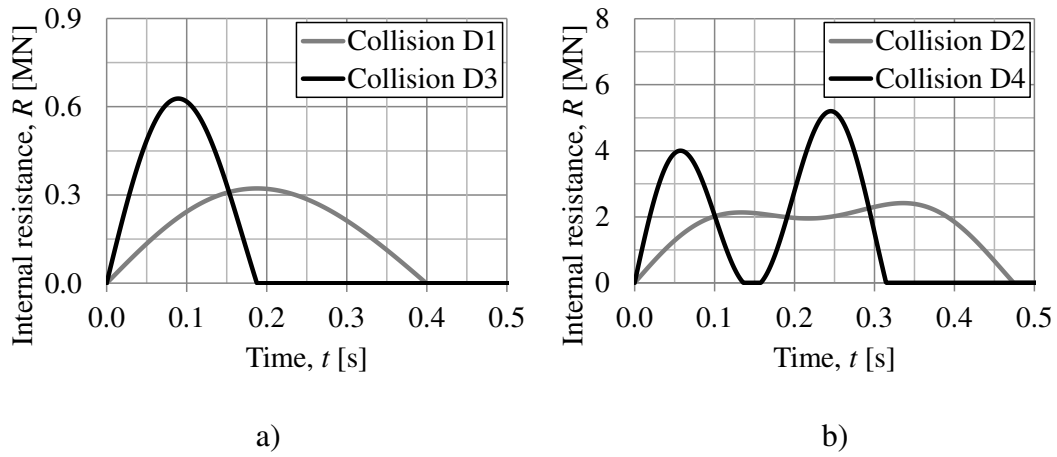
Figure B.23   Internal   resistance   of   body 1 R_1 for   a) collision D1   and   D3,   and b) collision D2 and D4.
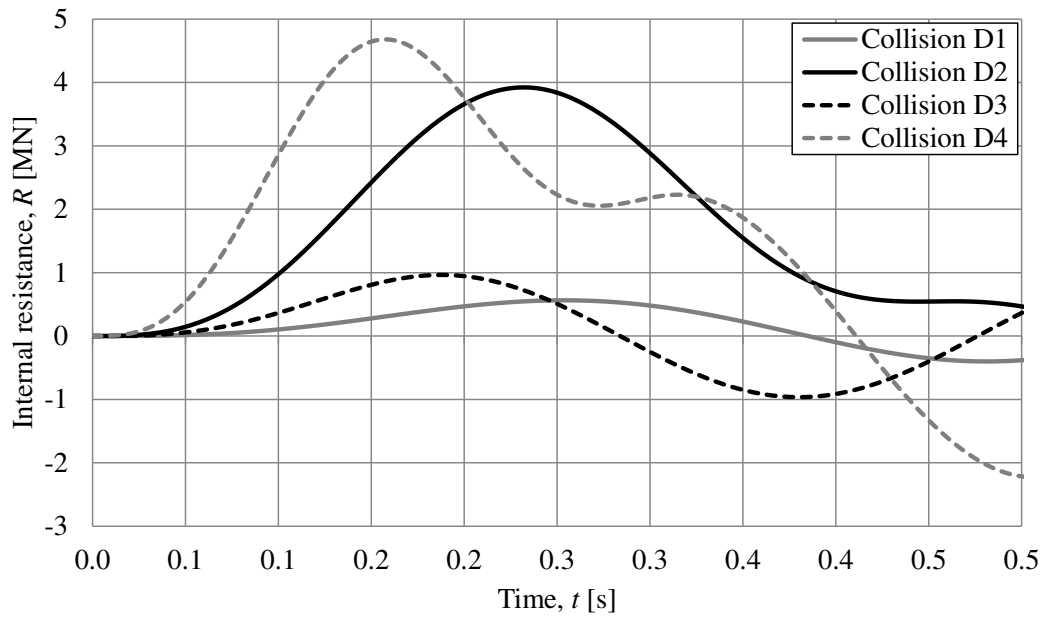
Figure B.24   Internal resistance of body 2 R_2 for collision D1-D4.

Appendix C 2DOF and FEM Comparison

C.1 Elastic body 1 and body 2 for a beam

In this section, results for collision E1 are presented according to the analysis discussed in Section 6.1.2.

Table C.1   *2DOF input parameters for the collision E1 with an elastic response for both body 1 and body 2.*

Case	α [-]	κ_{mF} [-]	k_1 [MN/m]	k_2 [MN/m]	m_1 [kg]
Collision E1	0.5	0.486	1	506.2	1 500

a)   b)
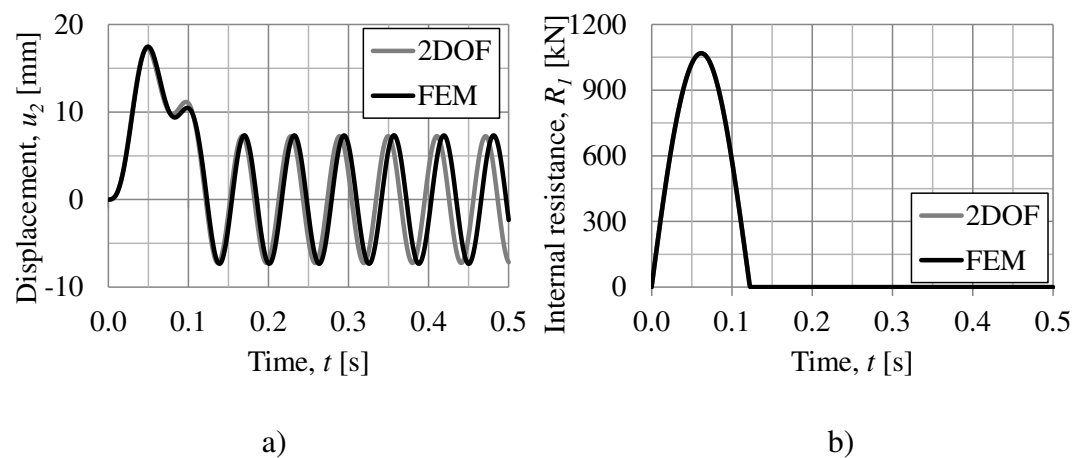
Figure C.1   *Comparison between the 2DOF model and the FE model for collision E1, a) displacement of body 2 u_2, and b) internal resistance of body 1 R_1.*

C.2 Elasto-plastic body 1 and elastic body 2 for a beam

In this section, results for collision F1-F4 are presented according to the analysis discussed in Section 6.1.3.

Table C.2   *2DOF input parameters for collision F1-F4 with elasto-plastic response of body 1 and elastic response of body 2.*

Case	α [-]	κ_{mF} [-]	k_1 [MN/m]	k_2 [MN/m]	m_1 [kg]	$R_{1,max}$ [kN]
Collision F1	0.5	0.486	1	506.2	1 500	500
Collision F2	0.5	0.486	1	506.2	1 500	250
Collision F3	0.25	0.774	1	899.8	1 500	500
Collision F4	0.25	0.774	1	899.8	1 500	250

a)

b)

c)

d)
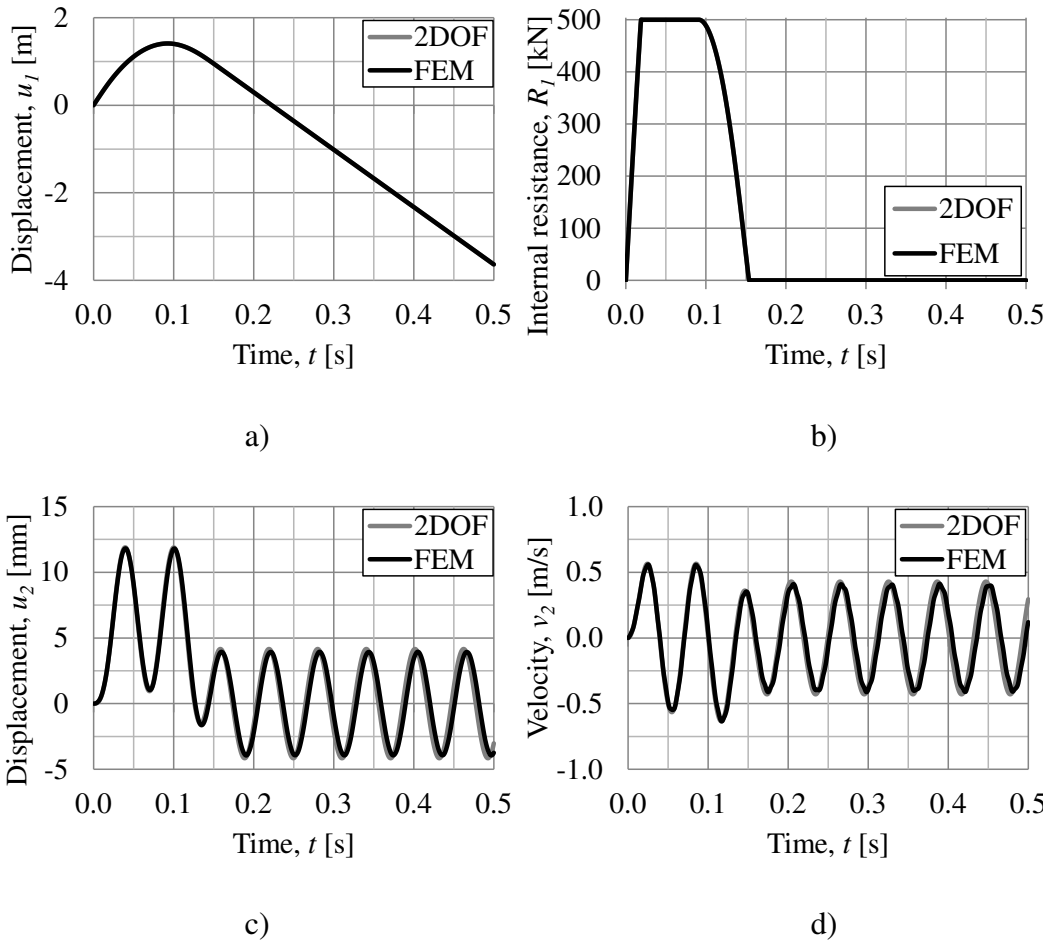
Figure C.2   *Illustration of the response for collision F1, a) displacement of body 1 u_1, b) internal resistance of body 1 R_1, c) displacement of body 2 u_2, and d) velocity of body 2 v_2.*
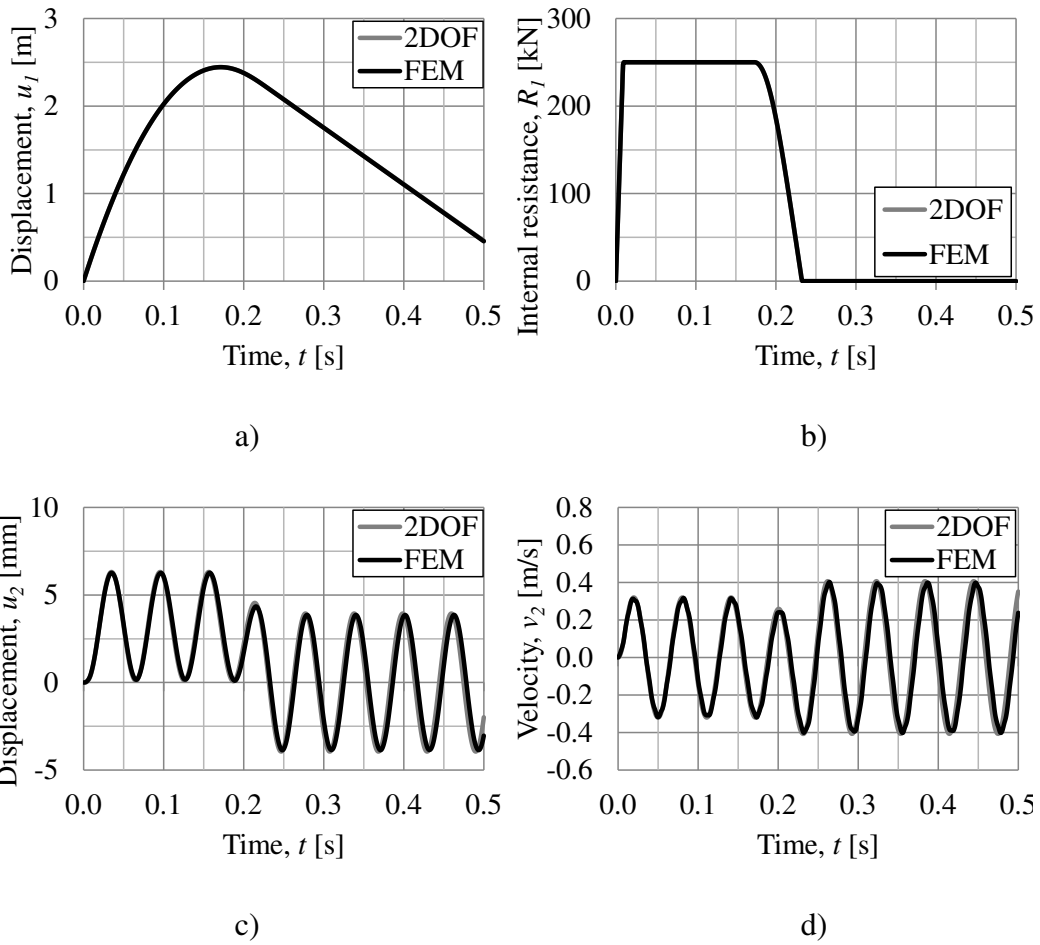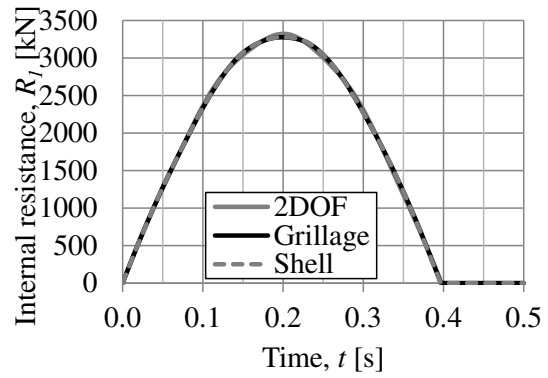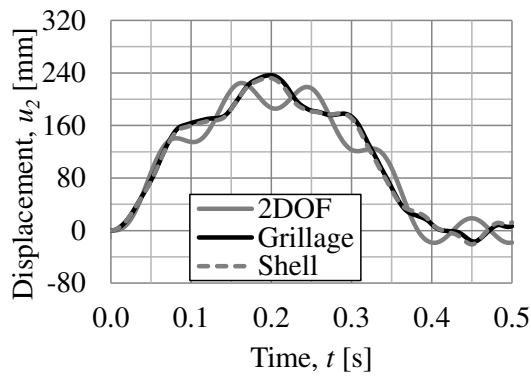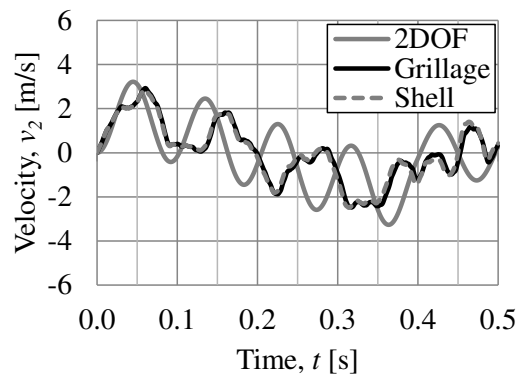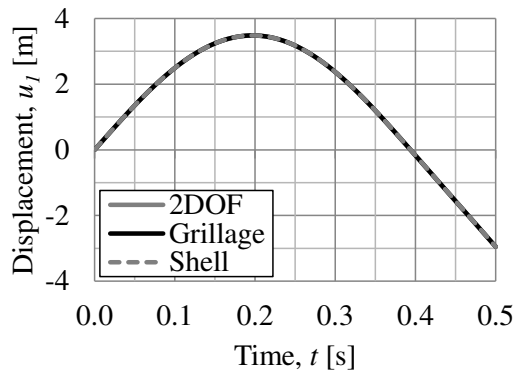
Figure C.3   Illustration of the response for collision F2, a) displacement of body 1 u_1, b) internal resistance of body 1 R_1, c) displacement of body 2 u_2, and d) velocity of body 2 v_2.
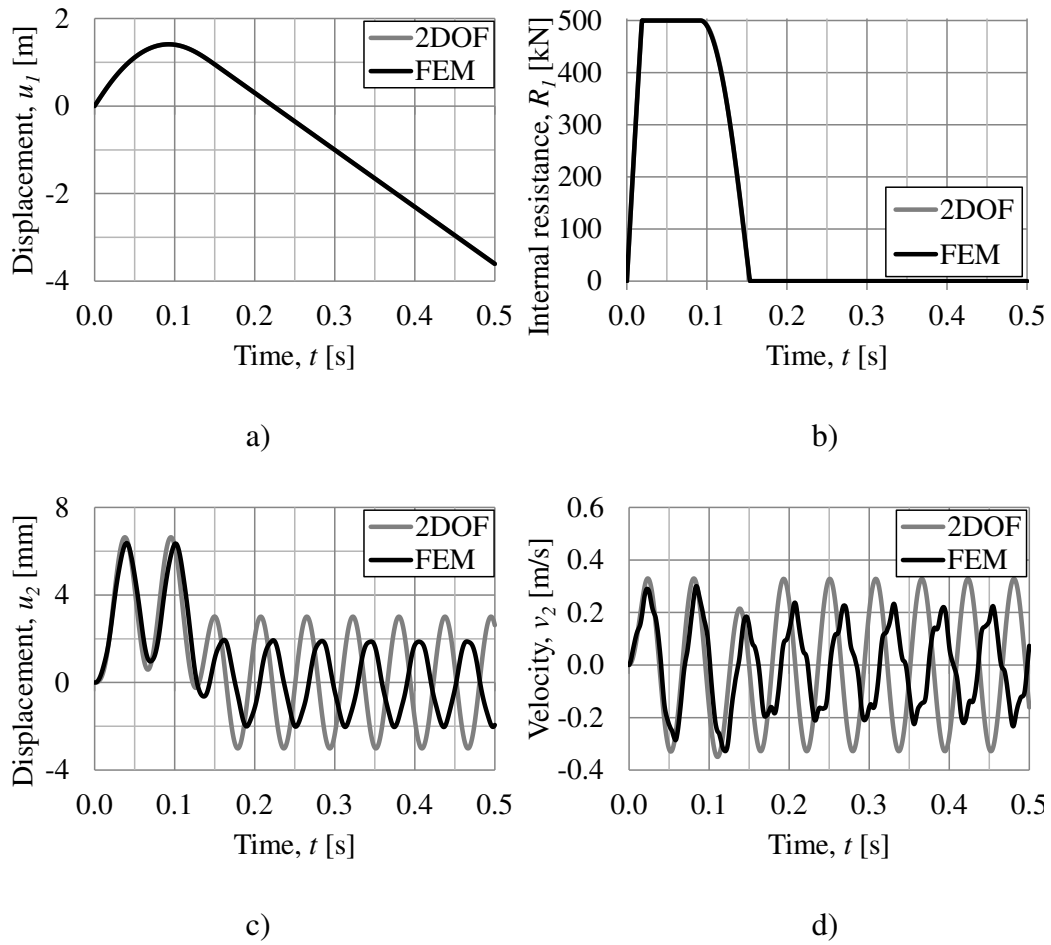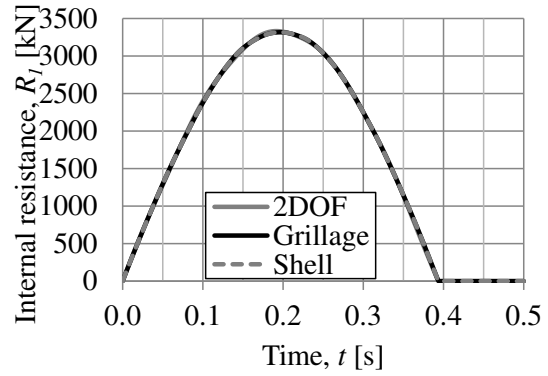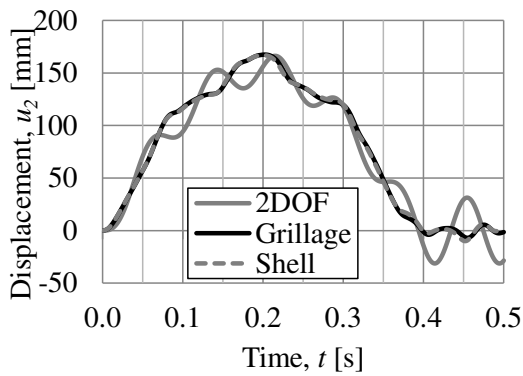
Figure C.4   Illustration of the response for collision F3, a) displacement of body 1 u_1, b) internal resistance of body 1 R_1, c) displacement of body 2 u_2, and d) velocity of body 2 v_2.
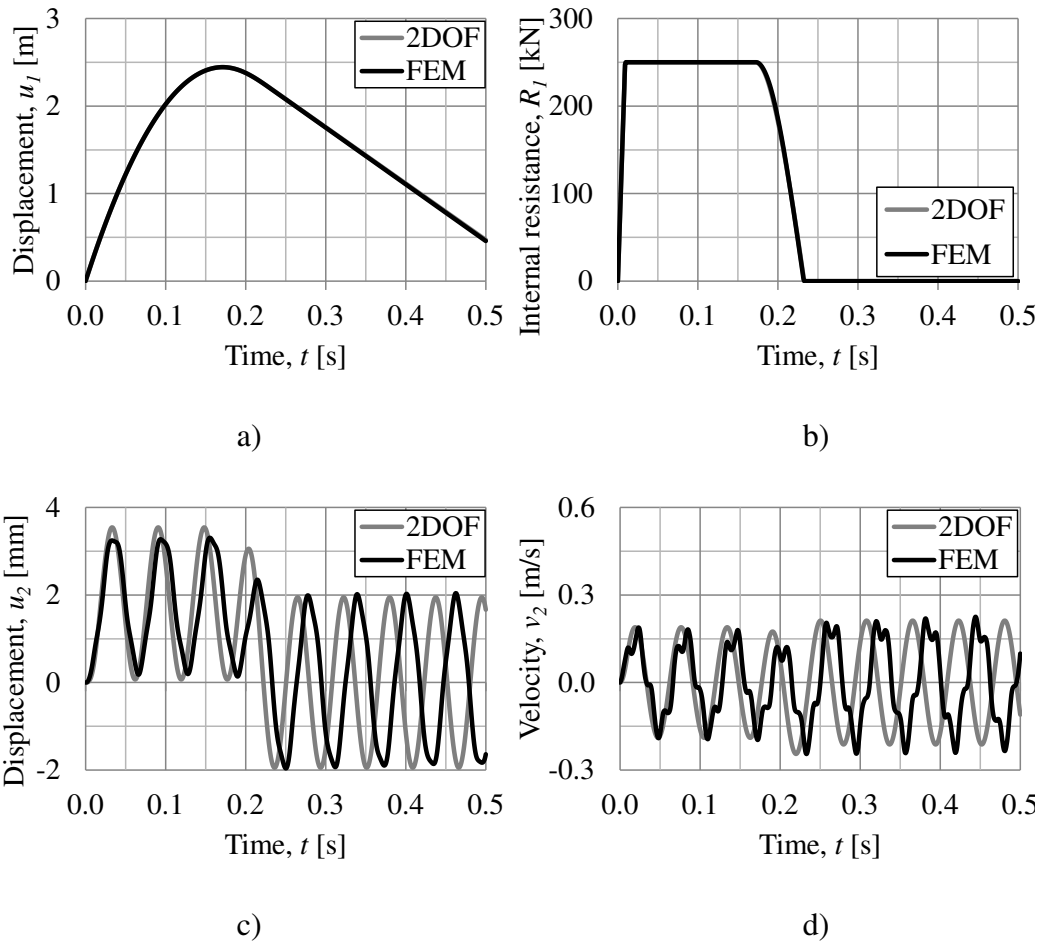
Figure C.5   Illustration of the response for collision F4, a) displacement of body 1 u_1, b) internal resistance of body 1 R_1, c) displacement of body 2 u_2, and d) velocity of body 2 v_2.
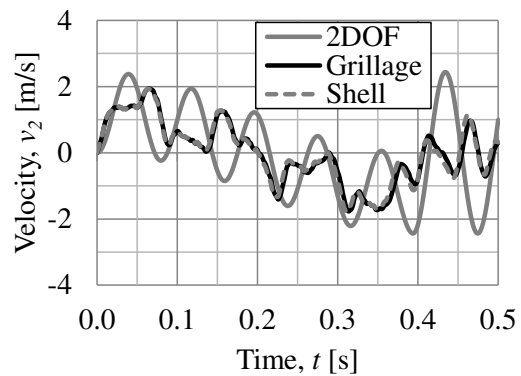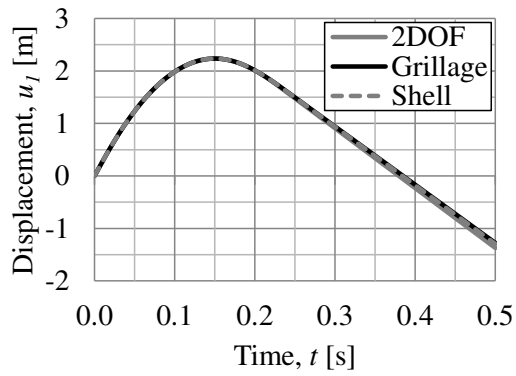
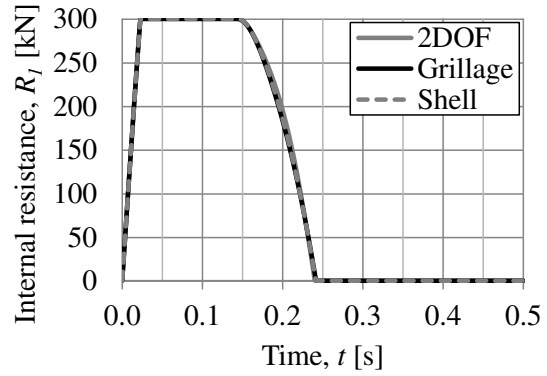## C.3 Elastic body 1 and elasto-plastic body 2 for a beam

In this section, results for collision G1a-G1c are presented according to the analysis discussed in Section 6.1.4.

Table C.3   *2DOF input parameters for collision G1a-G1c with different transformation factor κ_{mF} and with elastic response of body 1 and elasto-plastic response of body 2.*

Case	α [-]	κ_{mF} [-]	k_1 [MN/m]	k_2 [MN/m]	m_1 [kg]	$R_{2,max}$ [MN]
Collision G1a	0.5	0.486	1	506.2	15 000	3.1
Collision G1b	0.5	0.41	1	506.2	15 000	3.1
Collision G1c	0.5	0.333	1	506.2	15 000	3.1
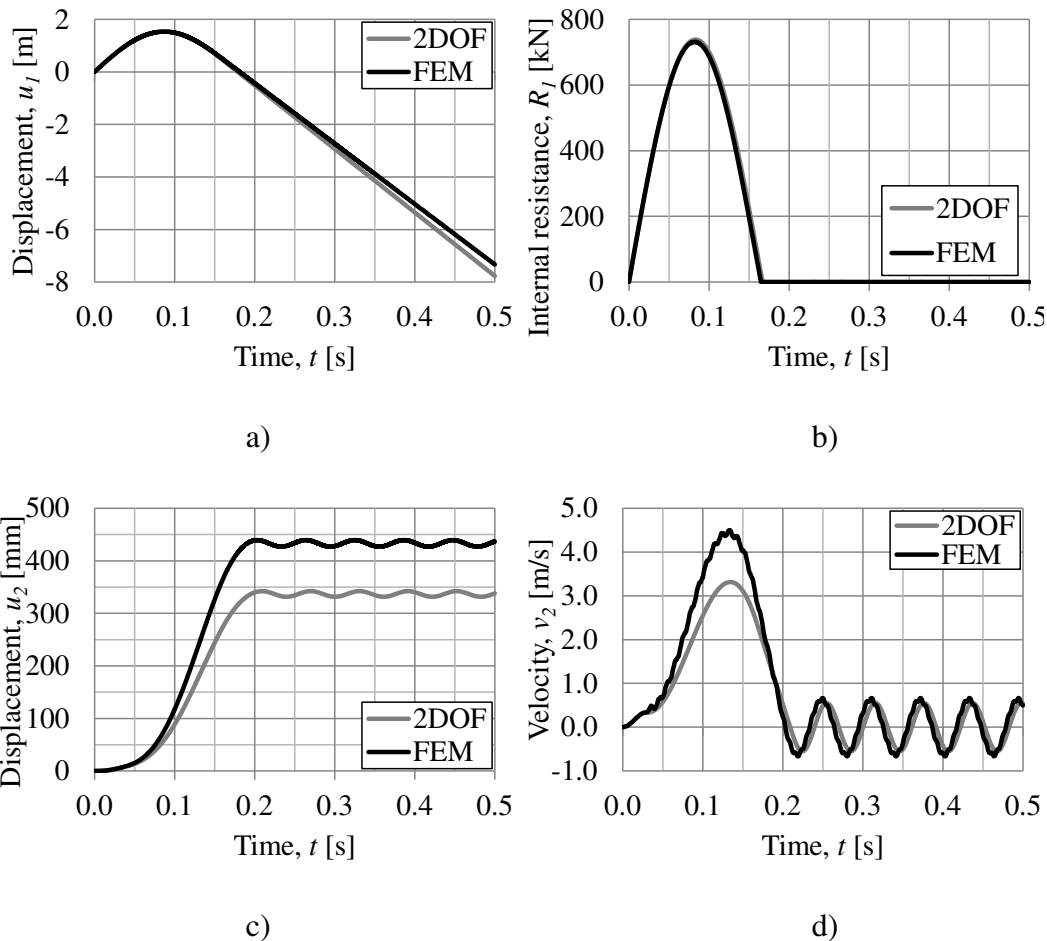
Figure C.6   *Illustration of the response for collision G1a, a) displacement of body 1 u_1, b) internal resistance of body 1 R_1, c) displacement of body 2 u_2, and d) velocity of body 2 v_2.*

a)

b)

a)

b)
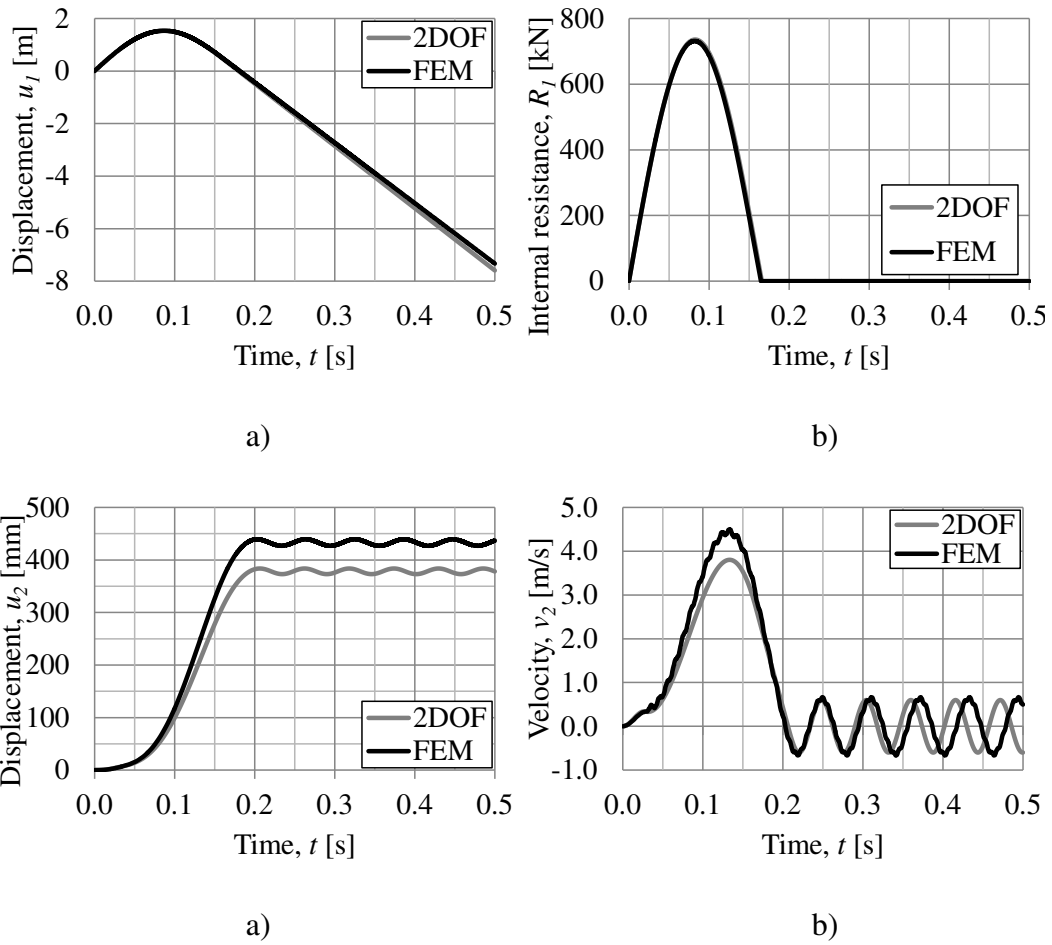
Figure C.7   *Illustration of the response for collision G1b, a) displacement of body 1 u_1, b) internal resistance of body 1 R_1, c) displacement of body 2 u_2, and d) velocity of body 2 v_2.*
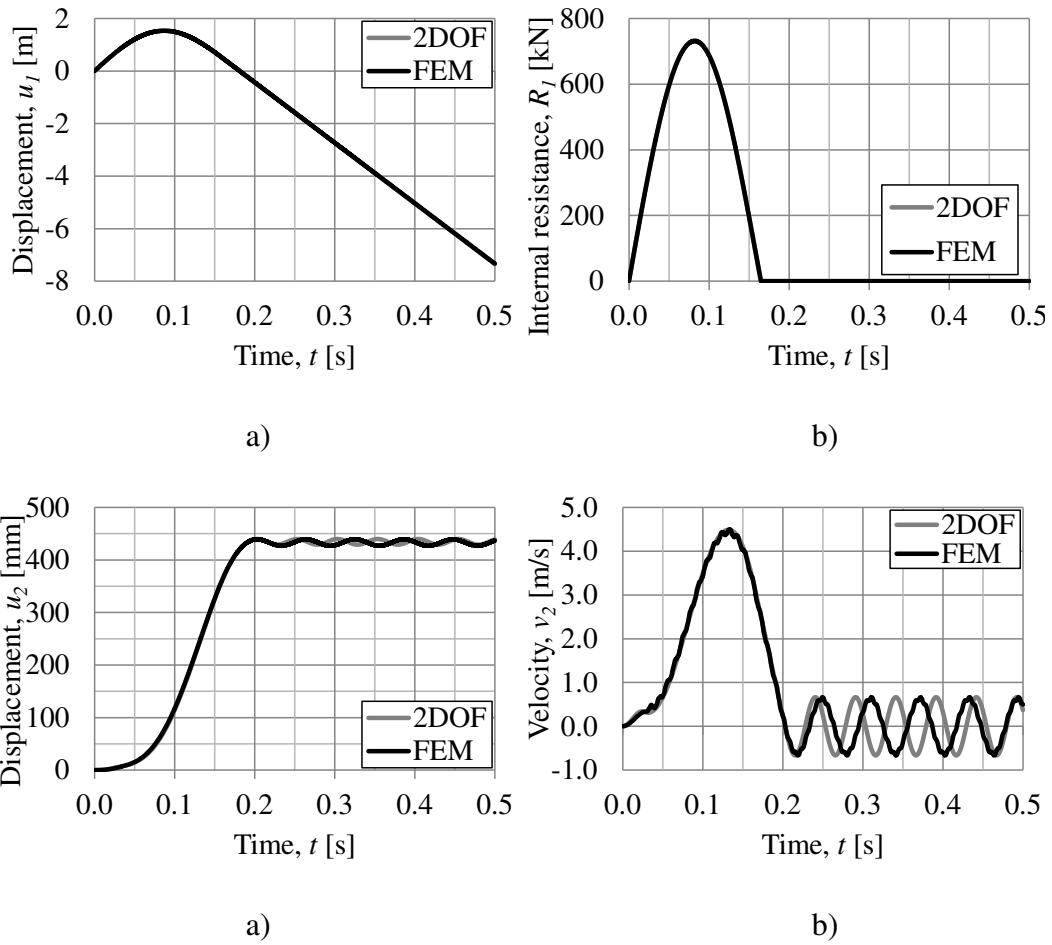
Figure C.8   Illustration of the response for collision G1c, a) displacement of body 1 u_1, b) internal resistance of body 1 R_1, c) displacement of body 2 u_2, and d) velocity of body 2 v_2.

CHALMERS, *Civil and Environmental Engineering*, Master's Thesis 2015:87

C.4 Elastic body 1 and body 2 for a slab

In this section, results for collision H1-H12 are presented according to the analysis discussed in Section 6.2.2.

Table C.4   2DOF and FE input parameters for collision H1-H12 with initial velocity $v_0 = 27.8$ m/s.

| Case	α_x [-]	α_y [-]	κ_{mF} [-]	k_1 [MN/m]	m_1 [kg]	k_{sl} [MN/m]
Collision H1	0.5	0.5	0.203	0.5	1 500	10.79
Collision H2	0.5	0.25	0.235	0.5	1 500	15.94
Collision H3	0.25	0.25	0.241	0.5	1 500	22.02
Collision H4	0.5	0.5	0.203	1	1 500	10.79
Collision H5	0.5	0.25	0.235	1	1 500	15.94
Collision H6	0.25	0.25	0.241	1	1 500	22.02
Collision H7	0.5	0.5	0.203	0.5	15 000	10.79
Collision H8	0.5	0.25	0.235	0.5	15 000	15.94
Collision H9	0.25	0.25	0.241	0.5	15 000	22.02
Collision H10	0.5	0.5	0.203	1	15 000	10.79
Collision H11	0.5	0.25	0.235	1	15 000	15.94
Collision H12	0.25	0.25	0.241	1	15 000	22.02

Figure C.9   Illustration of collision H1, a) displacement of body 1 u_1, b) internal resistance of body 1 R_1, c) displacement of body 2 u_2, and d) velocity of body 2 v_2.
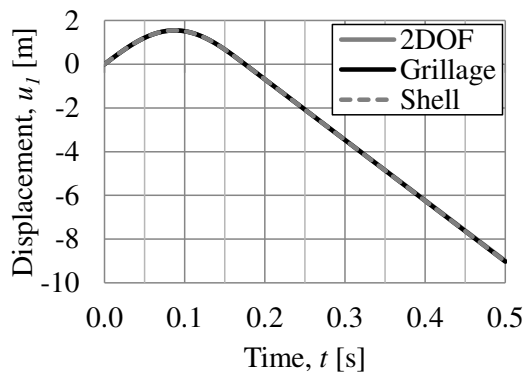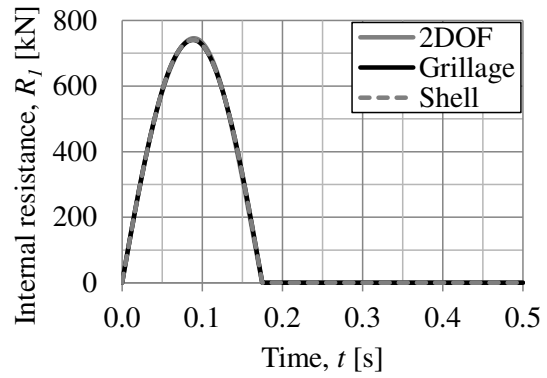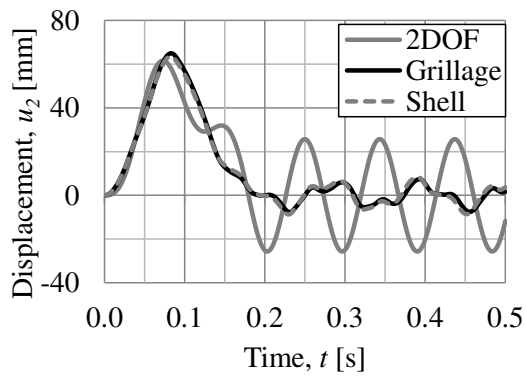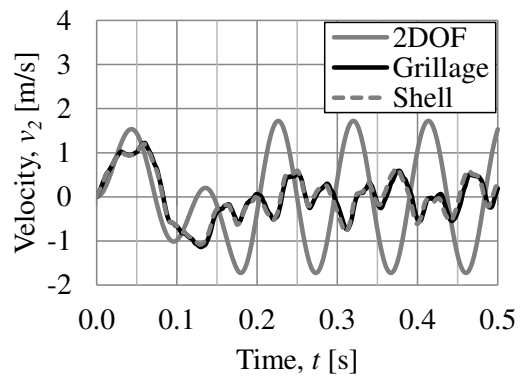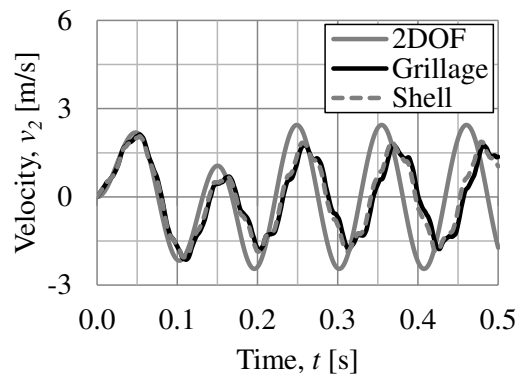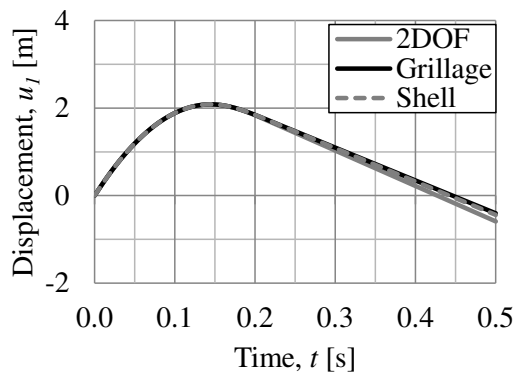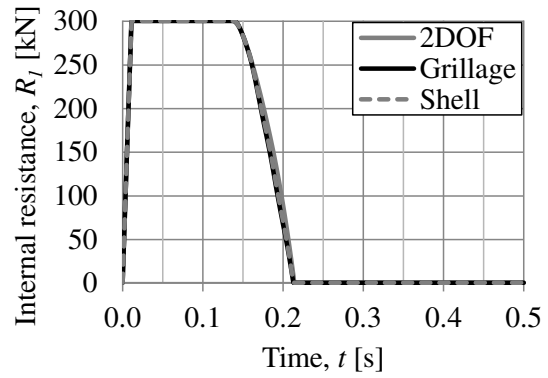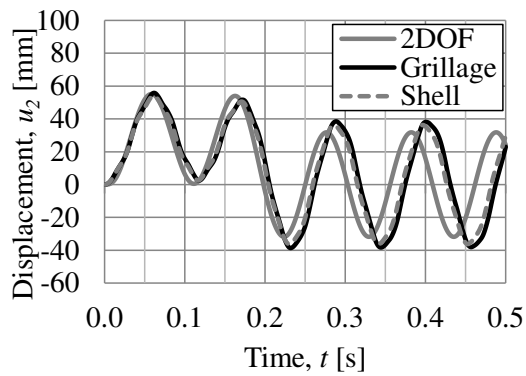
Figure C.10 *Illustration of collision H2, a) displacement of body 1 u_1, b) internal resistance of body 1 R_1, c) displacement of body 2 u_2, and d) velocity of body 2 v_2.*
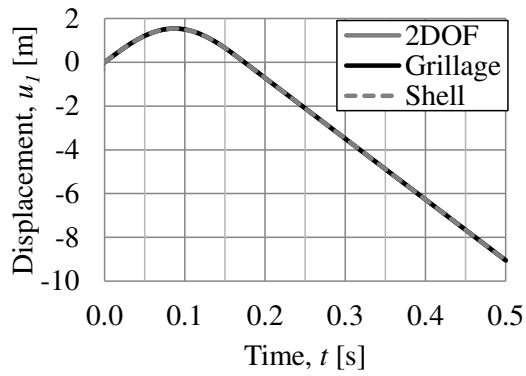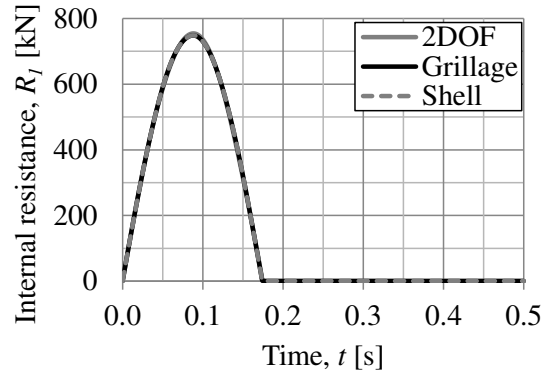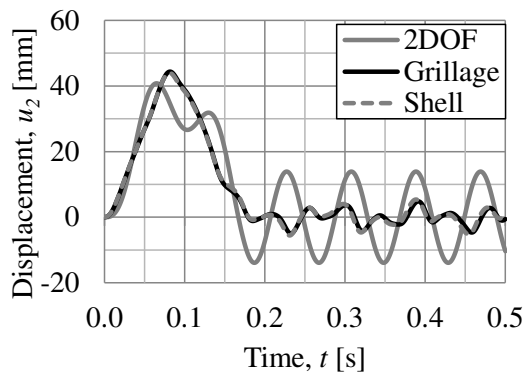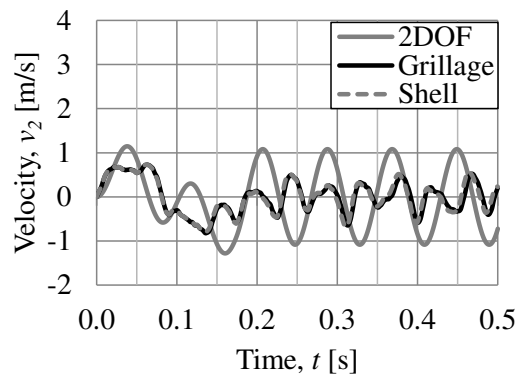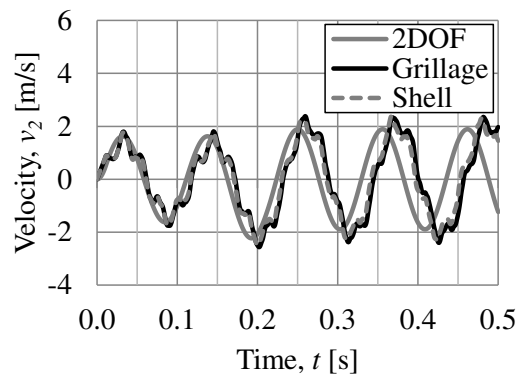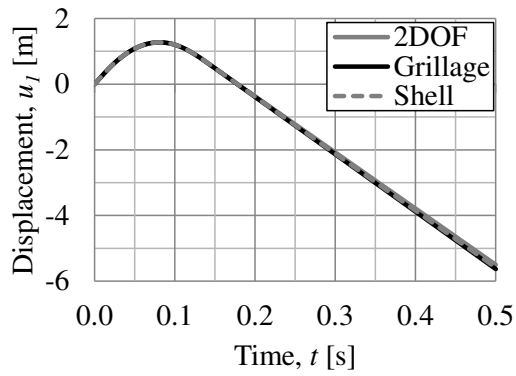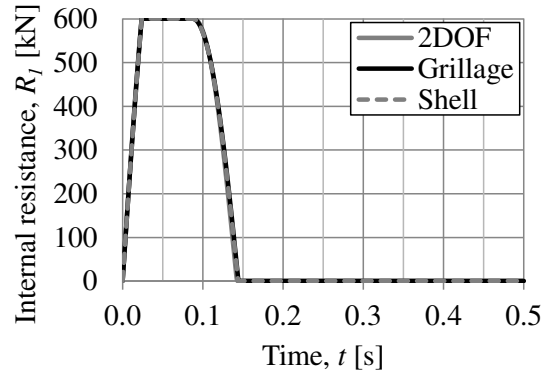
Figure C.11   Illustration of collision H3, a) displacement of body 1 u_1, b) internal resistance of body 1 R_1, c) displacement of body 2 u_2, and d) velocity of body 2 v_2.
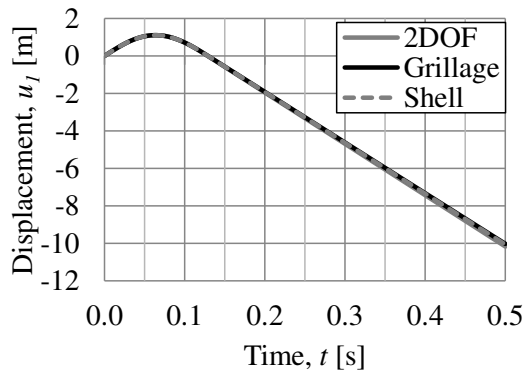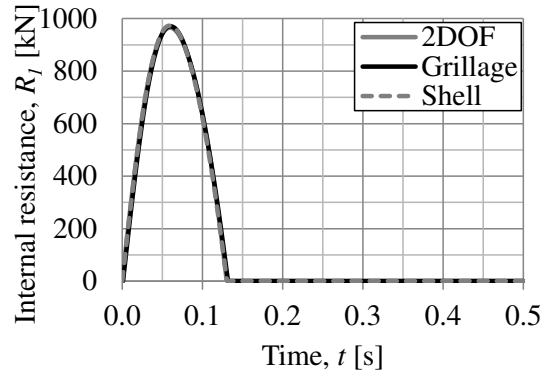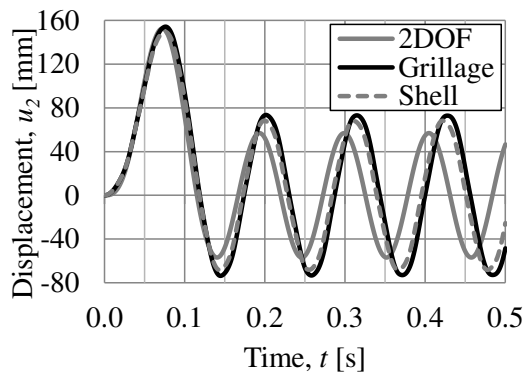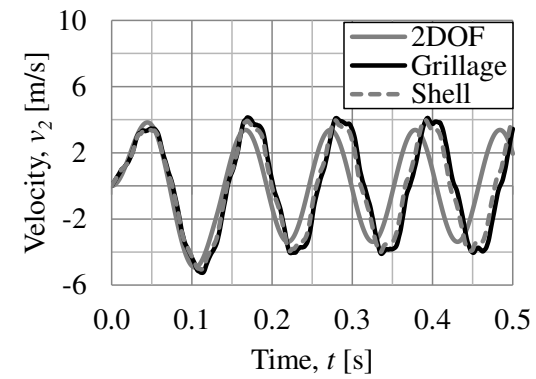
Figure C.12 *Illustration of collision H4, a) displacement of body 1 u_1, b) internal resistance of body 1 R_1, c) displacement of body 2 u_2, and d) velocity of body 2 v_2.*
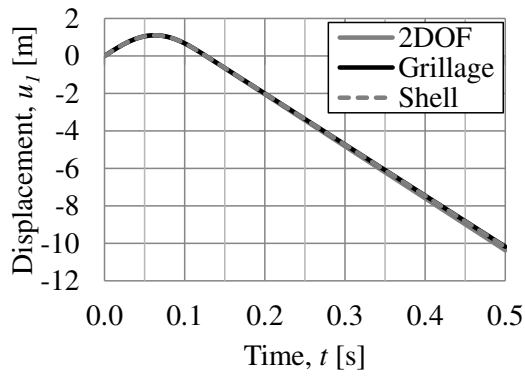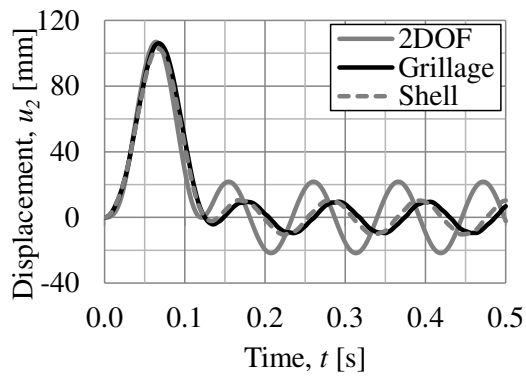
a)
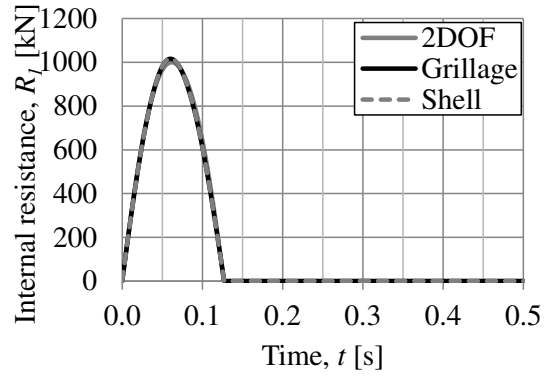
b)
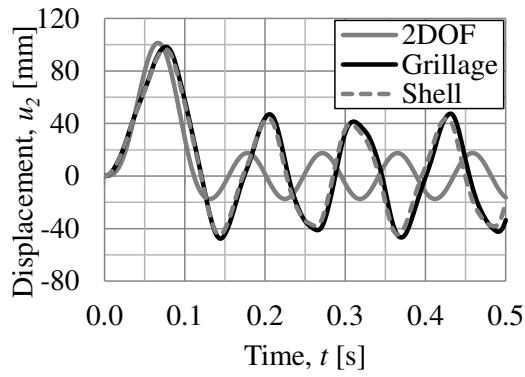
c)
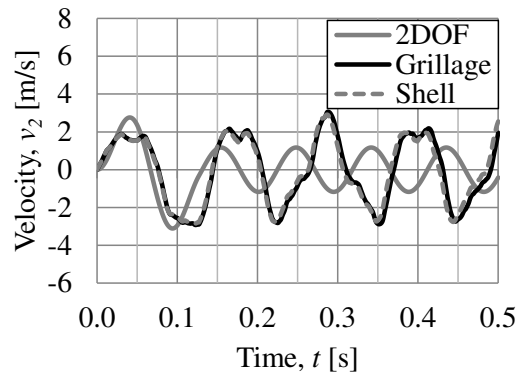
d)

Figure C.13   *Illustration of collision H5, a) displacement of body 1 u_1, b) internal resistance of body 1 R_1, c) displacement of body 2 u_2, and d) velocity of body 2 v_2.*
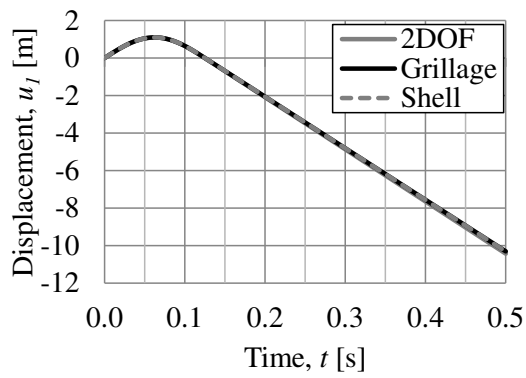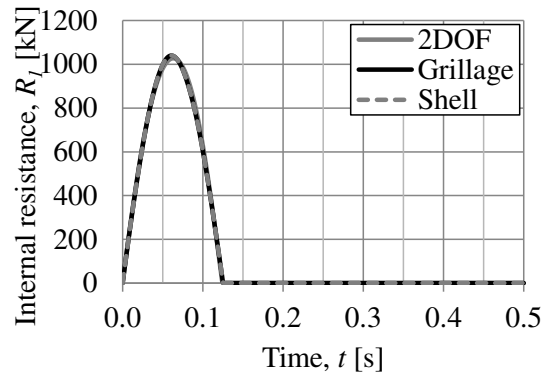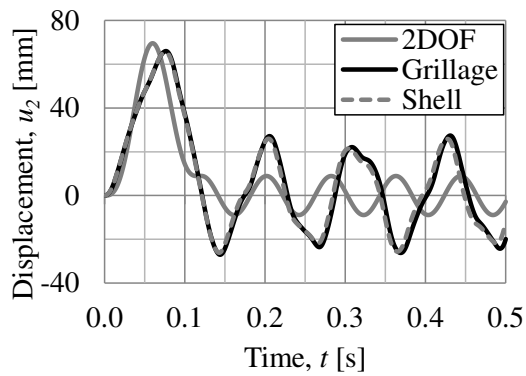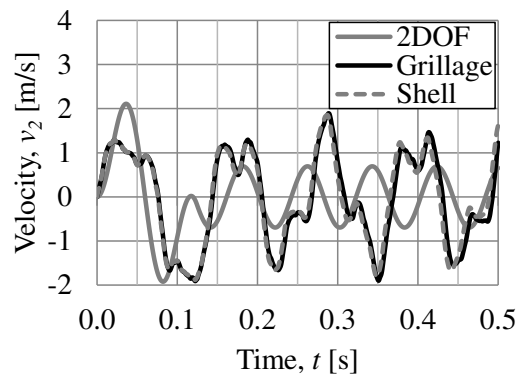
Figure C.14 Illustration of collision H6, a) displacement of body 1 u_1, b) internal resistance of body 1 R_1, c) displacement of body 2 u_2, and d) velocity of body 2 v_2.
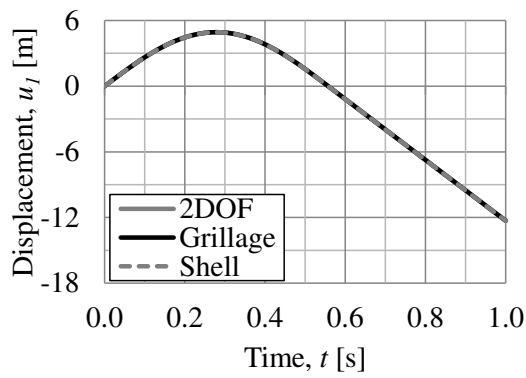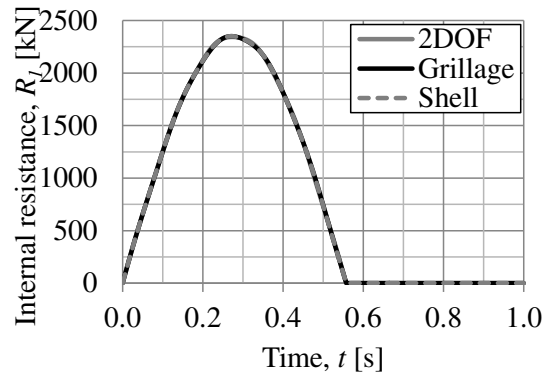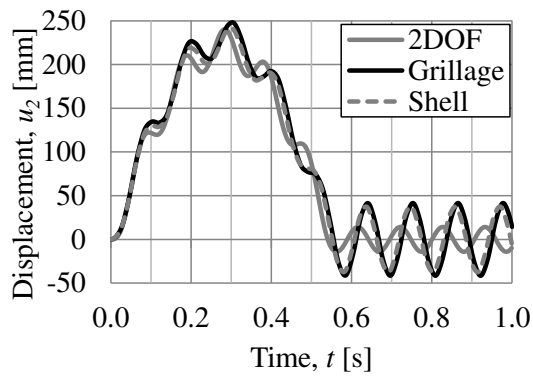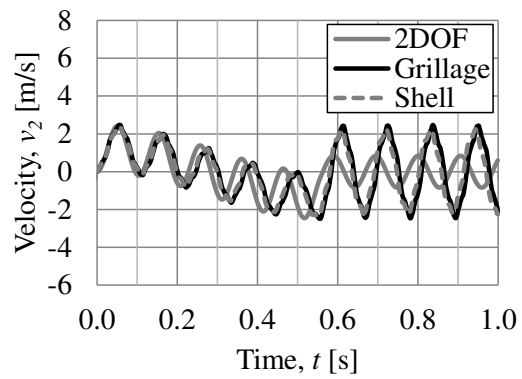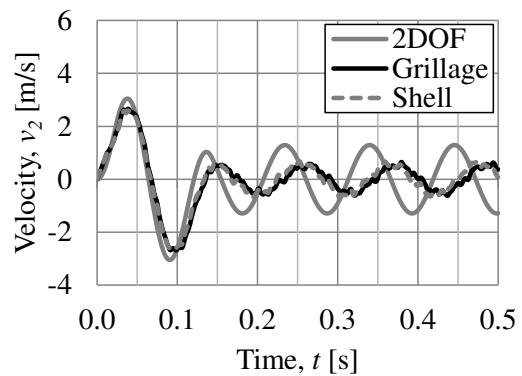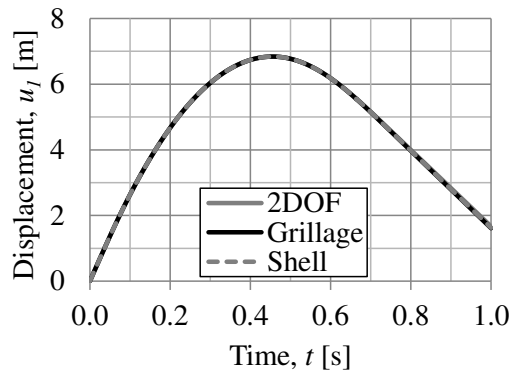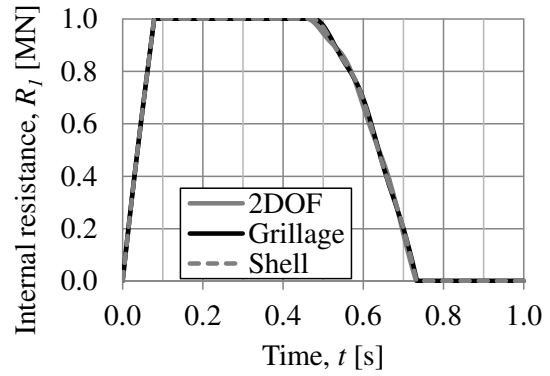
Figure C.15 *Illustration of collision H7, a) displacement of body 1 u_1, b) internal resistance of body 1 R_1, c) displacement of body 2 u_2, and d) velocity of body 2 v_2.*

CHALMERS, *Civil and Environmental Engineering*, Master's Thesis 2015:87
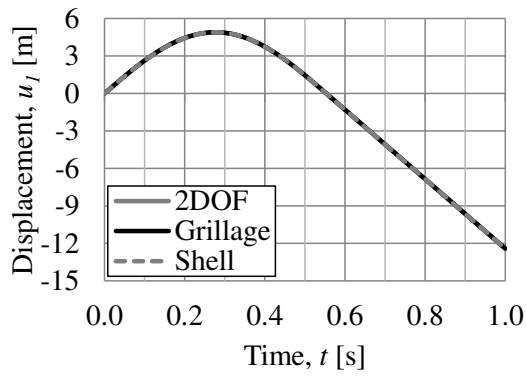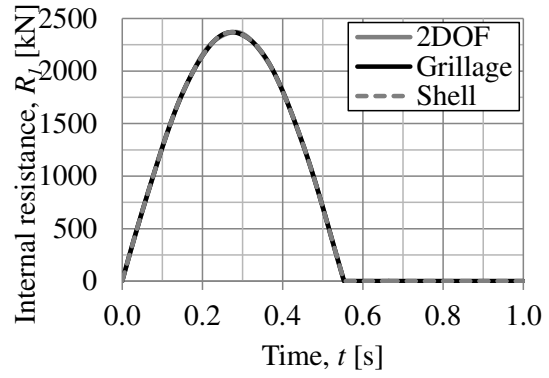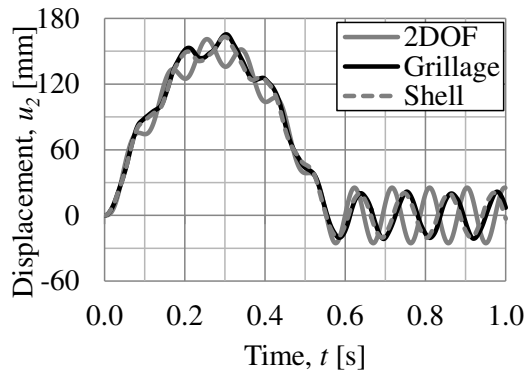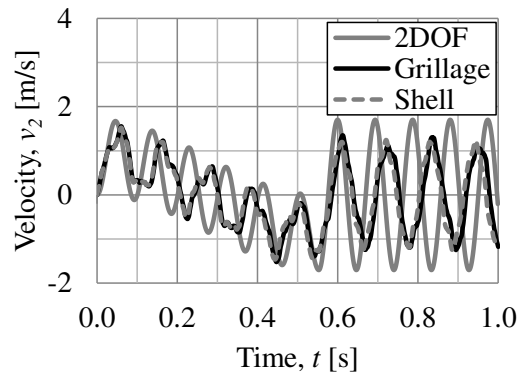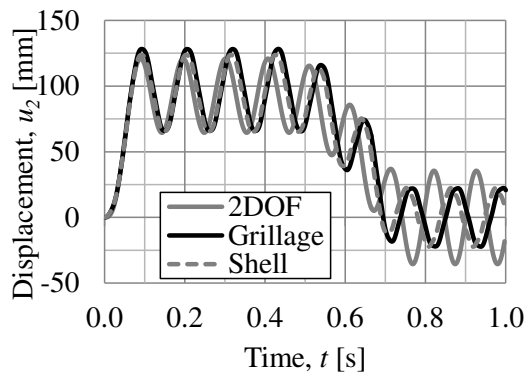
Figure C.16   Illustration of collision H8, a) displacement of body 1 u_1, b) internal resistance of body 1 R_1, c) displacement of body 2 u_2, and d) velocity of body 2 v_2.
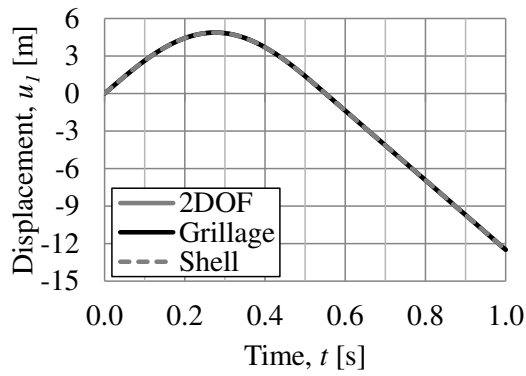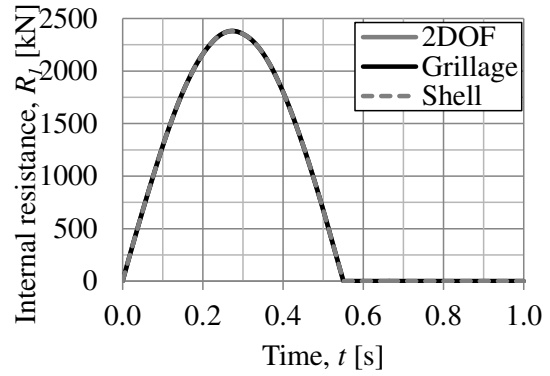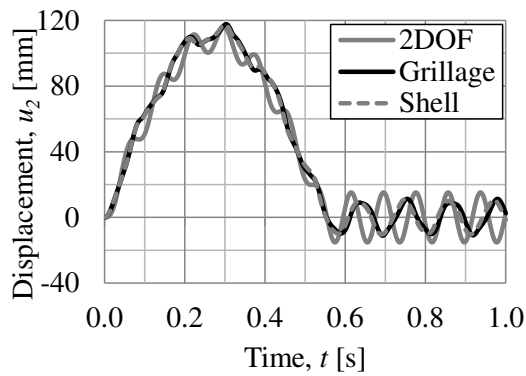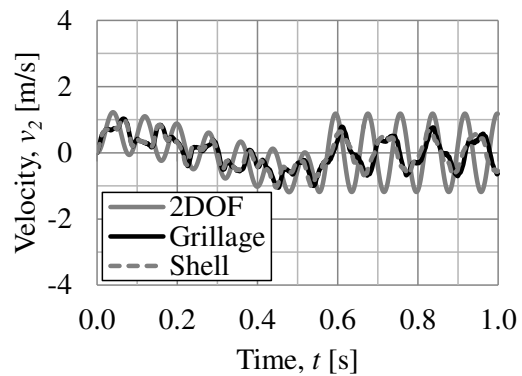
Figure C.17 *Illustration of collision H9, a) displacement of body 1 u_1, b) internal resistance of body 1 R_1, c) displacement of body 2 u_2, and d) velocity of body 2 v_2.*

CHALMERS, *Civil and Environmental Engineering*, Master's Thesis 2015:87
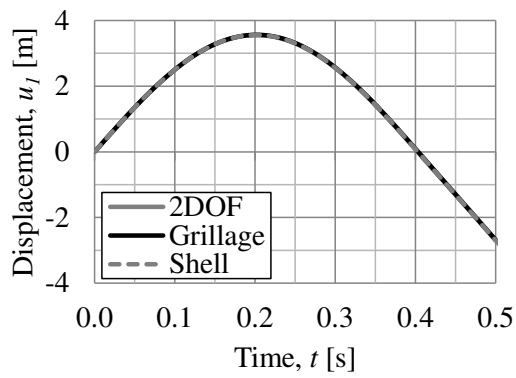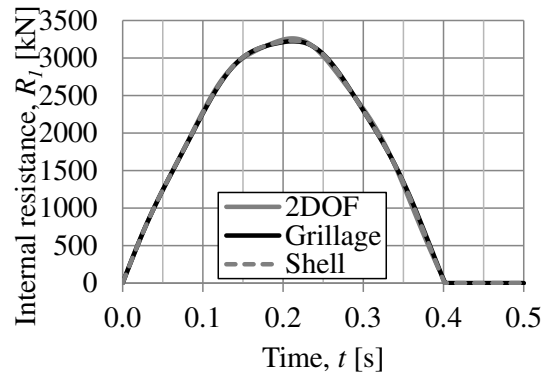
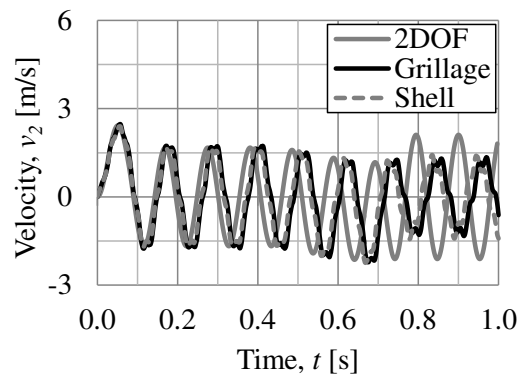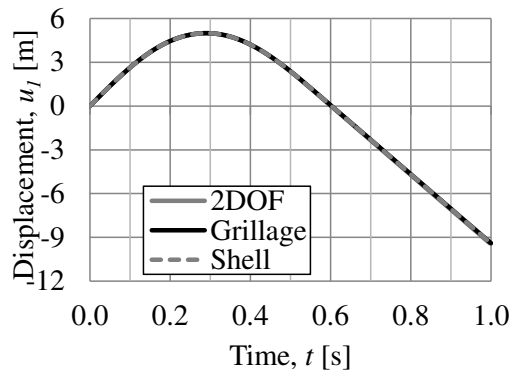a)   b)
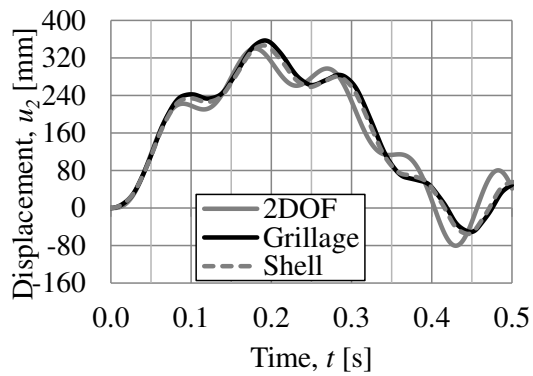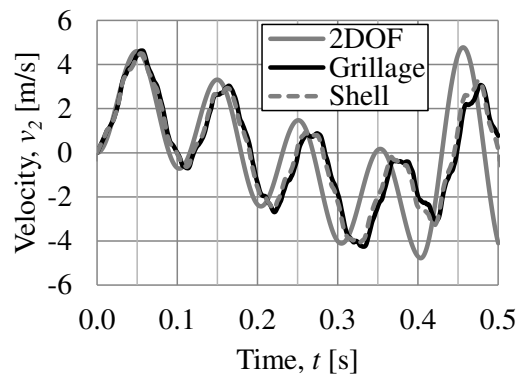
c)   d)

Figure C.18   Illustration of collision H10, a) displacement of body 1 u_1, b) internal resistance of body 1 R_1, c) displacement of body 2 u_2, and d) velocity of body 2 v_2.
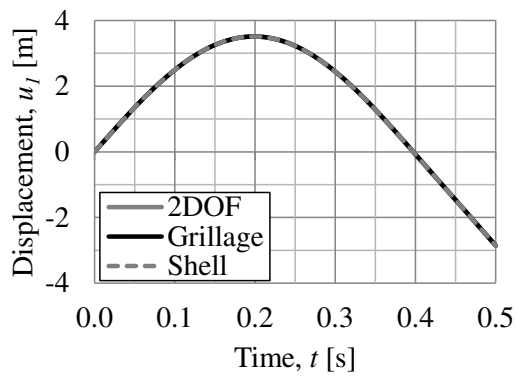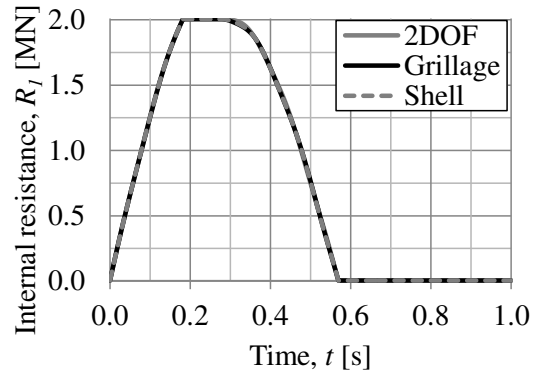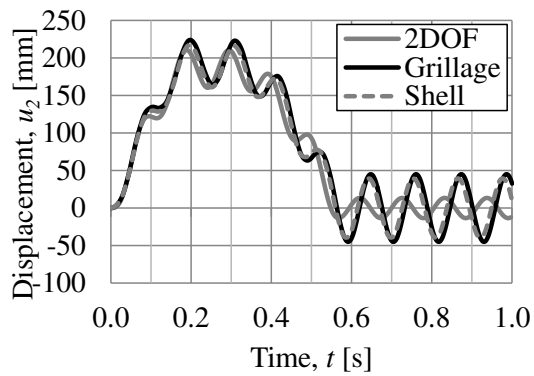
a)

b)

c)

d)

Figure C.19   Illustration of collision H11, a) displacement of body 1 u_1, b) internal resistance of body 1 R_1, c) displacement of body 2 u_2, and d) velocity of body 2 v_2.

Figure C.20 *Illustration of collision H12, a) displacement of body 1 u_1, b) internal resistance of body 1 R_1, c) displacement of body 2 u_2, and d) velocity of body 2 v_2.*
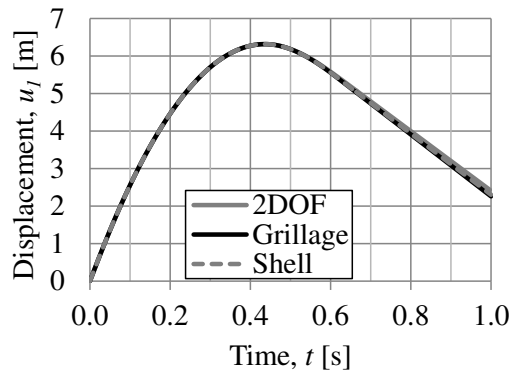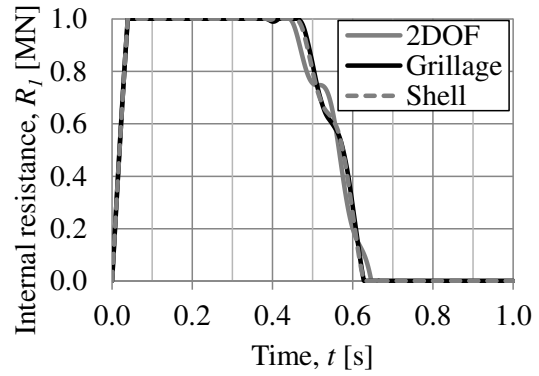
C.5 Elasto-plastic body 1 and elastic body 2 for a slab

In this section results, for collision I1-I8 are presented according to the analysis discussed in Section 6.2.3.

Table C.5 2DOF and FE input parameters for collision I1-I8 with initial velocity $v_0 = 27.8$ m/s. The point load is applied in the centre of the slab, i.e. $\alpha_x = \alpha_y = 0.5$, $\kappa_{mF} = 0.203$ and $k_{sl} = 10.79$ MN/m.

| Case	k_1 [MN/m]	m_1 [kg]	$R_{1,max}$ [MN]
Collision I1	0.5	1 500	0.3
Collision I2	0.5	1 500	0.6
Collision I3	1	1 500	0.3
Collision I4	1	1 500	0.6
Collision I5	0.5	15 000	1
Collision I6	0.5	15 000	2
Collision I7	1	15 000	1
Collision I8	1	15 000	2

Figure C.21 Illustration of collision I1, a) displacement of body 1 u_1, b) internal resistance of body 1 R_1, c) displacement of body 2 u_2, and d) velocity of body 2 v_2.
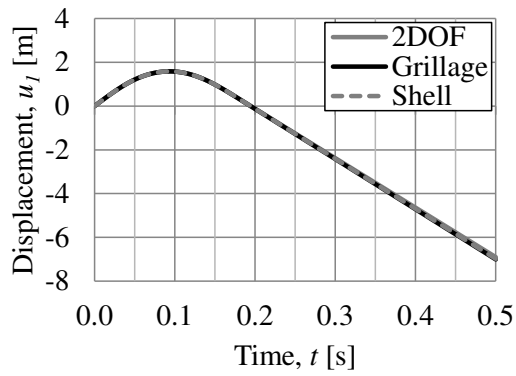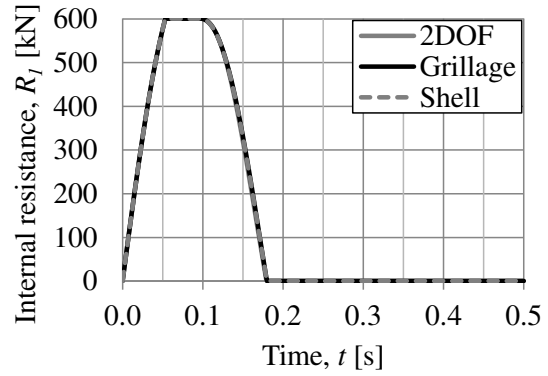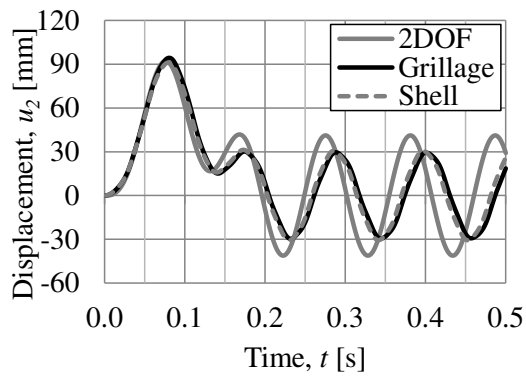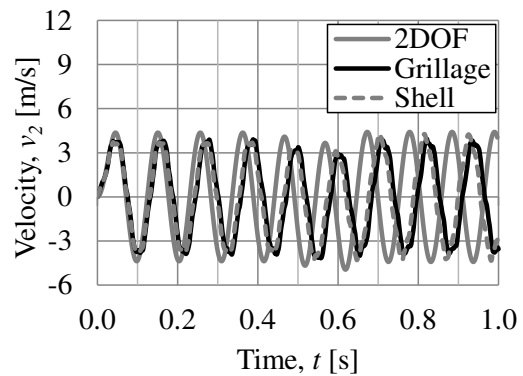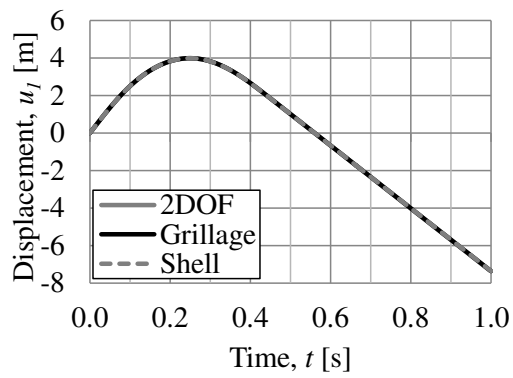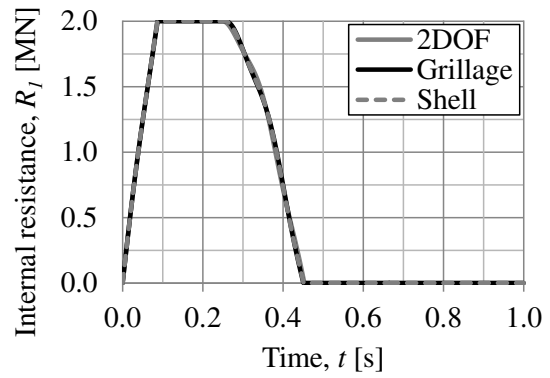
Figure C.22 Illustration of collision I2, a) displacement of body 1 u_1, b) internal resistance of body 1 R_1, c) displacement of body 2 u_2, and d) velocity of body 2 v_2.

Figure C.23   Illustration of collision I3, a) displacement of body 1 u_1, b) internal resistance of body 1 R_1, c) displacement of body 2 u_2, and d) velocity of body 2 v_2.
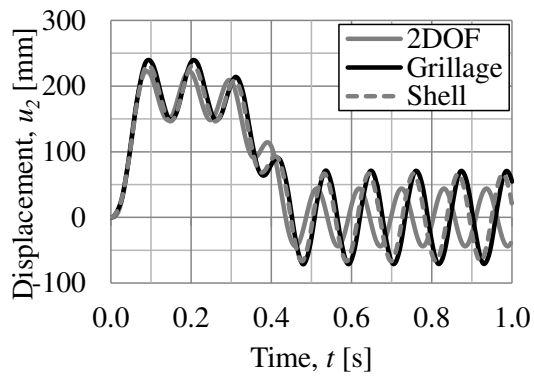
Figure C.24 *Illustration of collision I4, a) displacement of body 1 u_1, b) internal resistance of body 1 R_1, c) displacement of body 2 u_2, and d) velocity of body 2 v_2.*
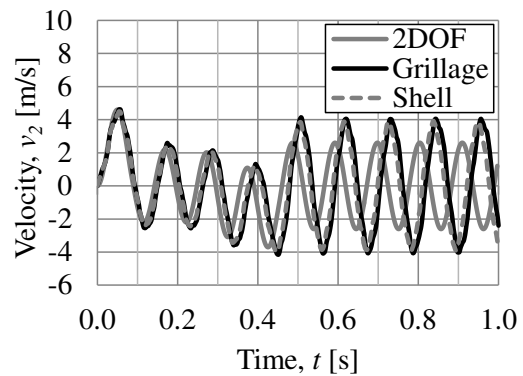
Figure C.25 *Illustration of collision I5, a) displacement of body 1 u_1, b) internal resistance of body 1 R_1, c) displacement of body 2 u_2, and d) velocity of body 2 v_2.*
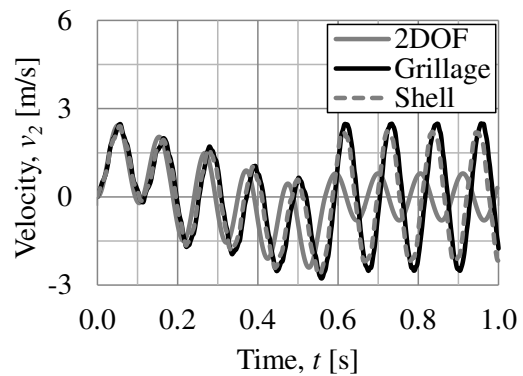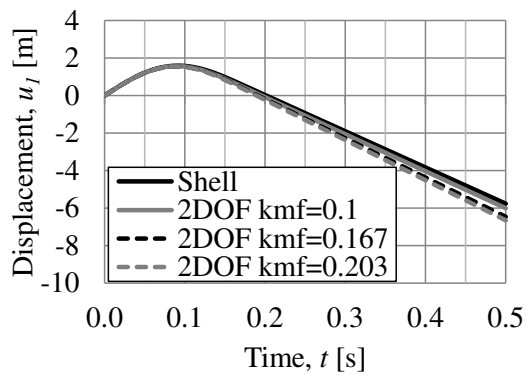
Figure C.26 Illustration of collision I6, a) displacement of body 1 u_1, b) internal resistance of body 1 R_1, c) displacement of body 2 u_2, and d) velocity of body 2 v_2.
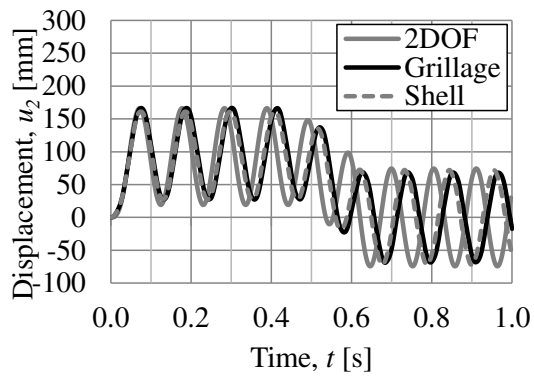
Figure C.27   *Illustration of collision I7, a) displacement of body 1 u_1, b) internal resistance of body 1 R_1, c) displacement of body 2 u_2, and d) velocity of body 2 v_2.*

Figure C.28 Illustration of collision I8, a) displacement of body 1 u_1, b) internal resistance of body 1 R_1, c) displacement of body 2 u_2, and d) velocity of body 2 v_2.

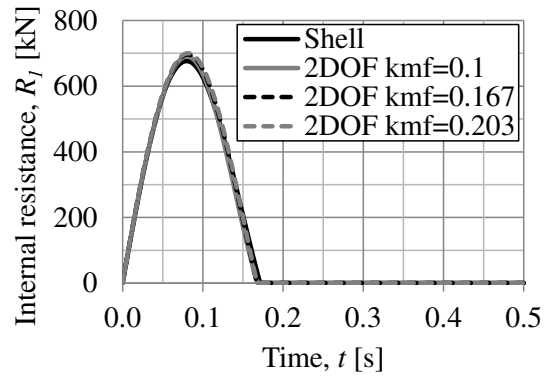## C.6 Elastic body 1 and elasto-plastic body 2 for a slab

In this section, results for collision J1-J12 are presented according to the analysis discussed in Section 6.2.4.4.

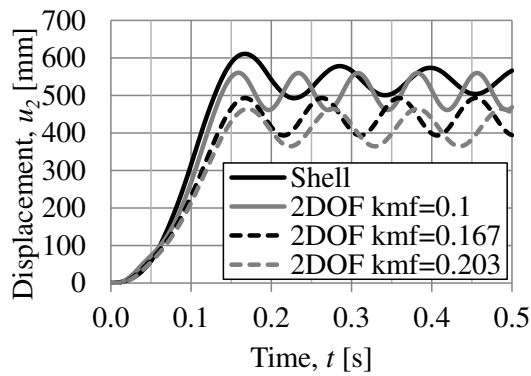*Table C.6   2DOF and FE input parameters for collision J1-J12.*

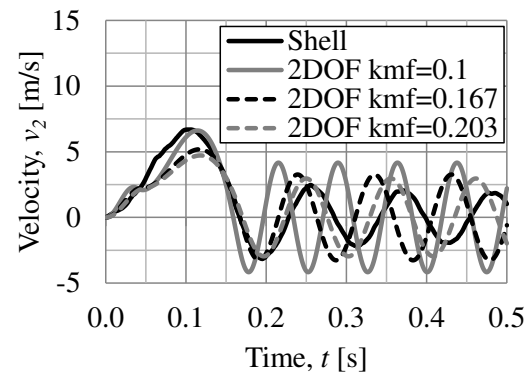| Case	α_x [-]	α_y [-]	k_1 [MN/m]	m_1 [kg]	v_0 [m/s]	2DOF k_2 [MN/m]	2DOF $R_{2,max}$ [kN]
Collision J1	0.5	0.5	0.5	1 500	27.8	10.79	537.7
Collision J2	0.5	0.25	0.5	1 500	27.8	15.94	537.7
Collision J3	0.25	0.25	0.5	1 500	27.8	22.02	716.9
Collision J4	0.5	0.5	1	1 500	27.8	10.79	537.7
Collision J5	0.5	0.25	1	1 500	27.8	22.02	537.7
Collision J6	0.25	0.25	1	1 500	27.8	22.02	716.9
Collision J7	0.5	0.5	0.5	15 000	10	10.79	537.7
Collision J8	0.5	0.25	0.5	15 000	10	15.94	537.7
Collision J9	0.25	0.25	0.5	15 000	10	22.02	716.9
Collision J10	0.5	0.5	1	15 000	10	10.79	537.7
Collision J11	0.5	0.25	1	15 000	10	15.94	537.7
Collision J12	0.25	0.25	1	15 000	10	22.02	716.9

Figure C.29   *Illustration of collision J1, a) displacement of body 1 u_1, b) internal resistance of body 1 R_1, c) displacement of body 2 u_2, and d) velocity of body 2 v_2.*
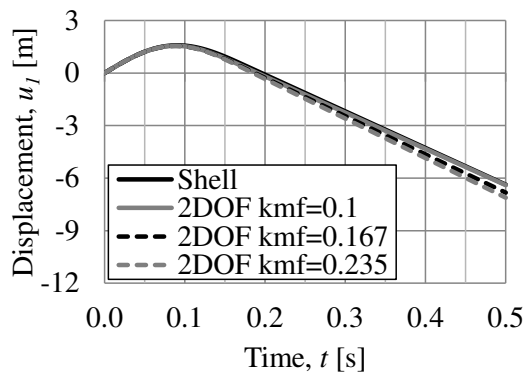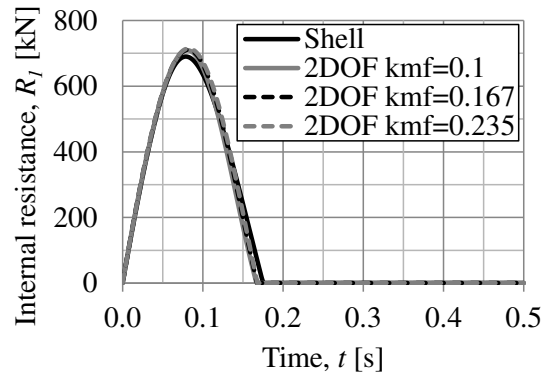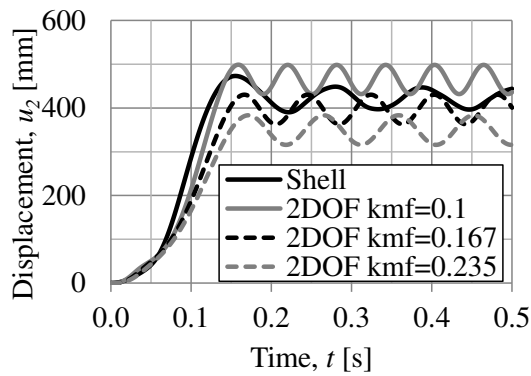
Figure C.30   Illustration of collision J2, a) displacement of body 1 u_1, b) internal resistance of body 1 R_1, c) displacement of body 2 u_2, and d) velocity of body 2 v_2.
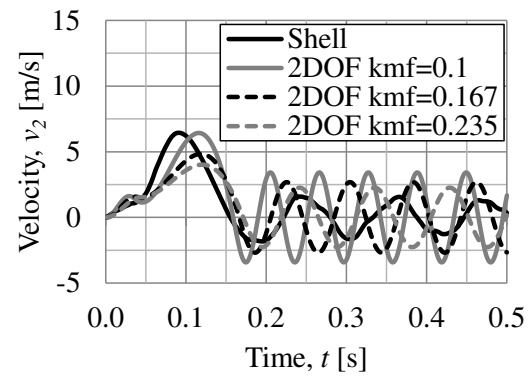
Figure C.31   *Illustration of collision J3, a) displacement of body 1 u_1, b) internal resistance of body 1 R_1, c) displacement of body 2 u_2, and d) velocity of body 2 v_2.*
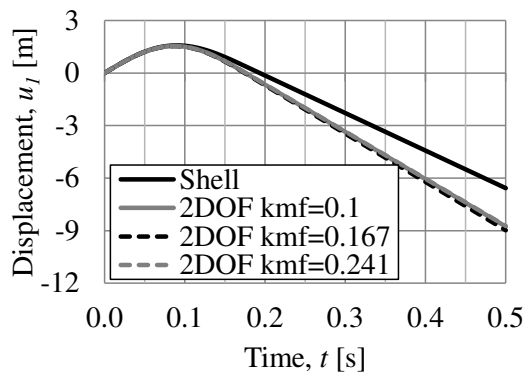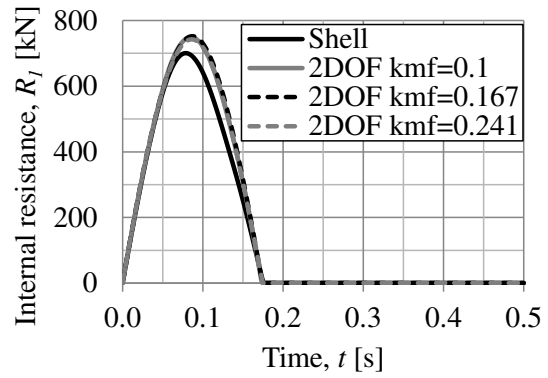
Figure C.32   Illustration of collision J4, a) displacement of body 1 u_1, b) internal resistance of body 1 R_1, c) displacement of body 2 u_2, and d) velocity of body 2 v_2.
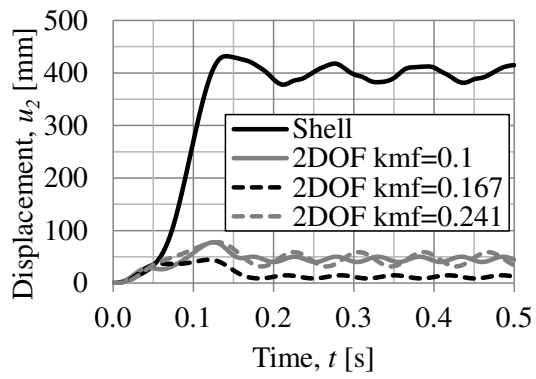
a)

b)

c)

d)

Figure C.33   Illustration of collision J5, a) displacement of body 1 u_1, b) internal resistance of body 1 R_1, c) displacement of body 2 u_2, and d) velocity of body 2 v_2.

CHALMERS, *Civil and Environmental Engineering*, Master's Thesis 2015:87
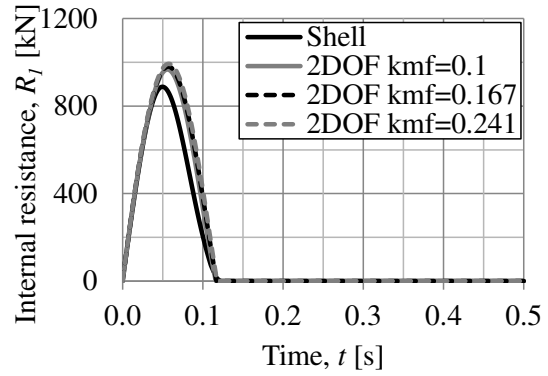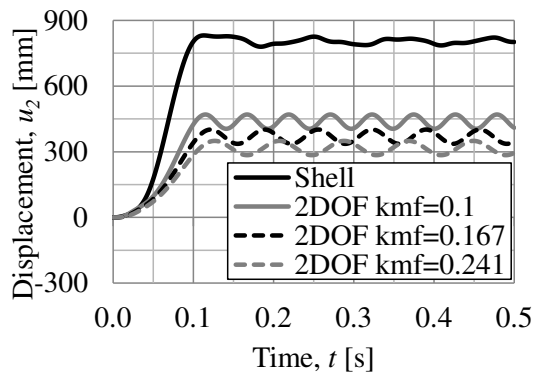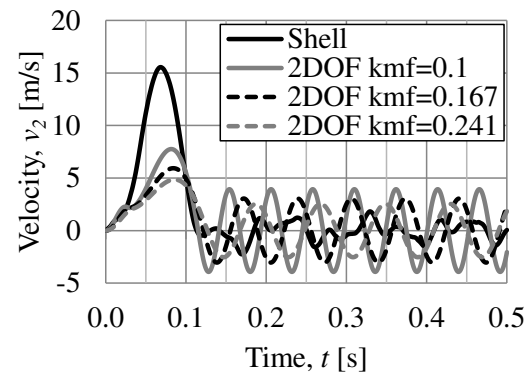
Figure C.34   Illustration of collision J6, a) displacement of body 1 u_1, b) internal resistance of body 1 R_1, c) displacement of body 2 u_2, and d) velocity of body 2 v_2.
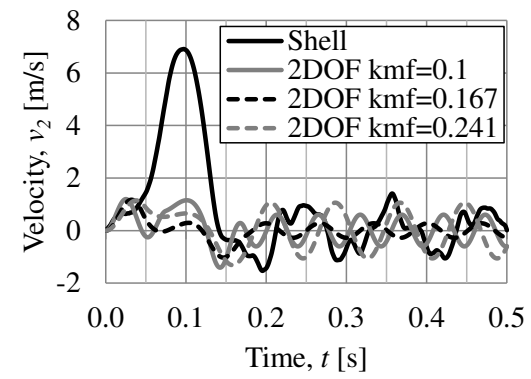
a)

b)

c)
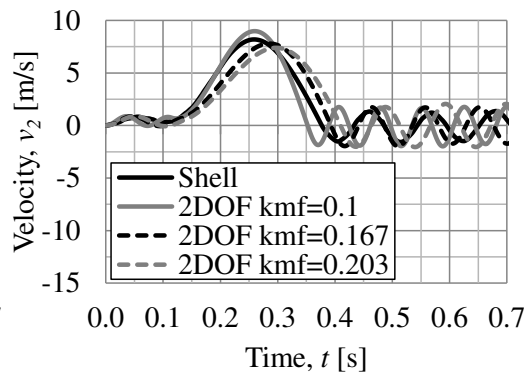
d)

Figure C.35   Illustration of collision J7, a) displacement of body 1 u_1, b) internal resistance of body 1 R_1, c) displacement of body 2 u_2, and d) velocity of body 2 v_2.
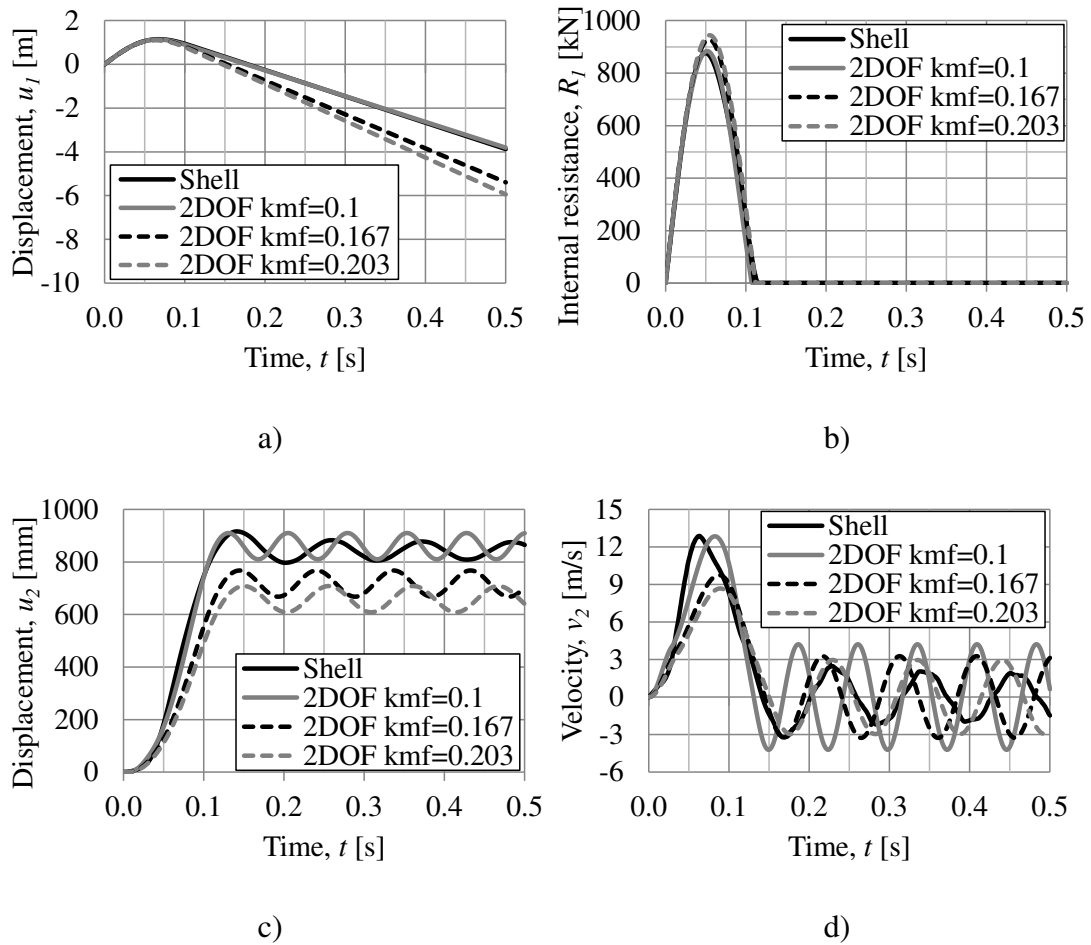
a)

b)

c)

d)
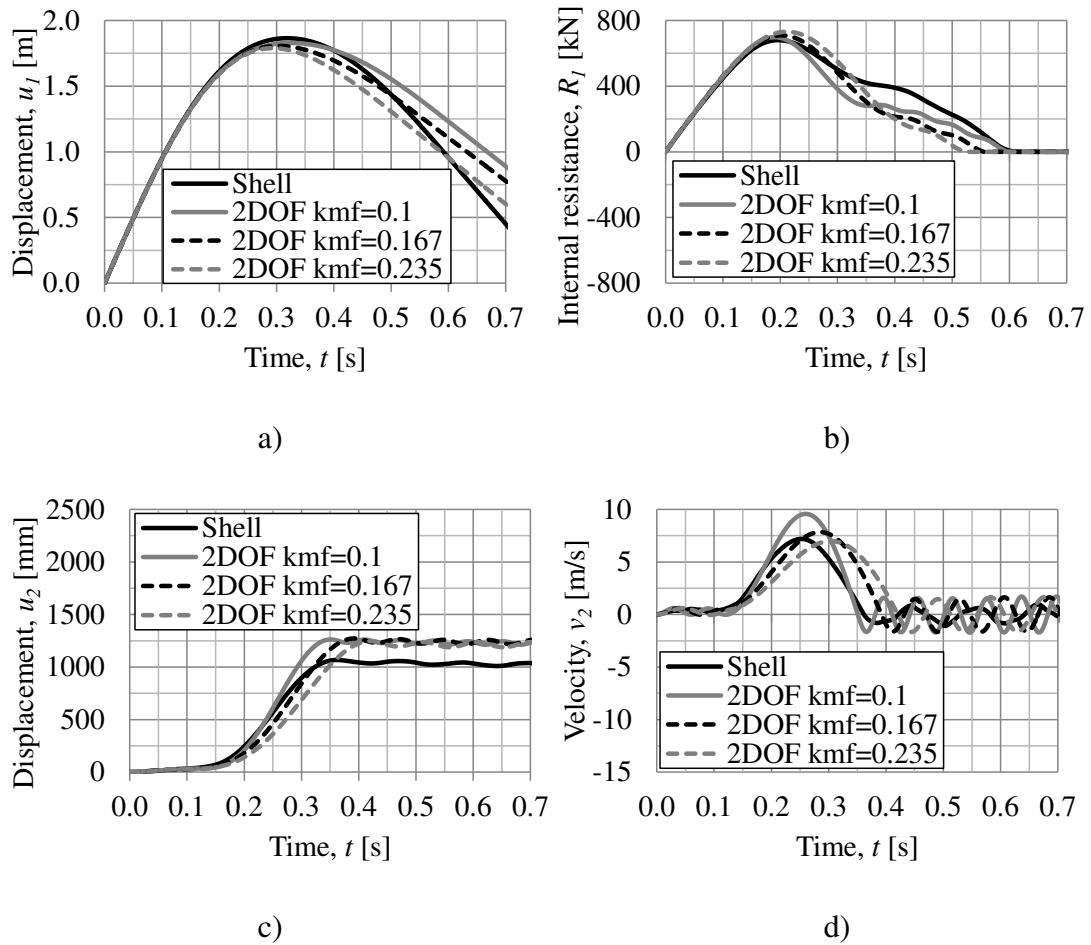
Figure C.36 Illustration of collision J8, a) displacement of body 1 u_1, b) internal resistance of body 1 R_1, c) displacement of body 2 u_2, and d) velocity of body 2 v_2.
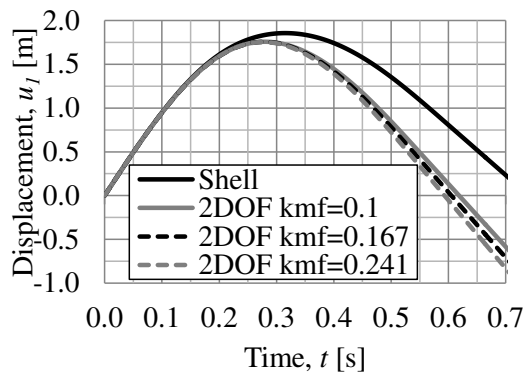
a)
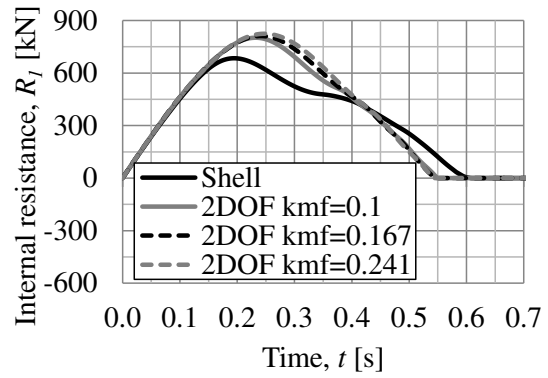
b)
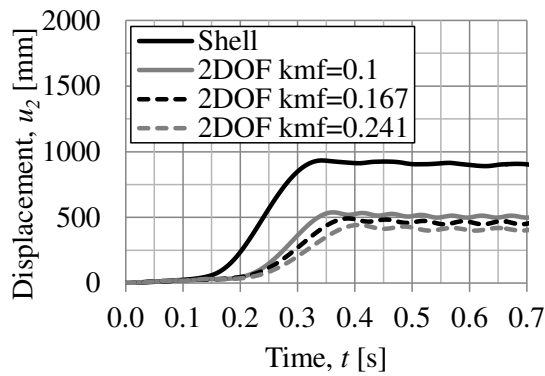
c)
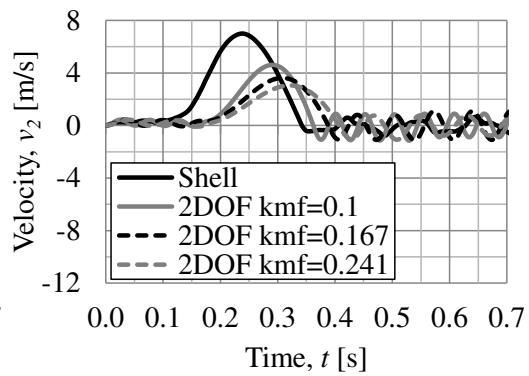
d)

Figure C.37   Illustration of collision J9, a) displacement of body 1 u_1, b) internal resistance of body 1 R_1, c) displacement of body 2 u_2, and d) velocity of body 2 v_2.
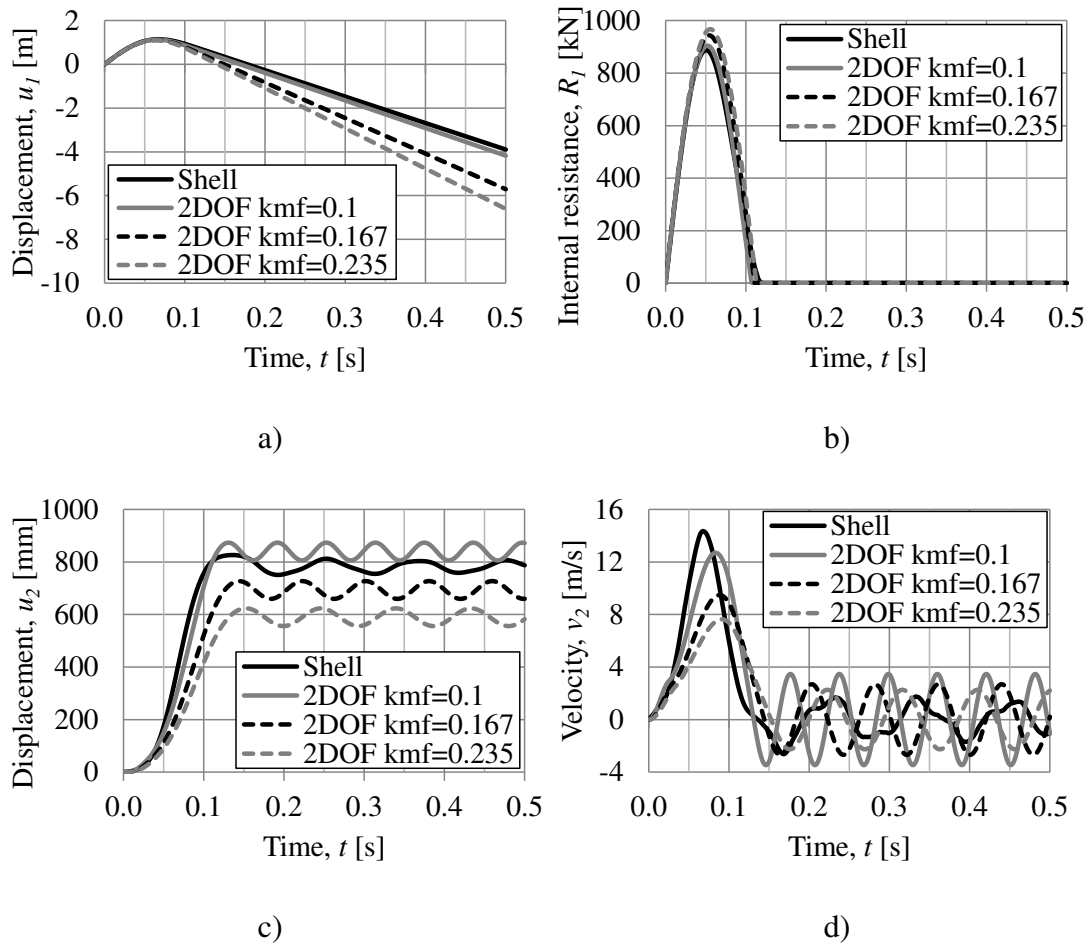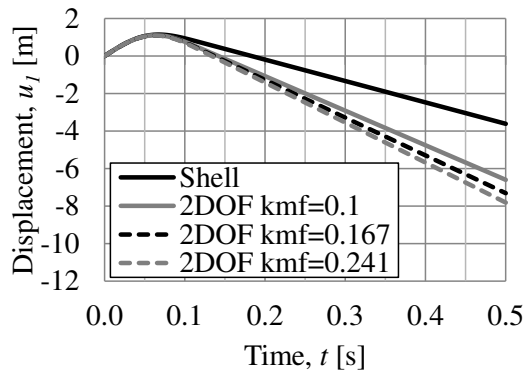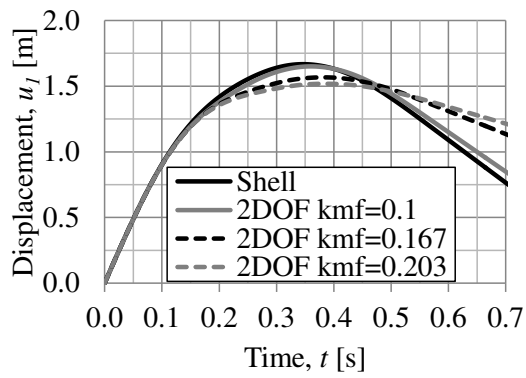
a)
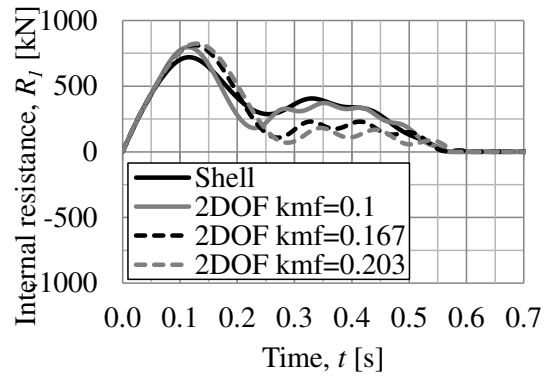
b)
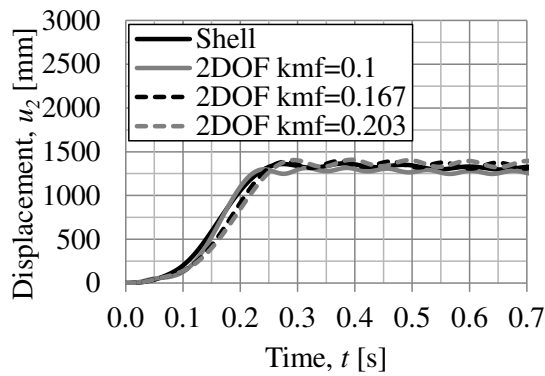
c)
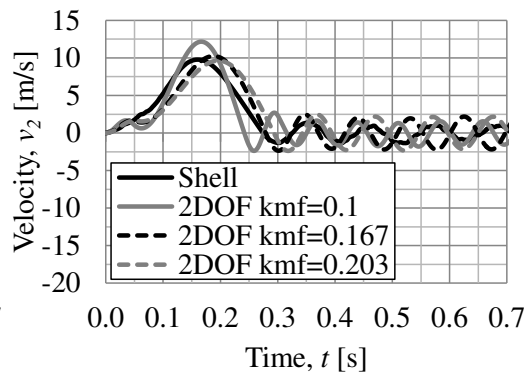
d)

Figure C.38   Illustration of collision J10, a) displacement of body 1 u_1, b) internal resistance of body 1 R_1, c) displacement of body 2 u_2, and d) velocity of body 2 v_2.
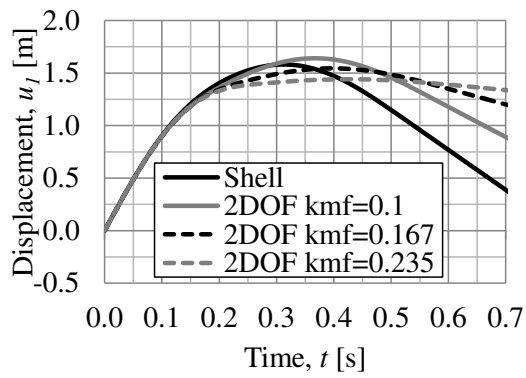
a)
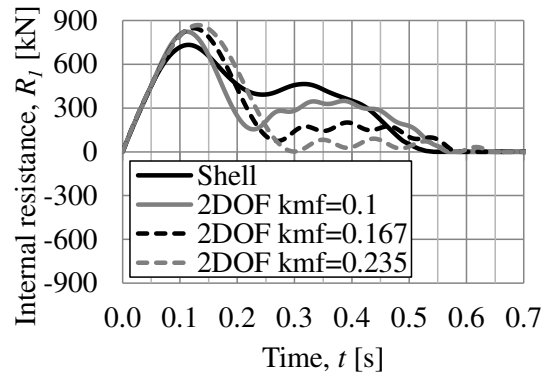
b)
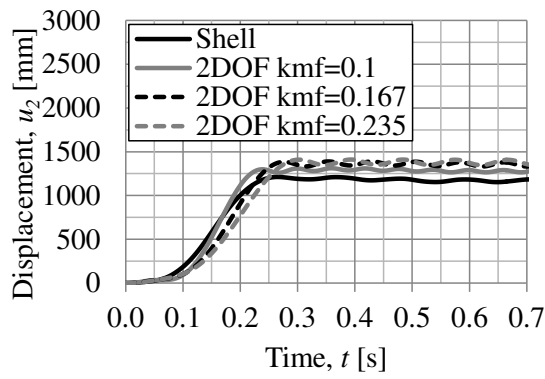
c)
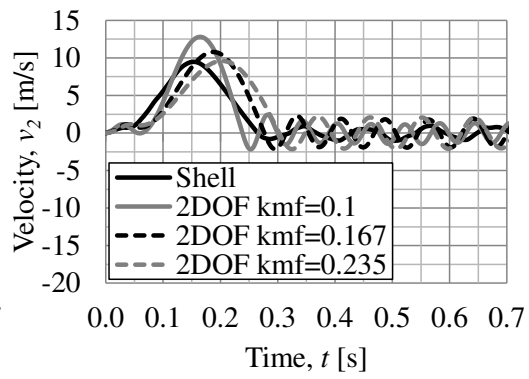
d)

Figure C.39   Illustration of collision J11, a) displacement of body 1 u_1, b) internal resistance of body 1 R_1, c) displacement of body 2 u_2, and d) velocity of body 2 v_2.

CHALMERS, *Civil and Environmental Engineering*, Master's Thesis 2015:87
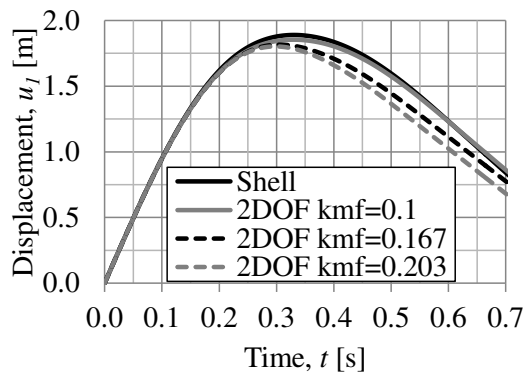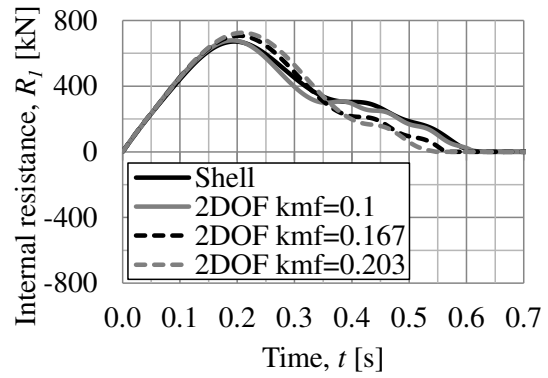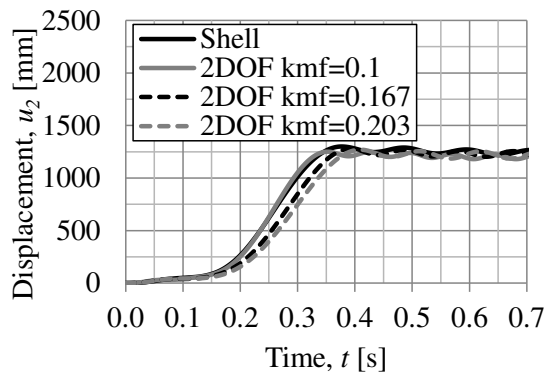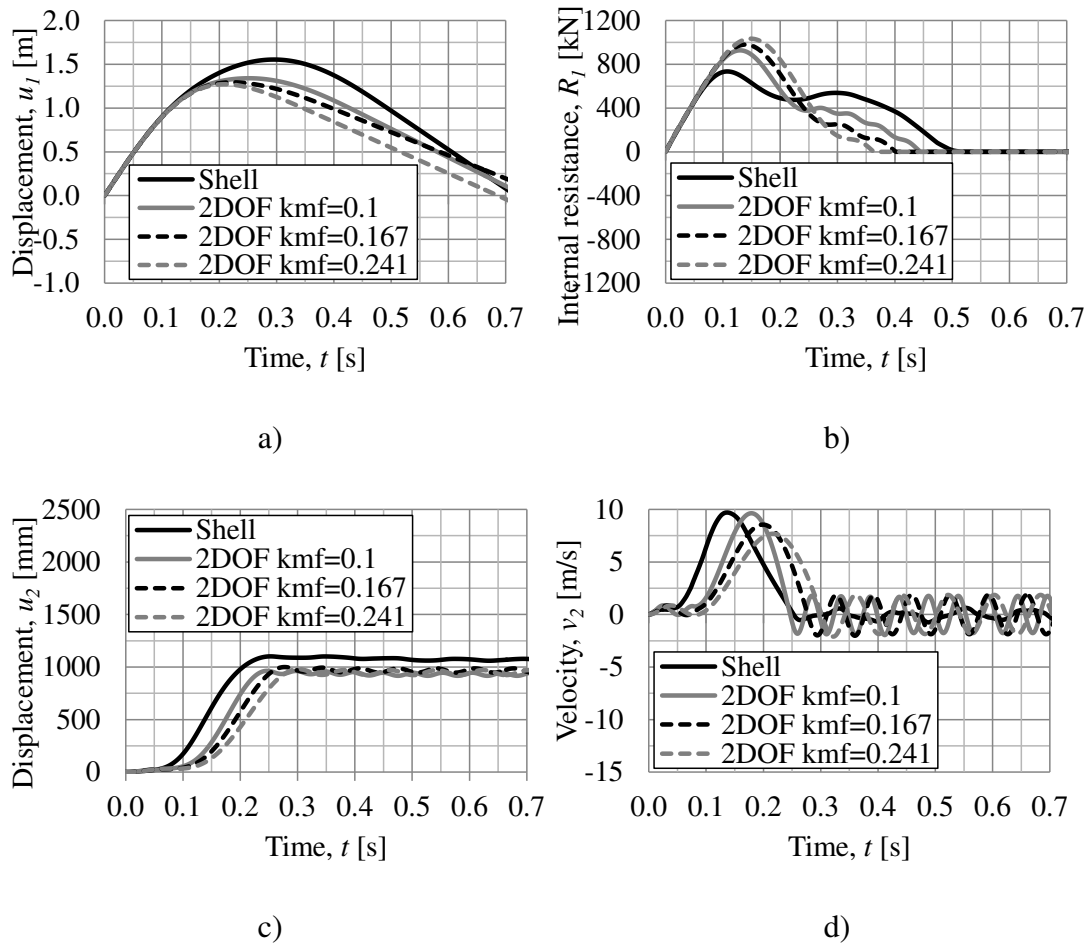
Figure C.40   Illustration of collision J12, a) displacement of body 1 u_1, b) internal resistance of body 1 R_1, c) displacement of body 2 u_2, and d) velocity of body 2 v_2.

Appendix D   Transformation Factors

D.1   Transformation factors for beams

In this section, transformation factors κ_m, κ_F and κ_{mF} are presented for beams subjected to a point load for different load cases where the system point is coinciding with the point of loading, by Asplund and Steckmest (2014).

Table D.1   Transformation factors for point loads at different distances from the support, with the system point coinciding with the point of loading, by Asplund and Steckmest (2014).

α	0.5	0.4	0.3	0.2	0.1
Elastic response					
κ_m	0.486	0.518	0.642	1.011	2.803
κ_F	1.000	1.000	1.000	1.000	1.000
κ_{mF}	0.486	0.518	0.642	1.011	2.803
Plastic response					
κ_m	0.333	0.333	0.333	0.333	0.333
κ_F	1.000	1.000	1.000	1.000	1.000
κ_{mF}	0.333	0.333	0.333	0.333	0.333

D.2   Plastic transformation factors for slabs

In this section, the plastic transformation factors κ_m, κ_F and κ_{mF} for a quadratic simply supported slab subjected to a point load are presented as a function of the displacement at the system point of body 2 u_2 for load case 1-3 presented in Section 4.4.2. The system point is coinciding with the point of loading. These transformation factors are derived from a FE model with shell elements and are unique for each load case. The slab is presented in Section 6.2.1.

a)

b)

c)

Figure D.1   *Illustration of the transformation factors as a function of the displacement at the system point of body 2 u_2 for load case 1 and a dynamic case based on collision J10 a) κ_m, b) κ_F, and c) κ_{mF}.*

Figure D.2 *Illustration of the transformation factors as a function of the displacement at the system point of body 2 u_2 for load case 2 a) κ_m, b) κ_F, and c) κ_{mF}.*

a)

b)
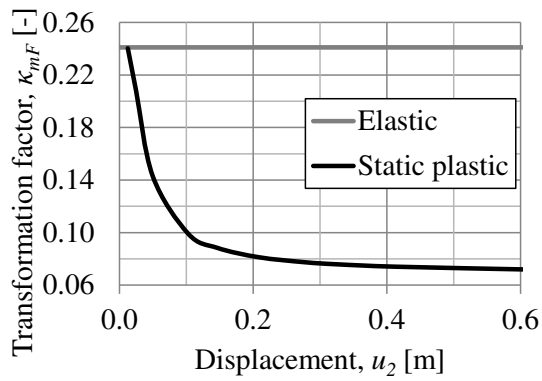
c)

Figure D.3   Illustration of the transformation factors as a function of the displacement at the system point of body 2 u_2 for load case 3 a) κ_m, b) κ_F, and c) κ_{mF}.

Appendix E   Load Factor βel

In this appendix is the relation between the load factor β_{el} and the frequency ratio f_1/f_2 presented for different values of the mass ratio m_1/m_2 used in Section 3.3, by Johansson (2014).

Table E.1   Values for load factor β_{el}, by Johansson (2014).

f_1/f_2	Hard	$\beta_{el} = R_2 / F_{2,el}$ [-]										
		m_1/m_2 [-]										
[-]	impact	0.10	0.20	0.50	1.0	1.5	2.0	3.0	5.0	10	50	100
0.000	1.000	1.000	1.000	1.000	1.000	1.000	1.000	1.000	1.000	1.000	1.000	1.000
0.005	1.006	1.005	1.005	1.005	1.005	1.005	1.005	1.005	1.005	1.005	1.004	1.004
0.050	1.050	1.050	1.049	1.049	1.048	1.047	1.046	1.044	1.041	1.032	0.986	0.993
0.100	1.100	1.099	1.099	1.098	1.095	1.093	1.091	1.086	1.076	1.048	0.874	0.925
0.125	1.125	1.124	1.122	1.118	1.110	1.103	1.095	1.080	1.050	1.005	0.802	0.651
0.150	1.174	1.172	1.171	1.166	1.158	1.150	1.141	1.125	1.091	1.006	0.874	0.578
0.175	1.158	1.157	1.156	1.153	1.148	1.143	1.137	1.123	1.092	1.002	0.672	0.517
0.200	1.083	1.084	1.085	1.087	1.090	1.091	1.091	1.086	1.066	0.981	0.615	0.461
0.225	1.180	1.172	1.165	1.143	1.108	1.074	1.042	1.027	1.024	0.949	0.563	0.420
0.250	1.268	1.258	1.249	1.221	1.176	1.134	1.094	1.021	0.976	0.915	0.515	0.382
0.275	1.348	1.335	1.323	1.288	1.233	1.182	1.134	1.047	0.927	0.879	0.479	0.352
0.300	1.418	1.403	1.389	1.347	1.281	1.220	1.164	1.063	0.899	0.843	0.447	0.324
0.350	1.536	1.515	1.495	1.437	1.349	1.269	1.196	1.069	0.873	0.776	0.389	0.281
0.400	1.625	1.598	1.572	1.498	1.387	1.288	1.200	1.051	0.830	0.713	0.347	0.248
0.450	1.689	1.656	1.624	1.534	1.400	1.284	1.183	1.016	0.777	0.655	0.310	0.221
0.500	1.732	1.693	1.655	1.549	1.395	1.264	1.152	0.971	0.722	0.602	0.281	0.200
0.550	1.757	1.712	1.668	1.548	1.375	1.232	1.111	0.920	0.667	0.552	0.256	0.182
0.600	1.768	1.717	1.668	1.534	1.345	1.192	1.064	0.867	0.627	0.506	0.235	0.167
0.650	1.766	1.710	1.656	1.510	1.308	1.146	1.014	0.814	0.605	0.465	0.217	0.154
0.700	1.755	1.693	1.635	1.478	1.266	1.098	0.964	0.763	0.583	0.429	0.202	0.143
0.750	1.736	1.670	1.608	1.442	1.220	1.049	0.913	0.714	0.560	0.405	0.188	0.133
0.800	1.710	1.640	1.575	1.402	1.173	0.999	0.863	0.667	0.537	0.386	0.177	0.125
0.850	1.680	1.607	1.538	1.359	1.126	0.951	0.816	0.624	0.513	0.367	0.166	0.118
0.900	1.646	1.570	1.499	1.315	1.078	0.903	0.770	0.583	0.489	0.349	0.157	0.111
0.950	1.609	1.531	1.458	1.270	1.032	0.858	0.727	0.548	0.466	0.332	0.149	0.105
1.000	1.571	1.490	1.416	1.225	0.986	0.815	0.687	0.518	0.445	0.316	0.141	0.100
1.125	1.471	1.387	1.310	1.117	0.883	0.721	0.606	0.456	0.397	0.281	0.126	0.089
1.250	1.373	1.288	1.211	1.020	0.797	0.648	0.543	0.408	0.358	0.253	0.113	0.080
1.375	1.283	1.198	1.122	0.936	0.725	0.588	0.492	0.377	0.325	0.230	0.103	0.073
1.500	1.200	1.116	1.042	0.864	0.666	0.538	0.450	0.350	0.298	0.210	0.094	0.067

Appendix F   Slab Modelling

F.1   Deformation shape for different load cases

In this section is the deformation shapes along a line for different load cases illustrated for both quadratic and rectangular slabs. The line and the point of loading are presented in each diagram.
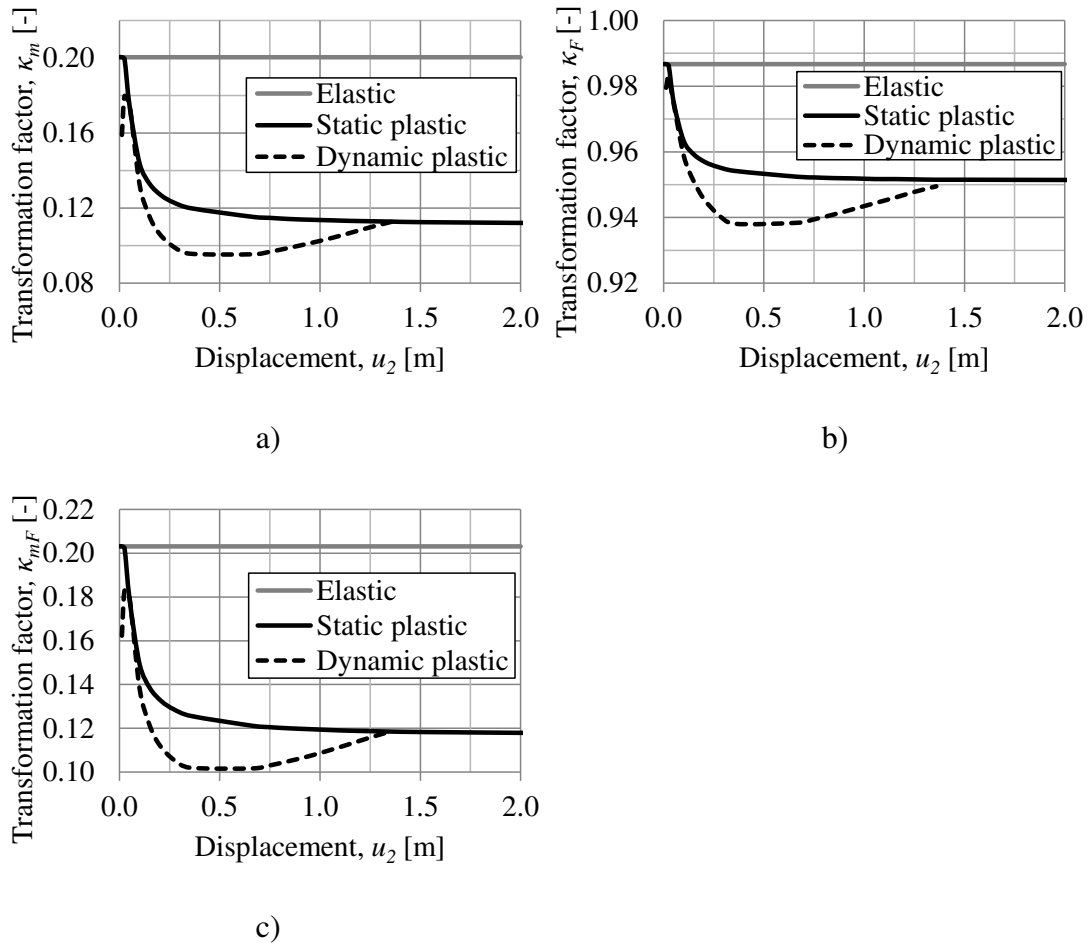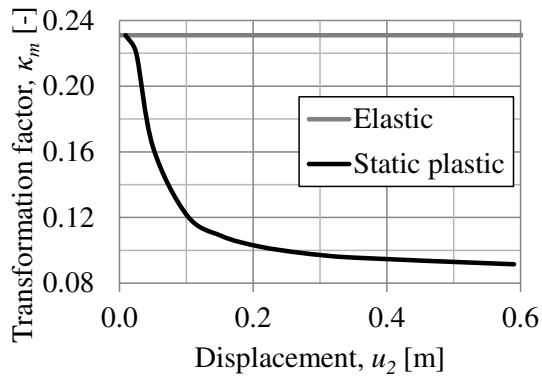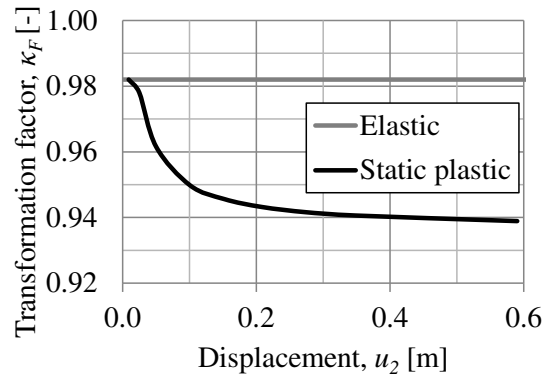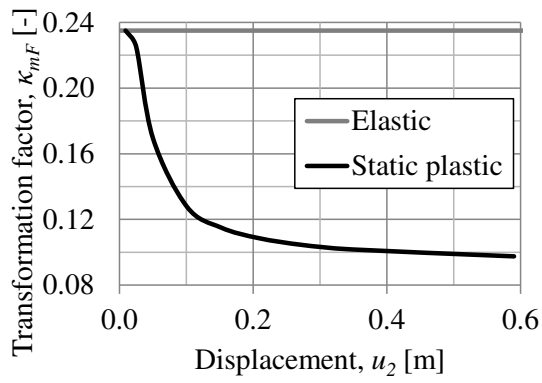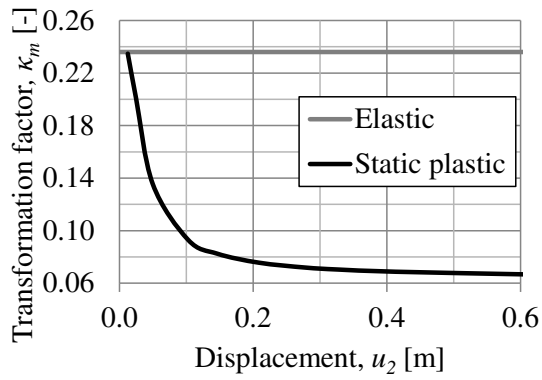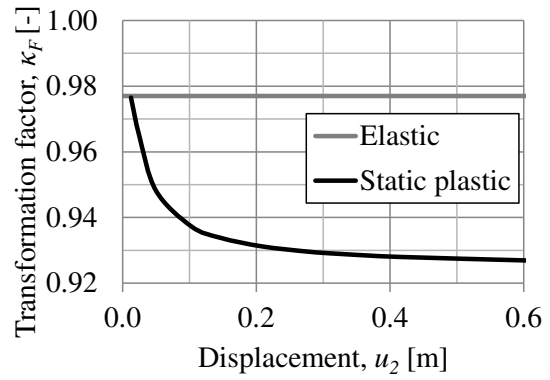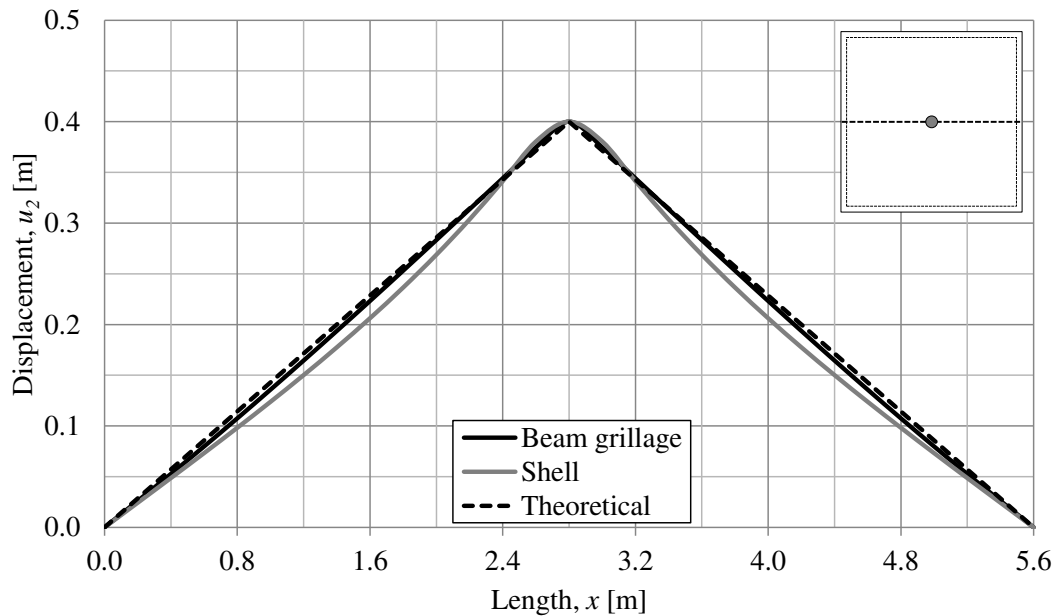

Figure F.1   *Illustration of the displacement of body 2 u_2 on a quadratic slab along a line for the theoretical assumed model, the beam grillage and the shell element model. The line and the point of point loading are presented in the upper right hand corner.*

Figure F.2   *Illustration of the displacement of body 2 u_2 on a quadratic slab along a line for the theoretical assumed model, the beam grillage and the shell element model. The line and the point of point loading are presented in the upper right hand corner.*
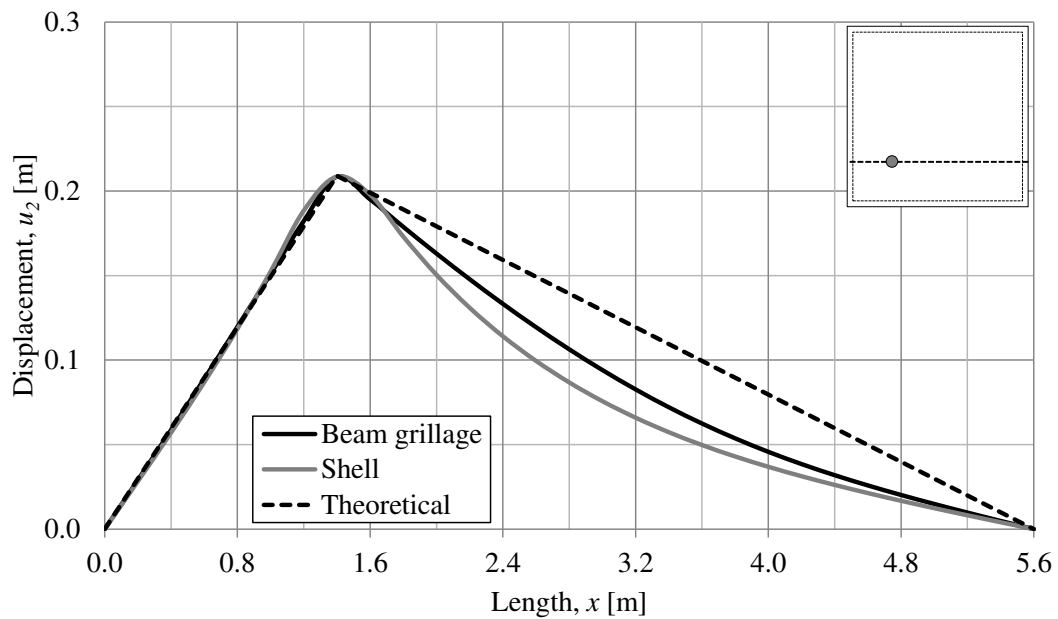
Figure F.3   *Illustration of the displacement of body 2 u_2 on a quadratic slab along a line for the theoretical assumed model, the beam grillage and the shell element model. The line and the point of point loading are presented in the upper right hand corner.*
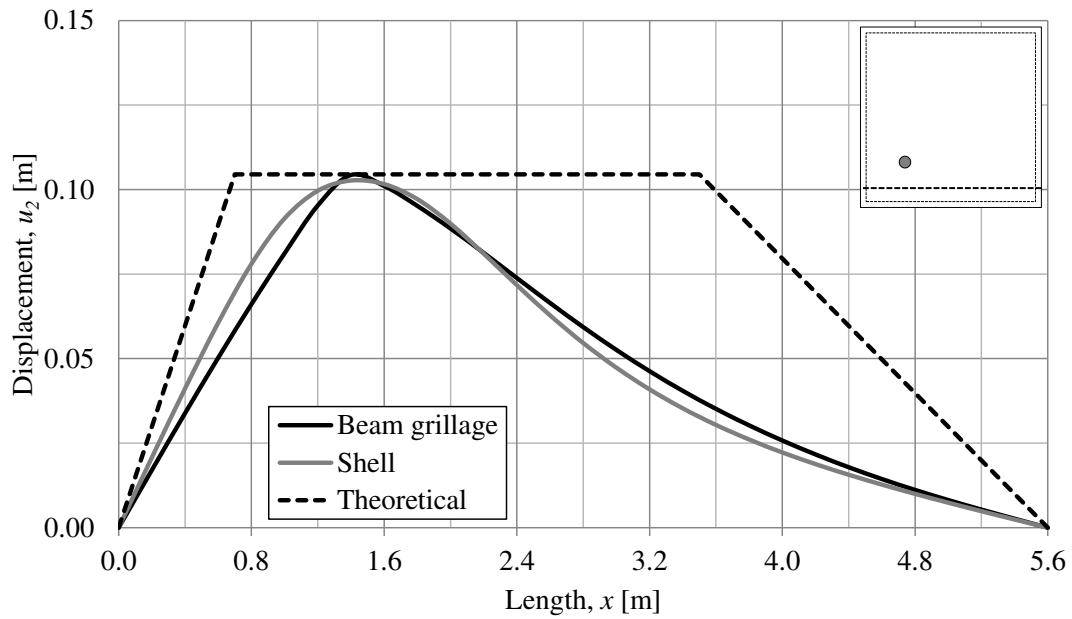
Figure F.4   *Illustration of the displacement of body 2 u_2 on a quadratic slab along a line for the theoretical assumed model, the beam grillage and the shell element model. The line and the point of point loading are presented in the upper right hand corner.*
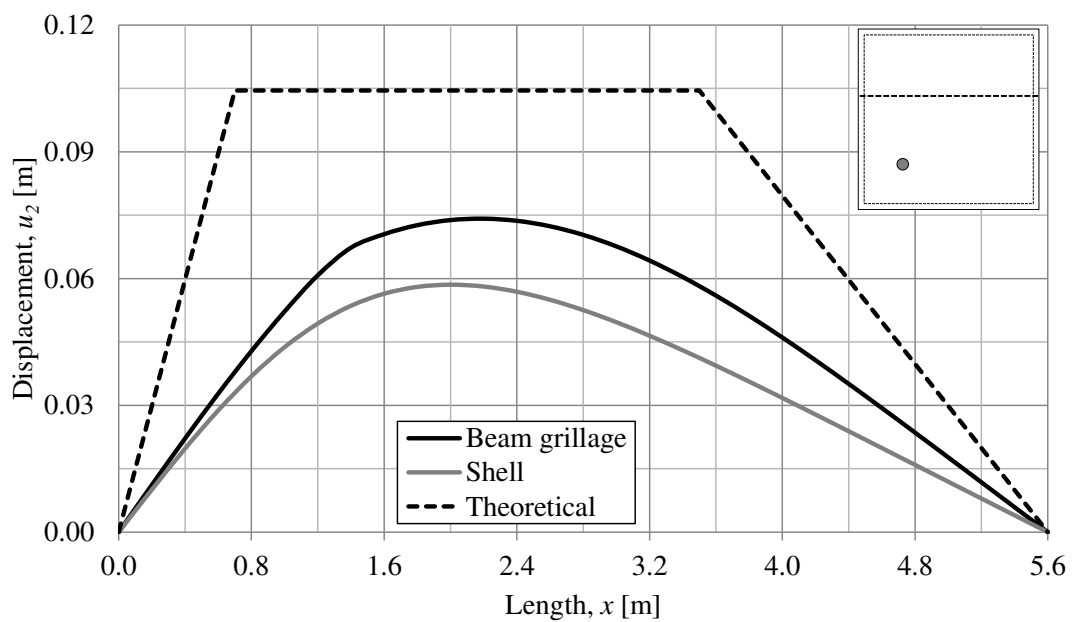
Figure F.5   *Illustration of the displacement of body 2 u_2 on a quadratic slab along a line for the theoretical assumed model, the beam grillage and the shell element model. The line and the point of point loading are presented in the upper right hand corner.*
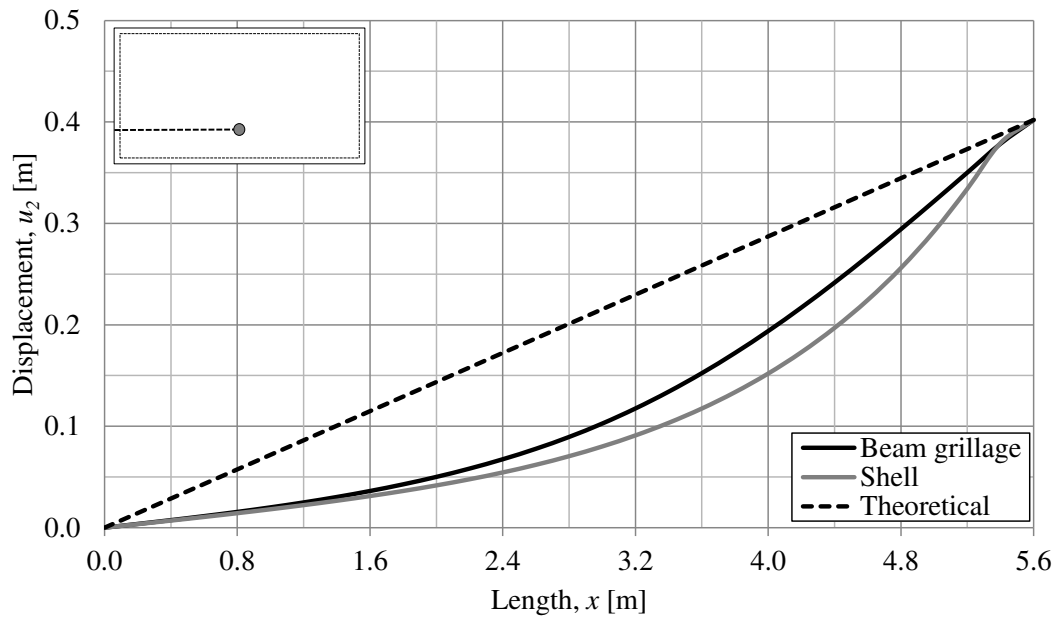
Figure F.6   *Illustration of the displacement of body 2 u_2 on a rectangular slab along a line for the theoretical assumed model, the beam grillage and the shell element model. The line and the point of point loading are presented in the upper right hand corner.*
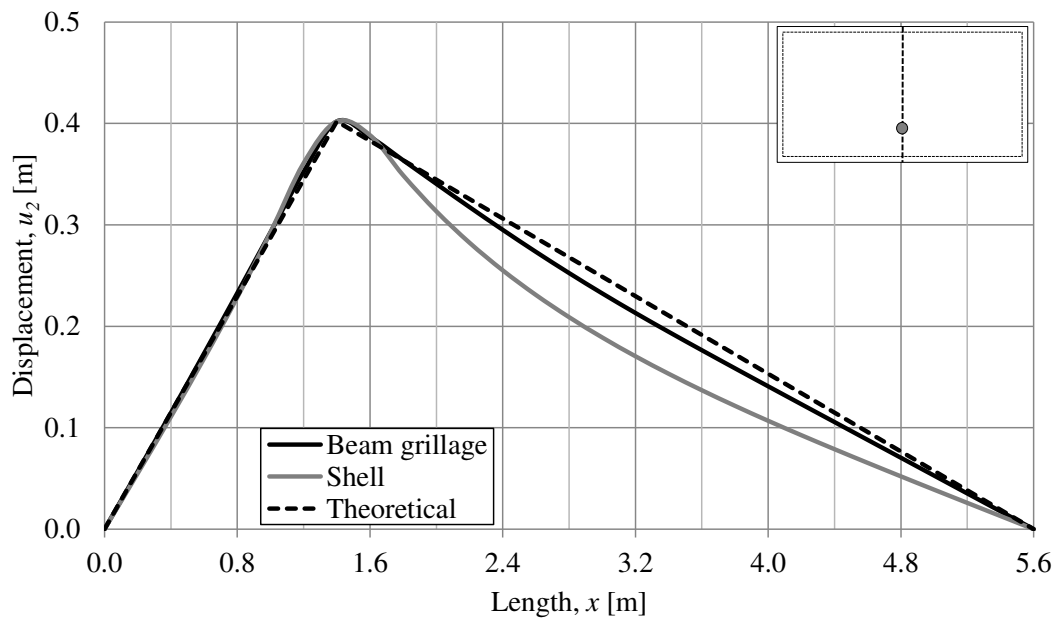
Figure F.7   *Illustration of the displacement of body 2 u_2 on a rectangular slab along a line for the theoretical assumed model, the beam grillage and the shell element model. The line and the point of point loading are presented in the upper right hand corner.*
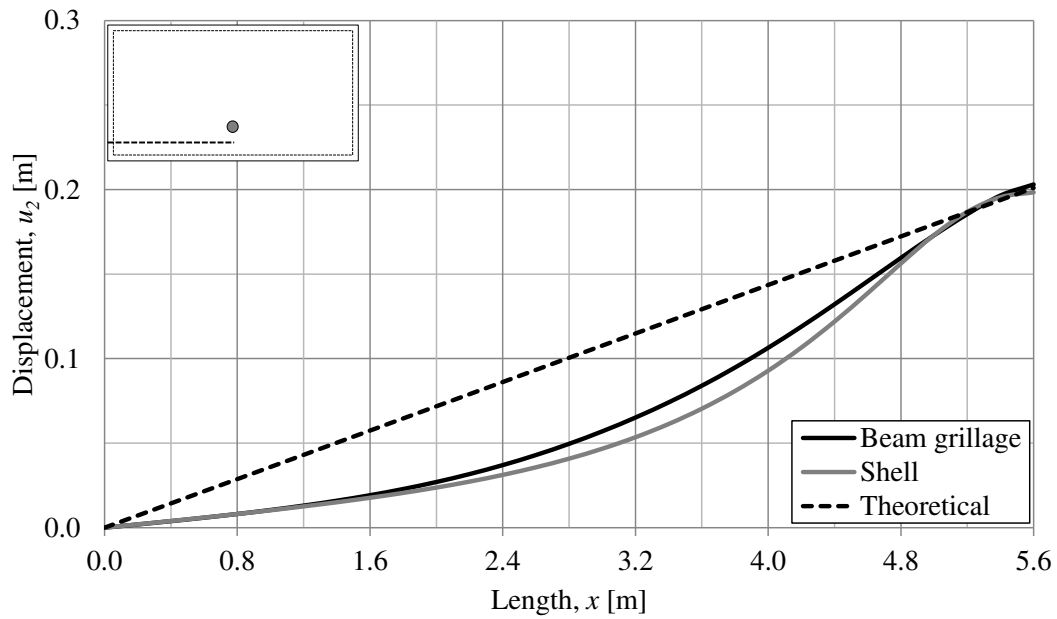
Figure F.8   *Illustration of the displacement of body 2 u_2 on a rectangular slab along a line for the theoretical assumed model, the beam grillage and the shell element model. The line and the point of point loading are presented in the upper left hand corner.*
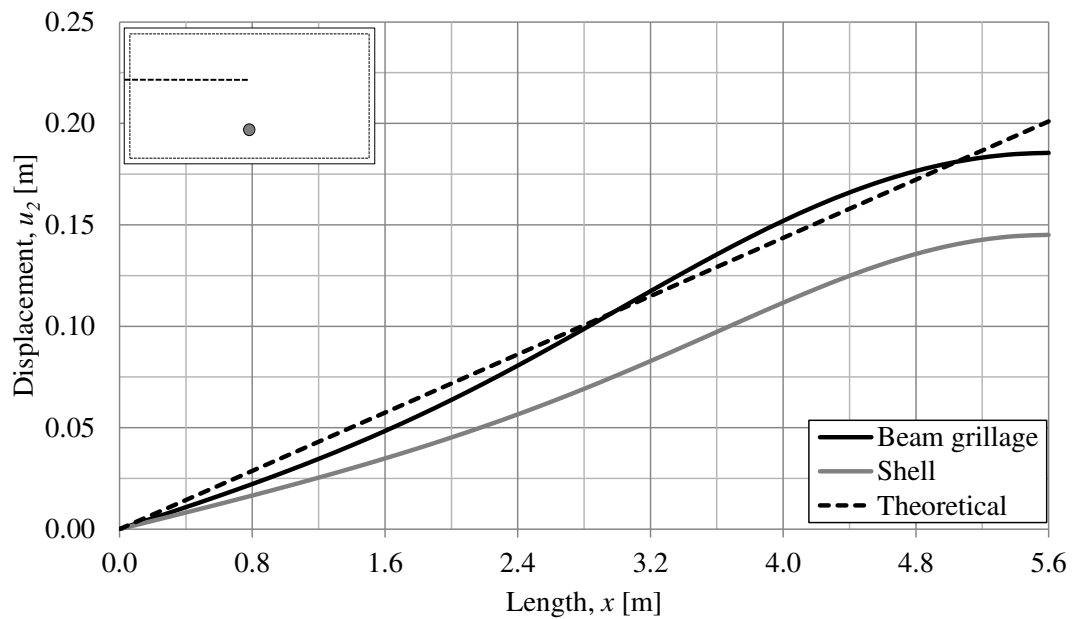
Figure F.9   *Illustration of the displacement of body 2 u_2 on a rectangular slab along a line for the theoretical assumed model, the beam grillage and the shell element model. The line and the point of point loading are presented in the upper left hand corner.*
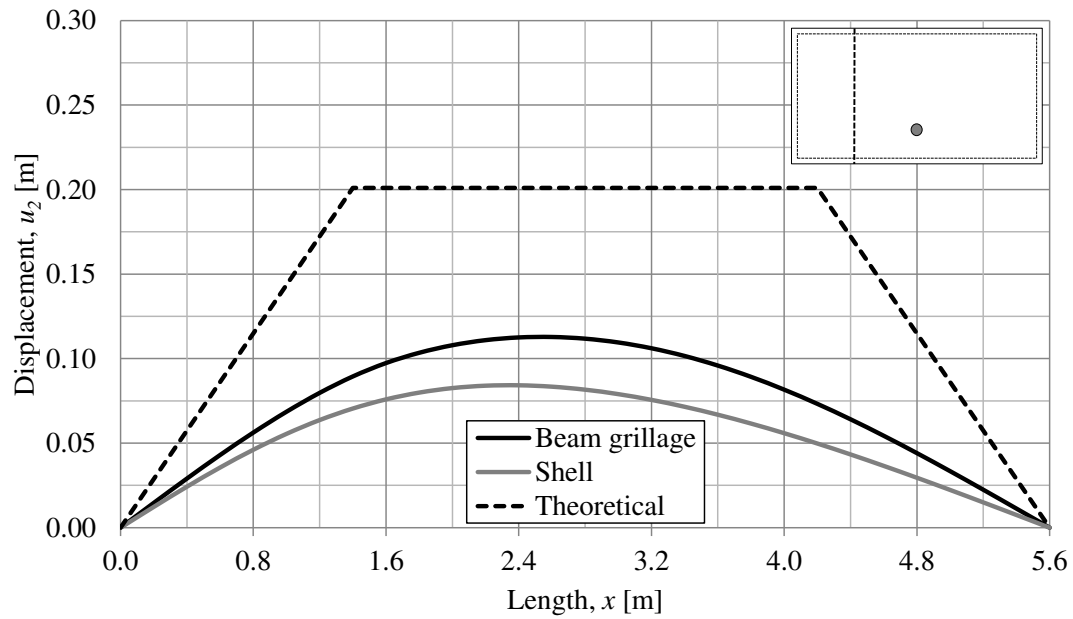
Figure F.10   Illustration of the displacement of body 2 u_2 on a rectangular slab along a line for the theoretical assumed model, the beam grillage and the shell element model. The line and the point of point loading are presented in the upper right hand corner.

F.2   Load-displacement diagrams

In this section are the load-displacement diagrams for load case 1-3 illustrated, which are discussed in Section 6.2.4.2. Additionally are two load cases for a rectangular slab illustrated.
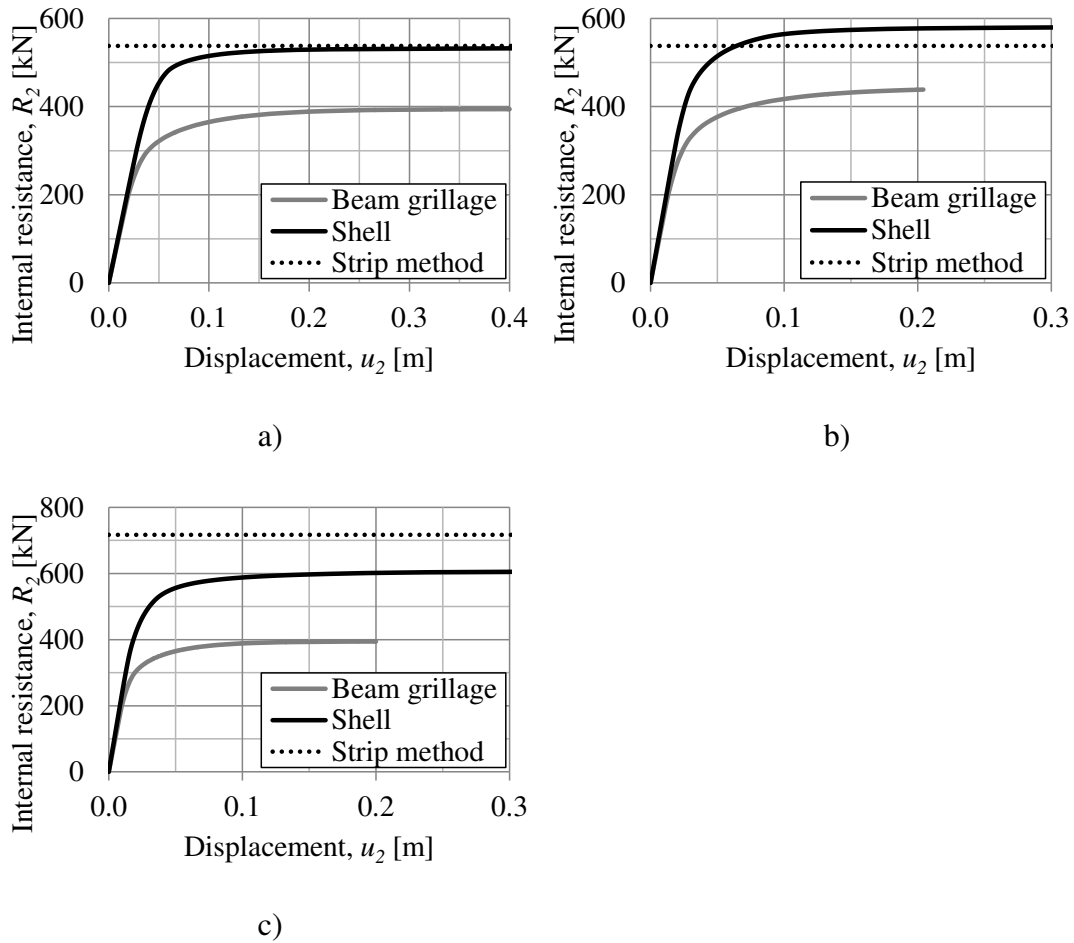
Figure F.11   Illustration of the load-displacement response on a quadratic slab of a beam grillage model, a slab modelled with shell elements and the expected load capacity obtained from the strip method, a) load case 1, b) load case 2, and c) load case 3.
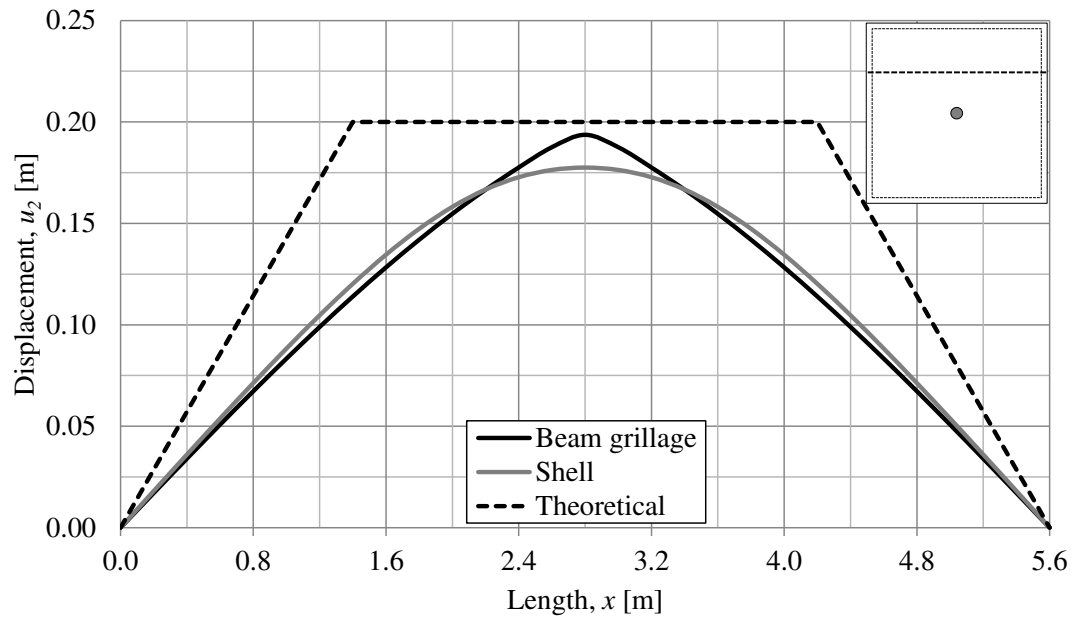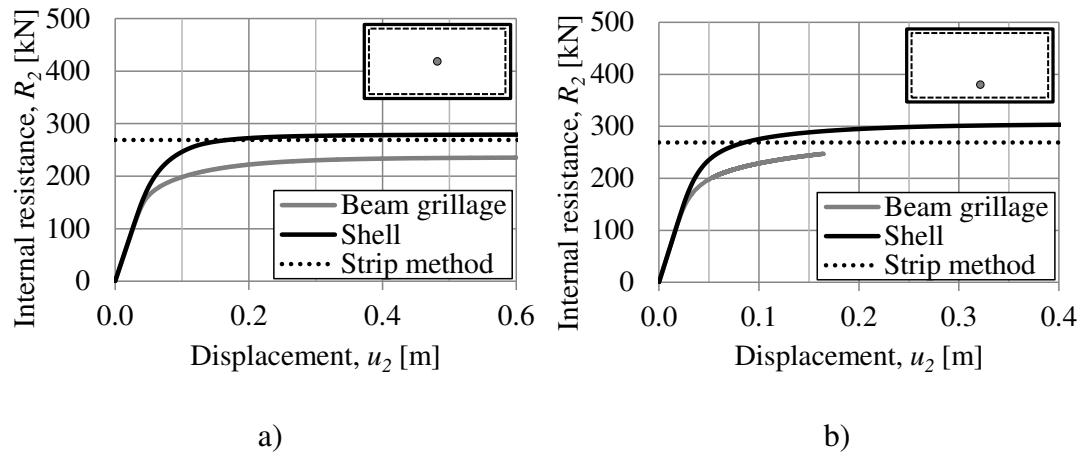

Figure F.12   Illustration of the load-displacement response on a rectangular slab, $l_x = 2l_y$, of a beam grillage model, a slab modelled with shell elements and the expected load capacity obtained from the strip method, a) with the point load acting as described in the top right hand corner, and b) with the point load acting as described in the top right hand corner.

F.3   Plastic strain distribution for shell element model

In this section, the plastic strain distribution diagram for various load cases on both a quadratic and a rectangular slab are illustrated in addition to the diagrams presented in Section 6.2.4.2. Purple and blue indicates that the strain is low or around the yield limit and red and pink indicates a very high plastic strain.

a)   b)
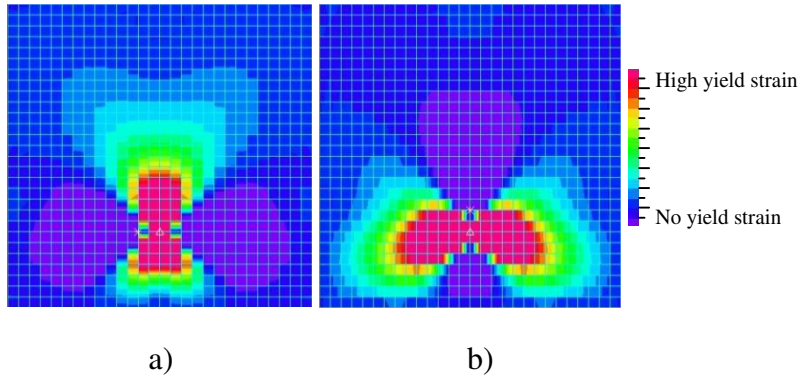
Figure F.13   Illustration of the distribution of the plastic strain for load case 2 in a) x-direction, and b) y-direction.
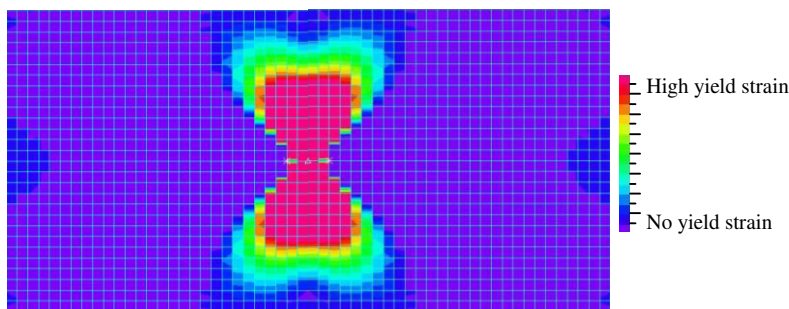
Figure F.14   Illustration of the distribution of the plastic strain in x-direction for a rectangular slab with side length $l_x = 2l_y$ subjected to a point load in the centre.
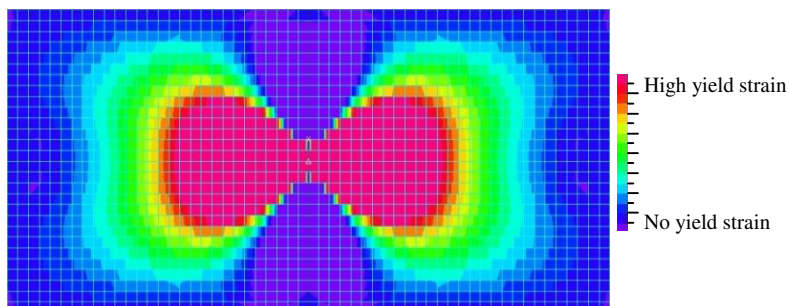
Figure F.15   Illustration of the distribution of the plastic strain in y-direction for a rectangular slab with side length $l_x = 2l_y$ subjected to a point load in the centre.

Appendix G   Mathcad Calculations

This appendix derives input parameters to ADINA and to hand calculations for the quadratic slab used in this thesis. Input parameters are derived for both shell and beam grillage elements. Input parameters for the beam are derived in the same way, but are not presented.

Input data

Geometry of the beam grillage beams:

$$l_b := 5.6\,m \qquad h_b := 0.2\,m \qquad w_b := 0.2\,m \qquad s_{rebars} := 200\,mm \qquad c_{cover} := 30\,mm$$

Material parameters for reinforced concrete:

$$E_{cm} := 33\,GPa \quad f_{cc} := 30\,MPa \quad \rho_{conc} := 2400\,\frac{kg}{m^3} \quad \alpha_R := 0.810 \qquad \beta_R := 0.416$$

$$E_s := 200\,GPa \quad f_{yk} := 500\,MPa \quad \phi := 16\,mm \qquad \varepsilon_{cu} := 3.5 \cdot 10^{-3} \qquad \upsilon := 0$$

$$\gamma_s := 1.15 \qquad \gamma_c := 1.5$$

Initial calculations

$$f_{cd} := \frac{f_{cc}}{\gamma_c} = 20 \cdot MPa \qquad\qquad f_{yd} := \frac{f_{yk}}{\gamma_s} = 434.783 \cdot MPa$$

$$d_{tens} := h_b - c_{cover} - \frac{\phi}{2} = 0.162\,m \qquad d_{comp} := c_{cover} + \frac{\phi}{2} = 38 \cdot mm$$

$$\alpha_s := \frac{E_s}{E_{cm}} = 6.061 \qquad\qquad A_{one.bar} := \frac{\pi \cdot \phi^2}{4} = 2.011 \times 10^{-4}\,m^2$$

$$m_b := \rho_{conc} \cdot l_b \cdot h_b \cdot w_b = 537.6\,kg \qquad A_{all.bars} := \frac{A_{one.bar}}{s_{rebars}} \cdot w_b = 2.011 \times 10^{-4}\,m^2$$

Double reinforced section in state III
Deriving of moment capacity, M_{rd}. This is for calculations around the s axis in ADINA, the manner of the calculations around the t axis are the same, but not presented.

x_{III} ansatz:

$$x_{III} := 33.22456\,mm \quad \text{(should be the same as } x_{III.control} \text{ later on)}$$

$$\varepsilon_{comp} := \frac{x_{III} - d_{comp}}{x_{III}} \cdot \varepsilon_{cu} = -5.031 \times 10^{-4} \qquad \varepsilon_{tens} := \frac{d_{tens} - x_{III}}{x_{III}} \cdot \varepsilon_{cu} = 0.014$$

$$\sigma_{comp} := min(\varepsilon_{comp} \cdot E_s, f_{yd}) = -100.613 \cdot MPa \qquad \sigma_{tens} := min(\varepsilon_{tens} \cdot E_s, f_{yd}) = 434.783 \cdot MPa$$

$$F_{s.comp} := A_{all.bars} \cdot \sigma_{comp} = -20.229 \cdot kN \qquad\qquad F_{s.tens} := A_{all.bars} \cdot \sigma_{tens} = 87.418 \cdot kN$$

Force equilibrium gives:

$$x_{III.control} := \frac{F_{s.tens} - F_{s.comp}}{\alpha_R \cdot f_{cd} \cdot w_b} = 33.22456 \cdot mm$$

$$F_c := \alpha_R \cdot f_{cd} \cdot w_b \cdot x_{III} = 107.648 \cdot kN$$

Moment equlibrium gives:

$$M_{rd} := F_{s.tens} \cdot d_{tens} - F_{s.comp} \cdot d_{comp} - F_c \cdot \beta_R \cdot x_{III} = 13.443 \cdot kN \cdot m$$

$$m_{rd} := \frac{M_{rd}}{w_b} = 67.213 \cdot \frac{kN \cdot m}{m} \qquad \sigma_{yield} := \frac{m_{rd}}{h_b^2} = 1.68 \cdot MPa$$

Double reinforced section in state II

In this section, curvature corresponding to moment capacity is derived. In these calculations it is symbolised as χ_{pl} and not $(1/r)_{pl}$. Equivalent elastic modulus E_{eq} is also derived in this section. This is for calculations around the s axis in ADINA, the manner of the calculations around the t axis are the same, but not presented.

x_{II} ansatz:

$$x_{II} := 34.51987 mm \qquad \text{(should be the same as } x_{II.control} \text{ later on)}$$

$$x_{cc} := \frac{x_{II}}{3} = 0.012\,m \qquad A_{cc} := w_b \cdot x_{II} = 6.904 \times 10^{-3}\,m^2$$

$$A_{II} := A_{cc} + (\alpha_s - 1) \cdot A_{all.bars} + \alpha_s \cdot A_{all.bars} = 9.14 \times 10^{-3}\,m^2$$

$$x_{II.control} := \frac{A_{cc} \cdot x_{cc} + (\alpha_s - 1) \cdot A_{all.bars} \cdot d_{comp} + \alpha_s \cdot A_{all.bars} \cdot d_{tens}}{A_{II}} = 34.51987 \cdot mm$$

$$I_{II} := \frac{w_b \cdot x_{II}^3}{12} + A_{cc} \cdot (x_{II} - x_{cc})^2 + (\alpha_s - 1) \cdot A_{all.bars} \cdot (x_{II} - d_{comp})^2 \ldots = 2.41573 \times 10^{-5} \cdot m^4$$
$$+ \alpha_s \cdot A_{all.bars} \cdot (d_{tens} - x_{II})^2$$

$$I_I := \frac{w_b \cdot h_b^3}{12} = 1.333 \times 10^{-4} \cdot m^4 \qquad EI_b := E_{cm} \cdot I_{II} = 797.191 \cdot kN \cdot m^2$$

$$\chi_{pl} := \frac{M_{rd}}{EI_b} = 0.017 \frac{1}{m} \qquad\qquad E_{eq} := \frac{I_{II}}{I_I} \cdot E_{cm} = 5.979 \cdot GPa$$

Torsion-twisting relation based on E_{eq}

These calculations are based on E_{eq}; the other torsion-twistion relations calculation are not presented, but they are calculated in the same manner. The calculations in this section are based on Lundh (2000).

$$F_1 := 0.42 \qquad F_2 := 0.83 \qquad \text{(For a quadratic cross section)}$$

$$W_v := \min\left(\frac{w_b \cdot h_b^2}{4} \cdot F_2, \frac{w_b^2 \cdot h_b}{4} \cdot F_2\right) = 1.66 \times 10^{-3} \cdot m^3$$

$$K_{eq} := \min\left(\frac{w_b \cdot h_b^3}{3} \cdot F_1, \frac{w_b^3 \cdot h_b}{3} \cdot F_1\right) = 2.24 \times 10^{-4} \, m^4$$

$$G_{eq} := \frac{E_{eq}}{2 \cdot (1 + \upsilon)} = 2.989 \cdot GPa$$

$$\boxed{M_v := W_v \cdot \sigma_{yield} = 2.789 \cdot kN \cdot m} \qquad \boxed{\varphi_{ref.eq} := \frac{M_v}{G_{eq} \cdot K_{eq}} = 4.165 \times 10^{-3} \cdot \frac{1}{m}}$$

Strip method calculations

These calculations are based on Engström (2014). The calculations in this section are for the quadratic slab used in this thesis. The load cases calculated are load case 1 where a point load is acting in the middle of the slab and a load case where the load is distributed over the whole slab. Other load cases and slabs are calculated in the same manner but are not presented.
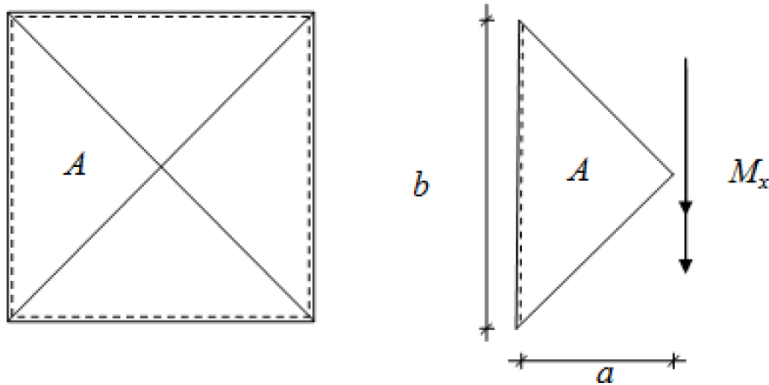
$$a := \frac{l_b}{2} \qquad b := l_b \qquad M_x := m_{rd} \cdot b$$

Point load:

$$P := \frac{M_x}{a} = 134.426 \cdot kN$$

$$F_{tot.Rd} := P \cdot 4 = 537.705 \cdot kN$$

(Each block take a fourth of the load because of symmetry)

Pressure load:

$$q_{Rd} := 6 \cdot \frac{M_x}{b \cdot a^2} = 51.439 \cdot \frac{kN}{m^2}$$

Appendix H MATLAB Algorithms

H.1 2DOF algorithm

```
%========================2DOF model===========================

% This program simulates a collision between two bodies with or
% without barrier using a two degree of freedom (2DOF) mass
% spring system. The 2DOF model is made of two masses and two
% springs connected to a fixed support and works for both
% elastic, plastic or elasto-plastic response.

%

% Program written by:   Jonatan Andersson   880626

%                       Johan Antonsson      900716

%

%             Date:    2015-05-05

%=============================================================

clear all

close all

clc

%====================Input data===========================
%Time interval:

time_interval=0.5; %[s]


%Properties of body 1:

m1=1500; %[kg] (Mass)

k1=1e6; %[N/m] (Stiffness, put to a very high number for an ideal
%               plastic response of body 1)

R1=0; %[N] (Put to zero if linear elastic analysis)

v1=27.8; %[m/s] (Initial velocity)

u_pl_max1=inf; %[-] (Maximum plastic displacement)

u1=0; %[m] (Initial displacement)

p1=0; %[N] (Initial force)


%Properties of body 2:

kappa_mf=0.203; %[-] (Transformation factor)

m_structure=15052.8; %[kg] (Mass of resisting structure)

k2=10.79e6; %[N/m] (Stiffness, put to zero for collision without
%                   barrier, put to a very high number for ideal
%                   plastic response)

R2=0; %[N] (Put to zero if linear elastic analysis)

v2=0; %[m/s] (Initial velocity)

u_pl_max2=inf; %[-] (Maximum plastic displacement)

u2=0; %[m] (Initial displacement)

p2=0; %[N] (Initial force)


%====================Initial calculations====================
%Time interval:

t=linspace(0,time_interval,time_interval*1000+1);


%Time step:

h=t(2);


%Relative mass of body 2:

m2=kappa_mf*m_structure;


%Maximum elastic displacement:

u_el_max=[R1/k1; R2/k2];

if R1 == 0
```

```
    u_el_max(1)=inf;

end

if R2 == 0

    u_el_max(2)=inf;

end


%Initial stiffness matrix:

K=[k1 -k1;

   -k1 k1+k2];


%Mass matrix:

M=[m1 0;

   0 m2];


%Initial velocity, displacement and force vector:

v0=[v1; v2];

u0=[u1; u2];

p0=[p1; p2];


%Predefining variables to save computational time:

u=zeros(2,length(t)+1);

v=zeros(2,length(t));

a=zeros(2,length(t));

Ek=zeros(2,length(t));

Ekpos=zeros(1,length(t));

Wi=zeros(2,length(t));

We2=zeros(1,length(t));

Ir=zeros(2,length(t));

dui=zeros(1,length(t));

u_pl=zeros(2,length(t));

R=zeros(2,length(t));


%================Central Difference Method (CDM)==================

%Using the Central Difference Method (CDM) to numerically
%calculate the displacement at different times


%Initial acceleration vector:

a0=M\(p0-K*u0);


%Starting displacement value:

u_start=u0-h*v0+h^2/2*a0;


%Start values for forces

p_n=p0;


%For loop to calculate displacements and other parameters at
%different times using the CDM:

for i=1:length(t)

    %Calculate the deformation of spring 1:

    dui(i)=u(1,i)-u(2,i);
```

```matlab
    %New additional plastic deformation for body 1:
    if dui(i) > u_el_max(1) && dui(i) > max(dui(1:i-1))

        dui_pl_1=dui(i)-max(max(dui(1:i-1)), u_el_max(1));

    else

        dui_pl_1=0;

    end


    %New additional plastic deformation for body 2
    if u(2,i) > u_el_max(2) && u(2,i) > max(u(2,1:i-1))

        dui_pl_2=u(2,i)-max(max(u(2,1:i-1)), u_el_max(2));

    else

        dui_pl_2=0;

    end


    %Updating the plastic deformation:
    if i ~= 1

        u_pl(:,i)=u_pl(:,i-1)+[dui_pl_1; dui_pl_2];

    end


    %Calculating reaction forces for spring 1:
    if dui(i) < 0 || u_pl(1,i) > u_pl_max1

        R(1,i)=0;

    else

        R(1,i)=max(0,k1*(dui(i)-u_pl(1,i)));

    end


    %Calculating reaction forces for spring 2:
    if u_pl(2,i) > u_pl_max2

        R(2,i)=0;

    else

        R(2,i)=k2*(u(2,i)-u_pl(2,i));

    end


    %Calculating current stiffnesses for spring 1:
    if dui(i)==0

        k1_cdm=k1;

    else

        k1_cdm=R(1,i)/dui(i);

    end


    %Calculating current stiffnesses for spring 2:
    if u(2,i)==0

        k2_cdm=k2;

    else

        k2_cdm=R(2,i)/u(2,i);

    end


    %Updating the stiffness matrix:
    K=[k1_cdm -k1_cdm;

       -k1_cdm k1_cdm+k2_cdm];


    %CDM equation:
    if i ~= 1

        u(:,i+1)=(M/h^2)\(p_n-(K-2*M/h^2)*u(:,i)-(M/h^2)*u(:,i-1));

    else

        u(:,i+1)=(M/h^2)\(p_n-(K-2*M/h^2)*u(:,i)-(M/h^2)*u_start);

    end


    %Calculating velocity and acceleration:
    if i~=1

        v(:,i)=(u(:,i+1)-u(:,i-1))/(2*h);

        a(:,i)=(u(:,i+1)-2*u(:,i)+u(:,i-1))/h^2;

    else

        v(:,i)=v0;

    end


    %Calculating kinetical energy for body 1 in positive
%   direction:
    if v(1,i) > 0

        Ekpos(i)=m1*v(1,i)^2/2;

    end


    %Calculating internal work for body 1 and 2:
    if i~=1

        Wi(:,i)=Wi(:,i-1)+(R(:,i)+R(:,i-1))/2.*(u(:,i)-u(:,i-1));

    end


    %Calculating external work from body 2 to body 1:
    if i~=1

        We2(i)=We2(i-1)+(R(1,i)+R(1,i-1))/2.*(u(2,i)-u(2,i-1));

    end


    %Calculating impulse from internal resistance:
    if i~=1

        Ir(:,i)=Ir(:,i-1)+(R(:,i)+R(:,i-1))/2*h;

    end

end


%Erasing the last u because it is out of the chosen time
%interval:
u=u(:,1:length(t));


%======================Other results============================
%Kinetical energy for body 1 and 2:
Ek(1,:)=m1*v(1,:).^2/2;

Ek(2,:)=m2*v(2,:).^2/2;


%Total kinetic energy in positive direction:
Ek_tot_positive=Ekpos+Ek(2,:);


%Frequency ratio:
freq_rat=sqrt(k1/m1)/sqrt(k2/m2);


%Mass ratio:
mass_rat=m1/m2;


%Load factor beta_el:
beta=max(R(2,:))/(v0(1)*sqrt(k1*m1));
```

H.2 Transformation factor algorithm

```
%=======================2DOF model=============================

% This program calculates the transformation factors that makes
% it possible to use mass-spring systems to model the behaviour
% of a slab

%

% Program written by:  Jonatan Andersson   880626

%                      Johan Antonsson      900716

%

%              Date:   2015-05-05
%================================================================

clear all

close all

clc


%========================Input data============================

F=1e5; %[N] Applied static force

system_node=421; %[-] The node where the load is applied

nodes=841; %Number of nodes


%=====================Extracting data==========================

%Opening txt file with all deflections of the slab

txtfil=fopen('u2_whole_model.txt');

    A=textscan(txtfil, '%s %s %s');

fclose(txtfil);


%Making the information from the txt file to a vector

for j = 1:length(A{3})

    str=A{3}{j};

    defl(j)=str2num(str);

end


%Extracting the deflection at the system node, u_s

str=A{3}{system_node};

u_s=str2num(str)


%===============Calculating transformation factors=============
%Calculating kappa_m

k_m=sum(defl.^2)/(u_s^2*(sqrt(length(defl))-1)^2)


%Calculating kappa_f for a load distributed over four elements

k_f=(4*u_s+2*(defl(system_node-sqrt(nodes))+defl(system_node-1)+

defl(system_node+1)+defl(system_node+sqrt(nodes)))

+defl(system_node-sqrt(nodes)-1)+defl(system_node-sqrt(nodes)+1)

+defl(system_node+sqrt(nodes)-
1)+defl(system_node+sqrt(nodes)+1))/(16*u_s)


%kappa_f for a point load

%k_f=1


%Calculating kappa_mf

k_mf=k_m/k_f


%Calculating the stiffness of the slab

k_sl=F/u_s
```

Appendix I   ADINA Command Files

I.1   ADINA command file for shell element model

```
**********INPUT DATA**********
PARAMETER E '5.979E9'
PARAMETER NU '0'
PARAMETER YIELDSTRESS '1.68E6'
PARAMETER YIELDSTRAIN '1'
PARAMETER ALPA '0.231'
PARAMETER DENSITY '2400'

PARAMETER MASSNODE '842'
PARAMETER POINTMASS '1500'
PARAMETER VELOCITY '27.8'
PARAMETER K '1E6'
PARAMETER TIMESTEP '1000'
PARAMETER STEPMAGNITUDE '0.001'

PARAMETER ALPAX '0.5'
PARAMETER ALPAY '0.5'
PARAMETER LENGTH '5.6'
PARAMETER THICKNESS '0.2'


**********PARAMETER CALCULATIONS**********
PARAMETER SUBDIV '$THICKNESS'
PARAMETER LOADPOINTX '$ALPAX*$LENGTH'
PARAMETER LOADPOINTX1 '$LOADPOINTX+$SUBDIV'
PARAMETER LOADPOINTXMINUS1 '$LOADPOINTX-$SUBDIV'
PARAMETER LOADPOINTY '$ALPAY*$LENGTH'
PARAMETER LOADPOINTY1 '$LOADPOINTY+$SUBDIV'
PARAMETER LOADPOINTYMINUS1 '$LOADPOINTY-$SUBDIV'
PARAMETER YIELDSTRESSMOD '$YIELDSTRESS/$ALPA'
PARAMETER MINUSK '-$K/16'
PARAMETER K1 '$MINUSK*4'
PARAMETER K2 '$MINUSK*2'
PARAMETER K3 '$MINUSK'


**********POINTS**********
COORDINATES POINT SYSTEM=0
@CLEAR
1 0 0 0 0
2 $LENGTH 0 0 0
3 $LENGTH $LENGTH 0 0
4 0 $LENGTH 0 0
5 $LOADPOINTXMINUS1 $LOADPOINTYMINUS1 0 0
6 $LOADPOINTX $LOADPOINTYMINUS1 0 0
7 $LOADPOINTX1 $LOADPOINTYMINUS1
8 $LOADPOINTX1 $LOADPOINTY 0 0
9 $LOADPOINTX1 $LOADPOINTY1 0 0
10 $LOADPOINTX $LOADPOINTY1 0 0
11 $LOADPOINTXMINUS1 $LOADPOINTY1 0 0
12 $LOADPOINTXMINUS1 $LOADPOINTY 0 0
13 $LOADPOINTX $LOADPOINTY 0 0
14 $LOADPOINTX $LOADPOINTY -1 0
@


**********SURFACES**********
SURFACE VERTEX NAME=1 P1=1 P2=2 P3=3 P4=4


**********BOUNDARY CONDITIONS**********
FIXITY NAME=HORN
@CLEAR
 'X-TRANSLATION'
 'Y-TRANSLATION'
 'Z-TRANSLATION'
 'OVALIZATION'

FIXITY NAME=HORNX
@CLEAR
 'Y-TRANSLATION'
 'Z-TRANSLATION'
 'OVALIZATION'

FIXITY NAME=HORNY
@CLEAR
 'X-TRANSLATION'
 'Z-TRANSLATION'
 'OVALIZATION'

FIXITY NAME=RULL
@CLEAR
 'Z-TRANSLATION'
 'OVALIZATION'
@

FIXITY NAME=SPRING
@CLEAR
 'X-TRANSLATION'
 'Y-TRANSLATION'
 'X-ROTATION'
 'Y-ROTATION'
 'Z-ROTATION'
 'OVALIZATION'

FIXBOUNDARY POINTS FIXITY=ALL
1 'HORN'
2 'HORNX'
4 'HORNY'
14 'SPRING'

FIXBOUNDARY LINES FIXITY=ALL
@CLEAR
1  'RULL'
```

```
2  'RULL'

3  'RULL'                                          PROPERTYSET NAME=2 NONLINEA=YES NK=2 NM=0 NC=0

4  'RULL'

                                                   PROPERTY NONLINEAR-K NAME=3

**********POINT MASS**********                     @CLEAR

MASSES POINTS                                      -1 $K1

@CLEAR                                             0 0

14 0 0 $POINTMASS 0 0 0                            1 0

@                                                  @


**********TIME STEP**********                      PROPERTYSET NAME=3 NONLINEA=YES NK=3 NM=0 NC=0

TIMESTEP NAME=DEFAULT

@CLEAR                                             EGROUP    SPRING    NAME=2    PROPERTY=1    RESULTS=STRESSES
                                                   DESCRIPT='SPRING1'
$TIMESTEP $STEPMAGNITUDE

@                                                  SPRING POINTS

                                                   @CLEAR

**********MESHING SLAB**********                   1 14 3 5 3

MATERIAL  PLASTIC-BILINEAR  NAME=1  HARDENIN=ISOTROPIC  E=$E   2 14 3 7 3
NU=$NU,
                                                   3 14 3 9 3
         YIELD=$YIELDSTRESSMOD        EPA=$YIELDSTRAIN
STRAINRA=0 DENSITY=$DENSITY,                       4 14 3 11 3

         MDESCRIP='Elastoplast'


                                                   EGROUP    SPRING    NAME=3    PROPERTY=2    RESULTS=STRESSES
EGROUP SHELL NAME=1 DISPLACE=DEFAULT MATERIAL=1 TINT=7    DESCRIPT='SPRING2'
RESULTS=STRESSES STRESSRE=GLOBAL,

         DESCRIPT='NONE'    THICKNES=$THICKNESS    TINT-   SPRING POINTS
TYP=NEWTON-COTES
                                                   5 14 3 6 3

SFTHICKNESS THICK-2D=VARIABLE                      6 14 3 8 3

@CLEAR                                             7 14 3 10 3

1 $THICKNESS 0 0 0 0                               8 14 3 12 3

@


SUBDIVIDE MODEL MODE=LENGTH SIZE=$SUBDIV NDIV=1,   EGROUP    SPRING    NAME=4    PROPERTY=3    RESULTS=STRESSES
                                                   DESCRIPT='SPRING3'
         PROGRESS=GEOMETRIC MINCUR=1

                                                   SPRING POINTS
GSURFACE NODES=4
                                                   9 14 3 13 3
@CLEAR
                                                   @
1

@                                                  **********APPLYING INITIAL VELOCITY**********

                                                   INITIAL VELOCITIES SUBSTRUC=0 REUSE=1
**********MESHING SPRINGS**********
                                                   @CLEAR
PROPERTY NONLINEAR-K NAME=1
                                                   $MASSNODE 0 0 $VELOCITY 0 0 0 0
@CLEAR
                                                   @
-1 $K3

0 0                                                **********MAKING IT DYNAMIC**********

1 0                                                MASTER ANALYSIS=DYNAMIC-DIRECT-INTEGRATION

@

                                                   ANALYSIS DYNAMIC-DIRECT-INTEGRATION
PROPERTYSET NAME=1 NONLINEA=YES NK=1 NM=0 NC=0


PROPERTY NONLINEAR-K NAME=2

@CLEAR

-1 $K2

0 0

1 0

@
```

I.2   ADINA command file for beam grillage model

```
*To avoid a large number of pages are the parts where points and
*lines are assigned and meshed excluded. There is a point in each
*intersection in the grillage and there is a line connecting each
*point vertically and horizontally. When there is a repetition of
*a command it is written as three dots "..." which means that the
*points and lines in between are done in the same way.


**********POINTS**********

COORDINATES POINT SYSTEM=0

@CLEAR

1 0 0 0 0

2 0.2 0 0 0

...

841 5.6 5.6 0 0

842 2.8 2.8 -1 0

@


**********LINES**********

LINE STRAIGHT NAME=1 P1=1 P2=2

LINE STRAIGHT NAME=2 P1=2 P2=3

...

LINE STRAIGHT NAME=1623 P1=783 P2=812

LINE STRAIGHT NAME=1624 P1=812 P2=841


**BOUNDARY CONDITIONS points**

FIXITY NAME=HORN

@CLEAR

 'X-TRANSLATION'

 'Y-TRANSLATION'

 'Z-TRANSLATION'

 'OVALIZATION'

@


FIXITY NAME=HORNX

@CLEAR

 'Y-TRANSLATION'

 'Z-TRANSLATION'

 'OVALIZATION'

@


FIXITY NAME=HORNY

@CLEAR

 'X-TRANSLATION'

 'Z-TRANSLATION'

 'OVALIZATION'

@


FIXITY NAME=RULL

@CLEAR

 'Z-TRANSLATION'

 'OVALIZATION'

@


FIXITY NAME=SPRING

@CLEAR
```

```
 'X-TRANSLATION'

 'Y-TRANSLATION'

 'X-ROTATION'

 'Y-ROTATION'

 'Z-ROTATION'

 'OVALIZATION'

@


FIXBOUNDARY POINTS FIXITY=ALL

@CLEAR

1 'HORN'

29 'HORNX'

813 'HORNY'

842 'SPRING'

@


**BOUNDARY CONDITIONS lines**

*The boundary condition "Rull" is assigned to all outer lines.

FIXBOUNDARY LINES FIXITY=ALL

@CLEAR

1 'RULL'

2 'RULL'

...

1623 'RULL'

1624 'RULL'

@


**********POINT MASS**********

MASSES POINTS

@CLEAR

842 0 0 1500 0 0 0

@


**********TIME STEP**********

TIMESTEP NAME=DEFAULT

@CLEAR

1000 0.001

@


*******MOMENT-CURVATURE/TORSION-TWISTING *******

FORCE-STRAIN NAME=1

@CLEAR

-0.003 -160000

-0.001 -160000

0 0

0.001 160000

0.003 160000

@


TWIST-MOMENT NAME=2

@CLEAR

-100 -2928.45
```

```
-0.004165 -2789

0 0

0.004165 2789

100 2928.45

@


MOMENT-TWIST NAME=2

@CLEAR

-1E6 2

0 2

1E6 2

@


CURVATURE-MO NAME=3

@CLEAR

-100 -14115.15

-0.017 -13443

0 0

0.017 13443

100 14115.15

@


MOMENT-CURVA NAME=3

@CLEAR

-1E6 3

0 3

1E6 3

@


CURVATURE-MO NAME=4

@CLEAR

-100 -13991.25

-0.019 -13325

0 0

0.019 13325

100 13991.25

@


MOMENT-CURVA NAME=4

@CLEAR

-1E6 4

0 4

1E6 4

@


**********MESHING SLAB**********

RIGIDITY-MOM  PLASTIC-MULTILINEAR  NAME=1  FORCE-AX=1  MOMENT-R=2
MOMENT-S=3,

MOMENT-T=4 DENSITY=1200 MASS-ARE=0.04,

ACURVE-T=UNSYMMETRIC TCURVE-T=UNSYMMETRIC BCURVE-T=UNSYMMETRIC
```

```
EGROUP  BEAM  NAME=1  SUBTYPE=THREE-D  MATERIAL=1  RESULTS=STRESSES
MOMENT-C=YES RIGIDITY=1 DESCRIPT='BEAM' SECTION=1


GLINE GROUP=1 XO=0 YO=-1 ZO=0

@CLEAR

1

2

...

811

812

@


GLINE GROUP=1 XO=1 YO=0 ZO=0

@CLEAR

813

814

...

1623

1624

@


**********MESHING SPRING**********

PROPERTY NONLINEAR-K NAME=1

@CLEAR

-1 -1000000

0 0

1 0

@


PROPERTYSET NAME=1 K=0 M=0 C=0 NONLINEA=YES NK=1 NM=0 NC=0


EGROUP SPRING NAME=2 PROPERTY=1 RESULTS=STRESSES


SPRING POINTS

@CLEAR

1 842 3 421 3 0  'DEFAULT'  'DEFAULT' 0 0

@


**********APPLYING INITIAL VELOCITY**********

INITIAL VELOCITIES SUBSTRUC=0 REUSE=1

@CLEAR

842 0 0 27.8 0 0 0

@


**********MAKING IT DYNAMIC**********

MASTER ANALYSIS=DYNAMIC-DIRECT-INTEGRATION


ANALYSIS DYNAMIC-DIRECT-INTEGRATION
```